Integration of Core and Log Data for the Petrophysical Analysis of Brae Conglomerates, North Sea.

Mark J.W.Deakin.

June, 1989

A thesis submitted for the degree of

Doctor of Philosophy of the University of London,

and for the

Diploma of Membership of the Imperial College.

Department of Geology,
Royal School of Mines,
Imperial College,
London, SW7 2BP.

BIBL
LONDON
UNIV

BEST COPY

AVAILABLE

Variable print quality

DEDICATION

This one's for Cheryl ...

ABSTRACT

This thesis describes an integrated petrophysical study on a sequence of Upper Jurassic conglomerates from the northern North Sea. The main objective was to resolve the apparent contradictions of reservoir quality and fluids content evident in the existing evaluation.

Formation evaluation is best accomplished by a combination of deterministic and statistical problem solving, with the will to model for and replace statistical/correlation techniques where possible. Conglomerate conductivity has been modelled as diffusion through a heterogeneous medium, in order to remove the influence of clasts from resistivity. An empirical chart and its equation are also derived from cored conglomerates, which provides sandy matrix resistivity. This can then be used with a single saturation equation, across the contrasting pore geometries of massive sands and conglomerates.

A saturation model is proposed which employs a free electrolyte formation factor, F_g, concerned with useable reservoir volumes. The model isolates shaly sand, grain and wettability effects to *non*-useable reservoir volumes by integrating capillary pressure data, or log correlations, to characterise the two pore-volumes. Independent saturation exponents are proposed for each pore-volume which further isolates any unwanted effects arising in the *non*–useable reservoir volume. A method is proposed for converting room temperature n values to reservoir temperature values.

A wide range of laboratory work was performed covering Optical Thin Sections, X-Ray Diffraction, Nuclear Activation, SEM and Special Core Analysis. These studies provided information for numerical Non-log-inputs, which have been integrated with continuous log data to predict the occurrence of clasts and evaluate the formation. The gathering and flow of all available information ideally follows the proposed scheme, reflecting objectively the importance of each item's role in the complete evaluation. The results of such an evaluation are presented graphically, interval by interval, through *Reservoir Type Signatures* which characterise reservoir flow units.

The conclusions of this evaluation applied to Well A contradict previous analyses, and place the well in a water zone, but intersecting residual oil, and local movable oil caught beneath any capillary barrier which has formed closure. The apparent contradictions in the original data are the result of filtrate invasion, and the inherent difficulties of evaluating low porosity complex reservoirs. Under such circumstances subtle observation of fundamental principles can assume greater significance than quantitative results, which frequently contain unnoticed assumptions. It is also evident that an S_{we} concept should be used to optimise log analysis; and that core has an essential, but preferably restricted role in petrophysics.

ACKNOWLEDGEMENTS

I would like to express my thanks to the staff of Occidental Caledonia plc, London, for providing me rocks and data, and assistance with funds to pursue this Ph.D. I would also like to express my gratitude and warmth to all those who have spurred me on through these four years of tunnel-vision. To my parents and family, mildly perplexed, but whose ever loving and generous hearts have provided me with succour and caring happiness; and to little Cheryl, for her special brand of sound practical advice, and her mountains of help with hardware, software, and harsh words of exasperated encouragement. To my fellow students in Room 3.31, whose company I have so greatly enjoyed, and whose friendship I trust will always be sustained; to Dr. Selley, my supervisor, for welcoming me into unchartered terrain, and providing me with that fresh and enlivening spirit to conquer yet more chapters! To all those helpful members of Imperial's staff especially Professor King for discussion, Gill Davies and Roy Hodgkinson for their agreeable assistance and Jon Cohen for his example of boundless energy. To Harold King at Marathon, generous with time and always ready to experiment, and to Chuck Keracik, my friendly but firm critic, to Mark Bilsland, fellow sufferer, and all those members of the SPWLA *London* Chapter who have made me feel, at least sometimes, that perhaps it is worth while.

CONTENTS

DEDICATION
ABSTRACT
ACKNOWLEDGEMENTS
CONTENTS
INTRODUCTION
---
1 PURPOSE
1.1 FORMATION EVALUATION PROBLEMS
Particular: The Inconsistencies Observed in Well A
General: The Need for Integrated Formation Evaluation
---
2 PREVIOUS WORK
2.1 GEOLOGICAL
2.2 PETROPHYSICAL
2.2.1 CORES AS A REFERENCE FOR LOGS
2.2.2 CORES AS A DATA SOURCE FOR LOG ANALYSIS
2.2.3 CORES & LOGS FOR THE PRODUCIBILITY OF CONGLOMERATES
---
3 PRELIMINARY THESIS WORK
3.1 HELMSDALE
3.2 CORE LOGGING PROCEDURE
3.2.1 DEPTH MATCHING CORE TO LOGS
3.3 GEOLOGICAL PERSPECTIVE
3.3.1 STRATIGRAPHIC AND STRUCTURAL SETTING
3.3.2 FACIES TRANSITIONS
3.3.3 LITHOLOGY AND GENESIS OF OBSERVED FACIES
3.3.3.1 CLAYSTONE FACIES (6)
3.3.3.2 CLAST AND MATRIX SUPPORTED CONGLOMERATE FACIES (1&2)
Debris Flows.
Fluidised Sediment Flows.
3.3.3.3 MASSIVE COARSE SANDSTONE AND BEDDED MEDIUM SANDSTONE FACIES (3&4)
Grain Flows.
3.3.3.4 INTERBEDDED SANDSTONES AND CLAYSTONES FACIES (5)
Turbidites.
---
4 BASIC THEORY
4.1 STATISTICAL ANALYSIS AND CAUSE & EFFECT
4.1.1 STATISTICAL

4.1.2 DETERMINISTIC
4.1.3 DETERMINISTIC / STATISTICAL COMBINATION
4.2 CONCEPT OF NON–LOG–INPUTS
4.3 CONCEPT OF RESERVOIR TYPE SIGNATURES, *RTS*
4.4 SCHEME OF INFORMATION FLOW
4.5 THE PROPERTIES & PRODUCTIVITY OF CLASTS cf. SANDY MATRIX
4.5.1 PROPERTIES
4.5.2 PRODUCTIVITY

---

5 PRELIMINARY IDEAS
5.1 CONDUCTIVITY, CLAY CONDUCTIVITY AND WATER FILLED POROSITY
5.2 RESIDUAL OIL AND PERMEABILITY
5.3 MULTI PARAMETER APPROACH TO ABSOLUTE PERMEABILITY
Parameters
5.4 CLAY DISTRIBUTION
5.5 EFFECT OF PARTIAL FLUSHING ON R_{xo}
5.6 WETTABILITY AND ELECTRICAL PROPERTIES
5.7 HYDROGEN INDEX OF RESERVOIR DRY CLAY MINERAL ASSEMBLAGE

---

6 SATURATION EQUATIONS
6.1 A SHORT HISTORY
6.1.1 EMPIRICAL SHALE VOLUME MODELS
6.1.2 THEORETICAL SHALE CATIONIC MODELS
Problems Remaining with Cationic Models.
6.1.3 THEORETICAL EQUATIONS WITH LOG DERIVED Q_v FUNCTIONS
6.1.4 THE DUAL POROSITY MODEL
6.2 THE SATURATION EQUATION
6.2.1 THE F_g SATURATION EQUATION - EXPLANATION OF VARIABLES
C_t.
S_{wt}.
$\emptyset_t$.
$\emptyset_e$.
C_w.
F_g: Geometrical Formation Resistivity Factor.
F_g: Wettability.
F_g: Continuous Prediction From Log Porosity - Constant Exponent.
F_g: Continuous Prediction From Log Porosity - Variable Exponent.

C_x.
n and y.
6.2.1.1 HOW IMPORTANT IS y ?
6.2.1.2 DETERMINING n and y.
Positive Features of the F_g Saturation Equation
6.2.1.3 THE PICKETT PLOT: m and g IN THE ABSENCE OF CORE DATA.
6.2.2 THE REPLACEABLE CONDUCTIVITY MODEL
6.2.2.1 DEFINITION OF REPLACEABLE AND NON-REPLACEABLE PORE VOLUMES.
6.2.2.2 FINAL S_w: P_c - S_w - R_t Method.

---

7 DIFFUSION & PERMEATION IN HETEROGENEOUS MEDIA
7.1 THE DIFFUSION EQUATION
7.2 APPLICATION TO CONGLOMERATE FORMATIONS
7.2.1 DERIVATION OF THE CONSTANT *"d"* FROM ACTUAL ROCK
Determining C_{om} & C_{oc}
7.2.2 SENSITIVITY OF CONSTANT *"d"* TO VARIATIONS ENCOUNTERED IN A NATURAL ASSEMBLAGE OF OIL BEARING CONGLOMERATES
7.3 DECONVOLUTION OF CONGLOMERATE CONDUCTIVITY - THE EMPIRICAL APPROACH
7.3.1 PRODUCING THE C_{tm} CHART
7.3.2 AN EQUATION FOR THE C_{tm} CHART

---

8 PARAMETER DERIVATION for RESERVOIR TYPE SIGNATURES & ERROR
8.1.1 NVSH
8.1.2 CLAST FINDING PARAMETERS & NVLOG
8.1.2.1 *vlogs* PARAMETER LISTING
8.1.4 CALCITE FINDING PARAMETERS
8.1.5 ENVIRONMENTAL PARAMETERS
drhocum
ncal
di
8.1.6 POROSITY PARAMETERS
8.1.6.1 $\emptyset_t$, TOTAL POROSITY METHOD
Correcting Porosity Tools for *vlogs*
Correcting Porosity Tools for $V_{dryclres}$ and *vlogs*
Calibration of $\emptyset_t$ to $\emptyset_{he}$
8.1.6.2 $\emptyset_e$
8.1.6.3 *NET* RESERVOIR QUALITY ROCK
8.1.7 FLUID TYPE PARAMETERS

SOX
BVO
8.1.8 PRODUCIBILITY PARAMETERS
Inappropriate Porosity / Permeability Data
ML
KE30
KO
KW
8.2 ERROR
Environmental Corrections
8.2.1 SYSTEMATIC ERROR
8.2.2 NON SYSTEMATIC ERROR
---

9 LABORATORY WORK

9.1 OPTICAL THIN SECTIONS
9.1.1 PURPOSE OF THIN SECTION EXAMINATION
9.1.2 SIGNIFICANCE OF *"Structural"* AND *"Dispersed"* CLAY USED IN POINT COUNTED PHASES
9.1.3 THIN SECTION DESCRIPTION SHEETS
9.1.4 THIN SECTION STATISTICS
Economy of Point Counts
Statistical Variation.
Significance of Facies.
9.1.5 QUANTITATIVE BULK MINERALOGY
9.1.6 INTRAFACIES HETEROGENEITY
9.1.7 A PETROPHYSICAL PLOT
9.1.7.1 DEDUCTION OF PETROPHYSICAL VALUES FROM THIN SECTIONS
9.1.7.2 INFLUENCE OF POINT COUNTED CHANNELS PER AXIS, MULTIPLIERS
9.1.8 DISTINCTIONS BETWEEN CLASTS AND MATRIX WHICH INFLUENCE LOGGING TOOLS
9.1.9 POROSITY & PERMEABILITY
9.1.10 TERNARY PLOT OF RESERVOIR QUALITY FROM THIN SECTION DATA
9.1.11 FLUID AND ELECTRICAL FLOW PATHWAYS WITH REFERENCE TO EXCESS CONDUCTIVITY
9.1.11.1 FLUID FLOW
9.1.11.2 ELECTRICAL FLOW
9.1.12 DIAGENESIS
9.1.12.1 POROSITY REDUCING AGENTS

9.1.12.2 DIAGENESIS HISTORY
Quartz
Clays
Organics
Pyrite
Carbonate
Oil Migration
Barite Fines
9.1.12.3 CONCLUSIONS REGARDING DIAGENESIS
Diagenetic Sequence
.....
9.2 X-RAY DIFFRACTION
9.2.1 PURPOSE OF X-RAY ANALYSIS
9.2.2 BULK SAMPLES
9.2.2.1 BULK MINERAL ABUNDANCE PER SAMPLE
9.2.3 CLAY FRACTION SAMPLES
9.2.3.1 CLAY FRACTION X-RAY DIFFRACTION RESULTS
Air Dried Glycolated Clay Discs
Ethyl-Glycolated Clay Discs
Heating @ 550°C for 1 hour
9.2.4 CONCLUSIONS REGARDING X-RAY DIFFRACTION
.....
9.3 SCANNING ELECTRON MICROSCOPE
9.3.1 PURPOSE OF SEM STUDY
9.3.1.1 QUANTITATIVE
9.3.1.2 QUALITATIVE
9.3.1.3 LIMITS OF SEM ANALYSIS
9.3.1.4 SEM RELATED Non-log-inputs
9.3.2 POLISHED SECTIONS, QUANTITATIVE
9.3.2.1 POLISHED SECTION PROCEDURE
9.3.2.2 POLISHED SECTION SAMPLE LISTING
9.3.2.3 POLISHED SECTION QUANTITATIVE INTERPRETATION TECHNIQUE
9.3.2.4 REPRESENTATIVE ENERGY DISPERSIVE SPECTRUMS
9.3.2.5 POLISHED SECTION INTERPRETIVE SHEETS
9.3.2.6 POLISHED SECTION WAVE DISPERSIVE K, Th, U
9.3.3 FRACTURED SURFACES, QUALITATIVE
9.3.3.1 FRACTURED SURFACE PROCEDURE
9.3.3.2 FRACTURED SURFACE SAMPLE LISTING
9.3.3.3 FRACTURED SURFACES STANDARD SCALE PHOTOGRAPHS AND RESERVOIR TYPE SIGNATURES, *RTS*
9.3.3.4 FRACTURED SURFACE PHOTOGRAPHIC CAPTIONS
9.3.4 MODIFICATIONS TO THIN SECTION DATA

	Point Counts
	Petrophysical Plot
9.3.5	NON-LOG-INPUTS
9.3.5.1	DRY CLAY MINERAL POINTS
9.3.5.2	DRY CLAY DENSITIES
9.3.5.3	DRY CLAY HYDROGEN INDEXES
9.3.5.4	*rhog*, HI_{matrix}
9.3.5.5	P_e
9.3.5.6	*Vclay dispersed : Vclay total*
9.3.5.7	K, Th, U
9.3.6	MODIFICATIONS TO X-RAY DATA
9.3.7	CONCLUSIONS REGARDING SEM STUDIES
9.3.7.1	ROLE OF SEM IN FORMATION EVALUATION
	.....
9.4	NUCLEAR ACTIVATION
	.....
9.5	CORE CONDUCTIVITIES
	Purpose of Electrical Experiments
	Sample Selection
	Laboratory Facilities and Limitations
9.5.1	METHOD
9.5.1.1	BRINES
9.5.1.2	CORE SAMPLES
9.5.1.3	OIL SATURATED SAMPLES
9.5.1.4	VARIABLE FREQUENCY DATA
9.5.2	RESULTS
9.5.2.1	CORE RESISTIVITIES Chronological Tabulation
9.5.2.2	INDIVIDUAL CORE PLUG FREQUENCY DATA
9.5.2.3	R_{xwe}, FLUSHED ZONE EFFECTIVE WATER RESISTIVITY
9.5.2.4	HYSTERESIS
9.5.2.5	R_t
9.5.2.6	TEMPERATURE
9.5.2.7	FORMATION RESISTIVITY FACTOL AND THE EFFECT OF TEMPERATURE
9.5.2.8	LABORATORY RESISTIVITY PLOTS, 77°F, 2kHz.
9.5.3	CONCLUSIONS REGARDING CORE CONDUCTIVITIES
9.5.4	DEMONSTRATION OF PREFERRED METHODOLOGY
9.5.4.1	CALCULATION OF n AT RESERVOIR TEMPERATURE FROM ROOM TEMPERATURE DATA
9.5.4.2	THEORETICAL EXAMPLES OF C_x

10 DRILL STEM TESTS, REPEAT FORMATION TESTS, FORMATION INTERVAL TESTS AND CAPILLARY PRESSURES
10.1 FLUIDS
10.1.1 ROCK VOLUMES CORRESPONDING TO PRODUCED FLUIDS
10.1.2 EXTRAPOLATION OF R_W VIA RECOVERED FORMATION BRINE AND SP LOG
10.2 FORMATION PRESSURES
10.3 *kh*
10.4 SKIN
10.5 CAPILLARY PRESSURES, P_C
10.5.1 METHOD
10.5.2 P_C PLOTS, PREDICTIONS AND RESULTS
10.5.2.1 CAPILLARY PRESSURE PREDICTIONS OF R_t
10.6 CONCLUSIONS REGARDING DSTs, RFTs, FITs and P_C s
10.6.1 S_{hmov}
10.6.1.2 EFFECT OF FILTRATE INVASION ON PRODUCED FLUIDS
10.6.2 FLUID PRESSURE GRADIENTS
10.6.3 CAPILLARY PRESSURE DATA

11 RECONNAISSANCE IN CORED & LOGGED WATER ZONE
11.1 FIELD WIDE TOOL NORMALISATION AND POROSITY MATCHING
11.2 PROCEDURE FOR ESTABLISHING MATRIX CONDUCTIVITY, C_{tm}
11.3 GENERATING LOG PARAMETERS FOR $\emptyset_e$, g & C_x: SANDY MATRIX
Pickett Plot
Compatibility of g with Switched $\emptyset_t$
11.3.1 $\emptyset_e$
11.3.2 PARAMETERS FOR C_x
m_{sand} and m_{shale}
11.4 PREDICTION OF LOGGED R_O: SANDY MATRIX
Conglomeratic Intervals
11.5 CONCLUSIONS REGARDING RECONNAISSANCE RUNS

12 NON-LOG-INPUTS
12.1 DEDUCTION OF THE DRY CLAY MINERAL POINT, DCMP
12.1.1 SHALE BED
The Dry Non Clay Mineral Point
The Wet Clay Mineral Point
The Dry Clay Mineral Point
Advantage of DCMP Over Book Values

The Dry Shale Point, *rhodsh*

12.1.2 QUANTITATIVE SHIFTS OF THE DRY CLAY MINERAL POINT FOR CHANGING CLAY MINERAL ASSEMBLAGES

12.2 V_{sh}

12.2.1 $V_{dry\ clay\ reservoir}$

12.2.2 CORRECTING $\emptyset_n$ FOR RESERVOIR CLAYS, $\emptyset_{nc}$ ($\emptyset_{nfac}$)

12.2.3 DISPERSED & TOTAL CLAY

12.3 *rhog*

12.4 S_{oc}

12.5 NON-LOG-INPUTS, LISTING

---

13 PROPOSED INFORMATION FLOW

---

14 RESULTS of INTEGRATED EVALUATION

14.1 RAW LOGS AND LOGGING COMPANY LOG ANALYSES

Resistivity

Microlog

14.2 CLAST PREDICTIONS, *vlogs*

14.3 POROSITY

14.3.1 *NET*

14.3.2 POROSITY ZONES

14.3.3 FRACTURES

14.3.4 APPENDIX 49

14.4 HYDROCARBON SATURATIONS, S_w

14.4.1 HAND HELD INTERPRETATION

14.4.2 RESISTIVITY RATIOS

14.4.3 APPENDIX 52: INVASION & CALCULATED PARAMETERS

14.4.4 APPENDIX 51A & B: S_{we}

14.4.5 OIL ZONE R_t PREDICTIONS FROM CAPILLARY PRESSURE DATA

14.4.6 MUDLOG, EPT and CORE HYDROCARBON SHOWS

Mudlogs

Electro-magnetic Propagation

Core S_{OC}

14.5 APPENDIX 53: BULK VOLUME FRACTIONS, SATURATION, PRODUCIBILITY, RESERVOIR TYPE SIGNATURES & SEM PHOTOMICROGRAPHS

14.5.1 RESERVOIR TYPE SIGNATURES, RTSs

14.5.2 SEM x45, x300 & x3000 PHOTOMICROGRAPHS

15 CONCLUSIONS
15.1 THE COMMERCIAL SIGNIFICANCE OF WELL A
15.1.1 ESSENTIAL OBSERVATIONS
15.1.2 INTERPRETATION
15.1.3 SIGNIFICANCE
15.1.3.1 PERMEABILITY TO BRINE INJECTION
15.1.4 EXPLANATION OF $R_t \neq R_O$
15.2 CRITICISM OF THESIS METHODOLOGY
15.2.1 *vlogs*
15.2.2 REVISED $\emptyset_t$ SWITCHING METHOD
15.2.2.1 DENSITY TOOL
15.2.2.2 SONIC TOOL
15.2.2.3 NEUTRON TOOL
15.2.3 THE F_g SATURATION EQUATION
15.2.3.1 USE OF CONSTANT S_{we} CONCEPT TO OPTIMISE LOG ANALYSIS
15.2.3.2 INDICATIONS OF AND SOLUTIONS TO PROBLEMATIC S_w
15.2.4 C_{tm} CHART
15.2.4 RESERVOIR TYPE SIGNATURES
15.3 SOME GENERAL STATEMENTS REGARDING FORMATION EVALUATION
15.3.1 A VARIETY OF DATA
15.3.2 USE AND ABUSE OF CORE
$\emptyset_{he}$, *rhog* , k_{hor} , k_{vert} , k_{ro}/k_{rw} , P_c, C_x
Estimating Closure from "oil-down-to" wells
S_w, n
Water Zone Core, m and R_w
Water Zone, General
Routine Core Analysis
15.3.3 DRILLING FLUIDS

REFERENCES / NOMENCLATURE

FIGURES, TABLES & PLATES

Fig p24 Stratigraphic context of the Brae conglomerates of Well A

Fig p27 Comparison of porosity, saturation and permeability from cores, logs and DSTs

Fig p28 A fan-delta complex, illustrating the topography and fan morphology as interpreted for the Brae area in late Jurassic time (Reproduced from Harms et al, 1981)

Fig p29 Brae field submarine fans model. (Reproduced from Stow et al, 1982)

Fig p34 Redrawn Helmsdale field map

Fig p36 Genesis of facies associations, Helmsdale (After Selley, 1985)

Fig p40 Stratigraphic and structural setting of South Brae

Fig p42 Upward facies transitions for Brae Group core

Fig p45 The relationship of various physical processes within a single gravity flow event (After Middleton & Hampton, 1973)

Fig p47 Generalised fan model (Walker, 1978)

Plate p49a Exposure of massive grain flow sands of facies 3, at Crakaig Station beach, near Helmsdale, N.E.Scotland

Plate p49b Exposure of bedded sandstone units of facies 3, at Crakaig Station beach, near Helmsdale, N.E.Scotland

Fig p53 The preferred relationship between cause & effect and statistical problem solving

Fig p55 Concept of Reservoir Type Signatures

Fig p58 Scheme of information flow for integrated evaluation

Fig p59 The main distinctions between a conglomerate's clasts and its sandy matrix relevant to formation evaluation

Fig p65 The relationship between Dispersed Clay and the *GR* tool response

Fig p65 Hypothetical plot to aid the modification of R_{mf}, (R_{xwe})

Fig p66 Wettability

Fig p71 Relation of porosity to Formation Resistivity Factor for consolidated sandstone cores, Gulf Coast (After Archie, 1942)

Plate p72 The shape and scale of porosity dictate its relationship to conductivity. (Carbonate, Khuff Fm, Saudi Arabia. Courtesy I.Al-Jallal)

Fig p73 Relation of S_W to R_t/R_O (After Archie, 1942)

Fig p76 Observed brine saturated rock conductivity with decreasing brine salinity

Fig p80 Log derived clay indicator, Q_{vn}, and apparent water conductivity, C_{wa}, from S_W=1 zones (Refer Juhasz, 1981)

Fig p81 Proposed change in C_{we} for dispersed and structural shales in sands of identical Q_{vn} and F^* (F^* is independent of C_{wesh}) (Modified from Juhasz, 1981)
Fig p85 Origin of $\emptyset_e$, simplified
Fig p86 A single sample dilution plot for C_x
Fig p87 Log log plot to determine exponent g to $\emptyset_e$
Fig p90 Nature of the change in resistivity for a change in individual terms of a series and parallel resistance model
Fig p90 Change in R_t/R_o with desaturation for rocks with and without excess conductivity. Schematic
Fig p91 Desaturation when C_x equals 50% of C_w/F_g, n=1.84 and y=1
Fig p93 Effect of y on S_{we} in Brae, industry standard: y=1
Fig p96 Pickett plot. Theoretical example
Fig p98 The pressure which determines water saturation in a reservoir
Fig p100 Hypothetical example of X_{pc} defined by height and pore geometry
Fig p101 Similarity of F_g and Replaceable saturation models.
Fig p108 Analogy of Archie"s $\emptyset$ -F concept with *%matrix sand-* F_{cgl}. Data from water zone logs and core clast:matrix ratios.
Fig p109 Instability in the calculated value of constant d from the equation in 7.2.1.
Fig p112 The C_{tm} Chart. Deduction of C_{tm} from logged C_t and *vlogs*.
Table p117 Summary of trial *vlogs* parameters.
Table p122 Calculated porosity responses to the common deviations from quartz matrix encountered in Well A.
Fig p122 Porosity tool application domains resulting from Table p
Table p123 Logic for total porosity switching routine.
Fig p124 Influence of clasts upon matrix density.
Table p124 Components influential to $\partial t\, matrix$.
Fig p126 Reduction in porosity caused by net overburden pressure (APPENDIX 40)
Fig p131 Pseudo relative permeability plot used for estimating single phase flow from calculated saturation.
Fig p132 Calibration of the selected log derived oil permeability predictor to actual oilzone test data. Scaling factor = 31
Fig p135 Slow and fast first arrival times (*dt*) as a function of geometrical distribution of equal volume fractions.
Fig p137 Sources of error.
Table p138 Average conditions for permeable Brae intervals of Well A.
Table p139 Non-systematic-error included in the corrected tool readings for average permeable Brae formation, Well A.

Table p140 Inputs with systematic and non-systematic error, for average permeable Brae, Well A.
Table p141 Semi-quantitative optimistic and pessimistic values, and credibility ratings,for mean permeable Brae. (Based on previous tables. Optimistic = low S_W)
Fig p145 Economy of point counts
Table p145 Statistical treatment of point counts
Fig p148 Relative abundance of point counts per channel per facies
Table p154 Influence of point counted channels per axes, multipliers
Fig p156 Three dimensional petrophysical plot deduced from thin section point counts
Fig p160 Reservoir quality from thin section point counts
Fig p165 Stability fields for kaolinite, illite and K-feldspar in aqueous solution
Fig p169 Diagenetic sequence
Table p171 X-Ray diffraction. Semi-quantitative, bulk mineral abundance per sample. Mean values per facies.
Fig p173 Relative abundance of each mineral across six facies, from X-Ray diffraction bulk samples. Semi-quantitative
Table p175 Clay fraction X-Ray diffraction results
Table p177 Summary of X-Ray results relevant to dry clay mineral points
Table p189 Modifications to opitical thin section data following SEM study
Table p190 Effect of stoichiometry on clay densities
Table p192 Book values of dry clay densities
Table p192 Density and Hydrogen Indexes of the threee dry clay mineral assemblages
Table p193 LDT & CNL tool response to the dry clay mineral assemblages of the three petrophysical rock types of Well A, deduced from laboratory and wireline data
Figp193 Review of stages 1 -> 8 followed to determine the density / neutron DCMPs
Table p194 Wave dispersive spectrum analysis of Shale type interval samples
Fig p196 Role of SEM in formation evaluation
Table p197 Values of radioactive elements from logs cf. nuclear activation of milled core
Fig p203 Movement of *Rxwe* with one pore volume and 12 pore volumes of mud filtrtae flushing
Table p211 Theoretical examples of C_x
Fig p213 Rock volumes associated with DST3's fluids and the same interval's mud filtrate (ignores wellbore)
Table p214 R_W as a function of DST brines and the SP log
Fig p214 R_W from DST brine extrapolated with the SP log
Fig p217 Composite of pressure information from FITs, RFTs, and DST 2A's P^*.Possible pressure boundaries are interpreted from the SP log, GR log and effective porosity calculation
Fig p221 Means of estimating S_{Wi} above ≈600ft (183m) of height, by using porosity

Fig p222 Water saturation versus reservoir fluids capillary pressures for six samples of varying porosity
Fig p223 The effect of a sample's porosity upon water saturation, at various capillary pressures or heights above FWL
Fig p224 The relationship between a sample's permeability and water saturation, at various capillary pressures or heights above FWL
Fig p229 Relationship between chapters 7 and 11 and solving for S_{we}
Fig p230 Matching $\emptyset_d$ and $\emptyset_{he}$
Fig p237 Deduction of the Dry Clay Mineral Point
Table p239 Book values of Dry Clay Mineral assemblages based on laboratory proportions and published figures
Table p240 Non-log information relevant to V_{sh} calculation
Table p241 The volumetric normalisation per rock type of *GRCC* using Non–log–data
Fig p241 Source of *GRCC* in Shale type interval
Table p244 Non-log-inputs
Fig p247 Generalised information flow for integrated evaluation, sequential
Fig p249 Information flow 1: Deriving *Non-log-inputs*
Fig p251 Information flow 2: Processing log and *Non-log-inputs*
Fig p258 Expected water zone invasion profile (left) and invasion profile commonly observed below 15400 (right)
Fig p262 *Calcclst*'s method of distinguishing calcified sandy matrix from clasts
Fig p265 Comparison of RTSs from known water and hydrocarbon bearing intervals within the Brae Formation
Fig p269 Decreased oil permeability due to water invasion into a zone at S_{wi}
Fig p274 Determining *rhof* for use of *rhob* in determining $\emptyset_t$. Plugs from clean intervals only
Fig p274 Determining the constant "c" for use of ∂t in $\emptyset_t$. Plugs from clean intervals only
Fig p275 Determining $\emptyset_{heres}$ in terms of $\emptyset_{nc}$. $\emptyset_{ng}$ is determined by the modal value of neutron response for the matrix of the core plugs. i.e. -0.02 for sand, 0.00 for limestone
Fig p278 Use of constant S_{we} concept to optimise Bulk Volume Hydrocarbon calculations
Table p280 Indications and recommendations regarding S_w equation error

APPENDICES

L = Retained at Imperial College Lyon Playfair Library
S = Sample include in "Selected Appendices"
p = Number of pages

S APPENDIX 1 GRAPHIC CORE LOG 81p
S APPENDIX 2 OPTICAL THIN SECTION DESCRIPTION SHEETS 103p
S APPENDIX 3 QUANTITATIVE BULK MINERALOGY PER FACIES 5p
L APPENDIX 4 3D PETROPHYSICAL PLOT COORDINATES
L APPENDIX 5 RESERVOIR QUALITY TERNARY PLOT COORDINATES
L APPENDIX 6 X-RAY DIFFRACTION BULK SAMPLE TRACES
L APPENDIX 7 X-RAY DIFFRACTION CLAY FRACTION TRACES
L APPENDIX 8 SEM SPOT PROBE "ZAF4" PRINTOUTS
S APPENDIX 9 SEM STOICHIOMETRIC INTERPRETATION SHEETS 34p
L APPENDIX 10 SEM WAVE DISPERSIVE SPECTRUM PRINTOUTS FOR K, Th, & U; Sample 1 (Excluded due to excessive bulk)
L APPENDIX 11 SEM WAVE DISPERSIVE SPECTRUM PRINTOUTS FOR K, Th, & U; Sample 2 (Excluded due to excessive bulk)
L APPENDIX 12 RFTs
S APPENDIX 13 MICROLOG: ANNOTATED REFERENCE LOG
L APPENDIX 14 DST 2A PRESSURE BUILD UP (HORNER PLOT)
L APPENDIX 15 DST 3 INITIAL FLOW / BUILD UP
L APPENDIX 16 DST 3A INFLOW PRESSURE @ 14501
S APPENDIX 17 DST 3A INFLOW ANALYSIS @ 14501
L APPENDIX 18A-F RAW LOG + CORE CLAST:MATRIX RATIO *"vcors"*
S APPENDIX 19 INITIAL PICKETT PLOT
S APPENDIX 20A-B *"g"* EQUALS 2.30
L APPENDIX 21 DETERMINING C_{xwe}, CLEAN CLAST FREE WATER INTERVALS
L APPENDIX 22A-D PLOTS OF C_x V LOG DERIVED C_x PARAMETERS
L APPENDIX 23 DETERMINING SCALING FACTOR FOR C_x PARAMETER WITH HISTOGRAM
L APPENDIX 24 INFERRED DIFFERENCE OF m_{sand} & m_{shale} USING $\emptyset_d$ AND ASSUMING $C_{wsand} = C_{wshale}$
L APPENDIX 25 LITERATURE SEARCH
S APPENDIX 26 X-RAY DIFFRACTION, SEMI-QUANTITATIVE BULK MINERAL ABUNDANCE PER SAMPLE
L APPENDIX 27 SHIFTED v UNSHIFTED CORE POROSITY
L APPENDIX 28 SPE 16518 WETTABILITY, EXCESS CONDUCTIVITY AND FORMATION RESISTIVITY FACTOR

L APPENDIX 29	FORTRAN ITERATION: EFFECT OF y ON S_w
L APPENDIX 30	SELECTED CLAST FINDERS
S APPENDIX 31	INPUTS FOR *vlogs* ON A 0-1 SCALE
L APPENDIX 32	$\emptyset_{he}$ HISTOGRAM, $\emptyset_c = 0.05$
L APPENDIX 34A-C	LOGGED R_o & PREDICTED R_o
L APPENDIX 35A-F	FREQUENCY PLOTS: $\emptyset_{he}$, *rhog* & $\emptyset_d$
S APPENDIX 36	SCHL 1:200 * LDL CNL GR * RUN 1
S APPENDIX 37	CORE LAB LOG: GR, k_{ah}, $\emptyset_{he}$, S_{oc}, DSTs & FACIES TYPE INTERVALS
S APPENDIX 39	SCAL: CAPILLARY PRESSURE DATA
L APPENDIX 40	SCAL: POROSITY AS A FUNCTION OF NET OVERBURDEN PRESSURE
S APPENDIX 41	SCAL: FORMATION RESISTIVITY FACTOR, m, AND RESISTIVITY INDEX, n
S APPENDIX 42A,B	AMALGAMATED RAW LOG DATA. PLOTS A&B
S APPENDIX 45	CONSTRUCTION OF TOTAL POROSITY
S APPENDIX 47	FINAL TOTAL POROSITY cf. HELIUM POROSITY
L APPENDIX 48A,B	RESISTIVITY RATIO. PLOTS A 1:200 & B 1:1000
L APPENDIX 49	EFFECT OF DIVIDING A V_{sh} TYPE PARAMETER BY $\emptyset$
L APPENDIX 50	THE EFFECTIVE POROSITY REQUIRED FOR A CONSTANT S_{we} CALCULATION
L APPENDIX 51A&B	S_{we} FROM F_g EQUATION, A=USING RTGLOB B=USING LLD
S APPENDIX 52	INVASION, AND OTHER CALCULATED PARAMETERS
S APPENDIX 53	BULK VOLUME FRACTIONS, POROSITY, SATURATION & PRODUCIBILITY, RESERVOIR TYPE SIGNATURES AND SEM PHOTOMICROGRAPHS
L APPENDIX 54	CYBERLOOK. ?RTCYBER. a=1, m=2.0, n=2.0, Rw=.028
L APPENDIX 55	CORIBAND 14585-14960. LLD. a=1, m=2.0, n=2.0, Rw=.028
L APPENDIX 56	CORIBAND 14585-16440. ILD. a=1, m=1.9, n=2.0, Rw=.025
L APPENDIX 57	GLOBAL 14585-16450. RTGLOB.a=1, m=1.9, n=2.0, Rw=.027
S APPENDIX 58A,B	DIL SLS GR RUNS 3, 4. 1:200
S APPENDIX 59A,B	DLL MSFL GR RUNS 1, 2. 1:200
L APPENDIX 60	MUDLOG
L APPENDIX 61	EPL GR RUN 1. 1:200
L APPENDIX 62	PORE SIZE DISTRIBUTION DATA, 4 SAMPLES
L APPENDIX 63	TRIAL PARAMETERS FOR VLOGS 4p
L APPENDIX 64	REPRESENTATIVE ENERGY DISPERSIVE X-RAY SPECTRUMS
L APPENDIX 65	LAB. RESISTIVITY (DILUTION) PLOTS 77°F 2kHz 10p

INTRODUCTION

This thesis results from a survey sent to a number of oil companies operating in the North Sea. The survey enquired of current pressing needs in formation evaluation which could benefit from Ph.D. level research. The response was encouraging, and following interviews it became clear that two companies were actually concerned with the same problem. This thesis presents a solution to that problem.

The problem involved a deep Central Graben appraisal oil well, Well A. A large amount of data was generated from Well A, including 750ft (229m) of core, an unusually comprehensive set of final logs, and three tested intervals. However, interpretations failed to provide a clear cut indication of the well's hydrocarbon content. The well was drilled with water based mud, and strong mud logging shows occurred during drilling. The 18 cores also contained significant residual oil, and computer processed logs computed a continuous oil column. However, DSTs flowed both oil and water with no apparent relationship to their relative vertical positions, or to adjacent log responses. The entire 2,000ft (610m) displayed no significant shift in resistivity, except for a general depth / porosity trend. The operator's main concern was therefore whether the large rock volumes penetrated by Well A were saturated with oil or with water.

The above explains the background to the project. The project itself began with a review of oil company reports and published papers on the area. A fieldtrip was made to rock outcrops at Helmsdale recognised as similar to rocks encountered by Well A (Selley, 1985). This was followed by attending various M.Sc. petroleum courses, drawing a detailed 1:12 scale core description, and studying petrophysical literature. Over this period sufficient knowledge of petrophysics was acquired to be able to view the data critically, and to plan a rational synthesis of the information. A guide to each chapter's place in the thesis is included below.

Chapter 1 explains the purpose of the study, the need for integrated evaluations, and the specific problems with Well A's interpretations. **Chapter 2** reviews previous geological work on conglomerates, and reviews methods of formation evaluation which use cores and logs. Early in the project depositional processes were believed to be an important key to

understanding Well A, thus **Chapter 3** reviews the lithologies and depositional processes of each of the facies revealed by core logging.

Chapter 4 goes on to introduce some underlying concepts, such as the nature of solving problems deterministically or statistically, and the important theme of transforming non-log-data into numerical *Non-log-inputs* for integration with logs. It also introduces the original concept of graphic, multi-parameter, *Reservoir Type Signatures* for characterising intervals, and gives the reader an idea of the intended flow of analytical data, in a simple schematic diagram. An ideal evolved as the project developed which was to quantitatively incorporate all the data in a manner which neither ignored or over-emphasised any one part. This appeared to be the essence of reconciling the data because of the contradictions which had been created by interpreting individual data sets.

Chapter 5 is not essential to the logic of the thesis, however all these preliminary ideas were considered in deciding the path to follow in Well A, and in some cases have been used directly, i.e. 5.3 and 5.7. The next three chapters cover the major theoretical section, in which the rationale for interpreting conductivity, and for incorporating non-log-data are discussed in some detail. **Chapter 6** reviews the development of saturation equations used in the industry, and goes on to propose an F_g saturation equation. The thrust of this work is that the reservoir's storage and producing capacities are controlled by effective, not total porosity, and that $\emptyset_t C_t$ anomalies in sandstones are sourced in the non-effective porosity. The F_g equation is an effective porosity saturation equation in which the anomalous affects of non-Archie conductivity, i.e. $C_t \neq S_w^n \emptyset_t^m / R_w$, appear in the second term.

$$C_t = (C_w / F_g) S_{we}^n + C_x S_{we}^{n-y}$$

The concept and derivation of each term is set out, and the equation is used later to evaluate Well A. The Replaceable Conductivity Model is derived and compared with the Fg equation, but is not applied to Well A due to lack of facilities. **Chapter 7** deals with the problem of using bulk log responses from conglomerates to evaluate the sandy matrix portion of the conglomerate. It explores the adaptation of a classical diffusion equation for heterogeneous media (Barrer 1967), to deconvolve the conductivity through clasts and sandy matrix.

$$D = l / l_A \left[\left\{ [l v_A \beta_A k D_A] / [l_A + (l_B \beta_B k D_A / \beta_B y D_B)] \right\} + \left\{ [(l_A - l v_A) \beta_A' D_B] / [l_A + (\beta_A' l_B / \beta_B' y')] \right\} \right]$$

Although this chapter appears complicated its aim is simply to provide the sandy matrix

conductivity, C_{tm}, for direct substitution into the F_g equation. Chapter 7 draws upon a separate data gathering exercise from numerous logged and cored, oil and water zone cores from the Brae field, courtesy of Marathon. Chapter 7 also creates an empirical chart for C_{tm} following the log's prediction of volume fraction clasts, *vlogs*. Finally, this empirical chart has been expressed in the form of an equation, for continuous solution of C_{tm} during computerised log analysis:

$$C_{tm} = (C_{t\,log} - 0.022t) / (1 - t + 0.110t), \quad where\ t = f.(vlogs)$$

Chapter 8 details the derivation of all the important parameters used in the evaluation, including vlogs the core calibrated log prediction of clasts; and the total and effective porosity parameters valid across the varying lithologies and borehole conditions of Well A:

$$\emptyset_e = \emptyset_t - vlogs\emptyset_c - (1-vlogs)V_{shsdymtx}\ \emptyset_{tsh}$$

$\emptyset_e$ is then used with relative permeability and DST kh values to provide an effective permeability predictor across all lithologies. Chapter 8 ends with a discussion of systematic and non-systematic error with particular reference to Well A.

Chapters 1-8 are therefore essentially a review of the existing situation and data, and theoretical considerations regarding the best use of the existing and future data.

Chapter 9 is a large chapter covering all the laboratory work carried out during the course of the Ph.D. It is divided into five sections and documents analytical work including thin sections, X-Ray diffraction, SEM, nuclear activation and core conductivity experiments. The thin sections compiled in APPENDIX 2 were an important influence on further work because of their ability to reveal pore geometry and establish mineralogy. Much of Chapter 9 was undertaken to eliminate certain lingering possibilities, such as clay formation damage and the detection of petrophysically problematic mineral assemblages. Chapter 9 was also undertaken to generate mineralogical data for log calibration. All the data generated in this chapter has, where possible, been used in the final log analysis. However, this large amount of laboratory work also created a purely non-quantitative background understanding of the well, and an appreciation of controls on formation evaluation generally. Chapter 9 includes a flow chart to help decide if SEM studies will assist during formation evaluation, since this work is time consuming and expense. The core conductivities section (9.5) investigates electrical properties for use with the F_g equation, but suffers from measurements at non-reservoir conditions.

Chapter 9 ends the data acquisition phase of the project. The remaining chapters deal with the interpretation of Well A, and the secondary objective of developing a general method for the rational integration of diverse formation data.

Chapter 10 is concerned with engineering data from Well A's DSTs, RFTs and capillary pressures. It gives a brief synopsis of the DST results, which suffered from a combination of mechanical problems and poor reservoir quality, to provide crude limits for *Non–log–inputs* and formation fluids. Formation pressures and *kh* values are examined to provide limits on the evaluation, but are in themselves inconclusive. Core capillary pressure data is used to assist resistivity interpretation.

Chapter 11 covers the theoretical ramifications of the study on Marathon's cored oil and water zone conglomerates used in Chapter 7. Chapter 11 is important because in the Marathon wells the saturation levels are well established, whereas saturation levels in Well A are the main problem. Known saturations enable the tripartite effect of clasts, excess conductivity and the sandy matrix saturation to be unravelled, and correlated to log derived parameters, for use where saturations are unknown. This chapter derives the F_g equation's porosity exponent, g, and excess conductivity parameter C_x. It also explains the operator's attitude to clasts in the chapter conclusions (11.4). **Chapter 12** can be thought of as the interface between the continuous log data and the discontinuous Non-log-data. Non-log-data is transformed into *Non-log-inputs* , and a list is compiled.

The proposed information flow of **Chapter 13** is important in helping the reader to place the details in their broader context. It was drawn up for this purpose, but is nevertheless an important record of the proposed flow of data necessary for a complete evaluation. Chapter 13 therefore addresses the secondary objective of the thesis.

Chapters 14 deals with the results, stepping sequentially through the evaluation, and comparing different methods of determining saturation. It is in this chapter that the basic problem becomes clearer, because by now the majority of unsettling doubts and novel explanations can either be discarded or bought to bear upon the final interpretation. The conclusions of **Chapter 15** reiterate all the essential observations, quantify the well formally in terms of Net Pay etc, and provide an explanation of all the data. The second part of the chapter criticises the thesis methodology and the methods commonly employed in formation evaluation, and makes specific suggests of how log analysis can be improved.

The thesis is primarily about Well A, and secondly about developing an ideal methodology for general usage which emphasises inviolate principles, as opposed to locally derived empirical solutions.

Effort has been put into making this thesis easily digestible, to that end it is best read sequentially with frequent reference to this introduction. Symbols appear in "Nomenclature". Chapter 13's explanatory diagrams, and the individual chapter conclusions are also intended to assist.

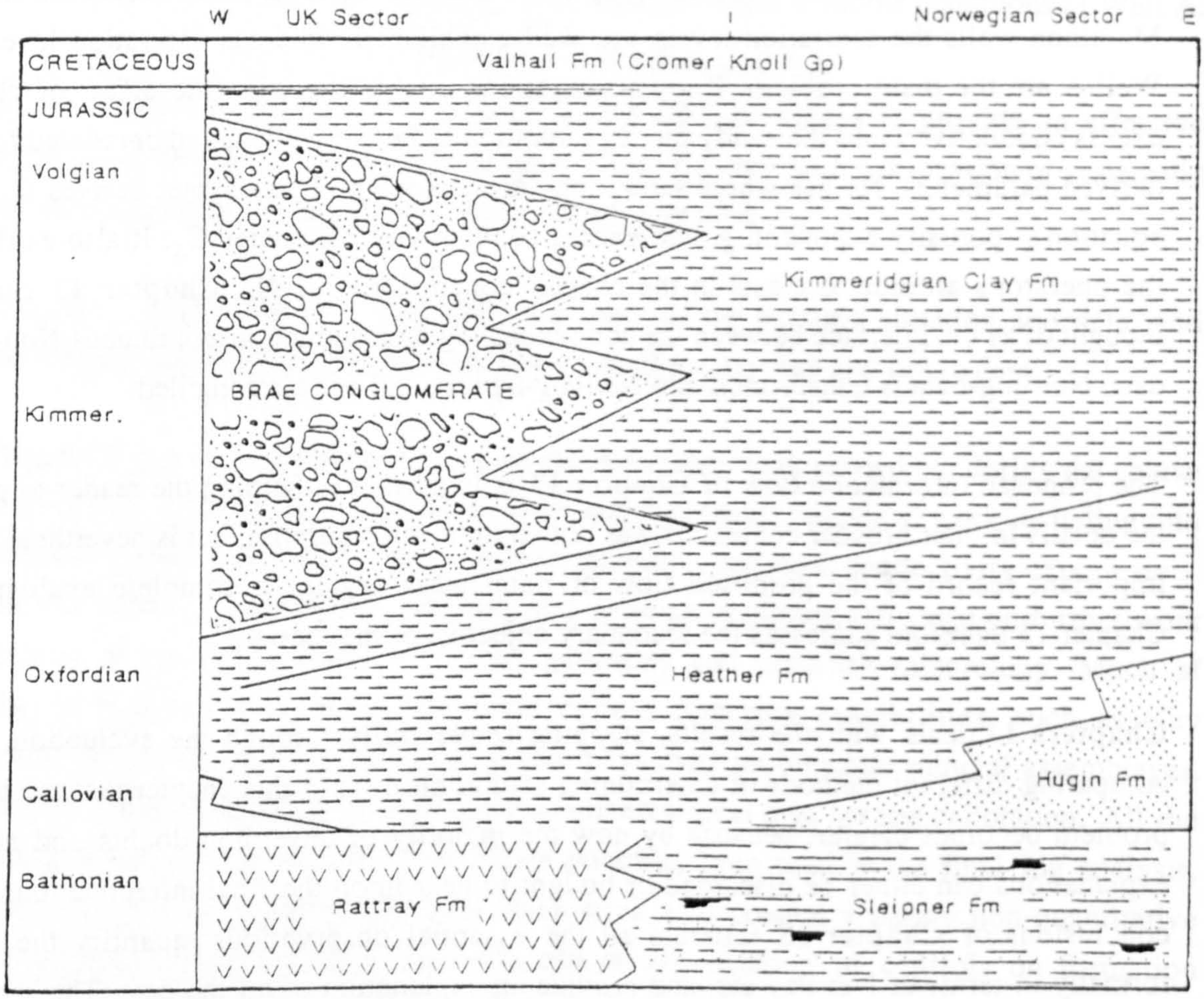


Fig p24 Stratigraphic context of the Brae conglomerates of Well A

1 PURPOSE

The synthesis of diverse sources of information from Well A into a confident appraisal of the well's commercial significance is the main purpose of this project. During the project a secondary objective evolved which was the development of a general methodology for the integration of formation evaluation data.

1.1 FORMATION EVALUATION PROBLEMS

The Inconsistencies Observed In Well A

A petrophysicist confronted with the various data from Well A would find that any single type of data, namely the cores, the logs or the DSTs, provides a significantly different impression from any other type. Although these data are suited to different reservoir properties some degree of agreement is usually expected. For example the character of logs might be broadly predicted from recovered core, or the results of production tests predicted from final logs. However in Well A's case this was not possible, even with a comprehensive set of final logs. Doubt was therefore cast upon the conditions of data acquisition which might otherwise have gone unquestioned. The more important problems specific to well A were:

1) Different intervals producing different fluids without the usual shift in log response.
2) Incompatible and equivocal indications of formation fluids from logs and from DSTs.
3) An uncertain vertical distribution of formation fluids with regard to the DSTs alone, even if the additional problems of logs and cores are ignored.
4) Incompatible porosity values from core analysis and standard log analysis.
5) Incompatible indications of formation permeability from core analysis absolute permeabilities and DST's effective permeabilities.
6) Unknown effect of conglomerate clasts upon the raw data and upon formation evaluation generally.
7) Lack of core over the only oil producing interval.
8) Unusually washed out and rugose hole creating a poor logging environment and large cement annulus behind casing.
9) Repeated mechanical problems during drill stem tests.

10) The operator's first encounter with a potentially commercial thickness of the Brae Formation, and at greater depths than other known producing intervals in this formation.

Although a straight comparison of porosity, permeability and saturation cannot be made between DSTs, logs and cores (cut with water based mud), the severe incompatibility of these data is shown overleaf:

Fig p27 Comparison of porosity, saturation and permeability from cores, logs and DSTs, compiled over DST intervals.

The comparison is compiled over the four tested intervals. It shows log-derived porosities and saturations over those intervals. It also includes chart book absolute permeabilities which assume $S_w = S_{wi}$ (Timur, 1968).

The Need for Integrated Formation Evaluation.

The problem that all geologists face when presented with apparently incompatible data is how to integrate the available information. Integration needs to provide a single credible assessment which can be used as the basis for decisions. Exploration or appraisal wells which penetrate deep, low permeability formations do not always provide readily interpretable data. For example mudlogs, wireline logs, routine or special core analysis, and DSTs can provide different indications of reservoir quality and fluids content. Future well location, spacing and objective depths remain unclear.

Successful integration of the wide variety of data arising from a key well entails geological and engineering knowledge which very probably lies beyond the scope of an individual, or even a team. This can result in information being ignored or incorrectly emphasised in the broader picture. Remotely acquired in-situ data and directly acquired laboratory data both have shortcomings which need to be understood and assessed before a reliable evaluation can proceed.

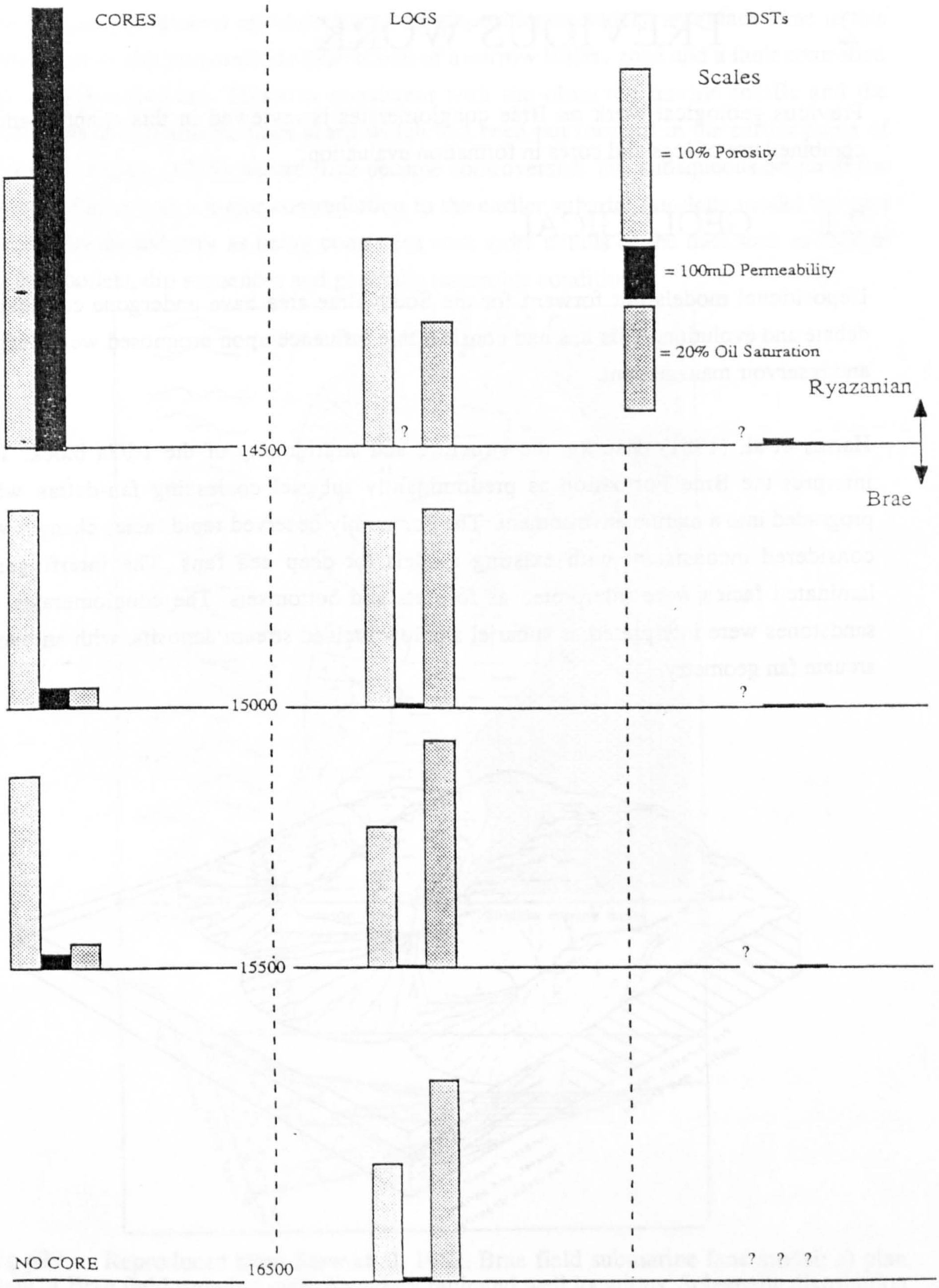


Fig p27 Comparison of porosity, saturation and permeability from cores, logs and DSTs, compiled over DST intervals.

2 PREVIOUS WORK

Previous geological work on Brae conglomerates is reviewed in this chapter, and the combined use of logs and cores in formation evaluation.

2.1 GEOLOGICAL

Depositional models put forward for the South Brae area have undergone considerable debate and evolution. This has had considerable influence upon prognosed well locations and reservoir management.

Harms et al, (1981) describe the structure and stratigraphy of the 16/7a block. They interpret the Brae Formation as predominantly subariel coalescing fan-deltas which prograded into a marine environment. The commonly observed rapid facies changes were considered inconsistent with existing models for deep sea fans. The interfingering laminated facies were interpreted as foresets and bottomsets. The conglomerates and sandstones were interpreted as subariel shallow braided stream deposits, with an overall arcuate fan geometry.

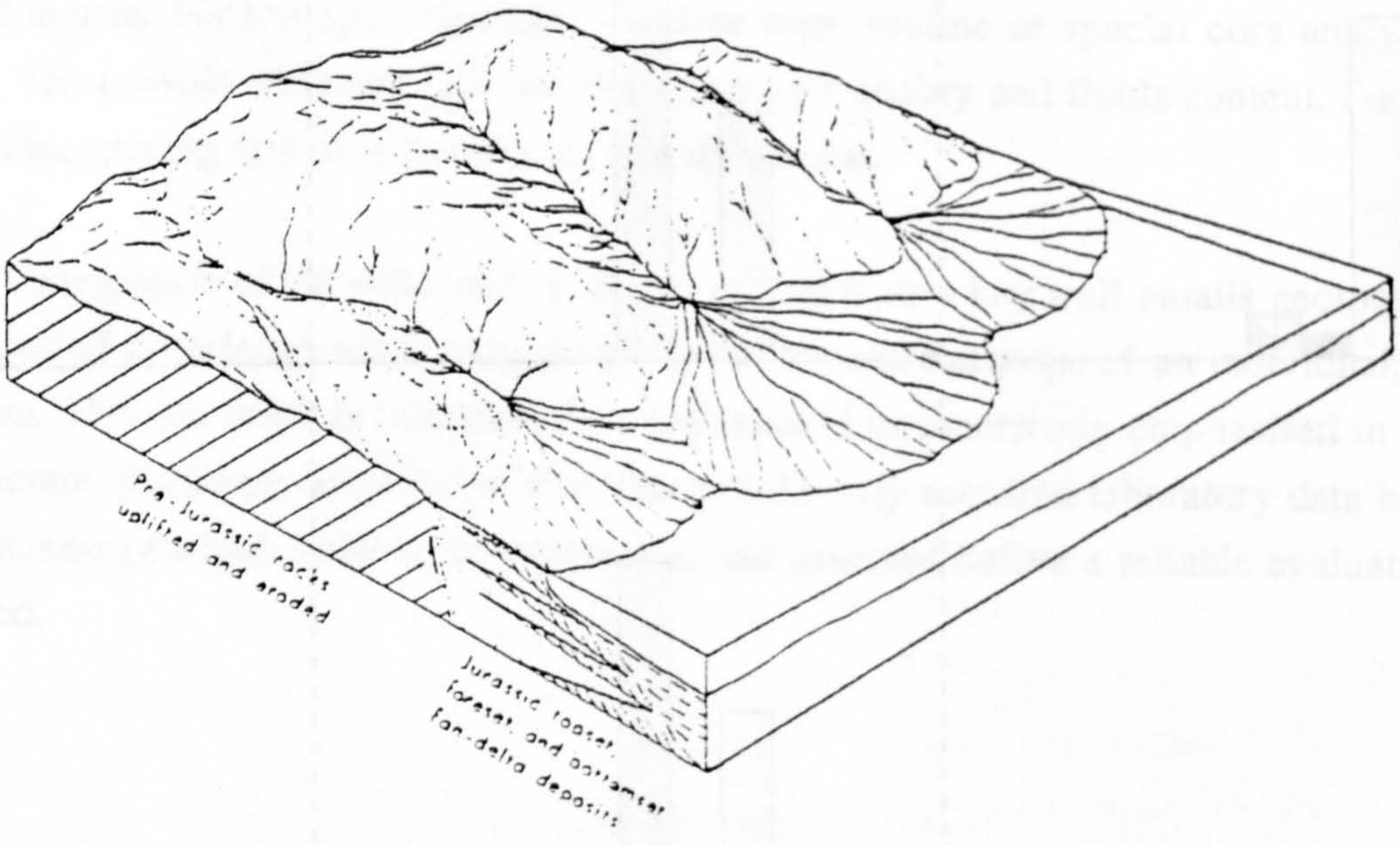


Fig p28 Reproduced from Harms et al, 1981. A fan-delta complex, illustrating the topography and fan morphology as interpreted for the Brae area in late Jurassic time.

Stow et al, (1982) make a broad review of fan depositional models, and place Brae in this context: the model proposed for Brae is that of a narrow littoral zone and a fault controlled shallow submarine fan. This was consistent with the observed marine fossils and the mechanism of a submarine fault scarp which had been put forward in the earlier paper of Neves and Selley, (1975); before Brae became controversial. The subaqueous origin of the observed facies was a major contradiction to the earlier subariel fan-delta model but was accepted by the industry as being consistent with more details of the data such as lack of ripples, rootlets, dip sequences and generally anaerobic conditions.

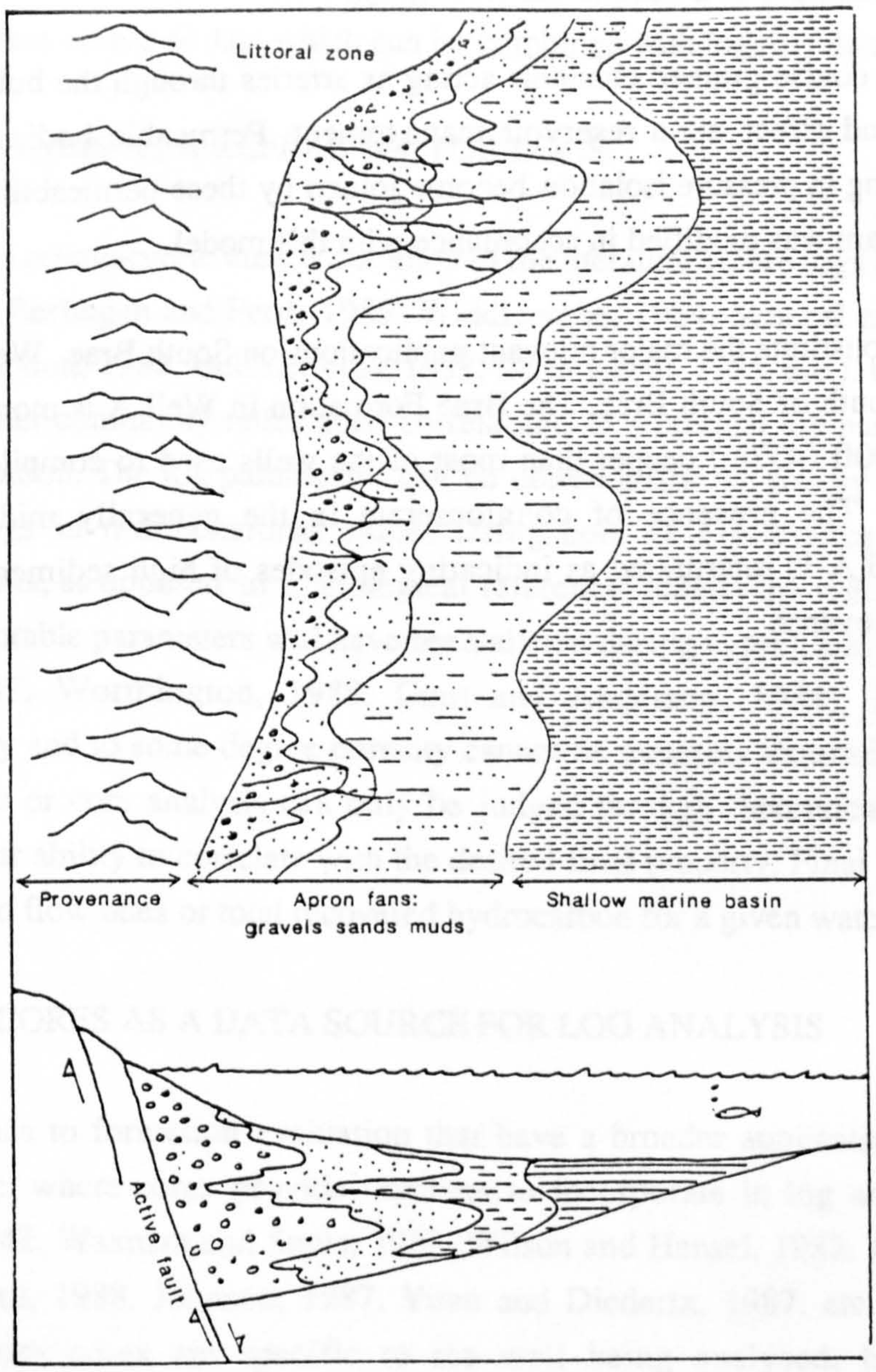


Fig p29 Reproduced from Stow et al, 1982. Brae field submarine fans model: a) plan view of Brae field showing main boundary fault and well locations. Schematic distribution of main facies groups shown by ornament. Solid and dashed lines indicate probable distribution of submarine-braided channel network; b) cross-section showing schematic basin fill sequence. Vertical facies megasequences related to periodic fault activity.

Turner et al, (1987) present a submarine fan model which accommodates many of the peculiarities of South Brae sediments. The model has been compiled from data gathered from a mature stage of field development. Deep feeder channels on the fan surface are filled with conglomerates and massive sands. The channels cut deeply into regionally extensive mudstone units of Kimmeridge clay. The mudstones are interpreted as a cessation of coarser clastic input in response to a tectonic or eustatic change. The graben margin fault movements are seen as dominating the type and arrangements of facies against the background of Kimmeridge clay deposition.

A model including coarse grained channels acting as arteries through the bulk of the fan body had a profound effect upon reservoir management. Permeable bodies previously conceived of as being in pressure isolation become joined by these permeability channels. The injection program was modified in accordance with this model.

The above papers constitute the major relevant publications on South Brae. Well A is nine kilometers to the south of South Brae. The Brae Formation in Well A is more distal and currently some 1500ft (457m) deeper than most of the wells used to compile the above geological models. The presence of conglomerate in the generally mid-fan facies associations of Well A is interpreted as indicating episodes of high sediment supply in response to tectonic events.

Do Not Lend Or Copy

2.2 PETROPHYSICAL

Most logging tools rely upon benign environmental conditions and empirical transforms to convey information about the subsurface. Tangible core samples therefore have greater credibility in formation evaluation than the indirect results of log analysis. It is beyond the scope of this thesis to include a detailed review of all literature concerned with logs, cores and tests, however petrophysicists have generally used core in one of two ways: Firstly as an independent reference which logging tools are expected to duplicate, and secondly as an independent source of data which can be combined with logging data.

2.2.1 CORES AS A REFERENCE FOR LOGS

Log analysis referenced to core is common in the literature where logs have been used in a novel way (Berlingen and Fertl, 1985. Widdicombe, 1984. Senecal and Mulhern, 1985. Serra and Abbott, 1982. Delfiner et al, 1987, Berteig et al, 1985. etc.). Using logs and core in this manner commonly relies upon correlations of empirical log parameters valid in a single formation. The log parameters can be deterministic or simply involve clusters of tool readings in n-dimensional space. Using core as a reference for petrophysical measurements, as opposed to a geological reference, entails the risk that almost all the cores measurable parameters will have been altered during cutting and extraction (Wendel et al., 1987. Worthington, 1988. Gant and Anderson, 1988). In-situ saturation, permeability and to some degree porosity cannot be precisely determined. Preference for log analysis or core analysis can only be judged through theoretical considerations or through their ability to correlate with the desired final property. Final properties could be hydrocarbon flow rates or total recovered hydrocarbon for a given water cut and flow rate.

2.2.2 CORES AS A DATA SOURCE FOR LOG ANALYSIS

Contributions to formation evaluation that have a broader application are those of the second type, where cores provide numbers to incorporate in log analysis calculations (Archie, 1942. Waxman and Smits, 1968. Wilson and Hensel, 1982. Cooke-Yarborough, 1987, Juhasz, 1988. Johnson, 1987. Yuan and Diederix, 1987. etc. This thesis.). The numbers from cores are specific to the well being analysed, but the method of incorporation can be exported to other wells. Success of the method in different formations serves as a test for the underlying theory. Truth of the results cannot always be known, and judgement in the case of saturation for example, tends to fall upon the internal consistency

of the theory which is not necessarily synonymous with the actual reservoir situation.

Logs with core have been used to predict the producibility of formations. Such methods make valuable use of core and log data but usually their success rests upon the peculiarities of one formation where a particular characteristic dominates the flow of hydrocarbons. In the case of the Lower Wilcox Sands, Texas, (Berilgen et al., 1985) for example kaolinite and chlorite are distinguished from illite and smectite with information from cores and logs, and the producibility is predicted.

2.2.3 CORES & LOGS FOR THE PRODUCIBILITY OF CONGLOMERATES

A computerised world literature search was conducted through the Imperial College terminal. Combinations of the following key words were used:

"conglomerate?",
"cores",
"well()log?",
"formation()evaluation", and
"petrophysic?".

The search did not reveal anything relevant that had not already been investigated (APPENDIX 25).

In this thesis conglomerate producibility is predicted through a quantitative combination of cores, logs and tested intervals.

3 PRELIMINARY THESIS WORK

This chapter represents early geological work on Well A's Brae Formation core. It provides a geological perspective for the project and decribes the depositional processes which gave rise to the observed facies.

3.1 HELMSDALE

There are two outcrops recognised in the literature as being broadly analogous to the Brae formation penetrated by Well A. One is on the east coast of Greenland (Surlyk, 1978a), and the other just south of Helmsdale, North East Scotland (Neves & Selley, 1985). Work began for this thesis with a solo field trip to the coastal outcrops of Kintradwell and Crakaig, Scotland.

The beds are an Upper Jurassic sequence of cobble-boulder conglomerates, medium grained massive grain flow sands, and carbonaceous siltstones. They are similar in age and generated from similar depositional processes as those in the well studied, which lies 230 kilometres offshore in the south Viking Graben.

A redrawn field map is shown overleaf.

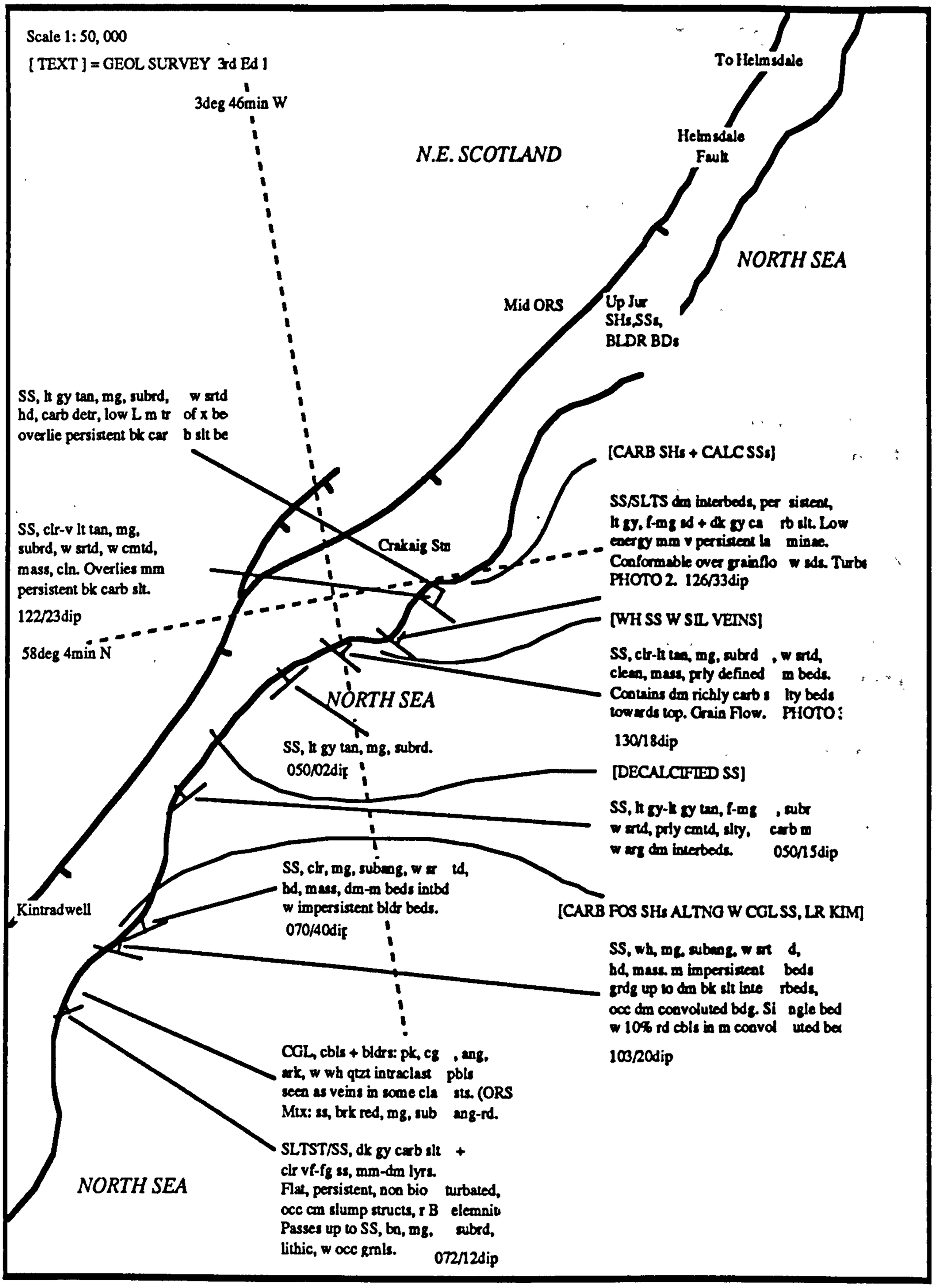


Fig p34 Redrawn Helmsdale fieldmap

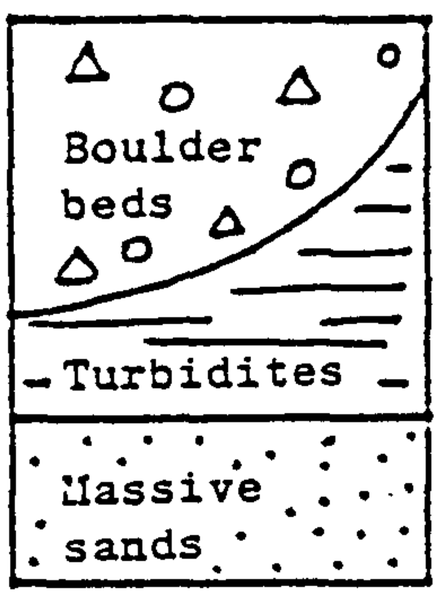
A literature review coupled with these field observations indicate a fault controlled depositional environment. The massive grain flow sands at the base of the observed sequence resulted from early Upper Jurassic (tensional) subsurface movements of the Helmsdale Fault. The instability caused in the overlying loose sediment was sufficient to initiate fluidised flows, producing the massive grain flow sands which pass upward into more persistent turbidite sands interbedded with carbonaceous fine grained deposits. The turbidites are the distal ends of flows of loose contemporaneous clastics initiated elsewhere along the fault line, or upslope from the faultline. These persistent beds are interrupted by rounded boulder beds of Old Red Sandstone clasts. Boulder beds in the midst of the lower energy turbidites result from significant fault movements which brought the lithified Devonian up and out to the submarine erosional surface as a scarp.

These high energy boulder beds are analogous to the basal sections of the "fining-upwards megasequences" mentioned in (3.3).

These rocks represent an exposure of depositional processes similar to those producing the conglomerates and massive sands of Well A. They were observed for this reason. Any problems arising from this interpretation of Helmsdale and its use in understanding Well A will not be strongly relevant to log analysis itself. However such problems may bear upon the efficient exploitation of any reserves penetrated by Well A.

Overleaf:

Fig p35 Genesis of facies associations, Helmsdale (After Selley, 1985).



OBSERVED

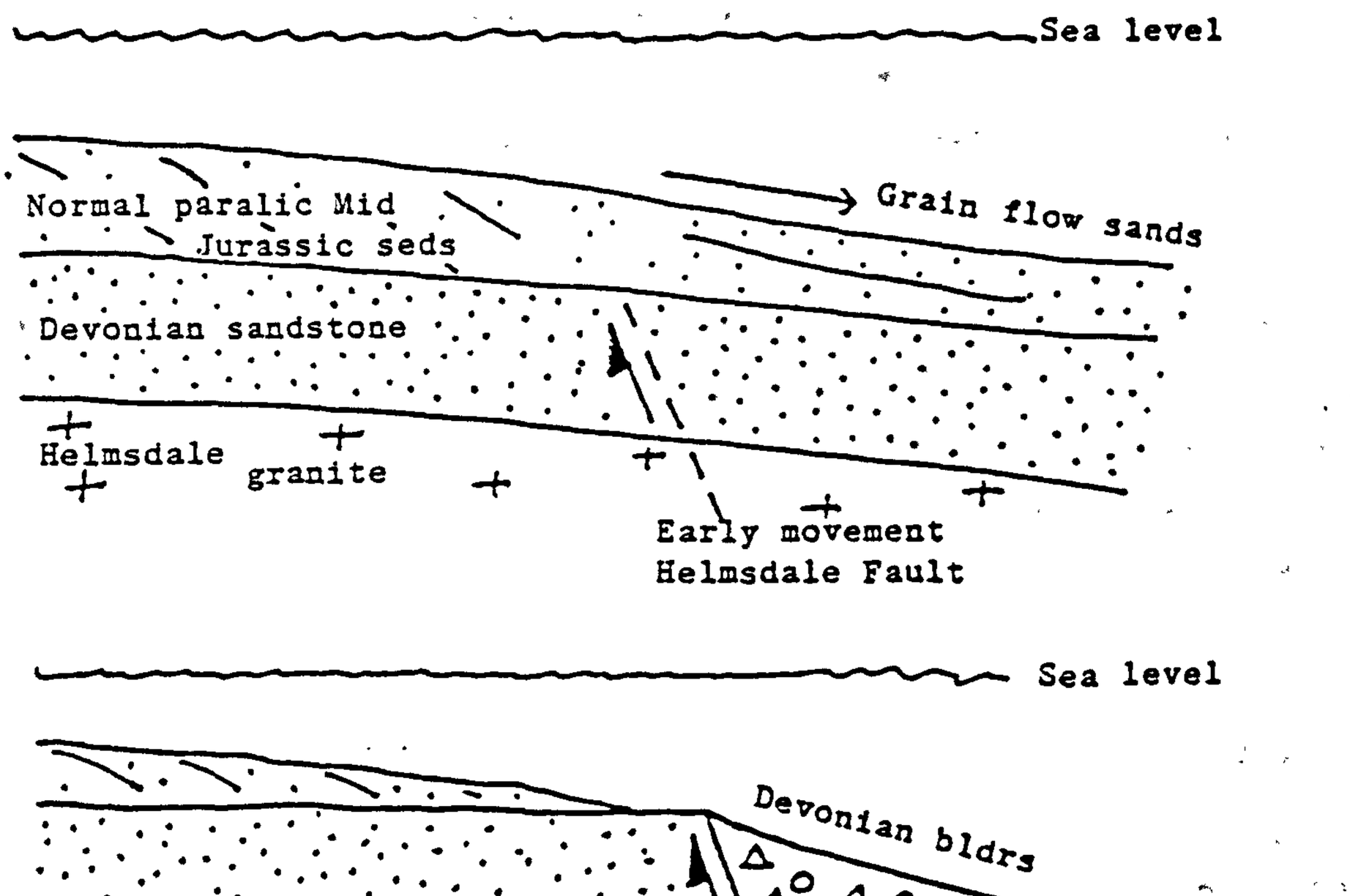


Fig p36 Genesis of facies associations, Helmsdale (After Selley, 1985).

3.2 CORE LOGGING PROCEDURE

A detailed 1:12 scale graphic log of the 750ft (229m) of core recovered from Well A was hand-drafted and later transcribed into the computer format of this thesis, (APPENDIX 1). Numerous observations were noted which served as a thorough grounding for subsequent mineralogical and petrophysical work.

Well A's core from the Brae Formation fell naturally into six facies which is coincident with later published work by Turner et al.(1987) Other workers (Stow et al, 1982) have subdivided Brae into more facies. This is not seen as beneficial for this particular core or the work of this thesis. The information required for further subdivision is nevertheless available in the 1:12 detail.

The six Facies Type Intervals are marked on APPENDIX 1, and are as follows:

Facies 1 Clast Supported Conglomerate
Facies 2 Matrix Supported Conglomerate
Facies 3 Massive Coarse Sandstone
Facies 4 Bedded Medium Sandstone
Facies 5 Interbedded Sandstones and Claystones
Facies 6 Claystone

The dilemma of scale for the demarcation of litho-facies was approached from the point of view of the wireline logs available, since the integration of this core with logs is the prime goal. The resolution of litho-facies recognition was therefore about one foot, in contrast to Turner et al's half foot.

Logs record physical properties. This required facies to be delineated in terms of observed lithology and not as an interpretation of depositional processes which might or might not have caused those lithologies. Interpretation of the physical processes which gave rise to the observed sequence will be dealt with later under (3.3.3).

3.2.1 DEPTH MATCHING CORE TO LOGS

Precise depth matching is an important pre-requisite for any integrated study. A considerable effort was put into depth matching in an attempt to minimise possible artifacts of integration. The microlog was chosen as the depth reference because of its superior vertical resolution, and its ability to characterise litho-facies more clearly than other tools. It was not the only log used for depth matching, all the logs were used to a greater or lesser extent. Depth matching on a five foot or greater scale was found to be easy, but attempts to refine this to two or three feet usually met with incomprehensible difficulty. It was finally conceded that the core was not actually the same volume of rock as that investigated by the logs and that reservoir (cm lateral) heterogeneity must account for small scale discrepancies. Although in Well A the core contractor's gamma ray log is potentially the best single means of depth matching it was not found to be useful due to its inadequate sensitivity. Criteria used for the foot by foot depth match were as follows:

1) Gamma Ray and core shale horizons.
2) Microlog positive separation and log resistivity compared with Core Lab permeability and porosity.
3) Logged bulk density decrease compared with Core Lab porosity increase <u>over non-clast bearing intervals only</u>.
4) Log resistivity and microlog signature compared with Devonian clasts in core.
5) Christensen[1] coring log sheets compared to core lithology.
6) Wireline gamma ray compared with Core Lab gamma ray.

When log processing facilities became available further attempts were made to refine the depth match between the core and microlog and between the logs themselves, which suffered from cable tension and stretch.

A plot of results is included as (APPENDIX 26) and (APPENDIX 27).

These should be scrutinised in conjunction with the vertical distribution of clasts. Clasts dominate log porosities but have no influence on core porosities because of the deliberate matrix biased sampling of the core contractor, severely undermining core to log porosity transforms. (APPENDIX 26, 27, 45, 47).

---

[1] Christensen Diamond Core Bit Co. record bit weight, pump pressure, drill rate and connection depths during coring runs which occ asionally reveal core break points and intervals over which core failed to enter barrel.

3.3 GEOLOGICAL PERSPECTIVE

3.3.1 STRATIGRAPHIC AND STRUCTURAL SETTING

The Brae Formation lies to the east of a major North-South trending fault. The coarse reworked clastics of The Brae Formation occur within the time of the Kimmeridge Clay Formation. Brae sediments become finer and thinner eastward and intercalations of Kimmeridge Clay facies occur within The Brae Formation. The Brae and Kimmeridge Clay formations are bounded to the west by an impermeable wall of cemented Devonian sandstone at the western faulted margin of the Viking Graben. The Brae Formation is therefore a local wedge shaped body of porous permeable rock lying within a regionally extensive kerogen rich claystone. (Mackenzie, 1986)

Tectonic activity from early Permian to the Palaeocene produced a series of horsts and grabens across the region which is now the North Sea. The Viking Graben is one such trough containing over 10,000ft (3048m) of Mesozoic sediments on its deeper western side, the trough being asymmetrical in cross section. The normal faulting at this westerly margin stepped progressively westwards into the Cretaceous producing a fault zone some three kilometres wide (Harms et al, 1981). The horst, the Fladen Ground Spur, to the west of this fault zone has thin to absent Mesozoic cover, and was the sediment source for the Brae Formation in Volgian times. A few kilometres east of the graben margin fault there is evidence of a small synsedimentary antithetic fault present in the Jurassic sediments, which is non sealing. (Cohen 1988, pers. comm.). This small fault of approximately 200ft (61m) throw (Turner et al, 1987), is related to the formation of the mini-graben to the west and low anticline to the east in the Jurassic sequence. See figure overleaf.

The wall of Devonian sandstone which is in contact with the Brae Formation at the graben margin fault is inferred to be impermeable to oil from the observed oil column height. Assuming this part of the trapping mechanism is not solely due to fault zone cementation the height of the oil column lends credence to the assertion later in this thesis that Devonian sandstone clasts do not contribute to reservoir volume. Recent evidence of the Devonian sandstones non reservoir quality comes from a well penetrating Devonian sandstone above the adjacent oil contact. (Cohen, 1988. Pers. comm.)

Overleaf: Fig p40 Stratigraphic and structural setting of South Brae.

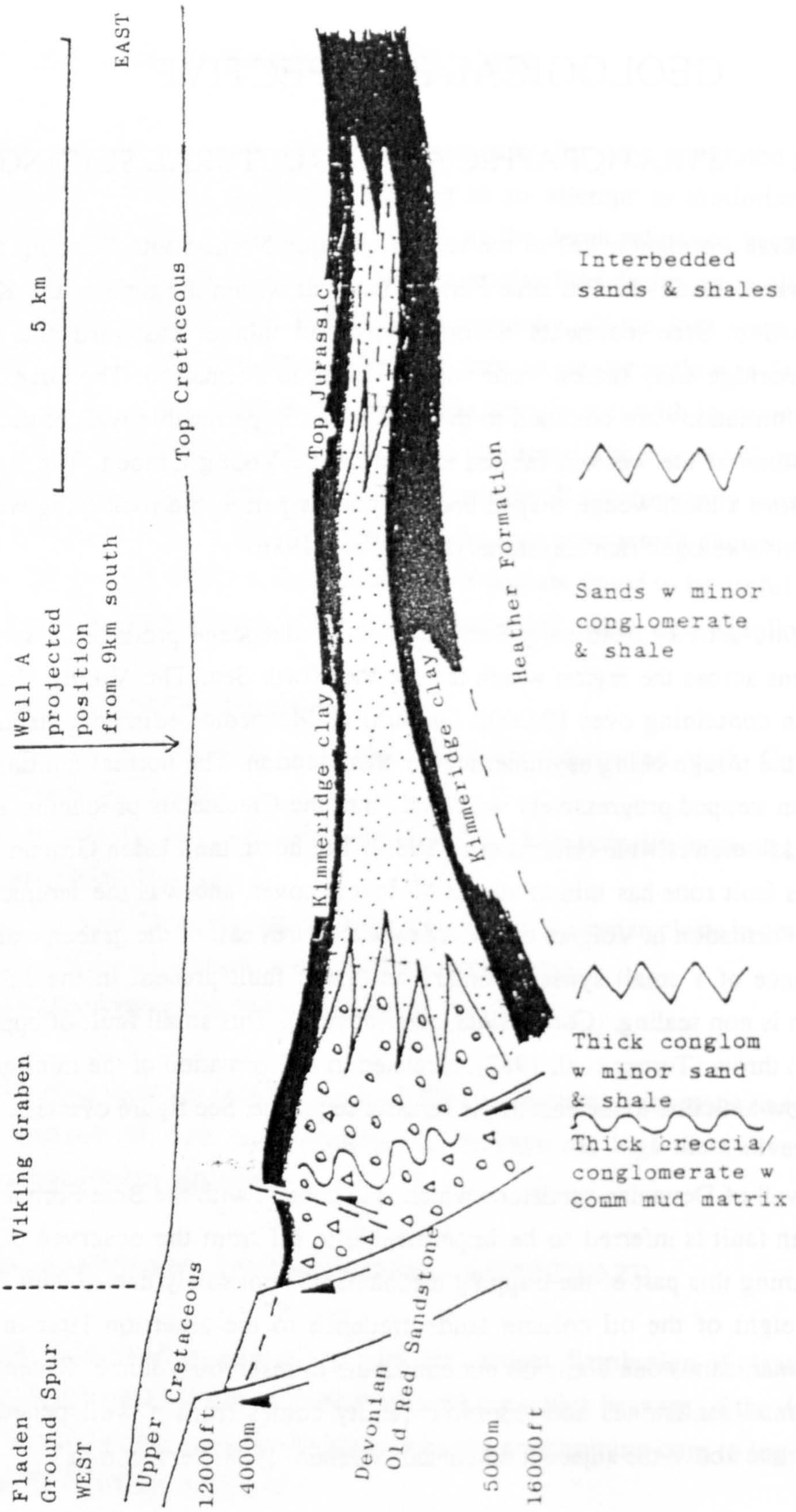


Fig p40 Stratigraphic and structural setting of South Brae

Do Not Lend Or Copy

3.3.2 FACIES TRANSITIONS

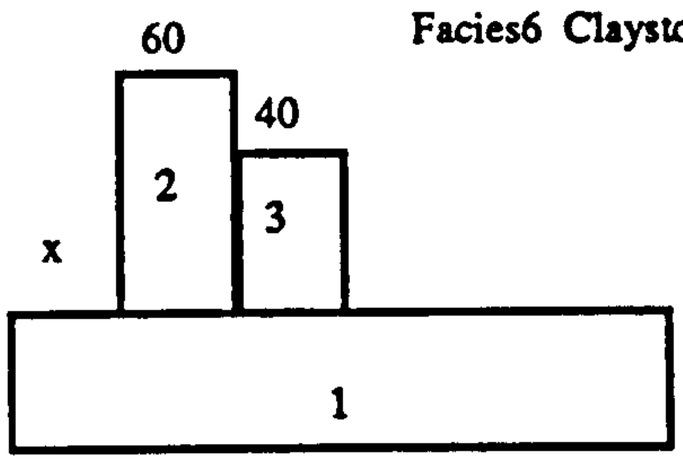
Statistical analysis shows that the facies are arranged in upward-fining sequences. Fig p39 shows matrix conglomerates passing to massive or bedded sands with an 80 percent frequency, and bedded sands passing to interbedded sands and claystones with a 72 percent frequency. This denotes a general fining upward trend within a single megacycle such as those cycles commencing at core depths 15300 (base of core), 15011 or 14655ft (4467m). (APPENDIX 1)

Although these diagrams are subject to the initial litho-facies categories, and the chosen coarseness of scale during facies delineation the inference is the same as that gained from a compressed scale core log. This shows large fining upward cycles, containing smaller fining upwards sequences, initiated by major movements of one or more of the graben margin faults.

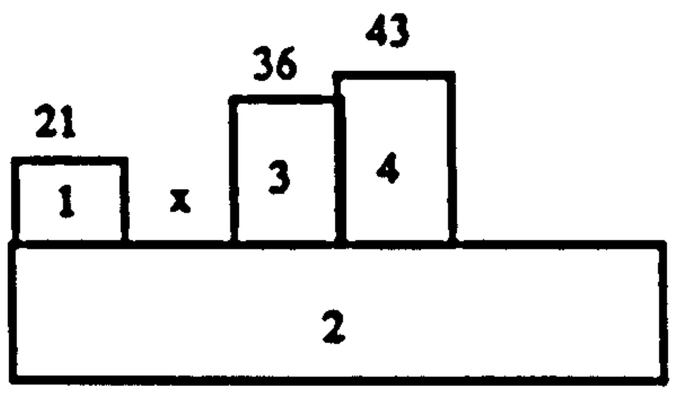
Transitions comprising a large percentage of all transitions for one facies, probably reflect causally related deposition. For example clast supported conglomerate overlain by matrix supported conglomerate with 60 percent frequency is likely to reflect the same depositional event. By contrast the 86 percent transition of facies 5 to 4 (laminated sand/shale to sandstone) is interpreted as a reflection of the chosen coarseness of scale. Transitions involving laminated facies will be sensitive to scale. The transition from 5 to 4 constitutes a hiatus between two depositional events. Delineation of finer laminae of claystone, facies 5, would have altered this diagram and broken down the same depositional event.

The 100 percent of facies 6 denotes the top of fining up cycles consistent with the concept of fining up megacycles. However this particular transition suffers from few observed occurrences.

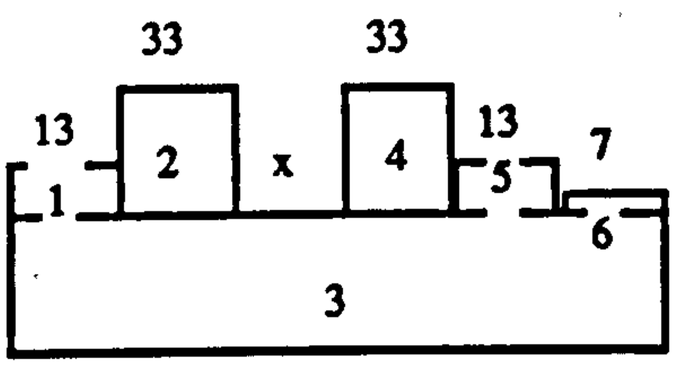
Facies1 Clast Supported Conglomerate
Facies2 Matrix Supported Conglomerate
Facies3 Massive Coarse S andstone
Facies4 Bedded Medium - Coarse Sandstone
Facies5 Interbedded Sand stones and Claystones
Facies6 Claystone



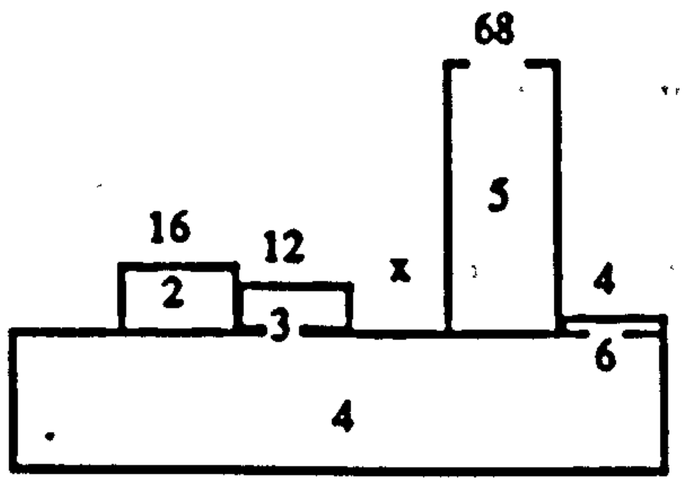
6% of all facies transiti ons



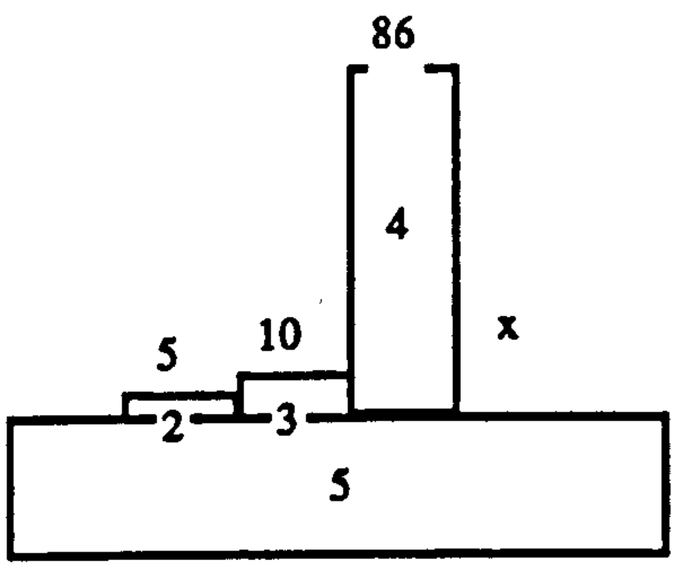
17% of all facies transit ions



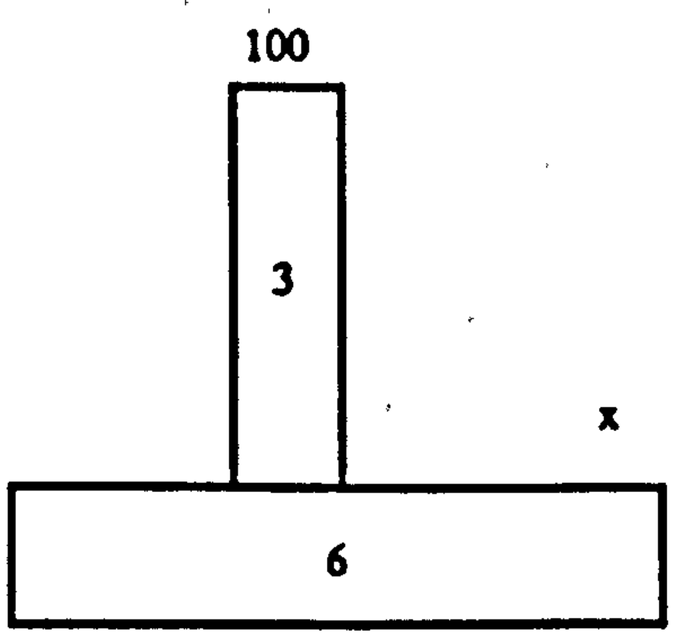
18% of all facies transit ions



30% of all facies transit ions



25% of all facies transit ions



2% of all facies transiti ons

Fig p42 Upward facies transitions in percent for Brae Group core

3.3.3 LITHOLOGY AND GENESIS OF OBSERVED FACIES

3.3.3.1 CLAYSTONE FACIES (6)

The Kimmeridge claystone facies is predominantly a dark brown, richly organic, earthy claystone. The claystone is Upper Volgian in this well (Operator) and equivalent to the diachronous regionally extensive marine Kimmeridge Clay Formation. Carbonaceous plant debris and mica flakes exposed on broken core surfaces are common features of this facies and enhance fissility along bedding planes. Diagenetic finely disseminated and framboidal pyrite is common in all the claystone intervals. The claystone's pyrite alters its petrophysical properties from those of the interstitial reservoir clays.

Nektonic fauna, unoxidised plant debris and little visible bioturbation, suggest quiescent anaerobic conditions close to the source of plant debris.

The claystone facies results from a cessation of coarse clastic input due to periods of reduced graben margin downfaulting.

The claystone is host to 1-10cm fine grain sandstone units (14073) interpreted as distal turbidites. A thin conglomerate (14084) with sharp top and bottom contacts, containing pebbles of fine grained sandstone and intraformational clayey fragments, indicates a debris flow unrelated to background clay deposition. This unit is a high pore pressure muddy debris flow. It results from early earth movements related to the larger upheavals which gave rise to the high clastic inputs of Ryazanian Sandstone.

The Claystone Type Interval (14655-63), situated within the Brae Formation, is slightly more sandy and less organic than the Kimmeridge itself. This type interval was chosen as being more representative of interstitial detrital clays in permeable intervals.

3.3.3.2 CLAST AND MATRIX SUPPORTED CONGLOMERATE FACIES (1&2)

The sandstone matrix of these two facies consists of medium to very coarse grained, occasionally granular, angular to subangular, moderately sorted quartz grains with rare chert, muscovite, pyrite, zircon and illite. Rare grey coloured grains of feldspar also occur. These rare components are petrophysically insignificant, except for illite, which is discussed in (6.2.1) and (9.5.4.2).

The apparent grain size has been increased by abundant quartz overgrowths. Detrital grain size has been estimated from thin sections as medium to coarse grain. Angularity has been similarly affected and detrital grains are estimated as subangular.

Barely visible silt grade intrapore debris, quartz or illite, is evident on many freshly broken core surfaces. The cement is predominantly quartz, calcareous cements are localised (15244) and not common in this core. Large volumes of calcite cement are common in South Brae wells. Calcite cement can be recognised below the cored interval of this well by a combination of log analysis parameters employed later in this thesis.

Compressed carbonised wood and plant fragments are common towards the top of depositional units. Burrows and body fossils are rare in this facies.

Clasts are predominantly a pale greeny-grey, fine grained, micaceous, feldspathic, argillaceous sandstone, with very low visible porosity. Parallel bedding is evident in the larger clasts, clast size ranging from pebbles to 75cm boulders (15367). Extremely low porosity rounded white quartzite pebbles make up approximately seven percent of clasts and tend to occur in limited horizons, possibly associated with a limited number of depositional events (15369). Jurassic grey shale clasts are present from the patchy Jurassic cover on the Fladen Ground Spur (Operator), but are volumetrically insignificant.

The sandstone clasts are interpreted as Devonian sandstone from the Fladen Ground Spur, see Fig p and Stow et al 1982. These clasts dominate the petrophysical evaluation of the Brae Formation. By contrast the pure quartz pebbles are not petrophysically significant (9.1.8). In keeping with this distinction quartzite clasts have been excluded from the Graphic Core Log's Clast:Matrix ratio.

The conglomerate facies typically have sharp basal contacts (15105), occasionally with rip-up clasts (many contacts have been removed for observation), and grade normally to massive sands. However some units reverse grade from matrix supported to clast supported conglomerate (15122); and some units exhibit sharp tops (15112). Such variations reflect single or multiple depositional events.

In a submarine environment these conglomeratic facies result from two gravity flow processes: debris flows and fluidised flows.

Debris Flows

The clast supported breccia conglomerates (e.g.15112-15121) are base of slope deposits, debris flows, of short transport length. They represent the erosion of a local upthrown submarine fault scarp or possibly canyon slumps (Nelson & Kulm, 1973) at the bottom of canyons cutting into the scarp wall. In debris flows the matrix itself provides support for clasts (Walker, 1984 p176) resulting in large clasts at the top of units. As the debris flow proceeds downslope, and the slope decreases, the rate of potential energy liberated becomes insufficient to overcome internal frictions; and the sediment halts.

Well A shows a lack of the muddy matrix breccias found in South Brae. This indicates either an active fault scarp where clay deposits had insufficient time to accumulate between debris flows, or a flow of sufficient duration for the net upward movement of water through the flow to carry away clays. This latter case is possible only when the unit shows some degree of normal grading.

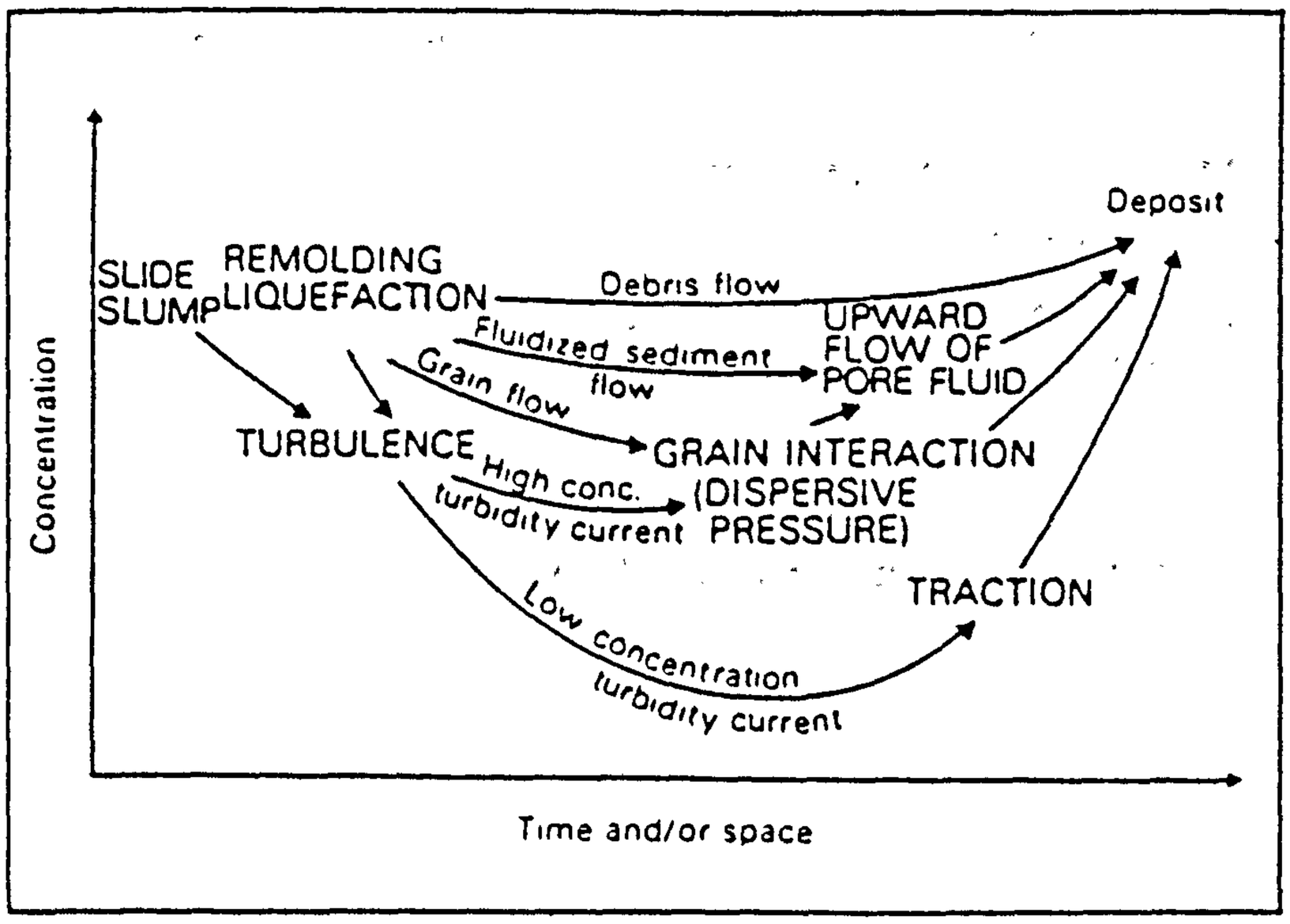


Fig p45 The relationship of various physical processes within a single gravity flow event (After Middleton & Hampton, 1973).

Fluidised Sediment Flows

The matrix supported conglomerates (14621-14643) are channeled fluidised flow deposits of greater transport length and generally lower sediment concentration than breccias. They are interpreted as reworked marine debris flows or reworked submerged fluvial deposits. The character of the conglomerates will be controlled partly by the original sediment, for example its sorting.

Earth movements destabilise the original loose sediments and a flow is initiated which cuts an erosive channel across the fan surface (La Jolla Fan California: Normark, 1970), or follows a previously cut channel. From South Brae facies mapping such channels at mid fan are typically one kilometre wide (Turner et al., 1984). As the flow proceeds down channel gravitational energy is liberated, resulting in high turbulence and clast collisions as the clast supporting mechanisms (Walker, 1984 p176). The Archimedian upthrust on a clast equals the weight of fluid the clast displaces. In the case of fluidised flows this weight provides considerably greater upthrust than water, due to the entrained sediment. Ungraded conglomerate indicates clasts have restricted movement within the flow. When the water:clast ratio falls below a critical level clast contact and internal frictions increase, turbulence rapidly decreases, the mass freezes, and the conglomerate is dumped.

In channels, water escape is restricted which prolongs the flow, allowing the mass to proceed some distance down channel. These high energy channels therefore explain a) roundness, b) lack of mud, and c) the presence of boulders in the generally mid-fan associations of Well A.

Overleaf: Fig p47 Generalised fan model (Walker, 1978).

Do Not Lend Or Copy

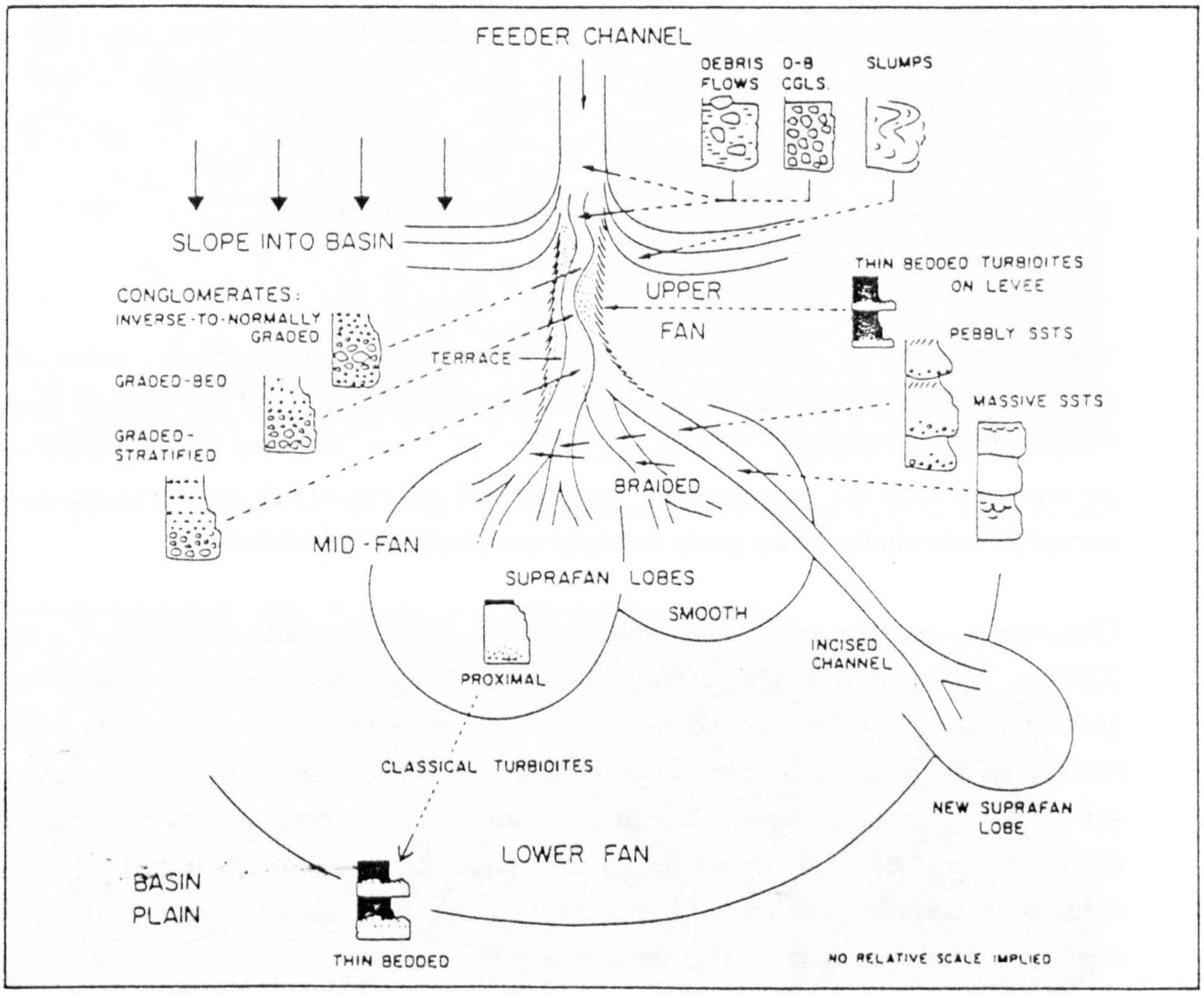


Fig p47 Generalised fan model (Walker, 1978).

Conglomerates that grade to massive sands resemble the graded "A" units of Bouma's proximal turbidites (Bouma, A.H., 1962). In Well A repeated "A" units are seen with no association to the lower energy "B", "C", and "D" units of a classic turbidite. Despite the attraction of the turbidite concept the facies arrangements of Well A extend beyond the turbidite model.

The geometry and orientation of these erosive permeability fairways, which penetrate the Brae Formation's lateral mudstones, is of the utmost importance to field development but beyond the data available for this thesis.

3.3.3.3 MASSIVE COARSE SANDSTONE AND BEDDED MEDIUM SANDSTONE FACIES (3&4)

The composition of the sandstone facies is medium to coarse grain, subangular, moderately sorted, quartz grains with carbonaceous detritus and minor chert and pyrite. Patches of leached feldspars occur as grain sized vugs. As in all facies quartz overgrowths are volumetrically the major cement, with isolated patches of calcite. These facies are petrophysically similar to the sandy matrix of the conglomerate facies.

Claystone rip-up clasts are common towards the base of the Bedded Medium-Coarse units (15094). The massive sands have sharp bases and tops typically showing very little grading with little or no sedimentary structures visible to the naked eye. Featureless massive units commonly overlie thin shale partings with no apparent erosion, indicative of grain flow sediment transport. Bedded units are frequently graded showing horizontal laminations and occasionally topped by thin shale partings (14988), clearly a single depositional event. As with other facies ripples are absent indicating sedimentation below wave base. Bioturbation and fossils are also absent.

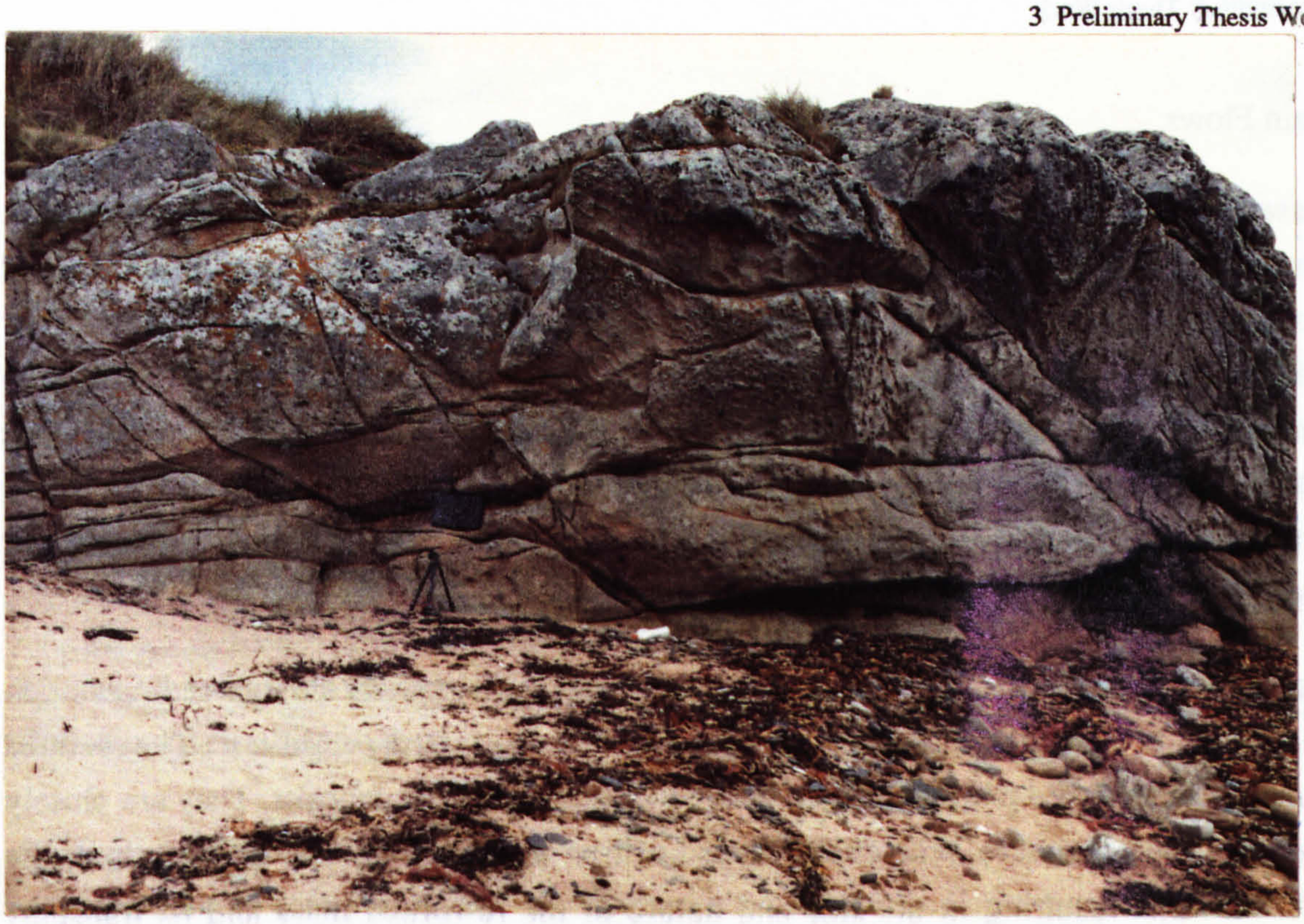


Plate p49a Exposure of the massive grain flow sands of Facies 3, at Crakaig Station beach, near Helmsdale, N.E.Scotland.



Plate p49b Exposure of the bedded sandstone units of Facies 4, at Crakaig Station beach, near Helmsdale, N.E.Scotland.

BIBL
LONDON
UNIV

Grain Flows

These facies result from grain flows, mass reworking in response to fault movements, storms, or any event providing sufficient energy to fluidise unconsolidated and gravitationally unstable sediment. They are of lower sediment concentration than debris or fluidised flows and incapable of supporting larger clasts. In grain flows "dispersive pressures" from grain collisions maintain the fluid properties of the mass (Lowe, 1976). These sandstones (Plate p49a) are typical of the mid fan associations of Well A, infilling partially filled erosive channels or spilling laterally from filled channels to create fan lobes.

Grain flows are part of a continuous spectrum of submarine gravity flow re-sedimentation process, from disorganised debris flows to finely laminated turbidites. The bedded sandstone units (Plate p49b) represent lower energy, more distal deposits. They are closely associated with massive beds due to their position in the energy / slope spectrum; the different units resulting in the size and nature of the reworked mass and its transport distance from Well A. These facies provide the best reservoir quality in this well.

3.3.3.4 INTERBEDDED SANDSTONES AND CLAYSTONES FACIES (5)

This facies consists of 30-95 percent centimetre-decimetre claystones interbedded with centimetre-decimetre sandstone beds. Claystones are typically dark grey, carbonaceous, silty, micaceous and occasionally bituminous. Thin beds sometimes show convoluted sedimentary structures (15079). Sands are fine to medium, subangular, well sorted, micaceous, and frequently grade through silt to clay. They contain carbonaceous detritus and horizons of sooty wavy laminations interpreted as plant remains (15066). Quartz overgrowths provide the cement.

Turbidites

Interbedded Sandstones and Claystones represent turbidites, covered exhaustively in the literature (based upon Bouma, 1962), and represent the distal end of reworked gravity flows capable of travelling considerable distances across near horizontal marine floors. They are erosive (15210) carrying rip-up clasts and leaving the tool marks of entrained pebbles on underlying soft sediment. Grain support is through turbulence. The beds are persistent, normally graded and frequently topped by clay. Where a considerable hiatus exists between events background Kimmeridge deposition is superimposed upon the flow (15215).

4 BASIC THEORY

"Basic Theory" covers the philosophy of solving problems in petrophysics, and introduces some of the ideas which are characteristic of this thesis. It also defines the petrophysical properties of the clasts and sandy matrix of the Brae conglomerates, which is fundamental to the project.

4.1 STATISTICAL ANALYSIS AND CAUSE & EFFECT

Formation evaluation can be approached from a deterministic and a statistical view point. Both have their advantages and areas of application.

4.1.1 STATISTICAL

Electronically stored and readily manipulated data lend themselves to powerful statistical techniques. For example petrophysicists can use stepwise multiple linear regression analysis to find the best linear equation relating dependent variables to an independent variable. i.e:

$$a_{predicted} = k_1 b + k_2 c + k_3 d..etc. + k_n$$

Additionally, facies which appear similar on raw log traces may be able to be distinguished statistically with multiple tools via discriminate-function-analysis, which provides mathematical functions for delineating groups of data plotted in n–dimensions.

In statistical approaches cause and effect are subordinate to correlation. An understanding of why certain parameters or data clusters correlate with the variable under investigation is not essential, providing the correlation is consistent. This approach has the advantage of by-passing the research time required to identify, understand and quantify all the influences upon the unknown variable[2], and can make use of data which may be too subtle to be incorporated in a cause and effect type of prediction. An example of statistical approaches are facies prediction from principal component analysis and modal distribution analysis (Wolff, 1982).

[2]Boron's high capture cross section enables low concentrations to significantly affect neutron porosity. However a correlation of neutron with core porosity will embrace this and other unknown effects. As long as Boron cannot be determined from wireline, coring and core analysis are required to make use of this knowledge. The funds consumed by this research and the required coring make simple correlation more cost effective for most if not all cases.

Statistical techniques may be used to predict pore fluids as well as rock type. This has been done to some degree by Raiga-Clemenceau (1984) in the Dual Porosity Model (6.1.4), and by Global processing (Mayer, 1980) which are both deterministic and statistical.

The overriding weakness of all correlation methods is knowing under what circumstances the correlation will be maintained. In practice this could mean correlations are valid in one formation or facies. Ironically, to know when circumstances become limiting entails an understanding of cause and effect; and so the analyst's deterministic thinking remains a valuable commodity. The analyst must understand the dominant casaul relationships at work or parameters which have absolutely no casual relationship may be correlated by chance alone. Correlation techniques such as MLRA are frequently excellent at "predicting" the data already in existence, such as core, but weaken below deterministic methods as conditions diverge from the existing data.

4.1.2 DETERMINISTIC

Deterministic methods involve theoretical models. The models provide equations which predict the cause of the measured effect; measured resistivity caused by oil saturation is an example. Deterministic methods assume all the influences upon the measured effect have been correctly accounted for, and that the equations may be used more generally than simple correlations. However, cause and effect methods frequently fail to take all the influences into account. The method becomes a special case of a general theory, or a slightly more general theory, in which additional influences are quantified. (The Archie equation becomes a special case of more generalised shaly sand models which corresponds to the case of zero shalyness.)

The advantage of the deterministic approach is an immediate answer without reference to samples of the unknown quantity to establish correlations, and generally, an appreciation of the causal relationships and the corresponding limits of the method. The weaknesses of the deterministic approach is that the equations may not properly quantify the causes of the effect, and may not include all the causes.

4.1.3 DETERMINISTIC / STATISTICAL COMBINATION

A deterministic approach has had to be developed in this thesis because water saturation is the single most important unknown. When the position of samples relative to the transition

zone is not known, reservoir specimens of water saturation cannot be taken and used as the basis for correlation, and so a theoretical model is essential. The accuracy of the model is improved by laboratory measurements of electrical properties. In this thesis where the cause of an electrical property is due to numerous and imperfectly understood influences, such as excess conductivity, the deterministic approach is put to one side in favour of correlation with the most statistically favourable parameter. This parameter is sufficiently understood to assume that the correlation will be maintained in the reservoir, although it is not considered necessary to understand precisely why this parameter has the best correlation; rather to accept that it is more capable of predicting excess conductivity than a parameter arising directly from a shaly sand model. See Fig p53 below, (6.2.1 C_x), (9.5.4.2) and (12.).

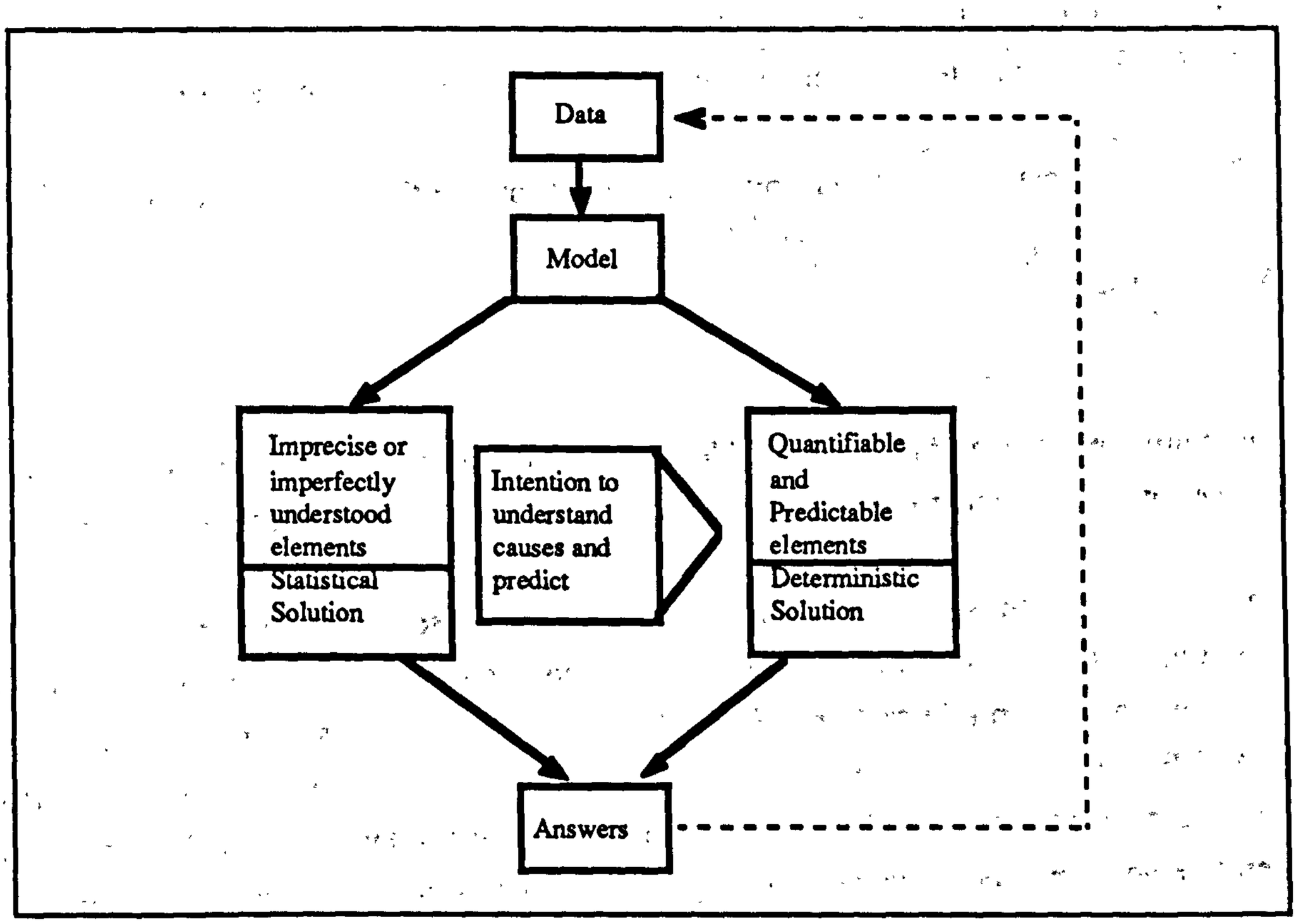


Fig p53 The preferred relationship between cause & effect and statistical problem solving.

A statistical analysis which searches for the least error between output parameters (8.2) and all inputs (12) is likely to be closest to reality only if the equations and constraints which have been used are an accurate and precise model of reality. Developing these solutions from the data provided for this thesis required additional time and computer facilities outside the range of this project.

4.2 CONCEPT OF Non–log–inputs

The internal consistency of log analysis is not a measure of its ability to yield information about the outside world, reality. Service companies use statistical error minimisations to provide incoherence factors. (Schlumberger, 1987 p121-122) This process of iteration reconstructs tool readings from a set of answers. The answers are synthesised from tool readings, response equations and constraints. If any of these three are invalid the solution which provides minimum "incoherence[3]" is necessarily not that which is closest to reality.

Non-log-inputs seek to make log analysis consistent with the outside world. This is done by providing external values for variables which are:

1) Usually generated within log analysis, e.g. a clay point on a neutron / density crossplot, or
2) Usually treated as constants by default, e.g. filtrate resistivity.

Non-log-inputs will also provide values to calibrate correlated tool readings, parameters, or accumulated parameters.

Optimum use is made of all the available well data by selecting the most appropriate data source for that particular formation parameter, or intermediate analytical parameter.

Non-log-inputs from special core analysis are already in use by the industry. e.g. Archie's *m* and *n*, porosities and grain densities. This approach has been developed further by deriving inputs from thin sections, X-ray diffraction, book values of mineral properties, SEM, electrical tests, nuclear activation, and finally drill stem tests. These inputs may secure certain parameters in log analysis which are conventionally internally derived and therefore not direct measurements, or may provide correlations for log analysis output.

The extensive experimentation involved in deriving the *Non-log-inputs* is also intended to uncover possible reason(s) for the anomalous behavior of Well A. (12.).

[3]Measure of discrepancy between logged and reconstructed tool responses

4.3 CONCEPT OF RESERVOIR TYPE SIGNATURES, "RTS"

Reservoir Type Signatures are a means of presenting integrated log analysis results. They are produced on an interval basis as opposed to the continuous curves of logs and are intended to succinctly characterise the interval under consideration. An interval might typically be a reservoir flow unit, a facies type interval or a drill stem test interval. The RTS is a histogram plot of numerous log analysis parameters (8). The parameters may result from combinations of tool readings with *Non-log-inputs* or from corrected single tool readings, and are grouped under sectors i.e.: Matrix, Porosity, Pore geometry, Clay type, and Saturation.

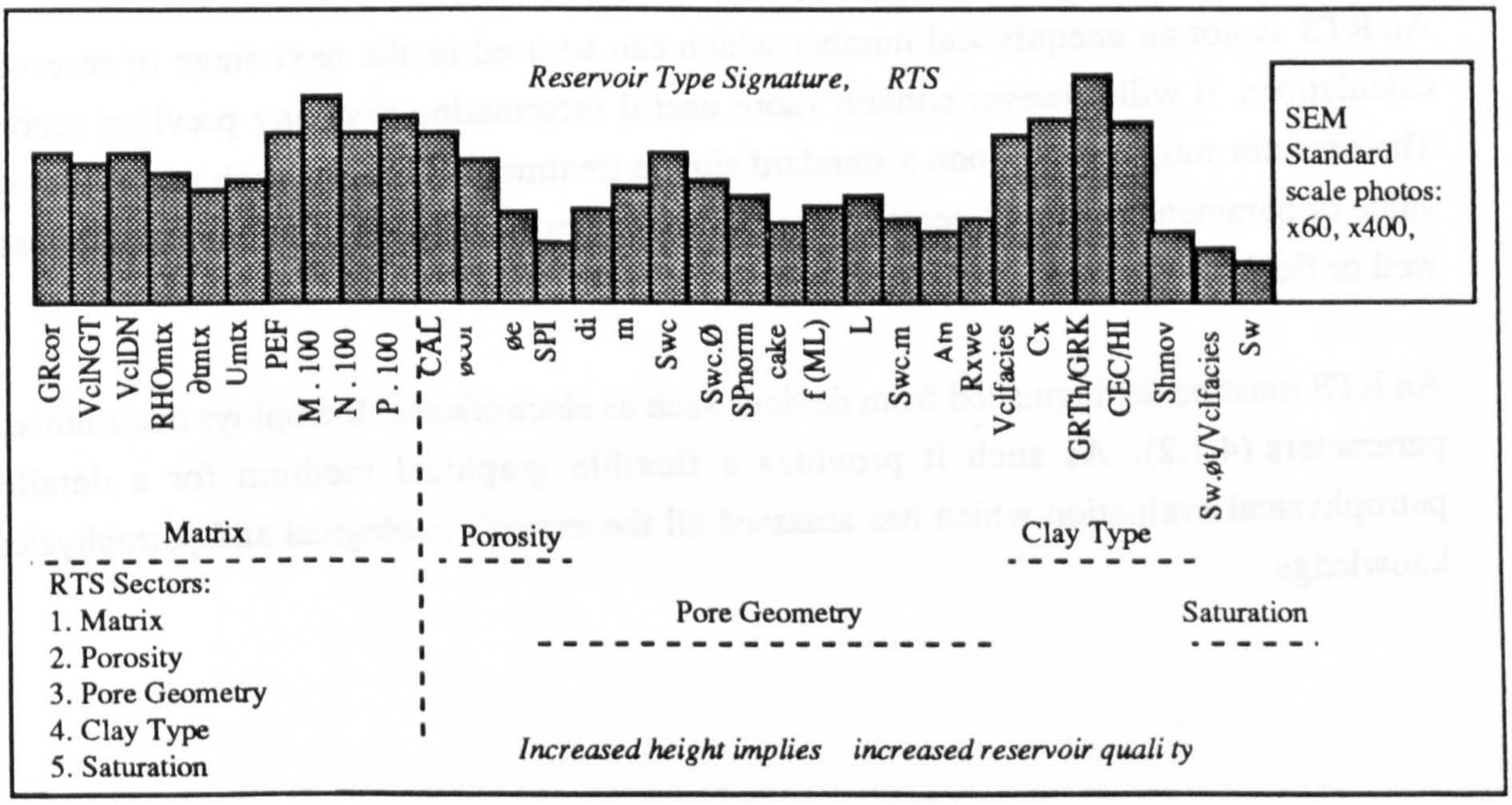


Fig p55 Concept of Reservoir Type Signatures

Unlike conventional log analysis each sector contains more than one description of the desired reservoir property. This represents the evaluation more comprehensively because relative heights of indicators within a sector is instructive to an experienced user in the same way that $\emptyset_{density} : \emptyset_{sonic}$ can relate pore geometry information. Different indicators represent different perspectives on the same reservoir property because different physical processes have been involved in their generation. In the case of clay type and pore geometry (or water saturation) to display only one parameter is to ignore information from other parameters which will also be influenced by the clay type or pore geometry. Parameters in sectors related to reservoir quality are designed to increase in height with

increased quality.

Standard scale SEM photographs of fractured surface core samples accompany the RTS for direct comparison with the Pore geometry sector.

An RTS is intended to portray the findings of an integrated formation evaluation graphically and comprehensively; in a manner relevant to testing or completion decisions; and to later more detailed analysis during field development.

An RTS can be generated over any interval[4]. It may be used by engineers for pore fluids and flow properties, or by geologists for diagenesis and lithology.

An RTS is not an unequivocal number which can be used in the next stage of reservoir calculations. It will however contain more useful information than any previous record. The operator must decide upon a standard simple treatment for RTSs, such as the average value of parameters within a sector, to obtain an accurate, standard set of numbers across a well or field.

An RTS must be distinguished from devices such as electrofacies. It employs deterministic parameters (4.1.2). As such it provides a flexible graphical medium for a detailed petrophysical evaluation which has amassed all the expert's geological and petrophysical knowledge.

[4]Non log inputs may be specific to one interval.

4.4 SCHEME OF INFORMATION FLOW

Fig p57 overleaf gives a basic indication of data flow; a primary aim being to predict production tests over untested, uncored intervals which might subsequently be of interest.

As *Non-log-inputs* are produced, and reconnaissance runs made, refinements to this scheme may become necessary.

Overleaf: Fig p57 Scheme of information flow for Integrated Evaluation.

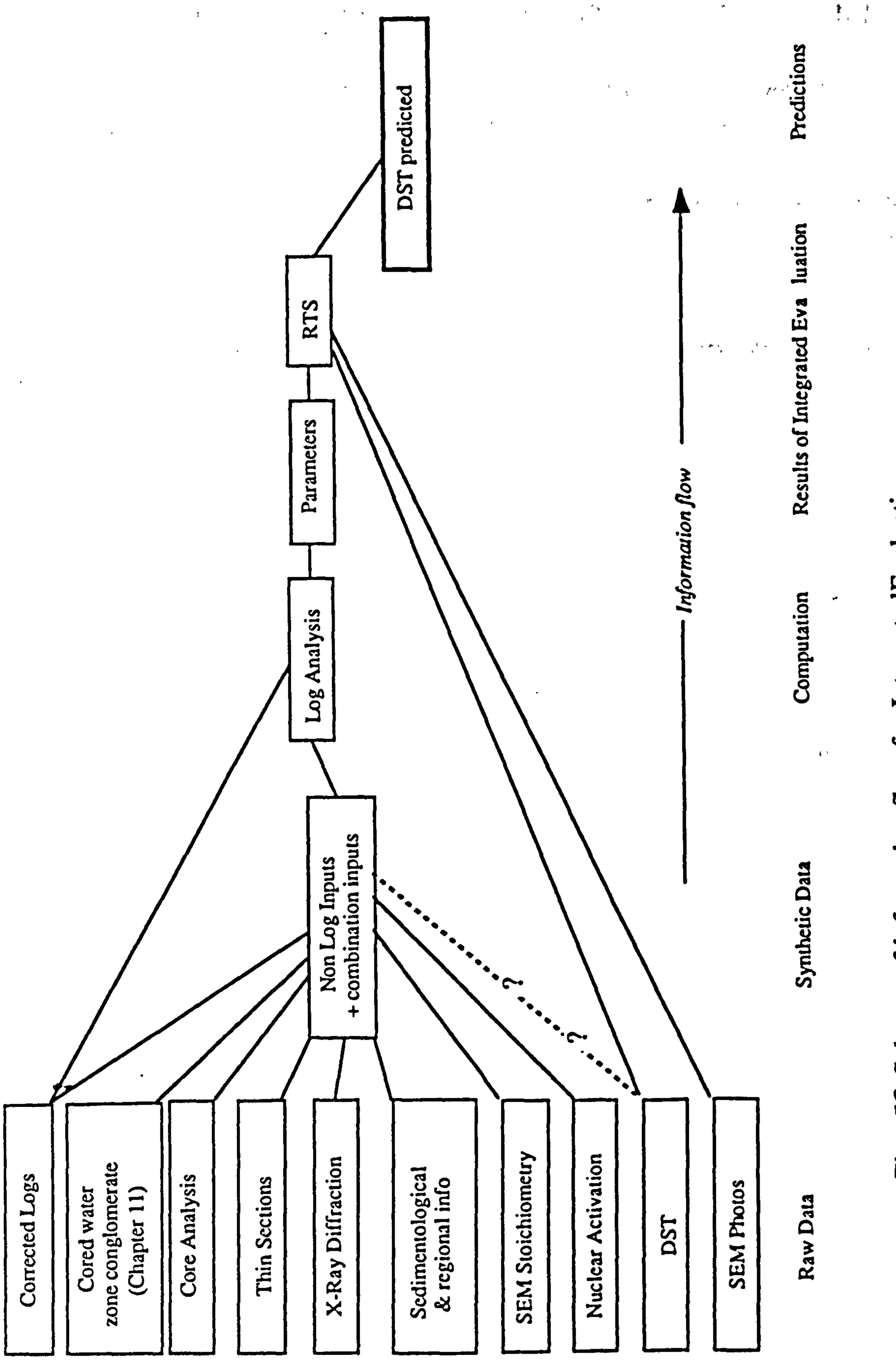


Fig p58 Scheme of information flow for IntegratedEvaluation

4.5 THE PROPERTIES & PRODUCTIVITY OF CLASTS cf. SANDY MATRIX

4.5.1 PROPERTIES

Geological clasts, typical petrophysical clasts and typical sandy matrix can be characterised from work in chapter (9), and from core analysis. Well A core analysis failed to adequately define the clasts, inparticular capillary pressure desaturation data was not available. (APPENDIX 32) indicates $\emptyset_{he}$=0.05. $khor$ ≈0.3mD suggest the assumption that $S_{wc\ clast} = 1$ is realistic. The means of estimating S_{wi} for sandy matrix detailed in (10.5.2) indictaes 0.05 porosity matrix to be water saturated up to 600 feet above free water level. The argillaceous nature of the clasts will further increase capillary threshold pressures for clasts. These considerations vindicate the $S_{wi} \approx 1$ assumption.

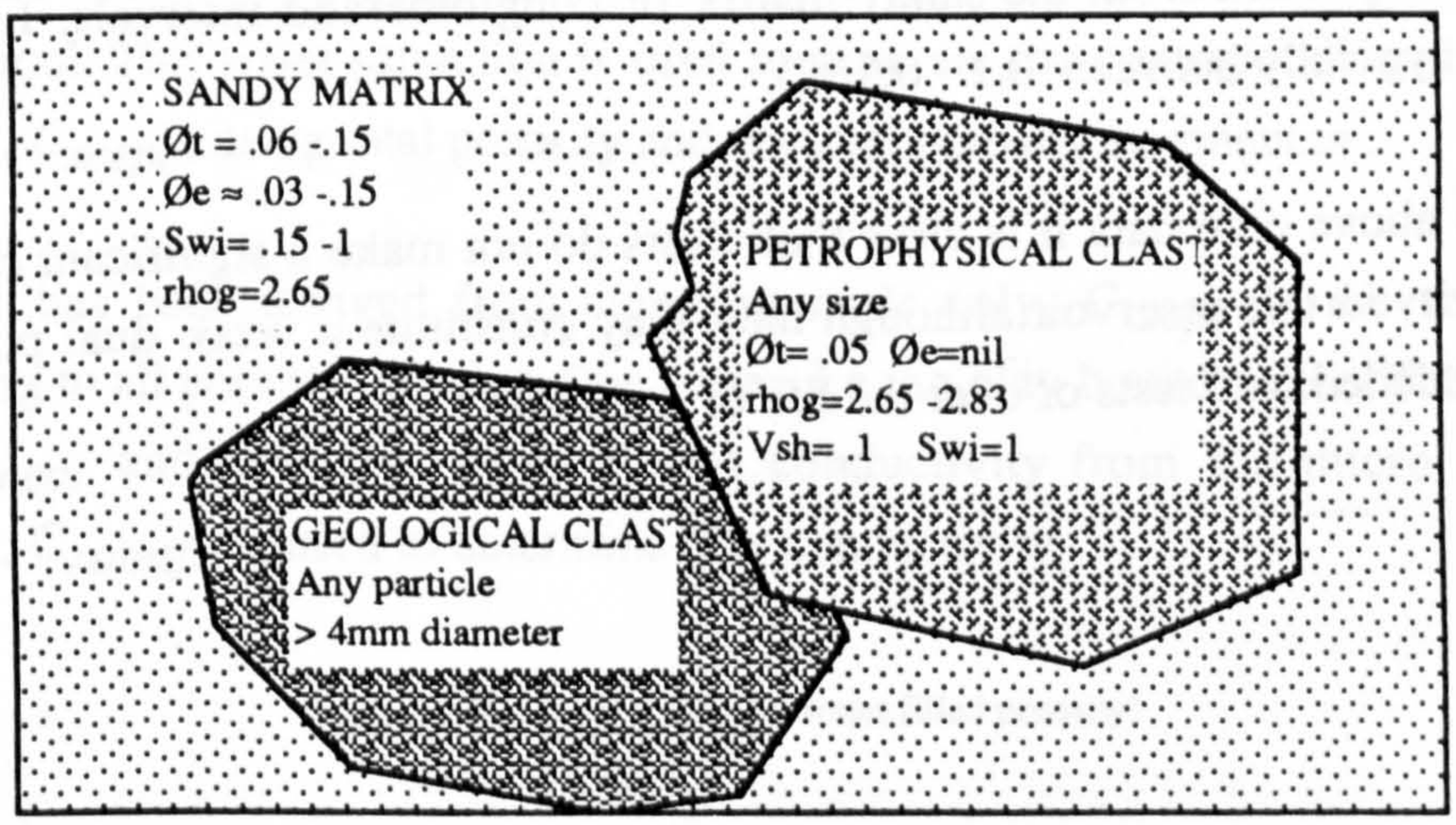


Fig p59 The main distinctions between a conglomerate's clasts and its sandy matrix relevant to formation evaluation.

4.5.2 PRODUCTIVITY

Core Analysis:	Clast Supported Conglomerate Type Interval
Average	k_{hor} = 7mD
	k_{vert} = 3mD

Core Analysis:	Matrix Supported Conglomerate Type Interval
Average	k_{hor} = 109mD
	k_{vert} = 72mD

Matrix permeability to clast permeability is > 20:1. These figures are averages for the intervals. Some clasts will be included in the matrix facies and some matrix in the clast facies, artificially bringing these figures together. Furthermore plugs have been preferentially taken from the sandy matrix of conglomeratic intervals. Individual clast plugs are typically between 0.1 - 0.5mD.

From the above core data it is clear that clasts do not make a significant contribution to productivity in this reservoir although they may constitute a weak dual porosity system during extended well tests or over the life of the field.

5 PRELIMINARY IDEAS

This chapter is a record of ideas concerning formation evaluation, some of which have been used in the derivation of *Non-log-inputs* or in the parameters of reservoir type signatures (4.). Ideas that require additional data which have not been used in this study are included for their theoretical content and possible use by others.

5.1 CONDUCTIVITY, CLAY CONDUCTIVITY AND WATER FILLED POROSITY

In this method flushed zone water saturation, S_{xo}, is determined from an electro magnetic propagation tool. This water saturation is used to generate the corresponding flushed zone conductivity, C_{xoept}, using total porosity and the total porosity exponent m.

Providing m has been derived from clean intervals only, C_{xoept} is the conductivity corresponding to all pore water being free water, i.e. no clay bound water. The difference between C_{xoept} and measured flushed zone conductivity from the micro spherically focused tool, C_{xomsfl}, is used to determine clay conductivity.

$$S_{xoept} = \emptyset_{ept} / \emptyset_t \quad (\emptyset_{ept} = \text{water filled porosity})$$

In the following equation m must be derived from clean intervals only.

$$C_{xoept} = S_{xoept}^{n} \cdot \emptyset_t^{m} \cdot C_{xwe}$$

C_{xwe} = effective conductivity of flushed zone water.

C_{xoept} = Predicted conductivity of clean flushed zone.

Differences in this predicted clean conductivity and actual conductivity is due to:

1) Clay conductivity.
2) Error in C_{xwe} due to a varying quantity of R_w in the flushed zone.
3) Geometric arrangement of total water content such that $L \neq .5$ in the Hanai-Bruggeman equation causing error in $\emptyset_{ept}$. (see Bruggeman, 1935 and Baker et al, 1985)

4) Deeper investigation of MSFL™ tool when water saturation varies across the depths of investigation of MSFL and EPT.

In fresh water, clayey permeable intervals 1 > 2+3+4

ie: $C_{xomsfl} - C_{xoept} = C_{clay}$

Waxman Smits, 1968:

$$C_t = \frac{C_w}{F^*} . S_w^n + \frac{BQ_v}{F^*} . S_w^{n-1}$$

C_{clay} is the equivalent term to (BQ_v / F^*)

Clavier Coates Dumanoir, 1977:

$$C_t = \frac{C_w}{F_o} . S_w^n + \frac{(C_{bw} - C_w) . V_q . Q_v}{F_o} . S_w^{n-1}$$

C_{clay} is the equivalent term to $((C_{bw} - C_w) . V_q . Q_v / F_o)$

Substituting C_{clay} in the W-S equation:

$$C_t = \frac{C_w}{F^*} . S_w^n + C_{clay} . S_w^{n-1}$$

Substituting C_{clay} in the D-W equation:

$$C_t = \frac{C_w}{Fo} . S_w^n + C_{clay} . S_w^{n-1}$$

Complex theories and assumptions are involved in W-S and D-W clay terms. The in-situ use of these equations also involves a Q_v transform - a circuitous approach to excess conductivity. By contrast C_{clay} is a relatively simple and directly measured parameter, at reservoir conditions. It has good vertical resolution and can be determined in both oil and water zones.

C_{clay}'s accuracy depends upon $\emptyset_{ept} . \emptyset_{ept}$ is subject to various systematic errors concerned with the geometrical distribution of volume fractions with contrasting dielectric constants, as revealed in Wharton et al., 1980; Sherman, 1983; Maple, 1985; Baker et al., 1985; & Schlumberger, 1987 p129-130. Nevertheless, it is additional information which can benefit evaluation. The petrophysicist must judge if the differences in C_{xomsfl} and C_{xoept} are caused primarily by C_{clay}, variations in m, or 2, 3 or 4 above by

considering:

1) V_{sh} cf. R_w,
2) changes in pore geometry, and
3) the borehole environment.

5.2 RESIDUAL OIL AND PERMEABILITY

Firstly plot core residual oil, S_{oc}, v core horizontal permeability, k_{hor} for oil zone core drilled with water based mud, to investigate any intra-coredata relationship. Secondly plot S_{oc} (core) and S_{xo} log to see if logs can predict S_{oc}. If so, S_{xo} log may be included in the Pore geometry *RTS* sector because of its relationship to k_{hor}.

5.3 MULTI PARAMETER APPROACH TO ABSOLUTE PERMEABILITY

Parameters

Tool readings are the result of numerous influences from formation solids, pore fluids and the borehole environment. The influence of the desired formation property is obscured by these numerous influences. A parameter is designed to combine tool readings (with or without *Non-log-inputs*) to minimise all but one influence. A parameter will be more sensitive to the desired property than a single tool reading.

Multi-Parameter Approach

Predictions of permeability are commonly based upon a single tool or parameter. Permeability, or any reservoir property, is controlled by various inter-related elements of the formation, such as surface area, tortuosity, clay morphology, clay bound water, porosity, mean pore-throat size, pore-throat size distribution etc. Parameters designed to be sensitive to one or a combination of these elements will be grouped together in the "Pore Geometry" sector of the reservoir type signature. By including parameters sourced from a

wide variety of physical processes, i.e. a wide variety of logging tool measurements, a fuller picture will be produced than depending upon one tool only.

Statistical treatment of the parameters is likely to uncover a better correlation with core permeabilities or DST *kh* mDft than any one single downhole measurement.

Parameters should include: (** = exponent)

E ** 2

S_{wir} ** -2

Mud cake

di

m

MLPROD

$S_{xo} - S_w$

5.4 CLAY DISTRIBUTION

The clay distribution as well as type and volume influences excess conductivity (Yuan & Diederix, 1987). Clay distribution is related to facies. There are potentially four producing facies in Well A, with at least three modes of clay distribution: The clasts of the conglomerates, the dispersed clays of the massive and bedded sands, and the structural clays of the interbedded facies. Log derived clay conductivity terms specific to each facies will predict clay's contribution to conductivity more precisely than a single term applied across all facies. Reservoir type signatures will predict facies in the absence of core data. Water zone R_O in known facies and computed R_O from the saturation equation can then provide the best clay conductivity term for each facies.

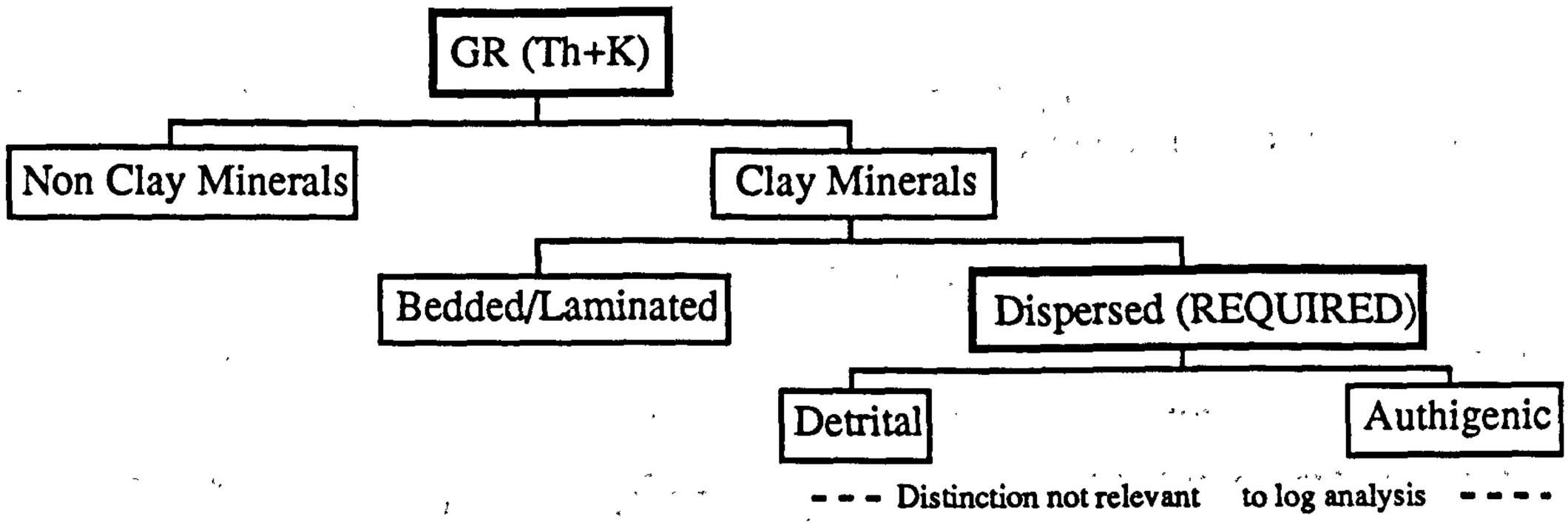


Fig p65 The relationship between Dispersed Clay and the *GR* tool response.

5.5 EFFECT OF PARTIAL FLUSHING ON R_{xo}

Some fraction of R_w remains in the flushed zone when R_{mf} invasion occurs. Less moved oil will be calculated if this is accounted for when $R_{mf} > R_w$.

The ability to moderate R_{xwe} between R_{mf} and R_w by use of a log derived parameter would improve moved oil calculations and inferred permeabilities. The fraction of pore water held at a given capillary pressure may provide an indication of R_{xwe}. If so S_w could be used to moderate R_{xwe} between R_{mf} and R_w. (Timur, 1968).

Experiment: Water saturation at a given capillary pressure is determined for a number of samples. Samples are resaturated with R_w before being flushed with one pore volume of R_{mf}. Sample resistivity, R_{ox}, is measured. R_{xwe} is determined by $R_{xwe} = R_{ox}/F$

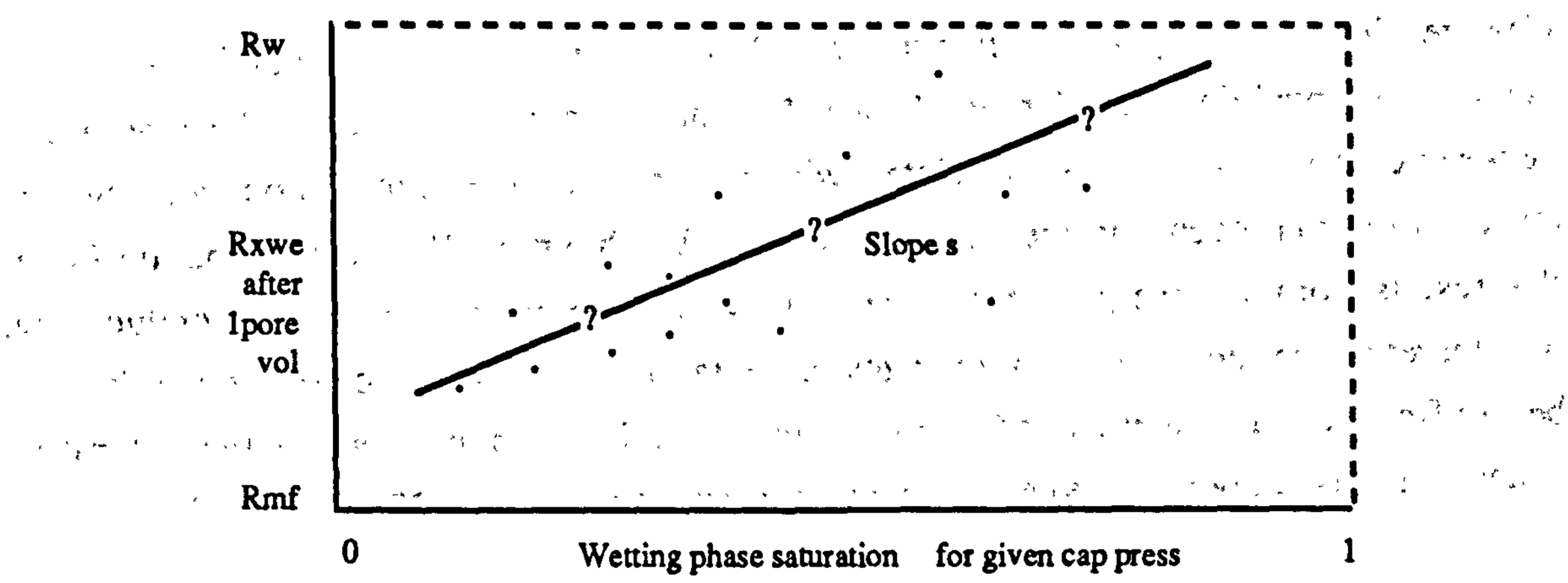


Fig p65 Hypothetical plot to aid the modification of R_{mf}, (R_{xwe})

The flushed zone saturation equation now becomes:

$$S_{xo}^{n} = R_{xwe} / (\emptyset^{m} R_{xo}) \qquad (9.5.2.3)$$

5.6 WETTABILITY AND ELECTRICAL PROPERTIES

Wettability is the contact angle measured from the solid through the water to the third phase (Dake, 1978 p344).

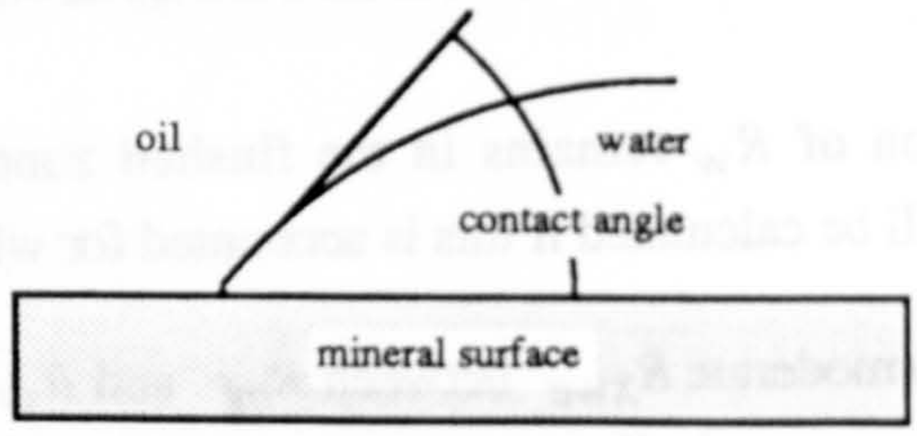


Fig p66 Wettability

It results from the balance of intermolecular cohesive and adhesive forces within and between the three phases. As such wettability is a surface phenomenon associated with the immediate vicinity of the solid surface.

Changes in wettability from reservoir to laboratory will cause changes in laboratory derived electrical data (Anderson, 1986). Distinction can be made (in the laboratory) between current flow that is associated with mineral surfaces, excess conductivity, and current flow that occurs in the free pore water (Worthington, 1985). A formation factor that results from the free pore geometry only, with no component of excess conductivity, will therefore be independent of changes in wettability. The influence of wettability will be confined to the excess conductivity and saturation exponent when the saturation equation is based upon this type of formation resistivity factor. (APPENDIX 28)

The flushed zone saturation equation now becomes:

$$S_{xo}^{n} = R_{xwe} / (\emptyset^{m} R_{xo}) \qquad (9.5.2.3)$$

5.6 WETTABILITY AND ELECTRICAL PROPERTIES

Wettability is the contact angle measured from the solid through the water to the third phase (Dake, 1978 p344).

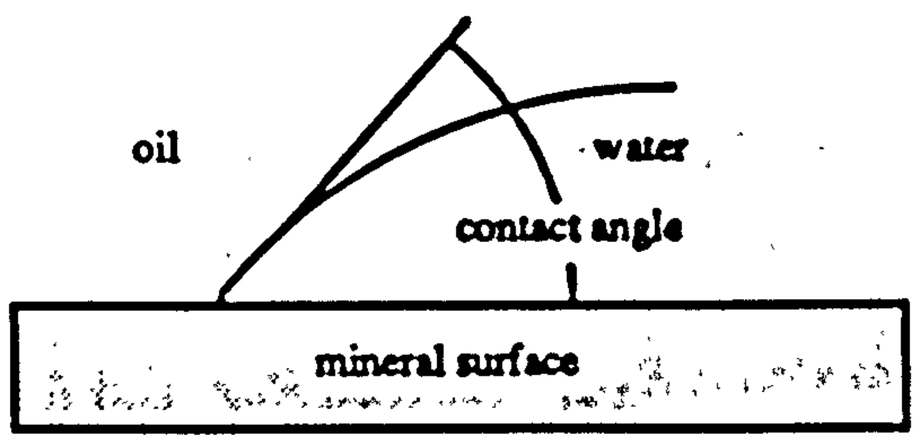


Fig p66 Wettability

It results from the balance of intermolecular cohesive and adhesive forces within and between the three phases. As such wettability is a surface phenomenon associated with the immediate vicinity of the solid surface.

Changes in wettability from reservoir to laboratory will cause changes in laboratory derived electrical data (Anderson, 1986). Distinction can be made (in the laboratory) between current flow that is associated with mineral surfaces, excess conductivity, and current flow that occurs in the free pore water (Worthington, 1985). A formation factor that results from the free pore geometry only, with no component of excess conductivity, will therefore be independent of changes in wettability. The influence of wettability will be confined to the excess conductivity and saturation exponent when the saturation equation is based upon this type of formation resistivity factor. (APPENDIX 28)

5.7 HYDROGEN INDEX OF RESERVOIR DRY CLAY MINERAL ASSEMBLAGE

Thin sections, X-Ray diffraction, scanning electron microscope and neutron density tool readings enable a Dry Clay Mineral Point to be determined on a neutron density crossplot. This is the borehole neutron density response of a solid assemblage of pure reservoir dry clays. **(12.1).**

6 SATURATION EQUATIONS

Chapter 6 deals with the complicated subject of translating resistivity into water saturation. It provides a brief history of the main developments in this field, and goes on to propose a new equation with a number of beneficial original features. This F_g equation is later used for analysing the sandy matrix. A second original equation which uses core capillary pressures is compared with the F_g equation but has not been used in Well A.

A conductivity saturation equation is perhaps most clearly understood when conceived of as a prediction of the conductivity a rock would have if its pores were entirely filled with brine. The particular values of the variables in the equation are characteristic of the rock and formation brine in question. More than 30 equations are in common use, most of which are empirical. Theoretical equations with a supposedly more general application involve assumptions which are not always true and in some cases require laboratory tests (Waxman and Smits 1968). An ideal equation is clearly one that is universally accurate and can be solved by reference to a continuous record of wireline measurements. Saturations from interpreted conductivity can be compared with saturations from a number of other methods: core capillary pressures versus saturation, converted to a height above free water level[31] versus saturation relationship, oil based mud preserved cores from above the transition zone (Woodhouse, 1987), and other logging devices such as the EPT™, GST™, TDT™ or NML™ tools.

In the final analysis saturations in the virgin formation are unverifiable, and dependent upon the accuracy of porosity calculations, all saturation methods have shortcomings, and force of argument is the final arbiter of the exact level of saturation and hydrocarbons initially in place.

[31] Capillary Pressure = Zero below Free Water Level. ™ Schlumberger trademark.

6.1 A SHORT HISTORY

Early interpretations of conductivity in the 1930's compared the resistivity of a known water bearing interval with the resistivity of the zone of interest. This was expressed empirically in the equation:

$$S_w = (R_o/R_t)^{0.5}$$

Variations in the resistance that different formations and different formation brines imparted to R_t were later accounted for by resistivity ratio methods. These compared two simultaneous resistivity readings in the same formation; one assumed to be from a volume of rock invaded by filtrate of resistivity R_{mf}, and a deeper one from a volume of rock containing formation water of resistivity R_w. Any increase in the ratio $R_{deep}/R_{shallow}$ was taken to indicate hydrocarbons. Since porosity tools did not supply a porosity value there was no requirement for porosity to be translated into a formation resistivity factor. However ratio methods suffer from the assumption of a step invasion profile in which $R_{shallow}/R_{deep} = R_{mf}/R_w$ in water zones. They also suffer from the presence of excess conductivity which obscures resistivity contrasts. Furthermore corrected $R_{shallow}$ and R_{deep} readings taken from impermeable shale formations are sometimes unequal, which reveals another source of error.

The ion-selective membrane effect of shale (Schlumberger, 1987.p18) influences the Spontaneous Potential (SP) log, and so using the SP log in shaly sand evaluation seems a natural choice. However the numerous and still poorly understood influences on this log and its need for a water based mud have prevented its quantitative universal use in saturation equations. Schlumberger's "R_{xo}/R_t Quicklook" method is a normalisation of the ratio method for changes in connate water salinity and shalyness (Poupon, Loy and Tixier 1954, Schlumberger 1987 p105). Also Yuan and Diederix (1987) have found core membrane potential measurements successfully predict clay conductivity. With enhanced SP vertical resolution (Tabanou et al., 1987), and invasion profile, and clay type information (Ruhovets & Fertl, 1982), the SP should become a greater contributor to saturation determination than was previously possible.

In 1942 Archie's Resistivity - Porosity plot related the resistivities of brine saturated core samples to their porosities. F is defined as the ratio of the brine saturated rock resistivity to the resistivity of the brine itself; $F = R_o / R_w$. This important characterisation of a rock was related to porosity by the slope of the plot, m .

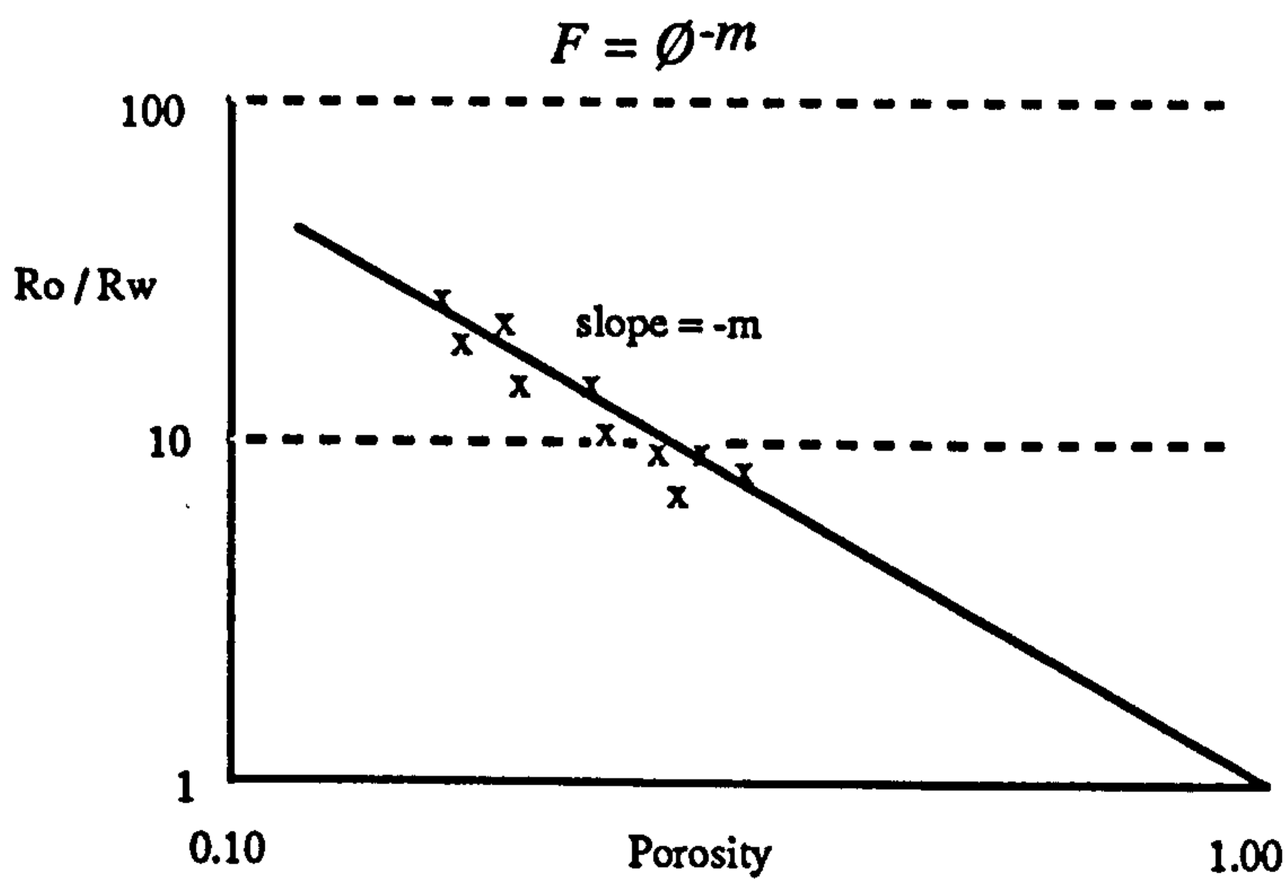


Fig p71 Relation of porosity to Formation Resistivity Factor for consolidated sandstone cores, Gulf Coast. (After Archie, 1942)

m is derived from a number of rock samples with a spread of porosities. m is an averaging technique which has no relevance to an individual sample unless the sample falls on this line. If this method is used to convert porosity into resistivity for an interval of rock which does not actually fall on a straight line passing through Porosity = 1 when $R_O/R_W = 1$ considerable theoretical problems are created. These were not apparent from the high salinity ranges, low clay contents and porosity types of these observations.(See Archie 1942, p55 & Fig.1,2). From observation of carbonate thin sections for example it would certainly seem improbable that porosity could be used to predict electrical resistivity (see Watfa & Nurmi, 1987).

Overleaf:

Plate p72 x25. The shape and scale of porosity dictate its relationship to conductivity. (Carbonate Khuff Fm. Saudi Arabia. Courtesy Ibrahim Al-Jallal)

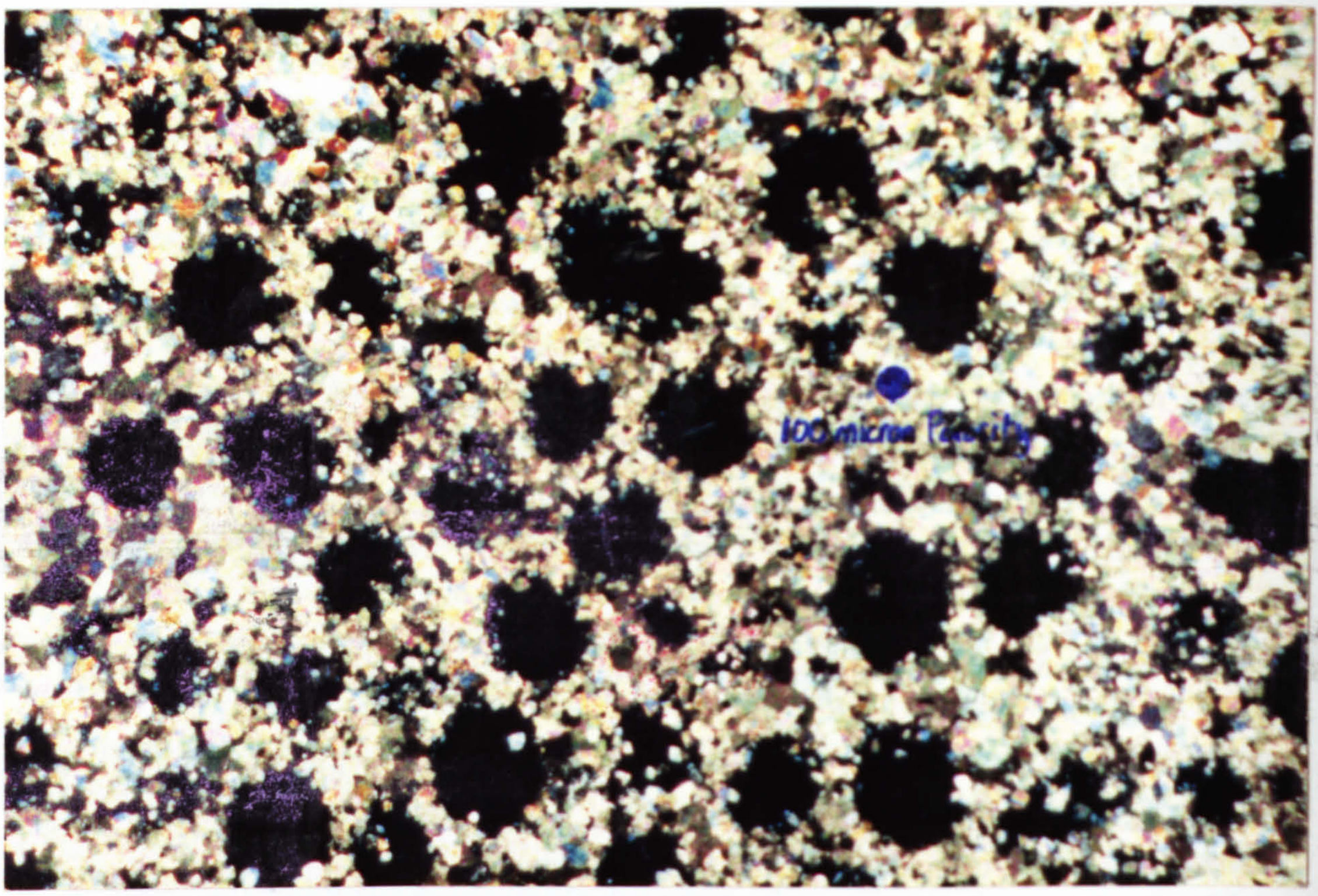


Plate p72 x25. The shape and scale of porosity dictate its relationship to conductivity. (Carbonate Khuff Fm. Saudi Arabia. Courtesy Ibrahim Al-Jallal)

For many reservoirs the conversion of porosity into conductivity is the single largest problem when calculating hydrocarbon levels. The size of the porosity exponent indicates the sensitivity of a formations water saturated resistivity to changes in porosity. (6.2.1).

Archie (1942) also observed a simple relationship between the ratio of measured resistivity to water saturated resistivity, and brine saturation above approximately 15 percent water saturation. This was expressed by the saturation exponent, *n*.

$$S_w^{-n} = R_t / R_o$$

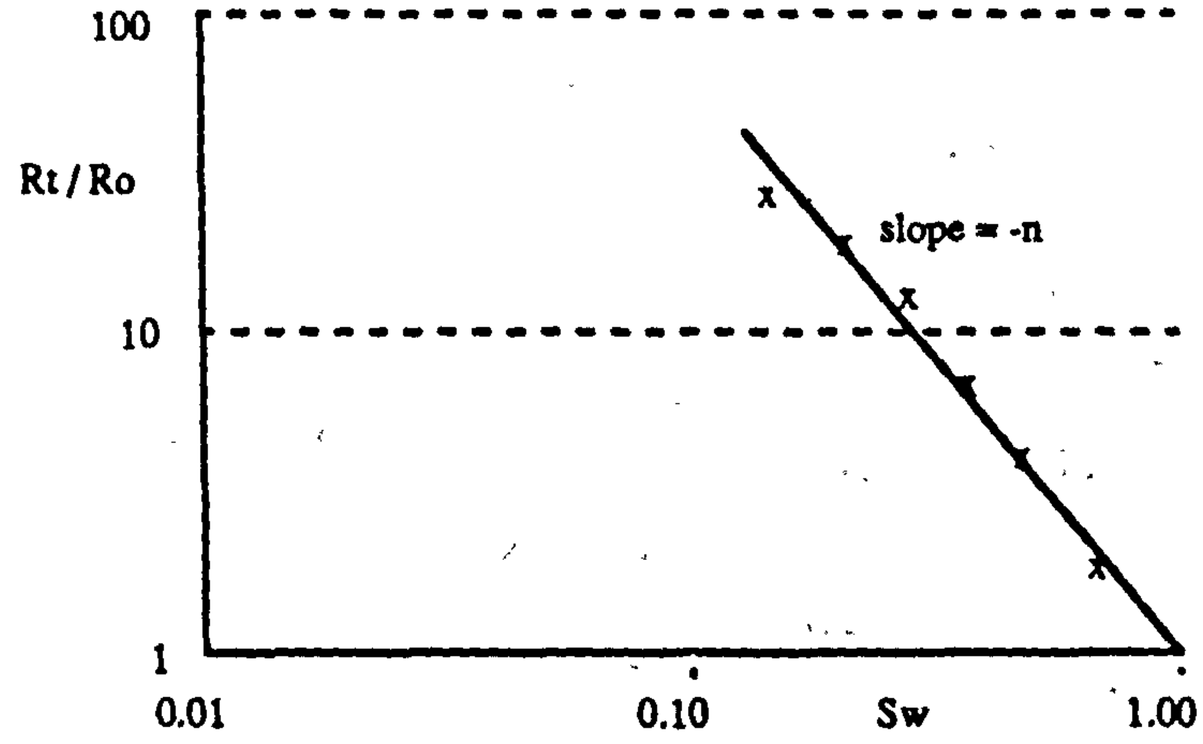


Fig p73 Relation of S_w to R_t / R_o (After Archie, 1942)

These admirably simple and pertinent observations on clean sandstones provide the cornerstone of log analysis to this day in the equation:

$$S_w^{n} = R_w / (\emptyset^{m} R_t)$$

This equation normalises the measured resistivity for the prevailing porosity. The porosity is converted into water saturated resistivity. This allows each level to be evaluated independently without the drawbacks of the ratio method.

Attempts to convert porosity into an electrical property in rocks dissimilar to those in which the concept originated has occupied the minds of log analysts since the 1950's.

In the 1950's it became clear that water saturated conductivity, C_o, could not always be predicted by C_w/F, and an additional conductivity was apparent, especially when C_w was small (Winsauer and McCardell 1953). This was attributed to clay conductivity.

6.1.1 EMPIRICAL SHALE VOLUME MODELS

In volume shale models this clay conductivity was quantified by referring to a tool reading sensitive to the volume fraction of clay minerals. The corresponding conductivity was calculated and subtracted from the total to give an estimate of the remaining free water. Commonly the tool reading at an adjacent shale bed was taken as the $V_{shale} = 1$ reference. These equations do not purport to have a theoretical basis although some degree of theory is involved in the basic idea. They are tailored to each rock, for example the Indonesia Equation of Poupon & Leveaux (1971) for shaly low salinity sands:

$$1/\sqrt{R_t} = [[V_{cl}^{(1-V_{cl}/2)}/\sqrt{R_{cl}}] + [\phi^{m/2}/\sqrt{a\,R_w}]] \cdot S_w^{n/2}$$

clay term clean term

In their own formations such equations frequently provide results as consistent with other data as the more sophisticated theoretical equations. Comprehensive data bases, a knowledgeable petrophysicist, and an informed use of computing power, may yet provide a universally accurate, and probably extremely complex, empirical saturation equation whose causal relationships may not be fully understood. The distinction between theoretical and empirical becomes more difficult to sustain as the subject is studied (see six pages forward). i.e. theoretical models are usually conceptualised under the impetus of an observed correlation. This begs the question of how many other correlations exist which are not yet recognised, i.e. has our theoretical model accounted for all causes of the measured effect? The distinctions and merits of theoretical and empirical problem solving have been discussed in (4.1).

6.1.2 THEORETICAL SHALE CATIONIC MODELS

With empirical models parameters are correlated without understanding the processes involved, and without an understanding of the conditions necessary to maintain that correlation. With theoretical models we understand, at least to some degree, the causal effect of a parameter.

Theoretical equations had to model the following:

1) At low salinities, an increasing absolute value for clay conductivity as the salinity was increased, up to a maximum clay conductivity value.(Patnode and Wyllie 1950).
2) A realistic resistor model which predicted conductivity for a diverse range of rock

types and variable saturations.

3) To approximate to the Archie relation in clean formations.
4) That C_t--> C_w as $\emptyset$-->1

Attention was focused on the subject of clay conductivity by Hill and Milburn in 1956, who showed a relationship between the clays effect on rock conductivity and Cation Exchange Capacity per unit of pore volume, Q_v. This work began a line of fruitful research. While all steps cannot be elucidated in this text the paper of Waxman and Smits (1968) has become an industry standard. Waxman and Thomas (1974) developed this approach by relating the equivalent conductance of the clay counter-ions to temperature and salinity. These equations allowed laboratory tests on reservoir cores to supply the necessary information to treat shaly sand analysis in a rational manner. They became the basis for equations using log data only[32] such as that of Juhasz (1981).

In essence the Waxman and Smits approach predicts an effective conductivity for the bulk pore water: the free and bound waters together, using cation exchange capacity, and then uses this effective R_{we} in the Archie equation as if the rock had no shale. Thus the W-S equation produces an R_{we} for the <u>total</u> porosity, and provides S_{wt}, the water saturation of that <u>total</u> porosity. This approach has a certain compatibility with logs in that it deals with total porosity.

The W-S model formulates clay conductivity as:

$$B\,Q_v S_w^{n^*-1} / F^*$$

B is the "equivalent conductance of clay exchange cations (sodium) as a function of C_w at 25°C" (Waxman & Smits, 1968). This is a composite factor resulting from ion concentration, ion species, temperature, and the geometrical distribution of the clay minerals in the rock. Any source of conductivity that is not correctly formulated for, or does not appear in the W-S equation, and that influences the C_o intercept on a C_o v C_w plot will be absorbed in B (Fig.1 Waxman & Smits 1968). For example replacing sodium with other cations will affect excess conductivity and laboratory B values (Hardwick, 1987).

---

[32] Saturation exponent n is not log derived by Juhasz; it is lab derived. See Conclusions and Woodhouse, 1987

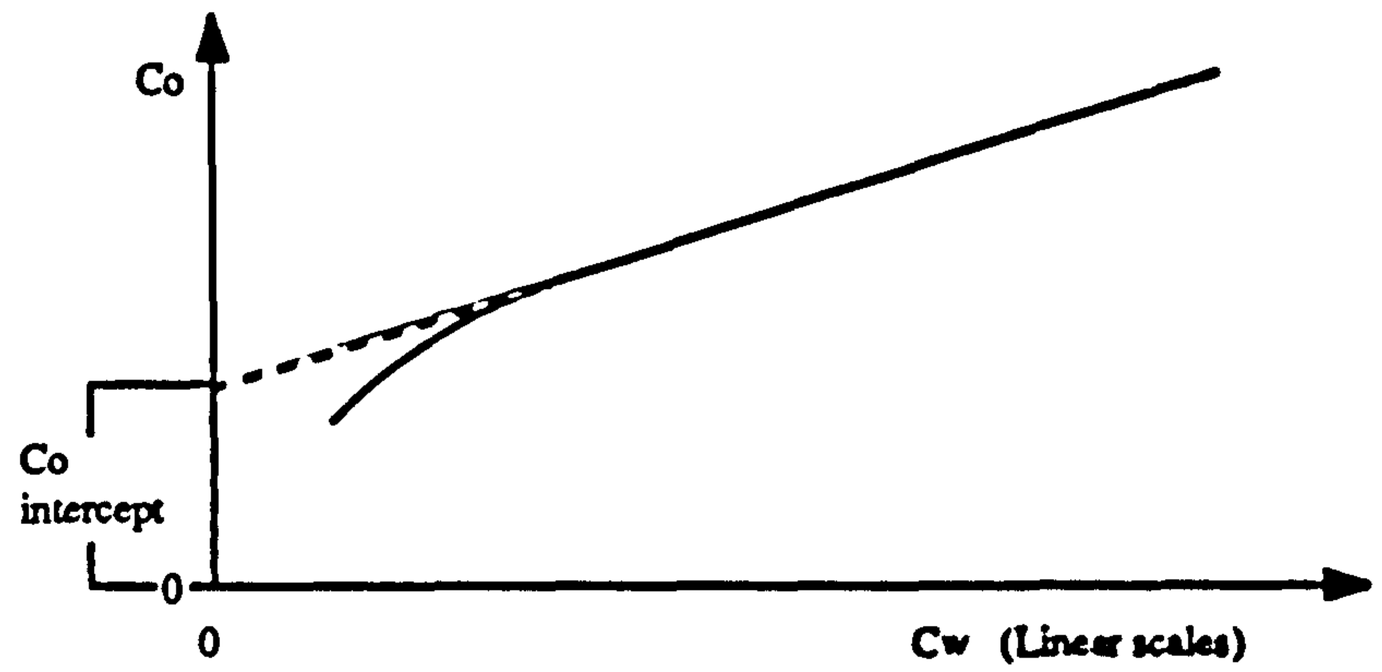


Fig p76 Observed brine saturated rock conductivity with decreasing brine salinity.

It is this intercept which is explained by BQ_v. With the value of Q_v known, if equations for B do not predict this intercept the equations for B must be considered inadequate. The composite nature of B can be appreciated by referring in the W-S paper to the standard deviation of the "§" values at low salinities, 0.159. All the influences on B are usually not appreciated in the literature. A recent exception to this is the paper of Yuan and Diederix, 1987.

The Dual Water model of Clavier et al. accounted for the deficiency of chlorine anions from a layer of bound water proximal to the clay surface, predicted by Gouy's diffuse layer model (Clavier, Coates and Dumanoir,1984). This treats the effective bulk water conductivity, C_{we}, as the result of two waters: bound clay water and free pore water. Based on W-S data the clay bound waters unit conductivity is "quasiuniversal" from different formations at the same temperature (next page:7).

The bound water conductivity is formulated as:

$$(C_{cw} - C_w)\, a V_Q Q_v S_{wt}^{n_o - 1} / F_o$$

Bound water conductivity is defined here as a function of salinity, the volume of anion deficient water, the equivalent conductivity of sodium counter-ions, saturation of the total pore volume, and a pore geometry consistent with the particular bound water volumes.

This complex paper partly deconvolves W-S B factor by replacing it with a salinity dependent function (Waxman & Thomas, 1974) and a clay bound water volume function. The geometry of the conducting volume of clay bound water itself, i.e. an m for clay bound water, as opposed to the geometry of the free pore water does not appear to be accounted for.

It also replaces W-S F^* with a formation factor, F_O, consistent with a particular salinity. F_O is consistent with the volume of clay bound water, arising in part from the equilibrating water's salinity. (APPENDIX 28: SPE 16415) Generally, a complex solution to a given data set is not to be preferred to a simpler solution, since its consequences are more numerous and carry greater probability of conflicting with future data (Occam,W. *c.*1349).

Problems Remaining with Cationic Models.

The problems remaining with both these approaches are as follows:

1) The electrical effects of clay distribution and clay surface geometry are contained in B and C_{CW} respectively. If distribution and geometry happen to be constant across the tested core and rock volume affecting R_t, then lab values of these clay terms will be relevant to log analysis. However any divergence of clay geometry which is manifested as a change in R_t will compute as a (false) change in S_W.

2) The experimental work and resulting equations are the result of approaching excess conductivity as though it were solely due to clay.

3) The excess conductivity of the clay itself is influenced not only by cation exchange capacity but also by exchangeable anions. Kaolinite with a CEC of 3–15meq/100g has replaceable $(OH)^-$ ions outside its structural sheets in the order of 1-2meq/100g (Deer et al., 1966 p257 & Dr H.F.Shaw pers comm. See also U.Schoen, 1953) The concept of "anion free" water, as expounded by Hill et al., 1979, proceeds on the assumption that anions are "substantially excluded" from bound water. The amount of "anion free" water is calculated from the chlorine concentration of the supernatent equilibrating water. In the case of clays with exchangeable cations and anions a double titration method should be used to determine total exchangeable ions. The total bound water will then be related to the total exchangeable ions, and to their total charge carrying capacity (Hill et al., 1979: Table 1). Although this effect is small in most rocks the assumption that CEC alone can satisfactorily account for the phenomenon of a C_O versus C_W intercept should not be forgotten.

4) The influence of changing saturations on the contribution of clay conductivity to total conductivity, the exact form of the parallel resistance model, is imprecise. Reducing

the S_W exponent n in the clay term by one amounts to a standardised approximation when in fact it is likely to vary with rock type, especially where one or more mineral phases have different wettabilities or unusual surface properties. (6.2.1.1)

$$C_{true} = C_{clean} S_w^{n} + C_{clay} S_w^{n-1}$$

5) Above transition zones, if the water saturation of the free pore volume is zero what can the salinity of this equilibrating saline solution be said to be, and consequently how is the clay bound water volume calculated from the salinity of a zero volume fluid?

6) Deriving the required data from logs for either of the above methods relies upon an empirical correlation of logging parameters with excess conductivity. Excess conductivity cannot be logged directly. In this respect at least, such models must be regarded as sophisticated volume "shale" models because the tools from which the log parameter is derived will always primarily be a response to basic volume fractions - not even to the geometry of those volume fractions. Recent high resolution tools (FMT[33]) may begin to address this basic weakness of log data but even then correlation will be the only way to use this new information.

7) The experimental work and resulting equations are the result of pure NaCl solutions as opposed to diluted/evaporated multi-ion natural formation brines taken from the same formation (Hardwick 1987).

6.1.3 THEORETICAL EQUATIONS WITH LOG DERIVED Q_v FUNCTIONS

Juhasz (1979) presented a unified approach to formation evaluation using the basic theory of Waxman & Smits but making use of the Hill, Shirley and Klein relationship between CEC and clay bound water volume (Hill, Shirley and Klein, 1979). Knowledge of the clay bound water volume allowed distinction between total and effective porosities. The resulting effective porosity water saturation values are more relevant to produced fluids. Q_v is continuously log derived from the neutron density combination calibrated to core sample clay types.

Defining effective porosity in this way:

$$\emptyset_e = \emptyset_t - \emptyset_{clay\ bound\ water}$$

[33] Schlumberger Formation Microscanner Tool

addresses one of the controls on what most geologists and engineers conceive of as effective (hydraulic) porosity (Hunt, 1985). The other main control is the mineral surface geometry, particularly the clays. From the photographs presented here (APPENDIX 2, APPENDIX RTS) it is evident that a complex network of walls and bridges may drastically reduce the effective porosity even if composed of low CEC clays such as chlorite or illite. (this thesis & Givens, 1987). It is this inability of logging tools to uncover surface geometries and the geometrical distribution of component volume fractions that remains a fundamental weakness throughout log based formation evaluation (Q_{vn}, next page). This inability of logs to reveal geometry enables thin sections for example, to provide an insight beyond the reach of the best log analysis.

A Shell method for deriving Q_v from logs in the absence of core is mentioned by Juhasz (1981). The following equation was frequently used by Shell in water zones to generate Q_v from logs. (B from temperature and R_w):

$$Q_v = 1/B\,(\emptyset_t^{-m^*}/R_o - 1/R_w)$$

Q_v and $\emptyset_t$ are then plotted and correlated. $\emptyset_t$ is then used to predict Q_v in zones where $S_w < 1$.

This procedure contains a number of speculative assumptions, the first of which is Juhasz's primary concern:

Firstly, when the Q_v-$\emptyset_t$ relation is well defined, that the reductions in total porosity are caused solely by increase in clay content. For example when an homogenous primary porosity had been differentially occluded by the growth of authigenic clay. However variations in $\emptyset_t$ due to sorting, feldspar dissolution, locally developed quartz overgrowths, local zones of organic matter or asphalt which respond as porosity - or any other local diagenetic phenomenon, are also possible. In hydrocarbon zones these would lead to an undetectable breakdown in the Q_v-$\emptyset_t$ correlation such that changes in R_t calculate as changes in S_w, when in fact they are changes in Q_v.

Secondly, that water zone diagenesis is identical to oil zone diagenesis.

Thirdly, that B may be calculated by referring only to R_w and temperature.

Despite their practical efficacy, these assumptions are invalid, especially in reservoirs affected strongly by diagenesis which have had an early emplacement of hydrocarbons.

Juhasz introduces the log derived parameter Q_{vn} which is conceived as the level of shale water saturation in the reservoir porosity. This parameter employs any clay sensitive log parameter, V_{sh}; the shale porosity of a shale bed intimately associated with the sands, $\emptyset_{tsh}$; and the reservoir porosity, $\emptyset_t$. Then:

$$Q_{vn} = (V_{sh}\ \emptyset_{tsh}) / \emptyset_t$$

In clastic sequences, where interbedded shales and the interstitial reservoir clays are original detritus, $\emptyset_{tsh}$ may be a relevant pointer to shale water volume in the reservoir. This is less probable for authigenic clays which may not be genetically related to interbedded shales. Water bearing clean to shaly sands are used to set up a C_{wa} (apparent water conductivity) versus Q_{vn} trend, where Q_{vn} is based upon any shale indicator. This indicator is then used in the hydrocarbon zone to predict C_{we}, the effective conductivity of the pore water residing in the total porosity system, a W-S concept.

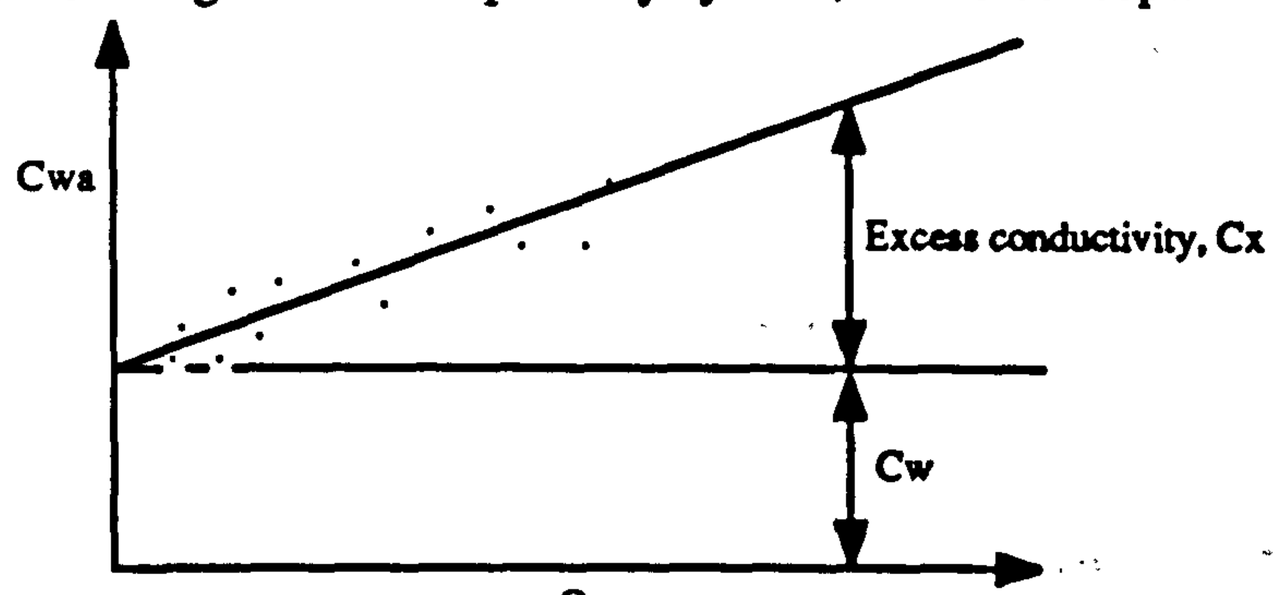


Fig p80 Log derived clay indicator, Q_{vn}, and Apparent water conductivity, C_{wa}, from $S_w=1$ zones (Refer Juhasz, 1981) Note: In cases where C_w is high (saline) excess conductivity will comprise a smaller fraction of C_{wa} and shaly sand evaluation approaches the Archie equation.

Q_{vn} is also described as a parameter which incorporates the effects of shale distribution. i.e. that variations in resistivity caused by shale distribution are accounted for by Q_{vn} when Q_{vn} is used in the Normalised Waxman-Smits equation. The following reasoning would suggest that this log derived parameter can only make such a powerful contribution to formation evaluation if a certain condition is met:

Thomas and Stieber (1975) use a mathematical example to describe the effect of shale distribution on the total porosity of a sand / shale mix. The pure sand has a fixed porosity of 0.35, the pure shale a fixed porosity of 0.15. The net porosities of the various sand / shale mixes which result from the various shale distributions are then mathematically calculated.

It is certainly true that in an otherwise fixed porosity sand, the effect of shale distribution is incorporated in Q_{vn}, even though it may not be quantitatively accurate in terms of conductivity[34]. Q_{vn} accommodates changes in total porosity caused by shale distribution or other factors such quartz overgrowths. Unfortunately the electrical influence, as opposed to the spatial influence, of changes in shale distribution are more difficult to resolve. In this sense Q_{vn} does not necessarily succeed in its electrical role.

The above can be clarified by consideration of two sands, each evaluated with the same $\emptyset_{tsh}$ values and with identical total porosities, F^* values, and shale volumes. Two such sands are theoretically possible. Suppose that one sand had this shale volume dispersed uniformly around the pore walls whilst the other had this same shale volume replacing isolated feldspar grains, a geological possibility. The first sand would certainly have a greater excess conductivity than the second, and yet their Q_{vn}'s would be identical since $Q_{vn} = (V_{sh}\ \emptyset_{tsh}) / \emptyset_t$. The F^*C_o axis below would thus have two vertically displaced points for the same Q_{vn} solely because of this difference in shale distribution.

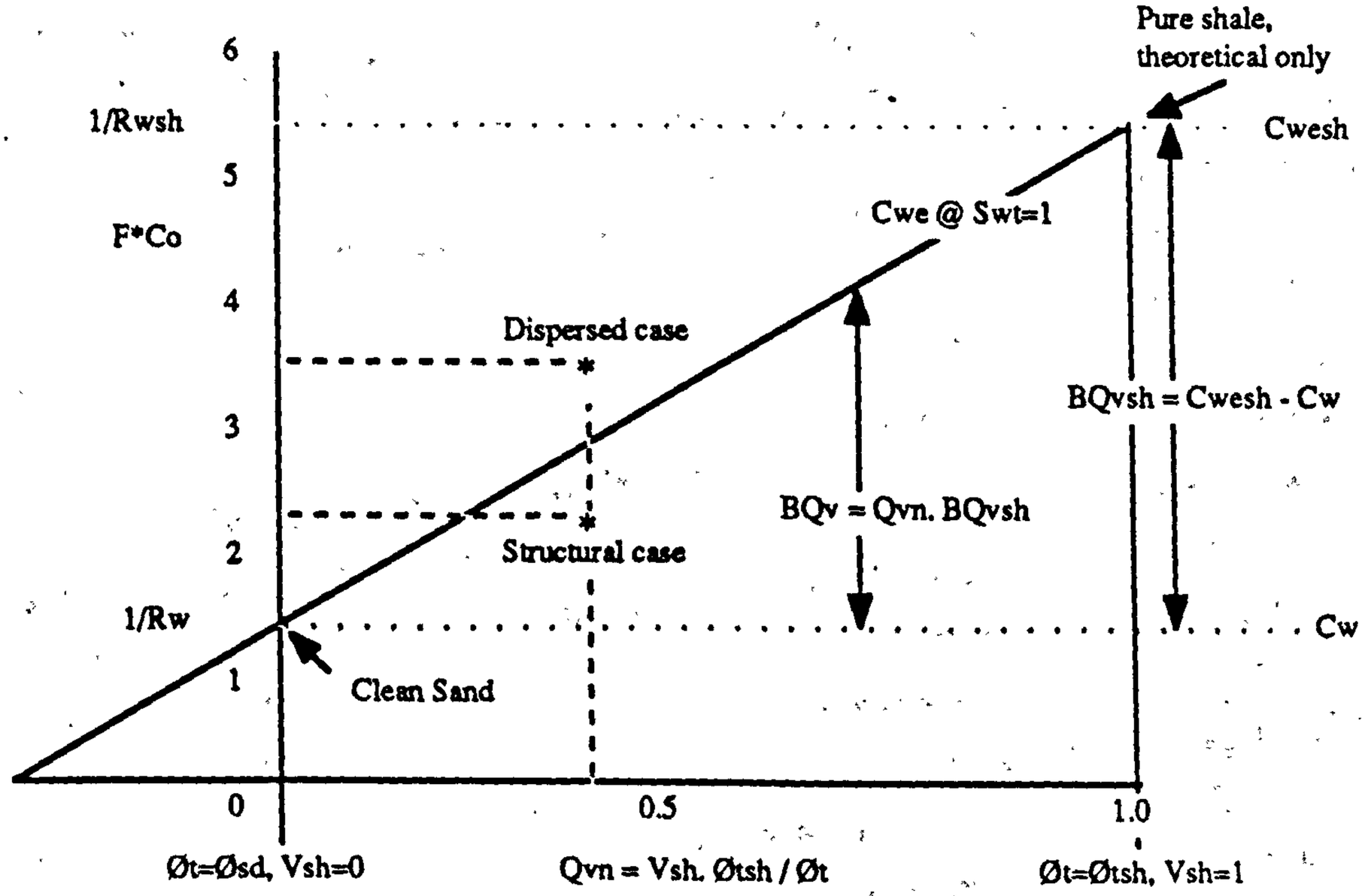


Fig p81 Proposed change in C_{we} for dispersed and structural shales in sands of identical Q_{vn} and F^* (F^* is independent of C_{wesh}). (Modified after Juhasz, 1981)

If $C_{wesh} > C_w$ then $C_{o\ dispersed} > C_{o\ structural}$
C_{wesh} = Effective water conductivity of shale.

---

[34] F_{sh} *i.e.* $\emptyset_{tsh}^{-m^*}$, is assumed to be relevant to interstitial reservoir clays.

In practice the Q_{vn} versus C_{wa} plot can be quite well defined across the water zone interval, especially if genetic units, with characteristic distributions, are treated separately. The following features will enhance this relationship:

1) Fresh formation water.
2) Homogeneous intergranular pore geometry (constant m).
3) One species, or a constant mix of clay species, across the interval.
4) Constant ratio of dispersed:structural:laminar clay across the interval (constant electrical effect per unit volume of clay).

Despite Q_{vn} being subject to these limitations, the shale conductivity term in which it appears can be log derived if a suitable water zone exists. This term is likely to have a closer correlation with C_x, over a wider range of rocks, than alternative purely empirical parameters (11). In heterogeneous rocks with complex diagenetic histories there is less reason to expect good correlation because of greater variations in 2, 3, & 4.

The Normalised Waxman-Smits Equation:

$$C_t = C_w \emptyset_t^{m^*} S_{wt}^{n^*} + [V_{sh} \emptyset_{tsh} / \emptyset_t] (C_{sh} \emptyset_{tsh}^{-m^*} C_w) \emptyset_t^{m^*} S_w^{n^*-1}$$

clean term shale term

also predicts C_t-->C_W as $\emptyset_t$-->1 in water zones, since V_{sh} -->0.

6.1.4 THE DUAL POROSITY MODEL

This model, the DPM, is an empirical synthesis of the dual water and W-S CEC models. The two waters, i.e. the dual porosities, are that of the free pore water and the clay bound water (CBW) each with their own m exponent for conversion to conductivity. The observation that a dual porosity type equation produces less scatter of computed S_W=1 points than a conductivity model is taken as justification for the dual porosity approach (Fig.1, Raiga-Clemenceau et al 1984). The DPM is developed by reworking the original W-S data. The CBW m is deduced from the regression of the C_o clay conductivity contribution versus CBW volume (Fig3: $\emptyset_t \emptyset = \emptyset_t V_q Q_v$) from all the W-S data at all four salinities. This results in an exponent of 0.86 for the CBW pore space. The clay saturation exponent, ncl, is determined by equating R_t in the W-S equation with R_t in the proposed DPM equation (p6). $\acute{R}_{wb}$, bound water resistivity, is calculated from an adjacent shale bed. The Dual Water model postulates that the conductivity of the clay water is universal depending mainly upon temperature[35] (Eqn 16, Clavier et al., 1984).

[35] Above approximately 23,000 ppm NaCl.

The DPM's accuracy will be influenced by any experimental or theoretical inaccuracies of the W-S study, and the accuracy of the log derived CBW volume.

$$(1/R_t)^{0.5} = (\emptyset^m S_w^n / a R_w)^{0.5} + (\emptyset_t - \emptyset_e)^{0.86} (S_w^{0.5n} / R_{wb})^{0.5}$$

clean term shale term

This log derived equation is a practical synthesis of theoretical and empirical work. It uses statistics to extract the best mean solution of a widely accepted theoretical model, the D-W model. Its main weaknesses are:

1) The requirement to determine $\emptyset_e$ from logs.
2) The excellent W-S data set is laboratory data and not in-situ data, and therefore cannot be identical to in–situ log parameters.
3) The W-S equation has had to be employed to obtain ncl.

This equation correctly predicts C_t -->C_w when $\emptyset_t$ -->1 only if a=1.

Numerous other saturation equations have been proposed but the ones outlined here are considered the most significant contributions. In 1982 Bussain derived a simplified Hanai-Bruggeman saturation equation at low frequencies, relevant to resistivity tools, by assuming that $1 >> (1-S_w)\emptyset_t$ (Bussain, 1982). Bussain's paper suggests classifying formations with respect to depolarisation factor, L, and rock matrix conductivity, o_r, as opposed to a and m . $a \neq 1$ can have no direct physical meaning whereas L and o_r are straightforward.

Besides the assumption that $1 >> (1-S_w)\emptyset_t$, Bussain's "Generalised Archie Equation" relies upon L and o_r, which are laboratory determined, so it does not have a continuous log derived solution. Furthermore the papers criticism of the W-S equation: that $C_t \neq C_w$ when $\emptyset_t$=1, is incorrect, since the W-S Q_v parameter necessarily goes to zero as $\emptyset_t$ goes to 1.

Predicting C_o in oil bearing shaly sands has consumed large amounts of intellectual effort compared with other formation evaluation problems. Shaly sand concepts are subtle and complex and yet rarely complete in their description of nature. Nevertheless in most reservoirs, where salinity is over 50,000ppm, inaccurate porosities, treating m as a constant when in fact it is a variable; using laboratory data for n; or being unaware of changing connate water resistivities will usually have a far greater effect on HIIP and producibility estimates.

6.2 THE SATURATION EQUATION

Log Analysts can do things in the laboratory that they cannot do in the borehole. In mind of this an *"F_g"* saturation equation has been developed prompted by the observation that wettability is a surface phenomenon - not a pore wide phenomenon. It is believed that Geometrical Formation Resistivity Factor, F_g, resulting from this concept will be independent of induced changes in wettability, with all wettability effects being confined to excess conductivity, C_x (APPENDIX 28). This study proposes two alternatives for the solution of water saturation, different in their interpretation of conductivity, the F_g model and the replaceable conductivity model.

6.2.1 THE *"F_g"* SATURATION EQUATION - EXPLANATION OF VARIABLES

For this equation reservoir samples are used to deduce:

1) Excess conductivity.
2) Geometrical formation resistivity factor.
3) A clean term saturation exponent.
4) An excess term saturation exponent.

with actual formation brines, temperatures and pressures.

The proposed F_g saturation equation:

$$C_t=(C_w/F_g)\,S_{we}{}^{n} + C_x\,S_{we}{}^{n-y}$$

C_t

The true conductivity of the undisturbed formation is a downhole measurement ($1/R_t$), the accuracy of which is subject to many influences, including but not limited to: the mud, invasion profile, adjacent beds, temperature, and the accuracy of other tools. Correction for such influences is discussed briefly in the 'Error' section.

S_{we}

The fraction of effective porosity saturated with brine in the undisturbed formation. The equation is solved for S_{we}. The desaturation plots which determine n and y (below) use total porosity for the points on the S_{wt} axis, in keeping with the Core Lab data already supplied (9.5.4.1). The resulting saturation exponents n and y are therefore calibrated to S_{wt}. For compatibility with the F_g equation the S_{wt} axis has to be converted to an S_{we} axis. This is done with the equations:

$$\emptyset_e = \emptyset_t - 0.05vlogs - (1-vlogs)V_{shsdymtx}\emptyset_{tsh}$$

$$S_{we} = 1-(\emptyset_t/\emptyset_e)\ (1-S_{wt})$$

$\emptyset_t$

Log derived porosity calibrated to core helium porosities performed on samples dried to 105°C for 72 hours. Core porosities measured at net confining pressure and corrected to uniaxial stress porosity (Juhasz, 1988). The F_g equation will use the sandy matrix value C_{tm} for C_t, and $\emptyset_e$ for porosity; $\emptyset_e$ residing in the sandy matrix only.

$\emptyset_e$

$\emptyset_e = \emptyset_t - 0.05vlogs - (1-vlogs)V_{shsdymtx}\emptyset_{tsh}$

This method of log deriving $\emptyset_e$ is important to the usefulness of the F_g equation. It links the F_g family of effective porosity parameters to the cornerstone of petrophysics: $\emptyset_{he}$. (6.2.1 *Fg:*...constant exponent.)

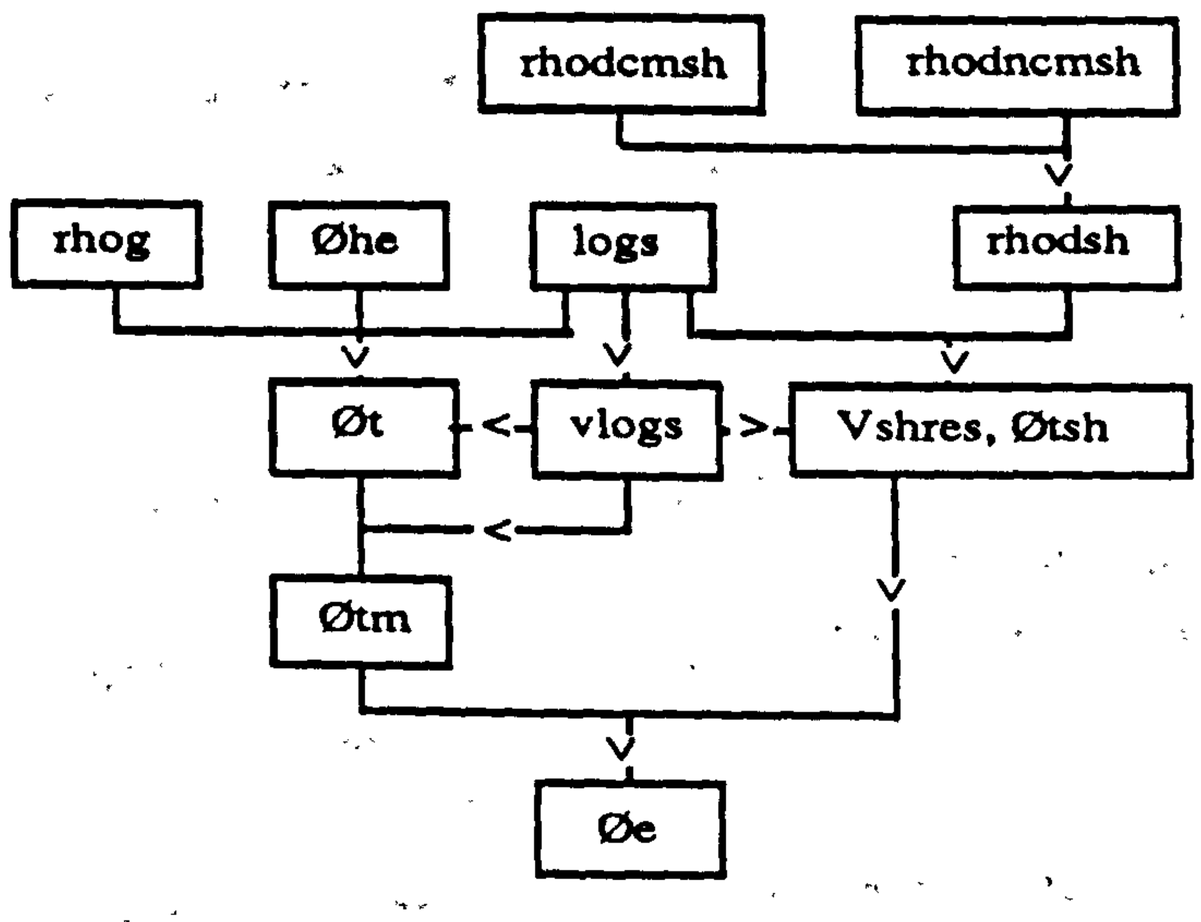


Fig p85 Origin of $\emptyset_e$, simplified (Vshres=Vshsdymtx)

C_w

The conductivity of the free formation brine is determined in the laboratory from measurement of uncontaminated recovered formation brine.

F_g Geometrical Formation Resistivity Factor.

The geometrical formation resistivity factor is defined theoretically as the conductivity of the free (replaceable) formation water, divided by the free waters contribution to C_o, water saturated conductivity. Although F_g is defined theoretically it is determined experimentally from the plotted value of the C_x intercept on the C_o v C_w plot.

$$F_g = C_w / C_{oe} = C_w/[C_o - C_x]$$

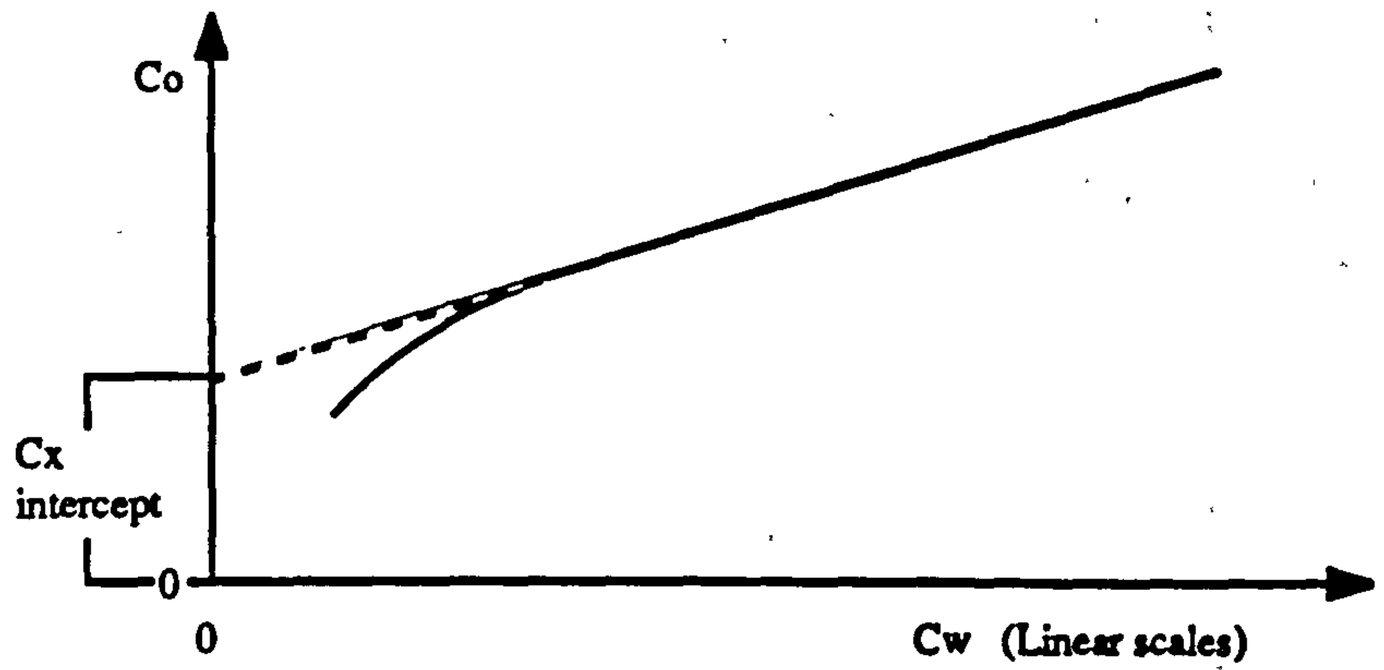


Fig p86 A single sample dilution plot for C_x

F_g is a function of the replaceable water geometry. When determined via the C_o v C_w plot F_g is more likely to be related to the geometry of hydraulic porosity than [$\emptyset_t$ - clay water] volume because of the variations in clay water geometries with shale distribution, and the difficulty of determining clay water with confidence. However when log porosities are used to predict F_g, clay water has to be invoked.

g may be empirically related to capillary pressure curves (pore throat size distribution) k_a and possibly $\emptyset_{he}$, commonly available data, since all are affected by pore geometry (Etris, et al, 1989). Although less expensive, this number would not be a theoretically exact determination of g, since strictly, g requires knowledge of C_{oe}.

In shaly samples F_g also becomes salinity dependent if the brine is fresh, ≈ < 24,000ppm, because C_x decreases. This is consistent with the variations in CBW volume at low salinities, enabling F_g to be more closely linked to the geometries of fresh water electrolytes than W-S F^*. F^* is defined by the C_o v C_w slope above the non linear

fresh water portion, even if the sample is from a fresh water formation.

F_g: Wettability.

F_g is defined as a water saturated parameter. Since no oil is present, wettability problems would not seem to be relevant. However, firstly, small changes in surface related conductivity will occur when surface properties have been changed (Mungan & Moore, 1968), even with no oil present. Secondly, the purpose of F_g is for use in intervals where the rock is not fully water saturated, thus wettability must be considered if we are to use F_g confidently where $S_w < 1$.

One of the advantages of this approach that F_g is not influenced by alterations of surface properties and therefore is not influenced by changing wettability, (APPENDIX 28).

F_g: Continuous Prediction From Log Porosity - Constant Exponent.

A porosity exponent is required to predict R_o from porosity in hydrocarbon intervals. If the log analysis does not penetrate a known water leg in a petrophysically similar rock a reservoir conditions $\log C_{oe}$ v $\log \emptyset_e$ plot is required to determine the exponent, g.

$\emptyset_e$ is that portion of the total porosity which is not involved with C_x. A portion of $\emptyset_t$ will be used for conducting C_x whenever C_x involves clays. An approximation to $\emptyset_e$ in the sandy matrix is [$\emptyset_t$-clay water]. Even if C_x is caused by non clay factors such as conductive filamentous pyrite, which does not involve porosity, clay water remains valid because in this case clay water calculates as nil, allowing all porosity to be correctly treated as $\emptyset_e$.

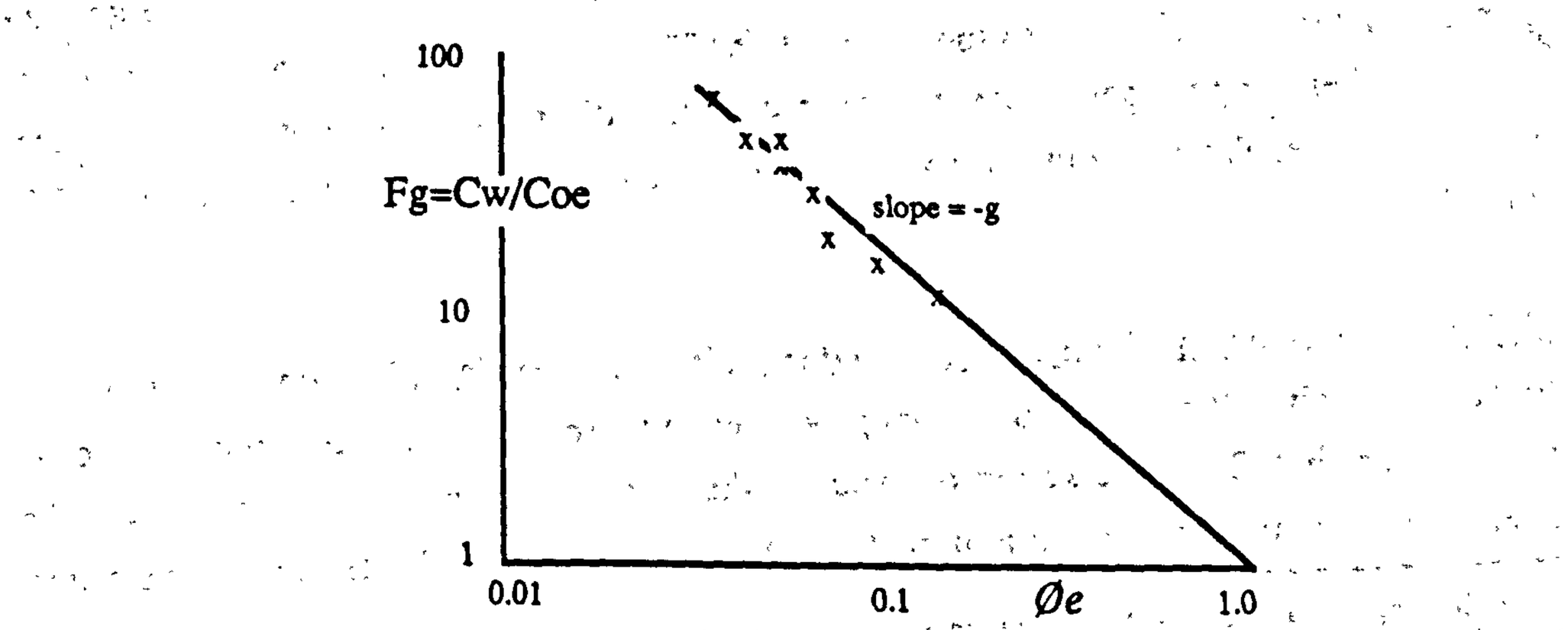


Fig p87 Log log plot to determine exponent g to $\emptyset_e$.

Unless all points lie on the line of slope -g then g is not actually a constant for all samples tested, and to treat it as a constant is an expediency. This is a cause of error in conventional log analysis where m is treated as a constant over intervals with varying degrees of shalyness, whose conductivity effects C_O and m . However, since g is derived from the free water conductivity only, it is more likely to be constant than m , derived from whole rock conductivity, and therefore subject to more variables. The only factor influencing g will be free water geometry. Free water geometry will be influenced by characteristics such as the ratio of intergranular:secondary porosity, vugs, stylolites, fractures etc. Unlike m, shale or rock matrix conduction will not influence g if C_x has been correctly determined.

F_g: Continuous Prediction From Log Porosity - Variable Exponent.

Since g is in fact not a constant,[36] any log derived parameter which can steer g is desirable. Porosity itself is a steering parameter when Archie's a from C_x=0 samples is observed not to be equal to 1. Because a must equal unity to satisfy the condition of R_O=R_W at 100% porosity, a plot where a≠1 tells us that a different porosity exponent is required for samples with different porosities (11.3). Other parameters may be able to steer g, for example comparing two S_{xo} devices, one of which is more sensitive to water geometry than the other, such as the MSFL™ and EPT™[37] (5.1). In saline formations predicting g will be more beneficial than predicting C_x.

C_x

Brine saturated excess conductivity is determined by extrapolation of the straight line portion of the C_O v C_W plot to the C_W=0 axis. This intercept is the conductivity which remains when the free pore water has been infinitely diluted to a non conductor. C_x does not involve speculation about the source of excess conductivity as do the CEC and CBW models.

C_x is the phenomenon which all shaly sand models seek to explain, but which may be due to quantitatively different, or additional processes to those modeled. It is common practise to proceed as if CEC is the key to oil bearing shaly sand analysis, when in fact C_x is the phenomenon which requires attention (6.1.2). In rocks with multiple conductive paths:

[36] While samples may fortuitously fall close to a line of slope g there is no basis to assume that the pore space of any one volume of rock will have precisely the same electrical shape as the pore space of any other volume of rock.

[37] Schlumberger Trade Mark

connate water, clay water, pyrite, interface conductivity etc., C_x should be determined from oil zone samples, and correlated with log derived parameters to provide continuous C_x. This statement assumes that different C_x values due to different diagenesis between the oil and water zone is more important than errors in C_x values caused by core handling in the tested samples. This dilemma should be treated on an individual basis following:

1) Petrographic diagenesis studies and,
2) Determining the presence/absence of uncleaned hydrocarbons affecting the apparent resistivity/porosity relationship; by destructive core analysis. (All hydrocarbons are porosity to log analysis.)

Unfortunately at formation water salinities below about 24,000ppm the rate of decrease of C_o with C_w accelerates (Fig.1: Waxman & Smits). This non linearity makes the determination of C_x more difficult. Extrapolation to C_w=0 for a sample with fresh formation water therefore involves an assumption.[38] The assumption is that a line of parallel slope would develop as C_w was increased if the CBW volume could somehow be held constant at its low salinity volume. A graphical solution is presented in the attached (APPENDIX 28). It concludes that the resulting C_x would be equal to or slightly smaller than its actual value. It should be noted that this potential error only occurs in fresh water formations. The error only concerns the accuracy of the correction for C_x required from C_x's value above 24,000ppm to C_x's value at the lower formation salinity.

C_x has a greater influence on calculated S_w at low S_ws. C_x will be influenced by changes in surface properties and therefore by changes in wettability.

n and *y*.

The saturation exponent *n* characterises the change in C_t for a change in S_w. A rock with a high *n* indicates one whose resistivity is highly affected by oil. It is arguably the most difficult parameter of Archie's original work to be made to realistically apply to complex rocks.

[38] This statement implies that non-linearity is caused solely by the clay component of excess conductivity. See Clavier et al., 1984 Fig. 9

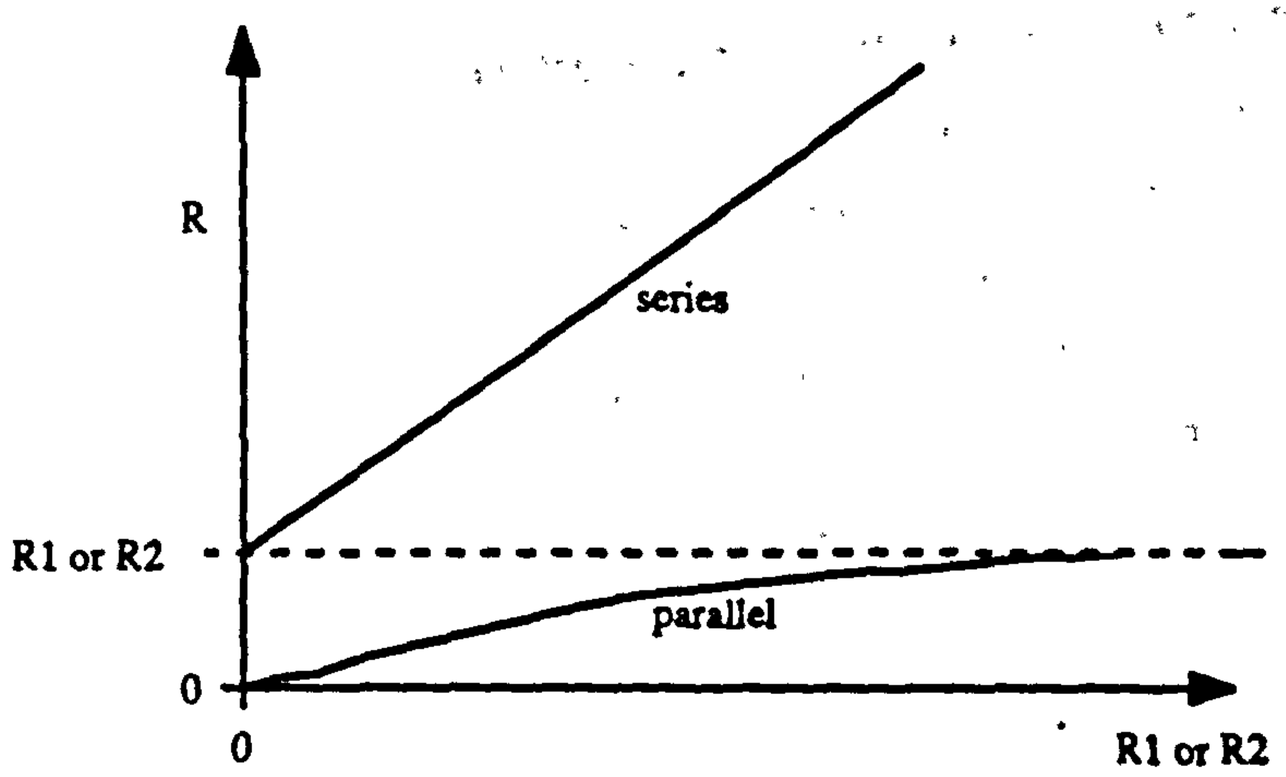


Fig p90 Nature of the change in resistivity for a change in the individual terms of a series and parallel resistance model.

As a sample is desaturated the replaceable pore water is expelled and clay conductivity, usually the largest component of excess conductivity, comprises a progressively greater fraction of the observed conductivity, as shown in Fig.2 of Patnode and Wyllie's 1950 paper. At reservoir temperatures R_t/R_O is therefore reduced, producing a flatter desaturation plot, corresponding to a lower n value (Givens, 1987).

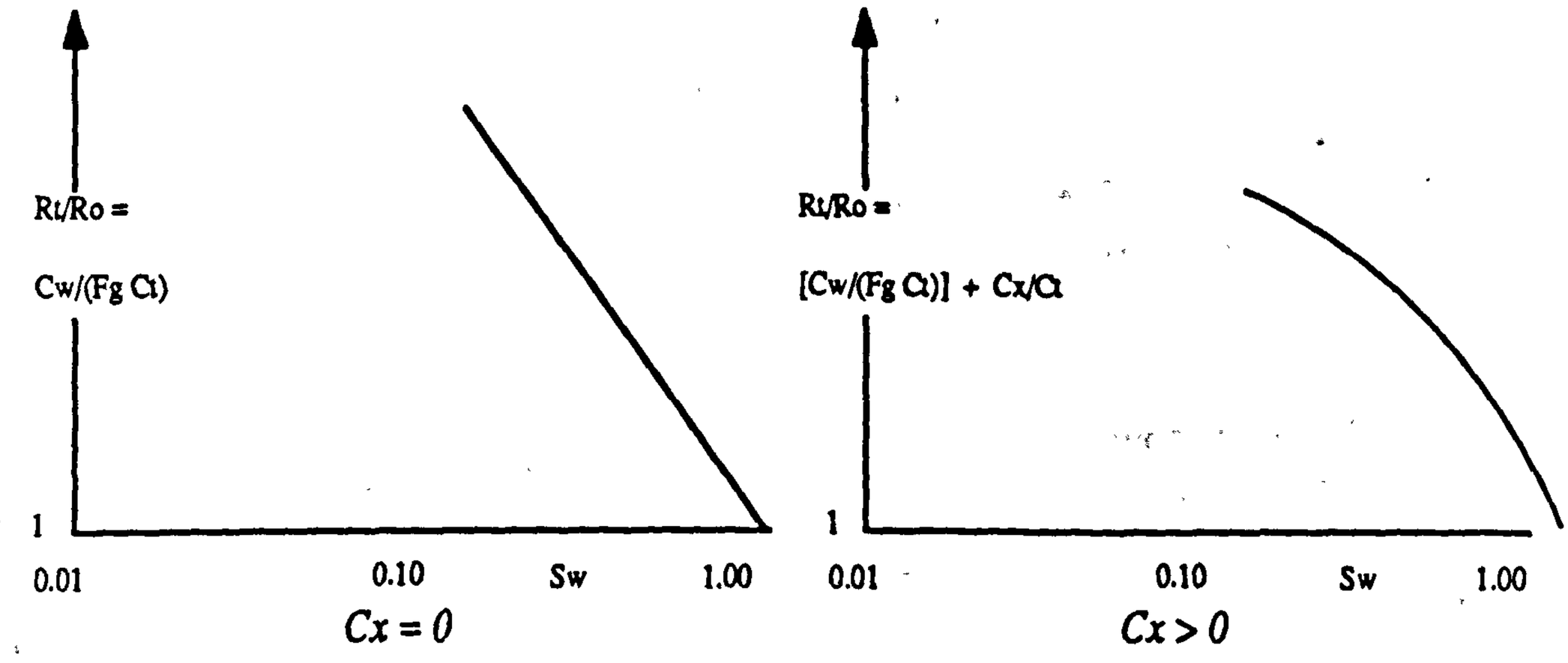


Fig p90 Change in R_t/R_O with desaturation for rocks with and without excess conductivity. Schematic.

When $C_x = 0$, $C_O = C_w / F_g$ and therefore $R_t / R_O = C_w / C_t F_g$

When $C_x > 0$, $C_O = (C_w / F_g) + C_x$ and therefore $R_t / R_O = [C_w / (F_g C_t)] + C_x / C_t$

This difference between clay and replaceable pore water conductivities as desaturation progresses is why the clay terms S_w exponent is conventionally approximated to n-1, while the clean terms S_w exponent is n.

Curvature of the desaturation plot indicates that $n \neq$ constant when $C_x > 0$, if n is defined by the slope of this line. Archie's equations did not include a term for excess conductivity, and like m , the exact significance of n becomes confusing when it is used for rocks with excess conductivity. From Archie's work on clean sands it seems logical to conclude that n is a constant with respect to S_w for the clean term of any saturation equation. However the saturation exponent's value for the excess conductivity term is problematic: The processes of excess conductivity vary and therefore the effect of desaturation on C_x varies. This problem is rarely isolated in the literature. The approach of this thesis is to nominate the C_x terms saturation exponent not as n-1 but as n-y, where $n > y > 0$. Although this introduces yet another variable, both n and n-y can be determined by the method outlined in (6.2.1.2)

An equation of the form:

$$C_t = (C_w / F_g) S_{we}^{\ n} + C_x S_{we}^{\ n-y}$$

does produce a curved desaturation plot as in Fig p below (pers com. P.Harris, 1987). The degree of curvature is a function of the $C_x S_{we}^{\ n-y}$ term.

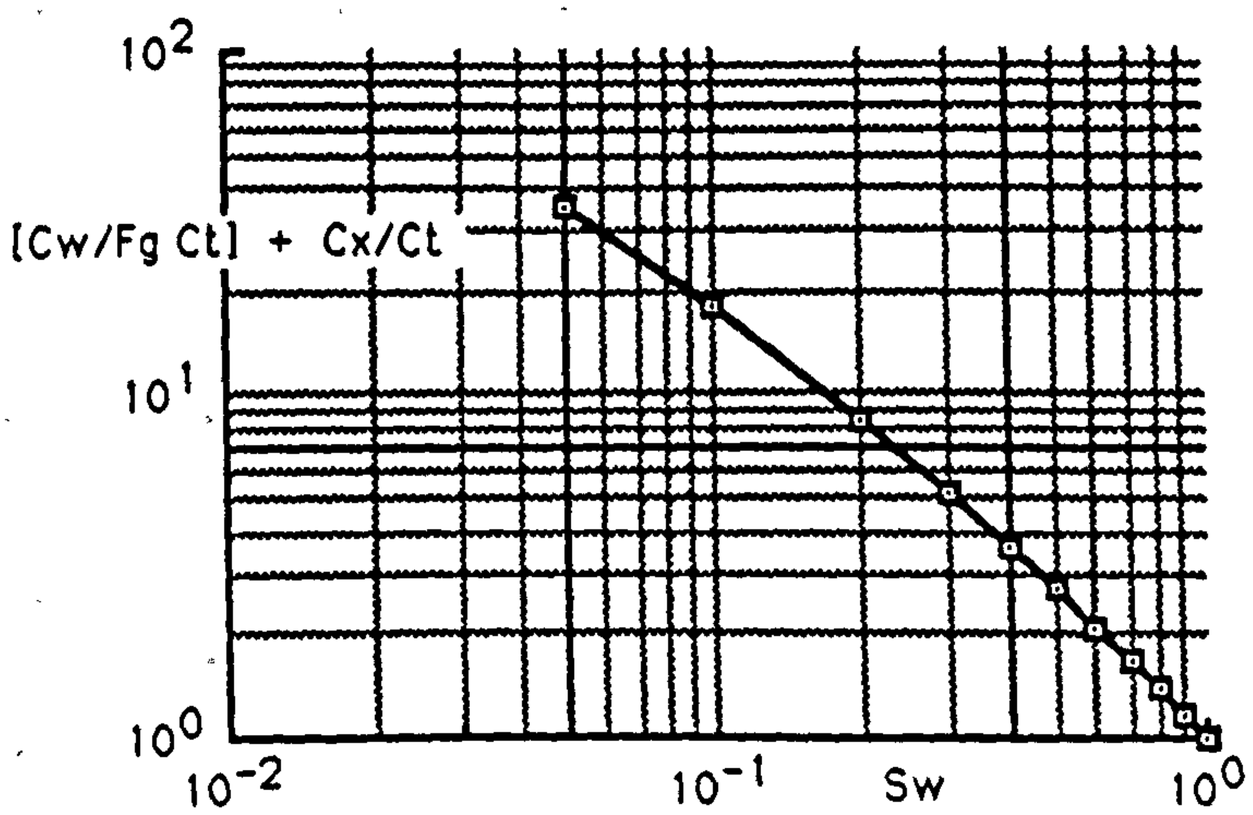


Fig p91 Desaturation when C_x equals 50% of C_w/F_g, n =1.84 and y =1

6.2.1.1 HOW IMPORTANT IS "y"?

Assuming n=2 and $n > y >$ 0, then the limits of the parallel resistance model:

$$1/R = [\,S_{we}^{n} / R_{clean}\,] + [\,S_{we}^{n-y}/R_{cx}\,]$$

are:

$$1/R = [\,S_{we}^{2}/R_{clean}\,] + [\,1/R_{x}\,] \quad \text{when } y=n$$

and,

$$1/R = [\,S_{we}^{2}/R_{clean}\,] + [\,S_{we}^{2}/R_{x}\,] \quad \text{when } y=0$$

The effect of changing y in the Brae Formation, using the F_g saturation equation, and the value n=1.84 has been calculated and plotted below, using the values for 14877ft (4535m) (Massive Coarse Sandstone) shown under (9.5.4.2)

$$C_t = [\,S_{we}^{n}\, C_w/F_g\,] + C_x S_{we}^{n-y}$$

at 14877 ft becomes:

$$0.233 = 0.523\, S_{we}^{1.84} + 0.248\, S_{we}^{1.84-y}$$

This equation cannot be solved analytically but can be solved by the Newton-Raphson iteration method. A Fortran program was written for this purpose, the results of which are shown below. (APPENDIX 29)

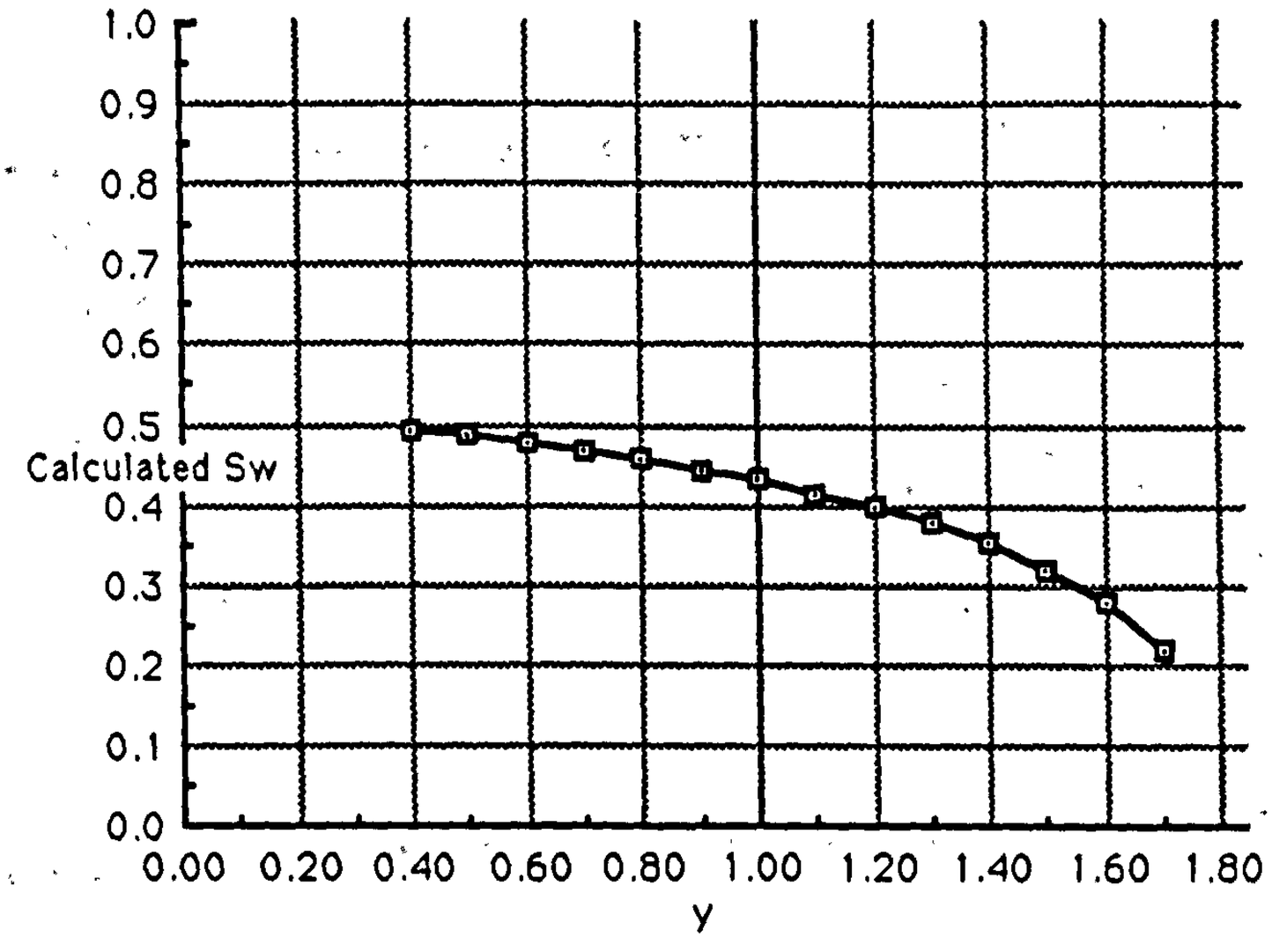


Fig p93 Effect of y on S_{we} in Brae, Industry standard: y=1

These calculations show an approximate three percent decrease in calculated S_{we} when y is moved by +0.2, through its industry standard of 1.0. The F_g equation shows S_{we} to be most sensitive to y in rocks with low C_ws, high F_gs and high C_xs; namely low porosity, fresh water formations, with a high proportion of microporosity - such rocks would be extremely difficult to evaluate with resistivity.

6.2.1.2 DETERMINING n and y.

When a desaturation curve is plotted at reservoir conditions the shape of the curve does carry information relevant to formation evaluation. Reducing it to a straight line and fixing the clean and excess conductivity exponents by the straight lines slope is to partially ignore this information. Even to use the tangent of the curve at a given saturation for n and n-1 does not address the actual value of y for that rock, i.e. the actual difference in exponents for the clean and excess terms. Clearly, in a near fully saturated rock changes in the replaceable brine conductivity strongly influence R_t. Conversely in rocks close to irreducible[39] water saturation R_t is strongly influenced by wettability and changes in excess conductivity, because at these low saturations replaceable brine has been largely

[39] No saturation is irreducible if capillary pressure is increased.

expelled whereas clay bound water remains as the major conductive path. The slope at S_W=1 is therefore most relevant to the clean term's exponent n, and the slope at S_{Wi} most relevant to the excess term's exponent n-y.

Given that the general form of the F_g saturation equation complies with an experimental desaturation plot a set of experimental C_t and S_{We} values, for an individual sample, can be used to determine values for n and y, iteratively, by the standard Newton method in two variables:

Given $C_W/F_g = a$ and $C_x = b$, (constants)
and a set of N results: C_{t_i} (i=1,2,3...N) at known S_{W_i} (i=1,2,3...N) solve:

$$C_{t_i} = a\,S_{W_i}^{n} + b\,S_{W_i}^{n-y} \quad \text{where } n > y > 0$$

in the least squares sense for n and y.
Let $n = \delta$, n-$y = \beta$, then solve the following two non-linear simultaneous equations for δ and β:

$$0 = \sum_{i=1}^{N} C_{t_i} S_{w_i}^{\delta} - a\sum_{i=1}^{N} S_{w_i}^{2\delta} - b\sum_{i=1}^{N} S_{w_i}^{\delta+\beta}$$

$$0 = \sum_{i=1}^{N} C_{t_i} S_{w_i}^{\beta} - a\sum_{i=1}^{N} S_{w_i}^{\delta+\beta} - b\sum_{i=1}^{N} S_{w_i}^{2\beta}$$

Solution of these equations provides independent saturation exponents for the clean term and excess conductivity term of the F_g saturation equation. This results in an equation of greater universality than W-S, D-W or DPM.

Do Not Lend Or Copy

Positive Features of the F_g Saturation Equation.

Less assumptions are involved in the F_g approach than the W-S or D-W approaches: no assumption is made about the source of C_x and the excess conductivity saturation exponent is not assumed to be n-1. The assumption of the F_g equation is only that the desaturation plot complies with the n and n-y form. This is certainly more universal than n and n-1 due to the increased flexibility y imparts to the equation. When C_x is not caused primarily by clays is when the W-S or D-W predictions may be expected to break down and likewise when y is most likely to deviate from unity. Wettability is likely to be a strong influence on the saturation exponent of the excess conductivity term (n-y), since excess conductivity and wettability are both associated closely with pore walls as opposed to pore centres. Unlike n-1, n–y could accommodate wettability and clay effects during desaturation, providing native wettabilities can be preserved during desaturation.

g will be more closely related to absolute permeability than m because it is only a function of $\emptyset_e$'s geometry. Thus the k_{hor} curve from core could be used with $\emptyset_e$ to generate a variable g across different rock types. See also (15.2.3.1).

The F_g equation as explained here is intended to be used in conjunction with cores tested at reservoir conditions, and if possible with reservoir fluids. Synthetic crudes and brines lacking polar compounds are likely to alter wettability and electrical measurements (Anderson, 1986a,b). These plots actually determine all the variables in the equation. Inputs for uncored intervals are then log derived by correlation of C_x with empirical log parameters. Parameters such as Q_{vn} may or may not be found to have the best correlation with C_x, and the contention is, that having followed a deterministic model thus far, correlation is now required to put the model to best use. With 20 or more laboratory C_x values a stepwise multiple-linear-regression-analysis (MLRA) involving $Th+K$, $\emptyset_n$-$\emptyset_d$, $\emptyset_t$, as independent variables, and C_x as the dependent variable, should now reveal the optimum use of these logging data. A linear expression between C_x and each independent variable must be deduced prior to this regression, and data should be edited to equally weight the full range of C_x, to avoid the creation of a meaningless statistical expression.

6.2.1.3 THE PICKETT PLOT: m and g IN THE ABSENCE OF CORE DATA

A Pickett plot is a crossplot of $\log\emptyset_t$ v $\log R_t$ (Pickett, 1966). A Pickett plot provides a straight line through water bearing intervals with the same pore geometry factor, m in this case, if these zones have insignificant excess conductivity. It also provides straight lines through other depths at constant water saturation; with the same m and C_x.

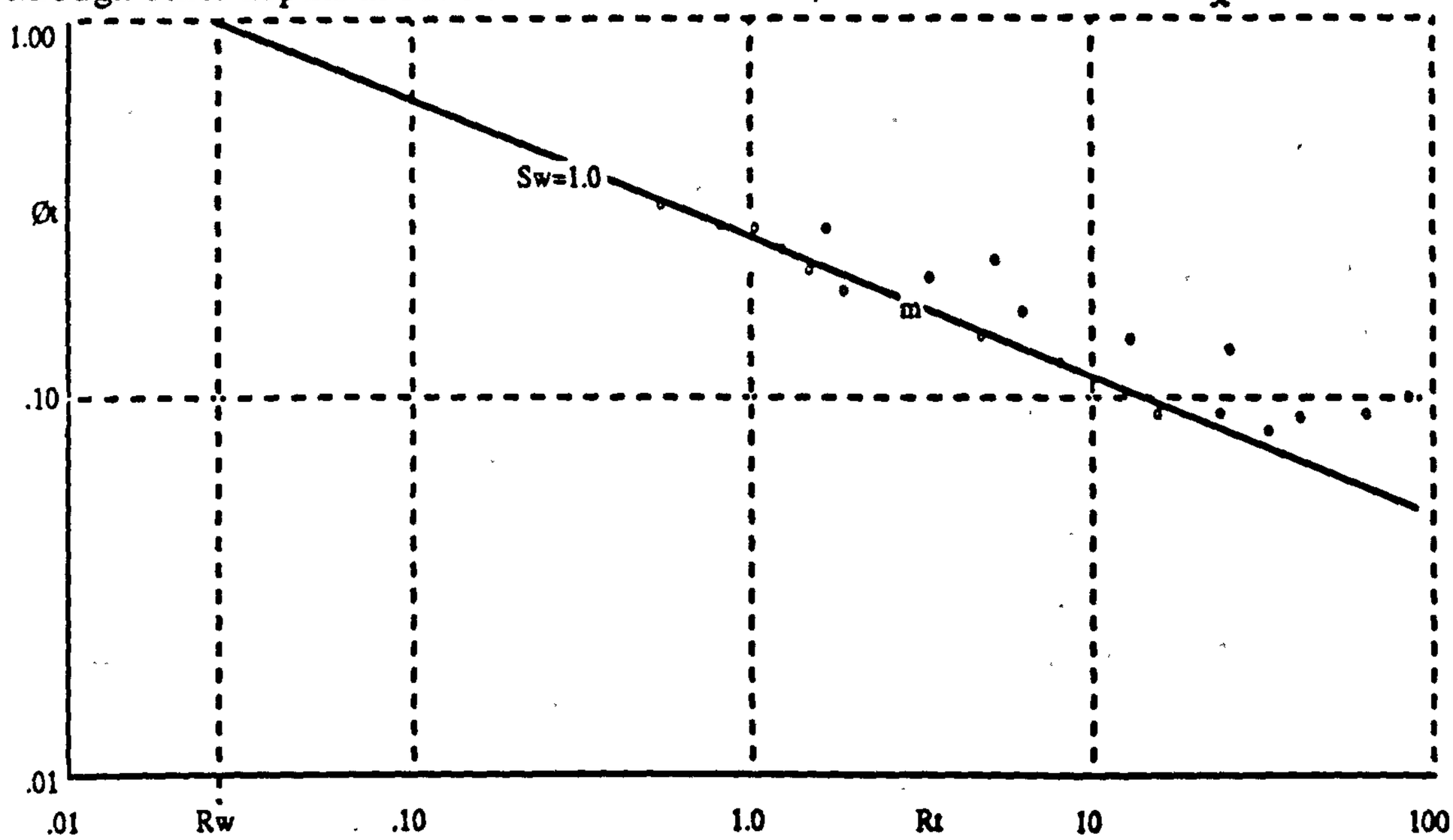


Fig p96 Pickett plot. Theoretical example.

Archie's m is related to C_O. g is related to $(C_O\text{-}C_x)$.
In zones where C_x is negligible g is related to C_O. It is evident therefore that in the absence of reliable F_g and C_x from reservoir conditions core data, g can be derived from a Pickett plot spanning water bearing clean intervals of the same rock type.

In these intervals because $C_O \approx C_O\text{-}C_x$, $\emptyset_i^m \approx \emptyset_e^g$ and $m \approx g$. We have therefore determined g from logs in clean water bearing intervals and can go on to compute F_g as a function of $\emptyset_e$. In this case we treat g as constant for lack of qualifying information.

This log method of determining the factor by which log derived porosity is to be converted into a logged conductivity should be superior to core analysis methods, especially when deep, low porosity cores have not been recovered and preserved with a view to delicate electrical measurements. Microfracturing caused during pore expansion and clay "trauma" will interfere with laboratory determinations of F_g and C_x. The crucial question is whether the effective pore geometry is similar above and below the hydrocarbon contact.

This can be qualitatively assessed by porosity, fluid corrected matrix parameters such as M, N, P; and clay typing such as $V_{shres}/(\emptyset_{\pi}\emptyset_{d})$, to highlight post emplacement authigenic changes. Even if such investigations show differences they still may not exceed the differences created between reservoir and SCAL.

The approach outlined in (6.2.1) is hoped to represent a comprehensive and exhaustive use of core for continuous log analysis. It is theoretically consistent with minimum assumptions, and maximum flexibility, and should therefore have a wide application. It borrows from other theory where corrections are necessary, but rests upon the C_o v C_w and desaturation plots of each sample. These plots are unfortunately time consuming and correspondingly expensive. Research into the economic acquisition of this data would be well justified.

6.2.2 THE REPLACEABLE CONDUCTIVITY MODEL.

This model is based upon the concept of conductivity which is replaceable by hydrocarbon emplacement and conductivity which remains after the rock has become saturated with hydrocarbon, i.e. non-replaceable conductivity. This is a realistic way of viewing the problem[40] because non-Archie behavior can be described as larger than expected conductivity, when clean oil flows from well tests spanning the high conductivity interval. i.e: residual conductivity when all movable water has been replaced by oil. The non-replaceable conductivity may be due to any source of conductivity, including but not limited to clays.

The replaceable conductivity is sourced from fluids which are free to move independently of pore walls. It will therefore be more closely related to hydraulic flow than C_o or Archie's m. Replaceable conductivity will also be related to hydraulic flow through its dependence upon tortuosity[41].

Laboratory measurements can be made of the replaceable and non-replaceable conductivities, and the corresponding replaceable and non-replaceable porosities. Unlike $\emptyset_e$ or V_{sh} models, this model is fully integratable with core data. It retains the basic advantage of a saturation model employing a porosity transform calibrated to helium core total porosities. The ability to calibrate against core is an undeniable advantage, however

---

[40] Under certain circumstances Archie's equation is unable to predict S_w or provide relevant information for production tests.

[41] R_o *clean=(Effective path length* ^{2} */Length* ^{2} *)* $(R_w/\emptyset)$ (Helander, 1983. p64)

total porosities include non-replaceable pore volume which does not contribute to storage capacity or to production rates. The two main concerns of the petrophysicist arise within the replaceable or useable pore volume. The replaceable conductivity model deals directly with the pore volumes that will or will not be affected by hydrocarbons, and also escapes from the preoccupation with cation exchange capacity.

6.2.2.1 DEFINITION OF REPLACEABLE AND NON-REPLACEABLE PORE VOLUMES.

The degree to which hydrocarbon replaces brine in the reservoir depends upon the pressure difference between the hydrocarbon and water phases, wettability, and pore size.

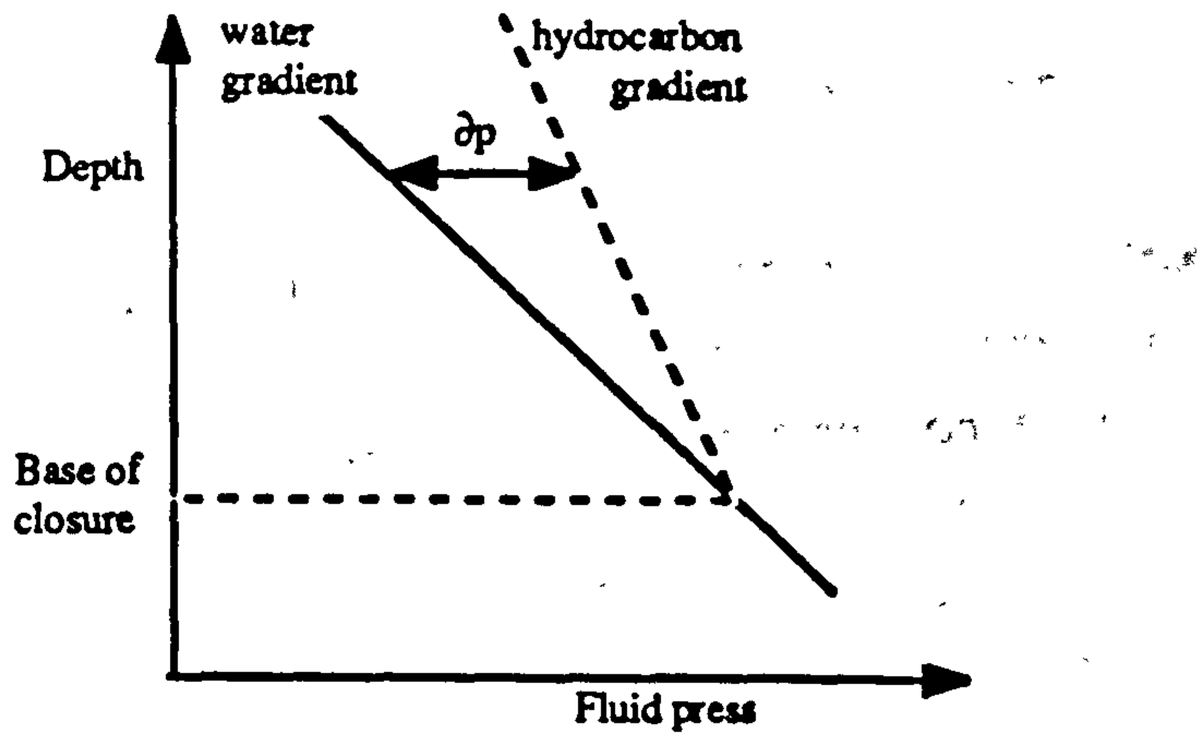


Fig p98 The pressure which determines water saturation in a reservoir.

A standard capillary pressure of 100psi using (where possible) formation fluids is arbitrarily chosen to differentiate replaceable and non-replaceable conductivities. In oil reservoirs this corresponds to approximately 1000ft(305m)[42] above the Free Water Level. The ability of the non wetting phase pressure to expel brine is sensitive to the term *TcosineØ* which is dependent upon the chemical nature of the phases present. Native state (Anderson, 1986a) samples, formation brine and hydrocarbon are therefore the preferred option for these laboratory measurements, however this may not be practical in many cases and the following is suggested:

Establish the P_C - S_W - R_t relationships with the Porous Plate Cell apparatus: use an Air-Brine desaturation system at reservoir temperatures (clays become conductive at high temperatures) on plugs with modal porosity for net pay intervals. Convert the P_C - S_W Air-

[42] P_C = *h.(rhowater-rhooil)/2.3* P_C =*psi, h=ft, rho=g/cc* . (Schlumberger,1987. p139)

Brine relation to a $P_C - S_W$ Oil-Brine relationship using the following two values of *TcosineØ* :

1) *TcosineØ* is measured on native state samples with actual formation brine and crude at reservoir temperatures and pressures, and also
2) on the Air–Brine–Sample system used for the desaturation plot (pers com. Gubbins, 1988).

Formation conditions P_C - S_W - R_t relationships are now established for typical porosities. $1/R_t$ at a formation conditions P_C=100psi is designated as X mho/m. X being the conductivity, at reservoir conditions, provided by the S_W remaining when crude has replaced brine to an extent equal to 100psi of capillary pressure.

The saturation equation used for this interpretation is:

$$C_t = C_w \, \emptyset_r^{\beta} \, S_{wr}^{n} + X \, S_{wr}^{n-y}$$

This equation gives the saturation of the pore space, $\emptyset_r$, which would be hydrocarbon filled by a formation hydrocarbon-brine capillary pressure of 100psi. Any conductivity above X indicates brine in the "replaceable" pore space.
When S_W -->0 of the P_C=100 replaceable pore space then C_t —>X.

6.2.2.3 FINAL S_W: P_C - S_W - R_t METHOD.

When the P_C - X relation existing in the reservoir has been revealed by the laboratory procedures, and the FWL has been determined from an initial S_W log analysis using X_{100}, then X_{100} in the equation may be replaced by X_{pc}, a function of height above FWL. However, $X_{pc} < X_{100}$, this is necessary to avoid X—>C_t as P_C-->0 below hydrocarbon water contacts.

In a reservoir of homogeneous pore geometry - in which all core plugs capillary pressure plots are identical X_{pc} would always be accurate. Changing pore geometries could be accommodated by a 3rd dimension for the *height* - X_{pc} plot, e.g. f.($\emptyset$,V_{sh}), such that X_{pc} lies on a surface defined by height and f.($\emptyset$,V_{sh}).

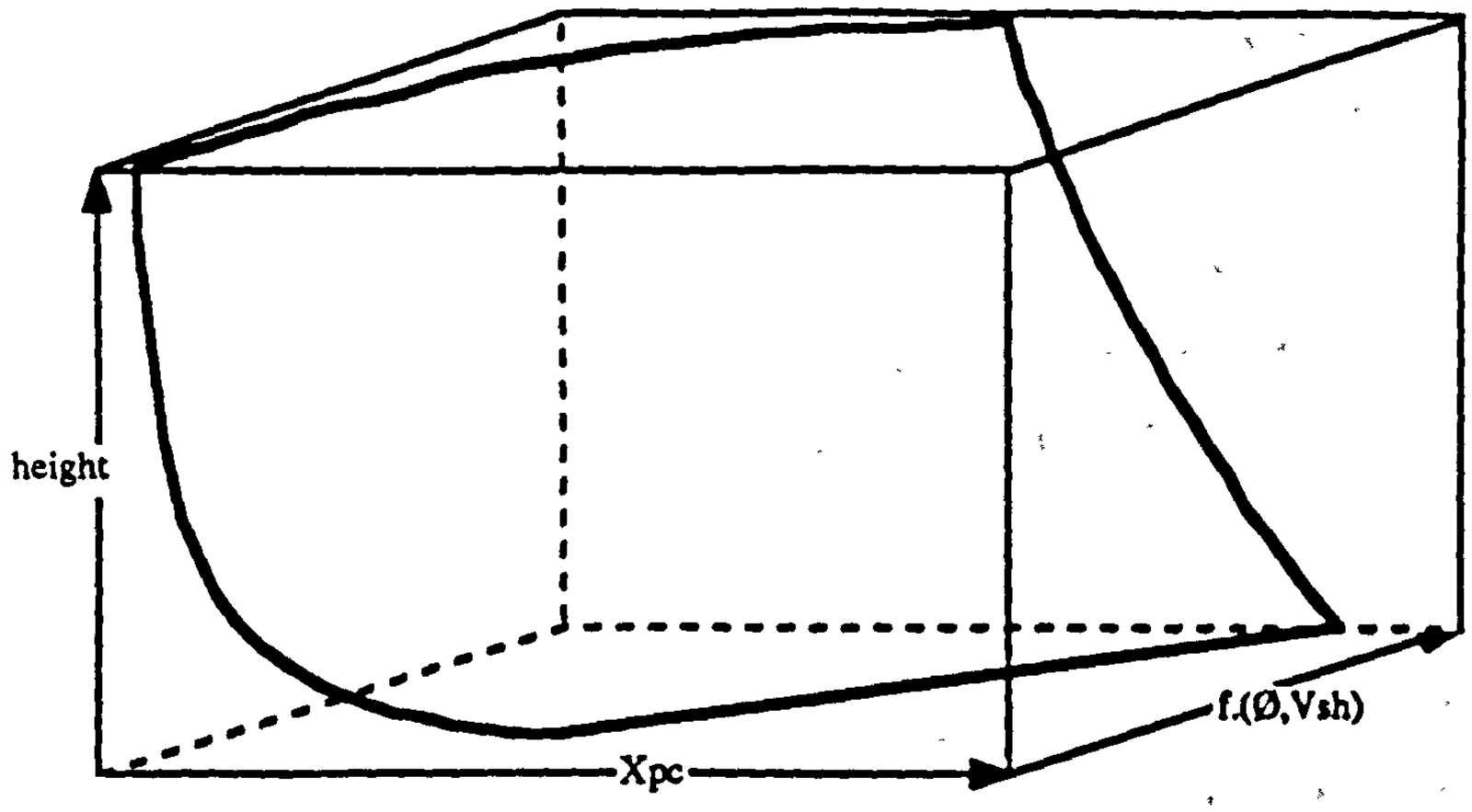


Fig p100 Hypothetical example of X_{pc} defined by height and pore geometry.

Because of its direct dependence upon the P_c - S_w relationship this S_w should provide the best log predictions of water cut. The ability of core analysis to reproduce reservoir conditions will be important to this S_w.

6.2.3 COMBINING THE "F_g" AND "*Replaceable*" MODELS

The F_g Saturation Equation and the Replaceable Conductivity Model are very similar concepts. They are both concerned with isolating 'free' or 'replaceable' pore volumes from 'bound' or 'non-replaceable' volumes. Successful determination of the non–replaceable volume, and its electrical properties at various replaceable pore volume saturation levels, S_{wr}, enable a correct evaluation of the replaceable pore volume, i.e. a correct analysis of the reservoir volume. A consideration of the two models reveals that air/brine capillary pressures at near reservoir conditions, simultaneous with conductivity measurements, can provide all the necessary information to 1) quantify the two pore volumes, 2) calculate a replaceable pore volume formation factor, and 3) provide saturation exponents for each pore volume.

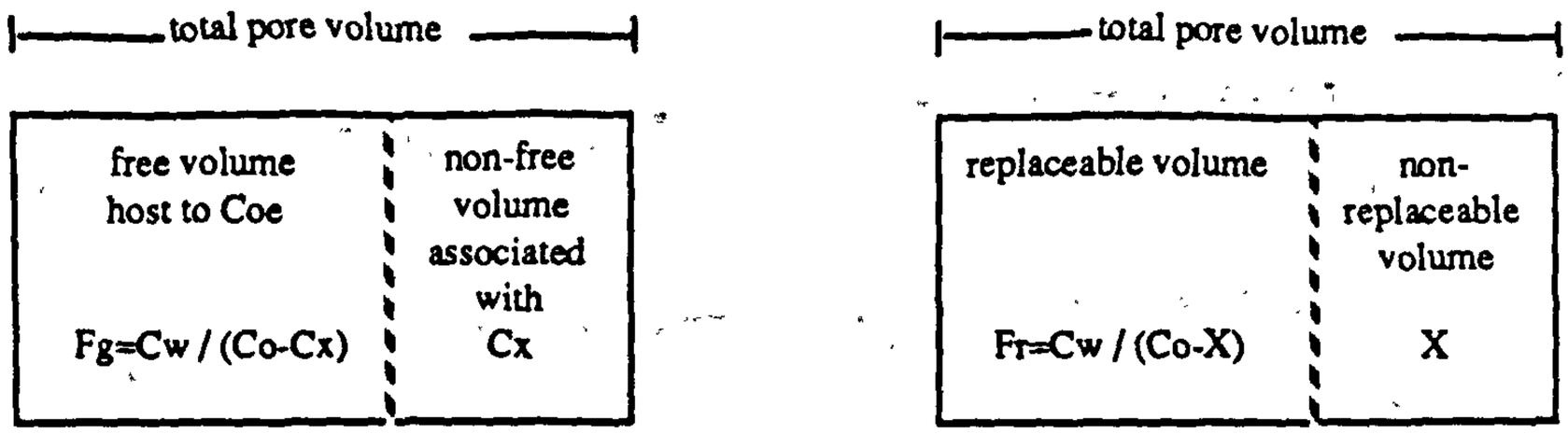


Fig p101 Similarity of F_g and Replaceable saturation models.

The F_g model allows C_x and F_g to be determined by a dilution plot, but the pore volume associated with C_x and F_g are not directly measurable by experiment, only through theoretical considerations. Conversely the replaceable and non-replaceable pore volumes are directly measurable, together with their corresponding conductivities.

$\emptyset_X = \emptyset_t \, S_{wt}$ @$P_{cA/B100psi}$

$\emptyset_r = \emptyset_t - \emptyset_X$

X = conductivity @ $P_{cA/B100psi}$, reservoir temperatures.

$C_r = C_o - X$

$F_r = C_w / C_r$

These are related in a saturation equation of the form:

$$C_t = C_w \, \emptyset_r^{g} \, S_{wr}^{n} + X \, S_{wr}^{n-y}$$

Saturation exponents are derived from a reservoir conditions desaturation plot as described in 6.2.1. The log derivation of $\emptyset_r$ and X rests upon correlation with suitable parameters, such as those mentioned elsewhere, particularly in (6, 8 & 11). The advantages of this model are that all "noise" effects on resistivity interpretation are isolated to the non–replaceable pore volume, its volume and conductivity are determined in the laboratory, allowing the signal from the useful reservoir volume to be interpreted with greater accuracy.

7 DIFFUSION & PERMEATION in HETEROGENEOUS MEDIA

Before the oil saturation of the sandy matrix can be known sandy matrix porosity and sandy matrix conductivity (C_{tm}) must be known; but tool readings are derived from both clasts and matrix. The object of this chapter is to explore means of deconvolving the sandy matrix conductivity from logs so it can be substituted in the F_g or Archie saturation equations.

It might be imagined that because clast porosities are lower than matrix porosities the effect of clasts in log analysis will be automatically dealt with via the log derived porosity computation. To some extent this is true; and is the assumption of most operators in this formation. However this is the case only if all the factors in the saturation equation are the same for both matrix and clasts. Optical thin sections suggested considerable differences in pore geometry and excess conductivity. Some qualifying investigation seemed necessary.

Clays and clasts cause problems because they have porosity which does not contribute to the reservoir and which conducts independently of the matrix porosity oil saturation. Clasts also have high and variable grain densities. V_{clasts} cannot be treated as V_{clay} because of the different electrical effect a geometry of large ball like objects has from the geometry of a more continuous and conductive network of V_{clay}.

Blood is like a conglomerate in that it consists of discreet objects dispersed in a continuous phase. Platelette counting techniques in medicine pointed towards work on diffusion in heterogeneous media as the most promising way of deconvolving the bulk conductivity of conglomerates. C_m can then be substituted for C_t in the saturation equation over conglomeratic intervals.

7.1 THE DIFFUSION EQUATION

Diffusion is a net movement of particles in response to a concentration gradient (see Nelkon & Parker, 1970 p236). The problem of understanding and predicting diffusion rates in heterogeneous media is a classical problem and has occupied the minds of many diverse workers for decades, amongst them, Graham, 1869; Maxwell, 1873; Bruggeman, 1935; de Vries, 1952 and more recently Barrer, 1967.

For the purpose of this problem, interpreting the conductivity of conglomerates, conductivity may be treated as a diffusion of charge in response to a potential gradient. Maxwells equations of electromagnetic theory may be solved for any combination of mingled phases. However, the interfaces must be completely defined in terms of shape and the contrasting physical properties which the interfaces separate. For a natural assemblage of clasts in sandstone this becomes extremely complex due to the irregular shapes, and the presence of more than a single interface of contrasting physical properties. Successive theoretical formulations for diffusion through a composite of phase A in a continuous phase B have been deduced for special cases. For example a suspension of spheres by Bruggeman (Bruggeman, 1935):

$$(1-v_A) = [(e_A - e)/(e_A - e_B)]\ [e_B/e]^{0.5} \quad \text{(Barrer, 1967)}$$

v_A = volume fraction discontinuous phase A

e = mean or gross dielectric permeability

e_A = phase A dielectric permeability

e_B = phase B dielectric permeability

Log analysts meet a variation on this equation during the interpretation of a formation's bulk dielectric constant in terms of porosity and depolarisation factor:

$$\emptyset = [(e - e_m)/(e_w - e_m)]\ [e_w/e]^{L} \quad \text{(Sherman, 1983)}$$

e = complex dielectric constant

e_m = rock matrix (solid grains) complex dielectric constant

e_w = fluid dielectric constant

L = depolarisation factor

None of the above formulations are general enough to accommodate irregular shapes and

sizes as well as small and large volume fractions of inclusions. The most general formulation was found to be a dispersion of rectangular parallelipeds. In this equation any dimension of the paralleliped may be varied to meet its neighbour, in one or more than one direction (Barrer, 1967). This model therefore accommodates inclusion volume fractions from 0-1, and inclusions of cubes, boxes, laminae, or rectangular rods in any one of three orientations; and predicts net diffusion (conductivity) of the whole assemblage. This rather complex equation has been chosen to represent conglomerates because of the broad range of geometries it accommodates.

The mean overall diffusion coefficient, D, is formulated thus:

$$D = l / l_A \left[\left\{ \left[l v_A \beta_A k D_A \right] / \left[l_A + (l_B \beta_B k D_A / \beta_B y D_B) \right] \right\} + \left\{ \left[(l_A - l v_A) \beta_A' D_B \right] / \left[l_A + (\beta_A' l_B / \beta_B' y') \right] \right\} \right]$$

(Barrer, 1967 p188), where:

l = total length of heterogeneous body, unity, $l = l_A + l_B$

l_A = fractional total effective length of charge through phase A

l_B = fractional total effective length of charge through phase B

v_A = volume fraction discontinuous phase A

k = partition coefficient

$y, \beta_A, \beta_B, y', \beta_A', \beta_B'$ = k dependent non parallel flow coefficients

D_A = diffusion coefficient of phase A

D_B = diffusion coefficient of phase B

When the diffusion model is used to model conductivity the partition coefficient, k, may be taken as unity (Winlowe, 1987): since there is no buildup of charge at interfaces, and the ratio of charge concentrations in A and B is unity (see also Barrer, 1967).

If $D_A < D_B$; then:

$$y<1,\ y'>1,\ \beta_A<1,\ \beta_B>1,\ \beta_A'>1,\ \beta_B'<1;$$

If $D_A = D_B$ the partition coefficient, k, is unity and all non-parallel flow coefficients become unity. (Barrer, 1967. p189)

7.2 APPLICATION TO CONGLOMERATE FORMATIONS

To apply Barrer's equation to conglomerate interpretation four assumptions are necessary:

1) $C_{t\ horizontal} = C_{t\ vertical}$
2) A particular geometry of parallelipeds exists which adequately describes the conductivity behavior of a conglomerate, when C_{tm} is a variable.
3) Non parallel flow coefficients = 1[43]
4) The clasts low porosity, ≈.05, high clay content and frequent encasement within a skin of diagenetic minerals makes their S_{wi} in the oil zone ≈ 1.0, i.e. C_{OC} = constant regardless of S_{wm}.

The above equation in log terms now becomes:

$$C_t = 1/d\left[\ \{\ [vC_{oc}\ ]\ /\ [\ d+(\ bC_{oc}/C_{tm}\ )\ ]\ \}\ +\ \{\ [(d-v)C_{tm}\ ]\ /\ [d+b]\}\right]$$

where:

C_t = conductivity true, log derived

v = volume fraction clasts, log derived

C_{oc} = conductivity of water saturated clast, constant

C_{tm} = conductivity true of conglomerate matrix

d = shape factor relevant to the effective length of charge through clasts

b = shape factor relevant to the effective length of charge through conglomerate matrix.

This is a general equation for water and oil zones. *a* and *b* may be conceived of as shape factors which convert the natural assemblage of clasts and sandstone matrix into the equivalent paralleliped geometry. Since under these circumstances unit lengths, not specific lengths, are used in the Diffusion Equation, the sum of the constants d and b is unity (Parker, 1987).

---

[43] This assumption was discussed with Winlowe and Parker of the Dept of Physiological Flow, Imperial College, and it was decided to proceed with this approach to the interpretation of conglomerate conductivity.

Therefore substituting $b = 1 - d$, the diffusion equation's simplest form becomes:

$$C_t = 1/d\left[\left\{\left[vC_{oc}\right]/\left[d+((1-d)C_{oc}/C_{tm})\right]\right\} + \left\{(d-v)/C_{tm}\right\}\right]$$

Having deduced the constant from actual rocks in the water zone, where $S_{wm} = 1.0$, the Diffusion Equation may be used to derive C_{tm} from the logged C_t and log derived v (*vlogs*) in intervals where $S_{wm} < 1$. C_{OC} is a constant.

7.2.1 DERIVATION OF THE CONSTANT *d* FROM ACTUAL ROCK

Rearranging for *d*, after considerable manipulation we have:

$$d^2\left[\left\{C_t(1-(C_{oc}/C_{tm}))\right\}-(C_{tm}-C_{oc})\right]+d\left[\left\{C_tC_{oc}/C_{tm}\right\}-C_{oc}+v(C_{tm}-C_{oc})\right]=0$$

After introducing the term C_{OC}/C_{tm} where possible and substituting $C_{OC}/C_{tm} = X$ we have:

$$d=\left\{C_{tm}[X/(1-X)]-vC_{tm}-C_t[X/(1-X)]\right\}/\left\{C_t-C_{tm}\right\}$$

In a known $S_{wm}=1$ interval a known value of *v* from core is now used to determine *d*.

Determining C_{tm} and C_{OC}

However, to solve for the constant *d*, C_{OC} and C_{tm} are also required for *X*. The exact value of these is more difficult to decide upon than is at first apparent. A large enough volume of 100% clasts does not exist over the large volume which typically influences R_t. The porosity and excess conductivity of the matrix which occurs in this near 100% clasts volume needs to be typical of the zone over which the Diffusion Equation is intended to be used. This problem was considered at length, and finally dealt with in the following manner:

It was thought best to obtain a good estimate of $F_{clast}:F_{matrix}$, without assuming $m_{clast} = m_{matrix}$. This was done from two independent sources of data.

1) $F_{clast}:F_{matrix}$ from laboratory core conductivities.

The average slope (F) of the typical coarse sand matrix plugs is:

$$52+53+91+77+68+53+77 / 6 = 79$$

The average slope of the clasts is:

$$200+395 / 2 = 298 \text{ (from table)}$$

$$F_{clast} : F_{matrix} = 3.8$$

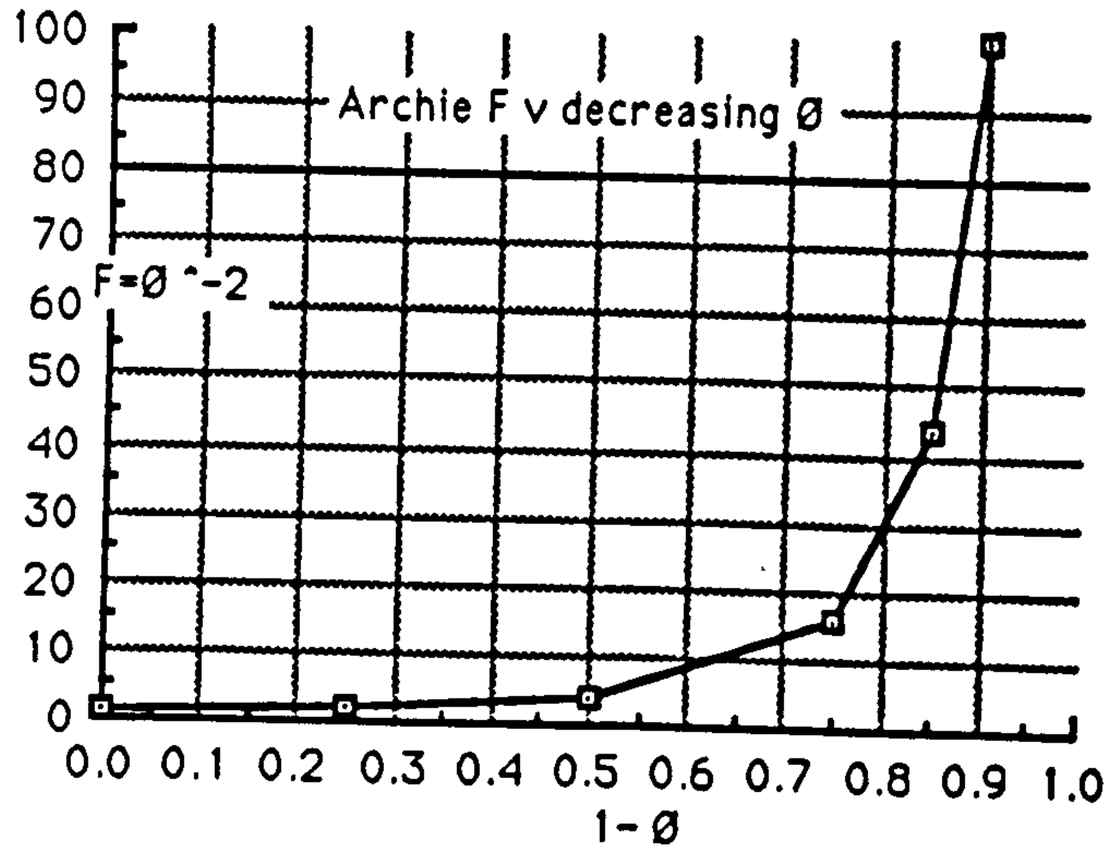
Note. At room temperature excess conductivity is negligible and Archie's F will be higher at room temperature than reservoir whereas F_g and F^* will be approximately equal to F measured at room temperature, i.e.

$$F_{measured\ rm\ temp} \approx F_{g\ res} = F^*_{res}.$$

2) $F_{clast}:F_{matrix}$ from core photographs and log R_O.

Clast to matrix ratio from core photographs can be coupled with corrected log R_Os. To obtain a meaningful plot the data set must be in the same formation, facies, and from similar depth and mud type (11.1). The data was obtained from Mr. H. King of Marathon Oil Co. It was tabulated as $\%clast$, C_{ocgl}, and $F_{cgl\ res\ temp}$ using C_w =35.71 (R_w =.028) and is plotted overleaf.

The form of the curve fitted to this plot is not obvious. The nature of the curve fit was based upon Archie's relationship. The analogy is that of a decreasing volume fraction of conductor, porosity, with an increasing F, the Archie situation, and, a decreasing volume fraction of the more conductive phase of the conglomerate, the matrix, with an increasing F for the bulk conglomerate. The fit is assumed to be a second order polynomial since Archie's m =2. Additional data from more water zone cored wells could clarify this relationship, however in this case the most had to be made from the limited data available.



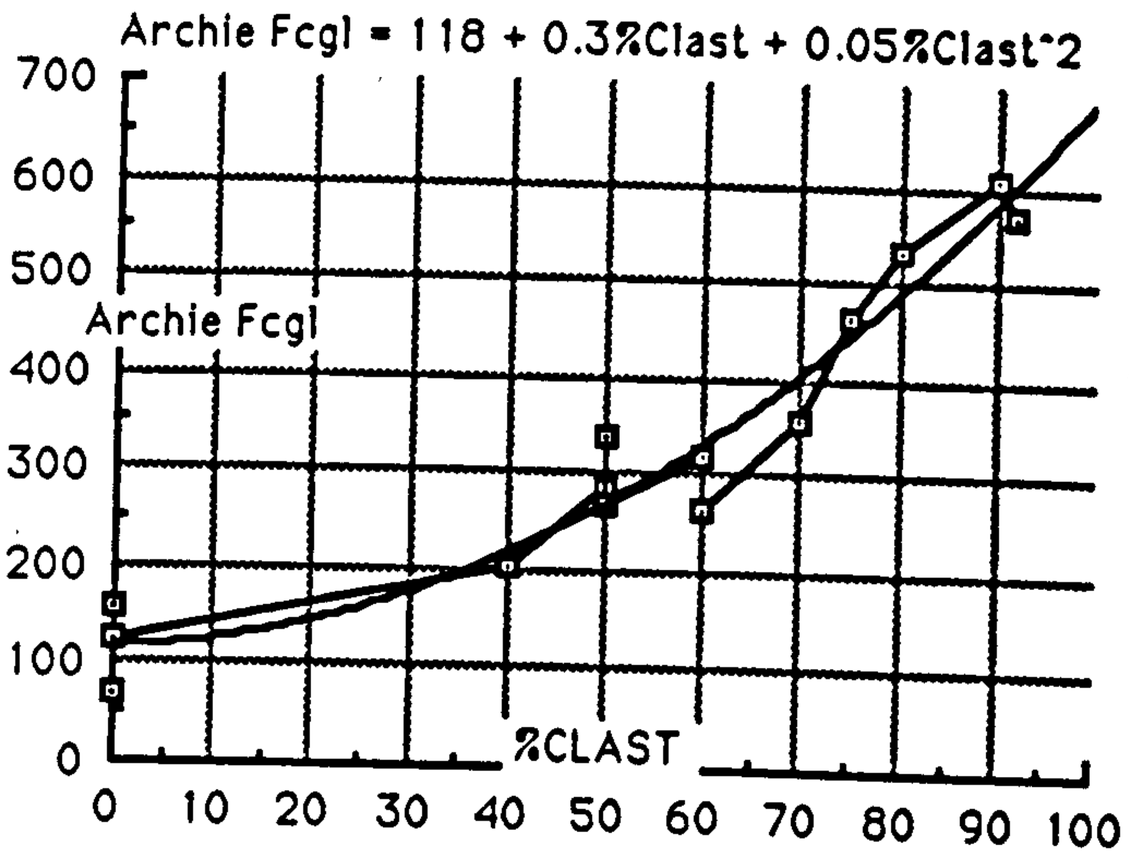


Fig p108 Analogy of Archie Ø-*F* concept with *%matrix sand-*F_{cgl}. Data from water zone logs and core clast:matrix ratios.

$$F_{clast} = 648, F_{matrix} = 118$$

$$F_{clast}:F_{matrix} = 5.5$$

Do Not Lend Or Copy

Both methods have significant error for different reasons, however the clasts and matrix do have divergent conductivities and the tool readings are convolved readings. These preliminary steps go some way towards the deconvolution of R_t.

The *Fclast:Fmatrix* value chosen was conservative at 4.1. This gives:

$$C_{oc} = .074, \quad C_{tm} = .303,$$

at reservoir temperatures in the water zone.

These values will now be substituted in the d, X equation, deduced four pages earlier, to solve for the constant d. We can then use C_{tm} in the saturation equation to solve for matrix sand oil saturation in conglomeratic intervals.

7.2.2 SENSITIVITY OF CONSTANT d TO VARIATIONS ENCOUNTERED IN A NATURAL ASSEMBLAGE OF OIL BEARING CONGLOMERATES

The equation for d(7.2.1) was solved for various values of v, volume fraction clast, and their corresponding logged water zone C_os. The results were tabulated and are plotted below.

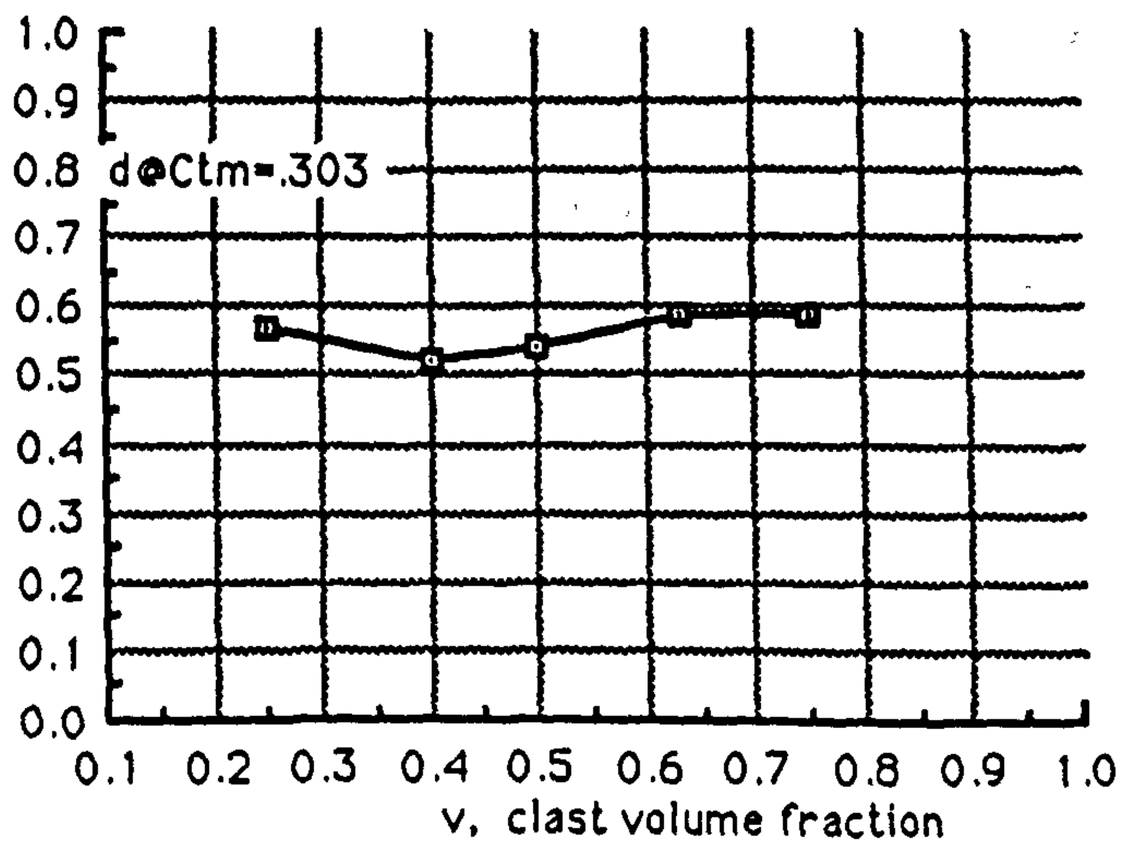


Fig p109 Instability in the calculated value of constant d from the equation in 7.2.1.

$$d \approx 0.57$$

However $d = f.(v, C_{oc}, C_{tm})$. C_{oc} is assumed constant. Determination of C_{tm} is the

object of the Diffusion Equation because C_{tm} matrix oil saturation can be determined from C_{tm} and $\emptyset_m$.

Various values of C_{tm} were calculated for various matrix oil saturations using Archie. The Diffusion Equation was then used to solve for C_{tm} using oil zone log values of C_t, core photograph values of v, and C_{oc} set at .074. It was found that the equation gave very low values of C_{tm}, corresponding to values for S_{wm} of 3-7%.

Although it is believed that the proper application of this equation is the theoretically sound and universal solution to the formation evaluation of conglomerates the inferred variance of d with the ratio $C_{tm}:C_{oc}$ requires iteration loops, or other procedures. Having already spent large amounts of time on this subject further research must remain beyond the scope of this thesis due to the limited time available[44].

The Diffusion Equation remains a strong candidate for solutions to problems of log interpretation which are currently dealt with empirically, the empirical solution only being available within one formation or facies. Calculating the "constant" d in <u>known</u> S_w intervals is a numerical index of that rocks component geometries over the volume of R_t because the Diffusion Equation was developed for a geometry of parallelipeds. d in bioturbated sands and shales for example could be indicative of horizontal fluid flow properties.

[44] Further research on this topic should be addressed to the footnoted assumption 3) on p104, and/or iteratively treating $d = f(C_m, C_{oc})$

7.3 DECONVOLUTION OF CONGLOMERATE CONDUCTIVITY: THE EMPIRICAL APPROACH

Core clast:matrix ratios, well defined OWCs and a good R_t log can be combined in a chart which solves for C_{tm}. The saturation equation may then be solved for the matrix unperturbed by the presence of clasts.

The first requirement is to create a chart from log data corresponding to the mean matrix porosity, porosity exponent and excess conductivity. i.e. a chart which depicts a typical S_{wm} - C_{tm} relationship. Normalising to the mean creates a matched data set for the C_{tm} chart and minimizes the error when calculating S_{wm}. R_w is taken as constant over the interval for which the chart is to be used.

The second requirement is to create a *linear* C_o to *%clast* relationship, a straight line plot. The horizontal axis parameter itself does not matter: its function is merely to introduce the influence of the clast:matrix ratio on the logged conductivity, in the simplest possible way. Linearity is achieved by converting the *%clast* axis into a $1/F_{cgl}$ axis. By definition $1/F_{cgl}$ has a linear relation to C_{ocgl} since

$$C_{ocgl} = C_w / F_{cgl}.$$

Since we have an equation for F_{cgl} in terms of clast:matrix ratio:

$$F_{cgl} = 118 + 0.3\%clast + 0.05\%clast^2,$$

the continuous clast:matrix ratio from logs can provide a point on the horizontal axis for any logged depth. Logged C_t and $1/F_{cgl}$ will intersect on a line of constant S_{wm}. This line is projected back to the matrix axis to the left which provides C_{tm}. C_{tm} and $\emptyset_{mt}$ are now used in the saturation equation in the normal manner.

Overleaf:

Fig p112 The C_{tm} Chart. Deduction of C_{tm} from logged C_t and *vlogs*.

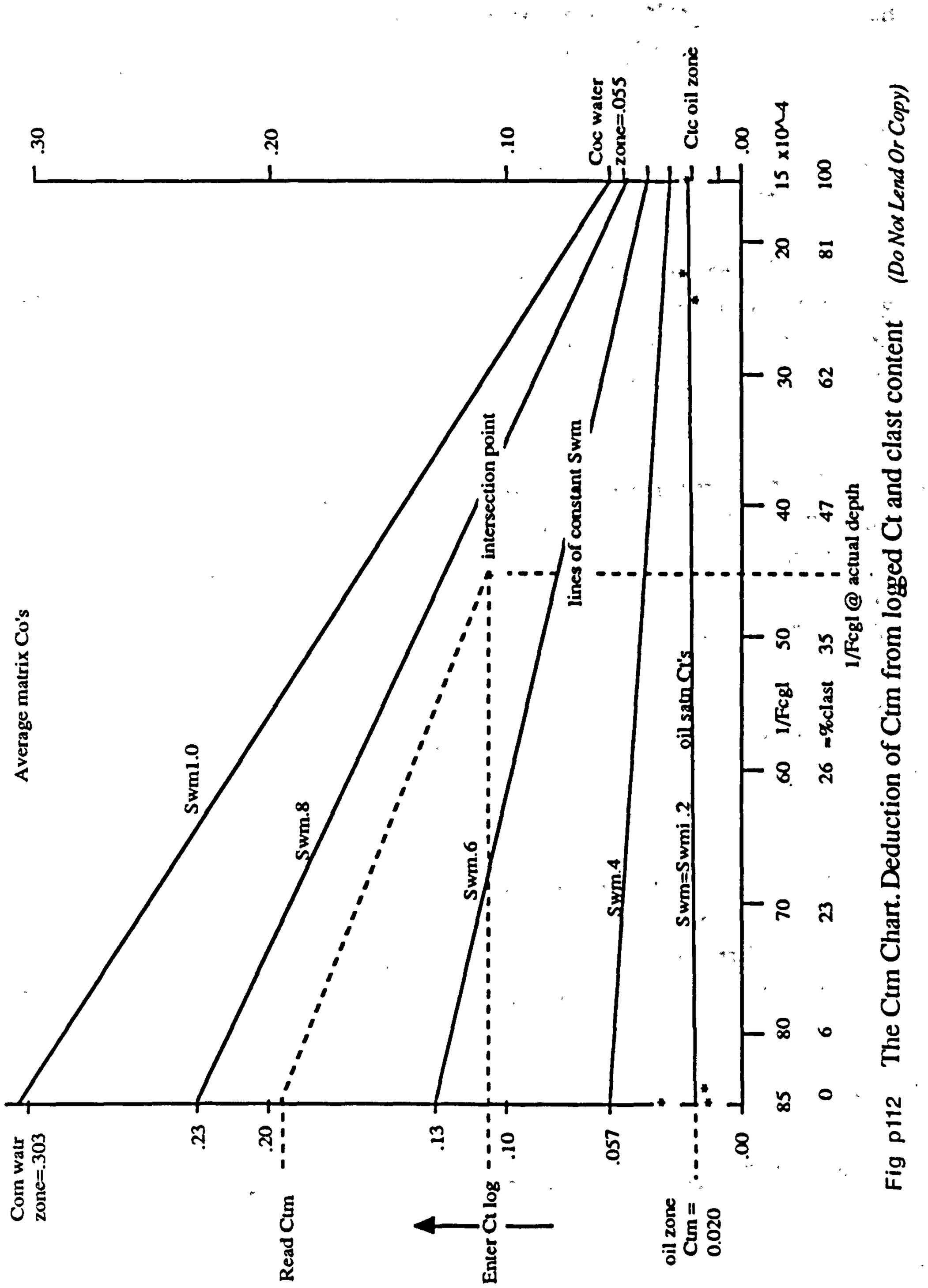


Fig p112 The Ctm Chart. Deduction of Ctm from logged Ct and clast content

Do Not Lend Or Copy

Lines of constant S_{wm} can be enumerated by calculating C_{tm} from the saturation equation for various S_{wm}s. When evaluating a conglomeratic interval projection leftwards along a line of constant S_{wm} to the matrix $0\%clast$ axis provides us with a C_{tm} relevant to the actual $\emptyset_t, \emptyset_e, g, C_x, n, y$ and S_{we} of that depth[45].

If $\emptyset_t, \emptyset_e, g, C_x, n$ and y are the same for the interval being assessed as the standard values used to create the chart, the chart value for S_{wm} will be correct.

If they are different then the intersection will simply be above or below the intersection that would have occurred if the interval had had standard values. If they are different the chart value of C_{tm} is used in the F_g equation the correct values of $\emptyset_e, g, C_x, n$ and y; and S_{wm} calculated.

7.3.1 PRODUCING THE C_{tm} CHART

The chart can be produced from an F_{cgl} v $\%clast$ plot, Fig p107. This can be generated from water zone logs after the first pass which determines clast:matrix ratio. This curve provides the F_{cgl} f.($\%clast$) equation which is the source of the water line in the C_{tm} chart. In this case the Marathon water zone data (11) has been used which resulted in the equation:

$$F_{cgl} = 118 + 0.3\%clast + 0.05\%clast^2$$

Since the equation is a best fit the C_{tm} chart will embody these mean values of $\emptyset_t, \emptyset_e, g$ and C_x. (n and y not relevant in water zones) The oil zone line is established through observation of oil zone C_ts and $\%clast$ from core photographs. "*" are these data points[46].

---

[45] This of course assumes that F_{cgl} for the interval being analysed would fall on the "*Swm1.0*" line if it were 100% water saturated, i.e. it corresponds to the *Fcgl / %clast* relationship implicit in the C_{tm} Chart.

[46] Slight separation between oil and water zone 100% clast conductivity reflects either a) the presence of (resistive) oil saturated matrix in the logged volume which gave rise to these points, b) a poor best fit F_{cgl} prediction @ 100% clasts due to a lack of true 100% clast logged volumes. This separation of C_{tclast} does not necessarily mean that oil has entered the clasts themselves. The assumption of $Swc\ clast = 1$ remains intact.

7.3.2 AN EQUATION FOR THE C_{tm} CHART

Automatic application of the C_{tm} chart during computerised log analysis can be achieved more easily with the linearisation of the *%clast* axis to $1/Fcgl$. The equation was deduced with the help of Dr. G.Wilson of the Department of Mathematics,
Imperial College.

Two assumptions are necessary:

1) C_{tm} (LHS) increases linearly with C_{tclast} (RHS) for increasing S_ws.
2) S_{wm} lines are straight.

First determine gradient of S_{wm} line at intersection point in terms of a, b:
y = Y.a + b, then:
.055 = .303a + b ...1
.024 = .020a + b ...2

a=.110, b=.022

Let t=0-1, on a linear scale, on the horizontal axis,
$z=C_{tlog}$, $y=C_{tc}$, and $Y=C_{tm}$ (required)
then:
(1-t).Y + t.(a.Y + b) = z
Y = (z-t.b)/(1-t + a.t)
gives the C_{tm} chart equation:

$$C_{tm} = (C_{tlog} - 0.022t) / (1-t + 0.110t)$$

t=c.($1/F_{cgl}$) + d (linear relation between t & horiz. axis)
0=85c+d...1
1=15c+d...2
subtract: -1 = 70c, c = -.0143, d = -85c,

d = 1.214

substitute d in:
t=c.($1/F_{cgl}$) + d,
t = [-.0143.($1/F_{cgl}$) + 1.214], and
F_{cgl} = 118 + 0.3%clast + 0.05%clast^2
may be substituted in the C_{tm} equation above:

$$C_{tm} = (C_{tlog} - 0.022t) / (1-t + 0.110t)$$

A check on this equation using the example of the intersection point gives:

$1/F_{cgl} = 46$, therefore

t = .56, therefore

$$C_{tm} = 0.19$$

confirming the correctness of the C_{tm} chart equation.

(7.3) therefore provides a means of logging sandy matrix conductivity, the conductivity relevant to the conglomerate's producible volume fraction, in terms of logged C_t and log derived clast volume, *vlogs*.

8 PARAMETER DERIVATION for RESERVOIR TYPE SIGNATURES & ERROR

Parameters are explained in (5.3). This chapter details some of the parameters used in the evaluation, in particular those included in the final *Reservoir Type Signatures*. Those described represent approximately a fifth of those experimented with.
The important steps in the evaluation are the derivation of:

$$- vlogs - \emptyset_t - \emptyset_e - C_{tm} - S_{we} - KO - KW$$

8.1.1 NVSH

NVSH is $(1\text{-}V_{shsdymtx})$ (12.2, Nomenclature) summed over the RTS interval. It is subtracted from unity so as to increase with increasing reservoir quality. It includes all clays not occurring in conglomeratic clasts.

8.1.2 CLAST FINDING PARAMETERS & NVLOG

Log derived clast finding formulae were written on the basis of laboratory work detailed in (9). A number of trial parameters were plotted as x-y plots. Plots consisted of the four basic elements of the formation requiring distinction on the x-axis, and the log values of the parameters adjacent to depth matched (3.2.1, APPENDIX 13, 27) cored intervals on the y-axis. These plots can be seen in :

(APPENDIX 63): Variation Of Trial Parameters, Adjacent To Cored Intervals, In Relation To The Four Basic Formation Characteristics Requiring Distinction.

Table p117 Summary of trial *vlogs* parameters

Parameter	x axis range		Trend	Credibility
VCLCGLGR	0	.120	fair	2
PORTD98	.19	.045	excellent	5
NPHISSC	.19	.045	fair	2, not used
PORSONIC	.19	.045	excellent	5 (rugosity tolerant)
SFLC	5	23	fair	3, not used
MSFL	5	23	good	3, not used
SFLMSFL	5	23	good	4
TP400RAT	0	2	v poor	0, not used
THKU1	3	7	v poor	0, not used
THKU	0	30	v poor	0, not used
EATT	230	140	fair	1, not used
TPL	10.8	9.3	fair	2, not used
PEF	2	5	fair	1, not used
TPMAP	10	5	v poor	0, not used
MLPROD	.20	0	fair	3, not used
MNORSMOO	10	2.5	excellent	5
CLASTGRP	250	650	v good	4
CLASTND	0	.06	fair	3
EPTATS	210	90	good	4
UMAASON	10	6	good	3
CALCCLST	4	0	nil	Not for vlogs

(CALCCLST distinguishes calcareous cement from clasts)

Discriminators: $2 < VCORS < 100$, $-.02 < DRHOC < +.02$

Useful parameters were converted to 0-1 over the range which predicted *vcors*. An "If–Then-Else" logic was used to extract this range, and to convert this portion of the parameter into a 0-1 value for *vlogs*.

Individual crossplots of parameters v *vcors* were also made and their correlations noted. (Software for multiple linear regression analysis of multiple parameters was not available.) Correlation with core was not the only consideration however e.g. carbonate cements in the deeper uncored interval would invalidate the use of correlations established in the upper interval; an example of why deterministic thinking should never be abandoned (4.1). The final *vlogs* parameters (8.1.2) are self explanatory. These curves were plotted against depth, (APPENDIX 30 and APPENDIX 31). The parameters deliberately cover the full range of physical processes induced in the formation by logging tools in order to provide a robust predictor: If a spurious influence in the uncored interval affects a parameter based on one physical process then other parameters, independent of this influence, will offset its affect on *vlogs*.

Exhaustive investigation of the NGL[47] curves failed to reveal an NGL parameter which

correlated with clasts, despite nuclear activation experiments (9.4) on carefully selected core samples. These indicated characteristic Th, K, and U ratios for clasts and matrix. The Schlumberger NGL repeat runs did not show any significant statistical problem.

The lack of porosity independent clast finders results in the porosity contrast between clast and matrix influencing *vlogs*. This was avoided as far as possible by using matrix sensitive parameters[48]. However the porosity contrast reduces with depth and so *vlogs* becomes less certain with depth.

The rock which provides *vlogs* is not the core but a slightly larger adjacent volume. It can be expected to deviate locally, and to be smoother than *vcors* , however it should equal *vcors* when summed over 10ft(3m) or more.

NVLOG is (1-*vlogs*) summed over the RTS interval. Like NVSH it is subtracted from unity so as to increase with increasing reservoir quality.

8.1.2.1 *vlogs* PARAMETER LISTING

V denotes input for *vlogs*. i= if, t= then, e= else.
See Nomenclature for explanation of abbreviations.

```
GRCSV
        i   30<GRCS<58
        t   (GRCS-30)/28
        e   0

PORTD98
        (2.65-RHOC)/(2.65-.98)

PORTDV
        i   25<GRCS<58
        i   .060<PORTD98<.140
        i   -.03<DRHOC<+.03
        t   1-((PORTD98-.060)/.08)
        e   0

RXO
        MSFL i < SFLC
        e   SFLC

PORSONIC
            .67(DT-56)/DT
```

---

[21] Mark of Schlumberger

[48] Traditional M,N, and P matrix parameters were computed and rejected. (Schl chart CP-8)

```
RXOV
            i    25<GRCS<58
            i    6<RXO<30
            i    0<PORSONIC<.115
            t    (RXO-6)/24
            e    0

CLASTGRP
            GRCS/PORSONIC

CLSTGRPV
            i    25<GRCS<58
            i    250<CLASTGRP<800
            t    (CLASTGRP-250)/550
            e    0

CLASTND
            NPHISSC-P

CLASTNDV
            i    25<GRCS<58
            i    0<CLASTND<.06
            t    CLASTND/0.04
            e    0

EPTATS
            EATT * TPL * PORSONIC

EPTATSV
            i    25<GRCS<58
            i    75<EPTATS<210
            t    1-((EPTATS-75)/120)
            e    0

UMAASON
            ((PEF * RHOE)-PORSONIC * 0.45)/(1-PORSONIC)

RHOE
            (RHOC+0.1883)/1.0704

UMAASONV
            i    5<UMAASON<10
            t    1-((UMAASON-5)/5)
            e    0

MNORV
            i    0<GRCS<58
            i    2.5<MNORSMOO<10      [ 3ft smoothing filter: 135531 ]
            t    (MNORSMOO-2.5)/7.5
            e    0
```

vlogs=
(GRCSV+PORTDV+PORSONV+RXOV+CLSTGRPV+CLASTNDV+EPTATSV+UMAASONV+2 MNOR)/10

8.1.4 CALCITE FINDING PARAMETERS

Calcification has been quantitatively distinguished from clasts on the basis of clasts gamma response and calcite's nil gamma response. An assumption of $\emptyset_m = 0.17$ prior to calcification is necessary for this calculation. Core data corroborates the *vcalc* calculation.

CALCI

i 2.35 < RHOC
t [(RHOC-.2 VLOGS)-2.35] / (2.65-2.35)

Fraction of Total porosity which is calcite cemented normalised to 0.17 total porosity.

VCALCI

i CALCI < 1
t CALCI * .17
e .17

Calcite volume fraction in shale free zones, 0.17 max allowable porosity occluded by calcite.

VSH

t (GRC-24) / (100-24)

VSHCALCI

t VSH * .17 * .91

Volume fraction calcite in shale zones. At VSH =1 all porosity has been preceded by shale. VSh * 0.91 allows 9% shale porosity to be calcite occluded.

VSHCALC

i VSHCALCI < VCALCI
t VSHCALCI
e VCALCI

VCALC

t VCALCI - VSHCALC

Removes portion of density that is shale leaving Øsh for calcite cement in shales. Note that CALCI includes clasts effects.

CALCCLST

TPL*NPHIC*GRCC* (RHOC - NPHIC) / SFLC

8.1.5 ENVIRONMENTAL PARAMETERS

drhocum

The absolute value of *drho* from the LDT[49] is summed over the *RTS* interval. Increased height indicates rugosity. This affects porosity and therefore all log analysis.

ncal

Caliper minus bit size summed over *RTS* interval.

di

Depth of invasion from tornado chart (Schl.Rint-2c) summed over interval. *di* is an ill defined parameter but nevertheless an extremely important quality control on R_t. Affects S_w. Crucial for R_{we} problem (15.1.4).

[49] Mark of Schlumberger

8.1.6 POROSITY PARAMETERS

8.1.6.1 $\emptyset_t$, TOTAL POROSITY METHOD

Accurate $\emptyset_t$ s are of fundamental importance in formation evaluation, inexact $\emptyset_t$ s at low porosities change calculations of S_{we}, BVO, and producibility. $\emptyset_t$ includes micro-porosity and most clay water (6.2.1). This formation requires special attention when deciding upon a method for calculating $\emptyset_t$. Thin section, X-Ray Diffraction and SEM results enabled an estimate of the tolerance the three porosity tools have to rock and borehole variations. In this sense non-log data have provided the basis for calculating total porosity from logging data.

Non-log-inputs for *rhog* sandy matrix, *rhogc* clasts, $\emptyset_{ndcmsh}$, $\emptyset_{ndcmres}$, and ∂t for clasts, sandy matrix and reservoir clays, have been used to show each tool's sensitivity to the lithologies and hole conditions of Well A, for a total porosity of 0.120.

Table p122 Calculated porosity responses to the common deviations from quartz matrix encountered in Well A.

Device	100% Quartz	10% Res Dry Clays	10% Carbonate	4% Pyrite	Simultaneous
Density	.120	.117	.116	.068	.061
Neutron	.120	.134	.121	.1197	.135
Sonic	120	.126	.111	.112	.109

Fig p122 Porosity tool application domains resulting from Table p122

Many of these disturbing influences on $\emptyset_d$ can be corrected for, but not perfectly.

The neutron-density string is an excellent lithologically compensating fluids/matrix tool combination, however certain conditions of rugosity, pyrite and low porosity indicate that the sonic tool provides a closer approximation to $\emptyset_t$ over limited intervals. Washouts cause cycle-skips and "road noise" on the sonic, but rugosity itself should not significantly increase first arrival time, if it can be detected. Rugosity is best seen on the Small Arm EPT caliper (APPENDIX 61). Unlike the density tool the sonic response is relatively tolerant to diverse mineral assemblages (Schl. 1985, p104-105). Intra-clay pyrite will tend to artificially lower density and to some extent sonic porosities, however there is no combination of tools or corrections that can overcome this phenomenon, unless neutron porosity is used in isolation.

Variations in matrix density, and sonic cycle skips occasionally favour $\emptyset_t$ equaling $\emptyset_{nc}$. In Well A the neutron tool responds primarily to fluid's large hydrogen index, not to matrix components. Neutron response is a function of the whole rock's neutron slowing length and its thermal neutron absorption crossection (R.Wiley, 1989). Although in some wells the latter is unpredictable and dramatic Well A sands appear to have a normal neutron response - one dominated by fluid *HI* , ie $\emptyset_t$. By contrast $\emptyset_d$ will show error at low porosities because rhobulk–>rhomatrix, and receiver count rates are low. This situation creates sensitivity to error in either *rhob* or *rhog* at low porosities. Thus although carbonate cemented zones will marginally increase $\emptyset_{nc}$ – which computes as hydrocarbon - the $\emptyset_{nc}$ error will be less than the $\emptyset_d$ error.

The tools least sensitive to the disturbing influences were chosen in respect of *vlogs*. The logic for total porosity is shown in the table.

Table p123 Logic for total porosity switching routine

vlogs < 0.2	=	Sands-Shales -->	Neutron Density porosity	=	Øn + Ød / 2
vlogs > 0.2	=	Conglomerates ->	Neutron Sonic porosity	=	Øn + Øs / 2
DRHOC > +/-0.03	=	Bad Hole ----->	Øs	=	Øs

This switching routine should be closely examined in conjunction with the DRHO, *vcors* and *vlogs*. (APPENDIX 45, 31 & 53 resp)

Before switching the separate tools have to be corrected for

1) *vlogs* ,
2) $V_{dryclres}$,

in a manner consistent with a total porosity determination. (see also 11.3)

CORRECTING POROSITY TOOLS FOR *vlogs*

Density

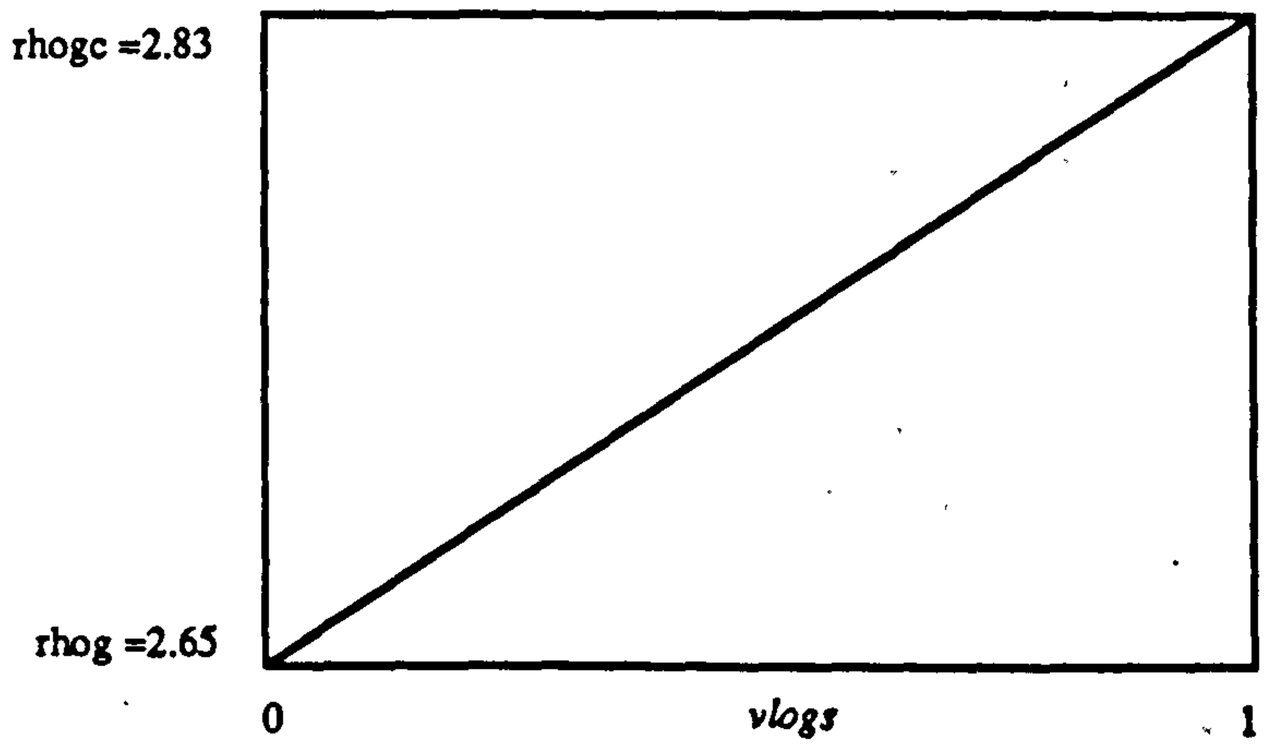


Fig p124 Influence of clasts upon matrix density

$$\emptyset dvlogs = [(2.65 + 0.18vlogs)-rhoc] / [(2.65 + 0.18vlogs) - 0.98]$$

Clast's pyrite and carbonate variations frequently render this correction invalid.

Neutron

$$\emptyset nvlogs = \emptyset n$$

No correction applied. Pyrite and carbonate approximately neutralise (12.2)

Sonic

The contrasting ∂s of the non *GRCC* inducing phases are deduced from mineralogy:

Table p124 Components influential to ∂t *matrix*

Mineral	∂t mtx	Sandy matrix		Clasts	
Quartz%	56	82.9	4642	59.3	3321
KFelds%	69	0.9	62	2.5	173
Calcite%	49	0	0	3.8	186
Pyrite%	39	0.6	23	8.6	335
Totals		84.4	4727	74.2	4015

If ∂t matrix sandy matrix = 56, ∂t matrix clasts = 56*4015/4727 = 47 .6

$$\emptyset svlogs = 0.67 (\partial t - [56-8.4vlogs]) / \partial t$$ (Raymer Hunt eqn.)

CORRECTING POROSITY TOOLS FOR $V_{dryclres}$ AND *vlogs*

Density

Before *GRCC* is used to estimate clays in the sandy matrix, clast's contribution to *GRCC* is subtracted.
vlogs 0 -> 1 increases *GRCC* by +28

In "shaly" non clast intervals when $V_{dryclres}$=1.0[50], *rhog* becomes *rhodcmres*: 2.79 (12.1).

$$rhogshaly = 2.65 + Vdryclres(2.79 - 2.65) = 2.65 + 0.14Vdryclres$$

When calculating *rhog* in clast intervals *GRCC*'s calculation of $V_{dryclres}$ has to be reduced since *vlog's* effect upon *rhog* has already been performed:

$$Vdryclres = 0.0051([GRCC-28vlogs] -23) \qquad (12.2)$$

Therefore in clast and shaly intervals:

$$rhog = 2.65 + 0.18\,vlogs + 0.14\,\{\,0.0051(\,[GRCC-28vlogs] -23\,)\,\}$$

$$rhog = 2.634 + 0.000714GRCC + 0.160vlogs$$

E.g. @ vlogs=0.4; GRCC=44; rhog = 2.73 g/cc

This equation yields the grain density required for $\emptyset_t$ from *rhoc* across clast and or shaly intervals.

Neutron

$$\emptyset_{nc} = \emptyset_n - [\,0.120 - 0.0051(GRCC-23)\,] \qquad (12.2.2)$$

Only a clay correction is required.

Sonic

∂ from density/sonic crossplots at approximately zero porosity suggest dry clay $\partial \approx$ 64µs/ft. (Pers comm. C.Skelt, Schl. 1987). Assuming this value:

$$\emptyset s = 0.67\,(\,\partial t - [56-8.4vlogs+8Vdryclres]\,)\,/\,\partial t \quad \text{(Raymer Hunt eqn.)}$$

GRCC responds to clays in the clasts and sandy matrix; the equation increases matrix travel times accordingly. This equation explains the favourable emphasise placed upon $\emptyset_S$ in conglomerates.

[50] Vdryclres will have an upper limit of about 0.5

The curves were then checked for equality over clean sand intervals (ref $g(11.3)$) and found to agree. The logic was applied and the pieces spliced as one curve, $\emptyset_t$.

An equation for $\emptyset_d$ using *rhog* =f.(*GRCC*,*vlogs*) might be thought preferable to switching. However the basis of this equation is averaged non-log data, and the possibility of unreal $\emptyset_t$ s from this method appears to be distinctly greater than the switching method, which not only corrects for these variations, but has already selected the tools least susceptible to these variations.

Calibration of $\emptyset_t$ to $\emptyset_{he}$

Porosity as a function of overburden pressure was available on five plugs (APPENDIX 40). This has been used to correct $\emptyset_{he}$ to in–situ porosity using:

$$\emptyset_{uniaxial} = \emptyset_{room} - (\emptyset_{room} - \emptyset_{NOB\ hydrostaically\ loaded})\,0.61$$

$$\partial\emptyset_{uniaxial} = 0.61\,\partial\emptyset_{NOB} \quad \text{(Core Lab, 1982. 13-3)}$$

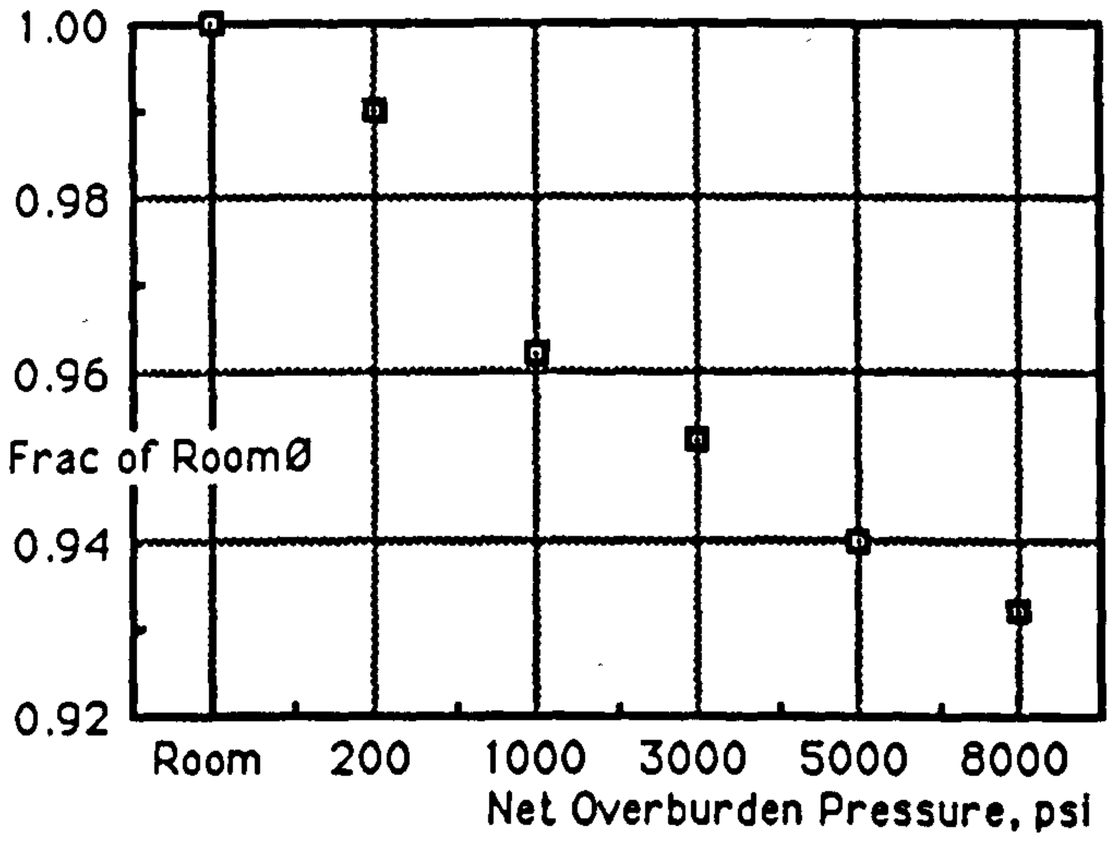


Fig p126 Reduction in porosity caused by Net Overburden Pressure (APPENDIX 40).

Overburden at mid reservoir	= 15,555ft(4741m) * 1.0 psi		(Core Lab, 1982)
Reservoir pressure at mid reservoir	= 8100 psi		(10.2)
Mean net overburden pressure	= 15555 - 8100	= 7454 psi	
At 7454NOB fractional $\partial\emptyset_{NOB}$	= 1.000 - 0.935	= .065	
Therefore fractional $\partial\emptyset_{unixial}$	= .61*.065	= .040	(Core Lab, 1982)
Compaction corrected $\emptyset_{he}$	= .96$\emptyset_{he}$		

Massive Coarse Sandstone Type Interval: (homogeneous lithology and mineralogy)

Ave $\emptyset_{he}$	.118 * .96	from core data listing
Ave $\emptyset_{heres}$	.113	
$\emptyset_t$, log	.130	
Shift $\emptyset_t$	-.017	

The weakness of this method is that it calibrates log porosity at .113, but not over lower porosity ranges. The rate of change in log porosity is taken as equalling the rate of change in actual porosity. The deeper lower porosity intervals with no core therefore suffer greater uncertainty.

8.1.6.2 $\emptyset_e$

A practical definition of effective porosity is the single most powerful tool for evaluating Well A. The formulation is based on log and Non-log information and correlates favourably with flow information from other Brae wells. It depends upon three variables:

$$Effective\ \emptyset = Total\ \emptyset - All\ clast\ \emptyset - sandy\ matrix's\ shale\ \emptyset$$

Assuming clast plugs were dried at 105°C see (APPENDIX 32) $0.05*vlogs$ removes clasts's porosity including any clay porosity in clasts. The only remaining non–effective pore volume is sandy matrix shale porosity. Shales may habour effective porosity containing recoverable gas (Truman, 1989), however, the 7,500psi net overburden, and oil environment of this well, require a $\emptyset_e$ definition which excludes shale porosity.

The whole rock V_{shres} parameter is converted to a sandy matrix parameter by the non–log information $V_{shclast} = 0.10$

$$\text{i.e.} \qquad V_{shsdymtx} = [V_{shres} - 0.10vlogs] \,/\, 1\text{-}vlogs$$

The remaining required parameter, shale porosity, is calculated from the DCMP data (12.1) from the shale Type Interval using $rhodcmsh$=2.75. Knowing the volumes and dry densities of the clay and non clay fractions allows the water volume, $\emptyset_{tsh}$, to be calculated. The equation assumes all shale porosity occurs in the clay minerals:

$$0.392*2.92 + (0.608\text{-}\emptyset_{tsh})*2.75 + \emptyset_{tsh} = rhoc$$

$$\emptyset_{tsh} = 0.14$$

Therefore:

$$Effective\ \emptyset = Total\ \emptyset - All\ clast\ \emptyset - sandy\ matrix's\ shale\ \emptyset$$

$$= \emptyset_t - vlogs\,\emptyset_c - (1\text{-}vlogs)\,\emptyset_{ish}\,V_{shsdymtx}$$

$$\emptyset_e = \emptyset_t - 0.05vlogs - 0.14\,V_{shsdymtx}\,(1\text{-}vlogs)$$

The $\emptyset_e$ calculation is partially tautological: *vlogs* is a function of $\emptyset_t$ and $\emptyset_e$ is a function of $\emptyset_t$ and *vlogs*. This weakness appears unavoidable, however its influence has been minimised by the special attention given to determining $\emptyset_t$ and *vlogs*.

$\emptyset_e$ is the basis of log derived flow units.

8.1.6.3 *NET* RESERVOIR QUALITY ROCK

Intervals of the Brae Formation classified as "net" are based upon the intervals potential as a producing rock. Arbitrary cutoffs for *GR* or porosity have been rejected in favour of data from production tests[51] from Well A, and two adjacent wells in the same formation but structurally higher. Tests spanned a wide range of reservoir qualities and *kh* values, enabling a choice of a cutoffs which effectively exclude the large thicknesses of clean sand with poor reservoir quality in Well A. The strongest candidate, when computed across all tested intervals, was $\emptyset_e \geq 0.05$; concluded from a reliable non-commercial test of 20 BOPD. This exercise also provided confidence in $\emptyset_e$ as a formation evaluation parameter. Also *NET* met the microlog (mudcake) parameter, $ML \geq 0.05$, (APPENDIX 30) to exclude any artificially inflated $\emptyset_e$ values caused by bad hole (15355) or variable matrix properties upon $\emptyset_t$. Therefore:

If $\emptyset_e \geq 0.05$ and,

If $ML \geq 0.05$,

Then *NET*=1.0

8.1.7 FLUID TYPE PARAMETERS

SOX

Flushed zone oil saturation, summed. Log derived $S_{ox} = 1 - S_{xo}$ where:

$$C_{xo} = C_{xwe}\,\emptyset_e^{\beta}\,S_{xe} + C_x\,S_{xe}^{n-y}$$

BVO

Bulk volume oil. $(1\text{-}S_{we})\,\emptyset_e$, summed.

---

[51] Data not available

8.1.8 PRODUCIBILITY PARAMETERS

Inappropriate Porosity / Permeability Data

The only data related to the foot by foot variations of reservoir permeability was core k_{hor} values. Although these values probably contain considerable error their spread was used in crossplots to select the best log derived absolute permeability parameter, but not to calibrate that parameter. A crossplot of $\emptyset_{he}$ v k_{hor} was produced by the operator but not used in this thesis. Although a permeability predictor is required a core porosity/permeability crossplot equation would have been founded upon poor data, for at least two reasons:

1) Core plugs were not sampled every twelve inch, but (apparently) taken preferentially from areas showing good sand, thus biasing the porosity / permeability relationship to one based upon better than average pore geometries.
2) Both porosity and permeability will be affected when withdrawn from the 15000ft(4572m) of overburden, but dissimilarly. Porosity will inflate but can be corrected to near reservoir conditions by overburden SCAL. Low permeabilities will also inflate, due to the increased porosities, and also to numerous other causes such as induced microfractures or altered clay morphologies in sheet like throats. A reservoir porosity/permeability equation based upon this core data would be misleading.

The selected log permeability parameter was calibrated to DST *kh* values (*KE3O*).

ML

The microlog was the best log for delineating thin permeable intervals through its detection of conductive mudcake. The MINV and MNOR curves were combined in at least 15 ways to establish a correlation with core because it was visually clear from the log that the traces carried important information. Shale disrupts the response and had to be included in the ML parameter:

ML = Σ(2000(MNOR - MINV)**2 / (MNOR+MINV)**2.2) / GRCC**1.8*

This useful empirical parameter effectively quantifies the human eyes interpretation of the microlog, and is also useful for facies delineation, particularly BMS from MCS. ML is an additional and usefully independent condition which must be satisfied if an interval is to produce.

The remaining parameters used to predict producibility resulted from laborious efforts to correlate log parameters with k_{hor} and scale them with DST *kh* values. *khs* were from oil bearing intervals in wells adjacent to Well A. *khs* from probable water intervals in Well A were unusable (10.3). The basic sequence was as follows:

1) Select the most suitable absolute permeability predictor by referring to core horizontal permeabilities in clast free intervals.
2) Approximately correct this permeability for two phase flow.
3) Sum the effective permeability predictor over oil leg tested intervals.
4) Calibrate the summed value to known DST *kh* values by using a scaling factor.
5) Use the absolute permeability in (1), similarly scaled, to predict single phase flow in water zones.

Further detail on these steps follows:

KE30

KE30 results from the *KE3* ($\emptyset_e$**3) curve. The absolute permeability curves, *KE3* and *KTIME* were found to be the two strongest correlations with core absolute permeabilities. Experimentation was made with approximately 20 equations based on the literature (Timur, 1968. Lolley, 1984. Johnson, 1987 etc) using $\emptyset_t, \emptyset_e, vlogs, V_{shmtx}, S_{wt}, S_{we}$; the usual log permeability parameters; $\emptyset_e$ accommodates conglomerates. The *KTIME* (Timur, 1968[52]) curve did not provide a better correlation with core permeabilities and was dropped. *KTIME* requires the interval to be at 'irreducible' water saturation which at this stage seemed unlikely.

KE3 and *KTIME* were not scaled to core mD values because:

1) Core values represent relative changes rather than absolute in-situ values.
2) Core plugs have been preferentially taken from sand matrix not rigorously sampled each foot, and,
3) The curves are required to predict DSTs not core analysis.

Conversion of *KE3* from absolute to effective permeability to oil was achieved through:

1) S_{wt}.
2) A fixed S_{or} cutoff of 0.30.

[52] *((100*(E**2.25)) / Swt)**.5* , above transition zone.

3) A variable irreducible water cutoff with a minimum value of 0.15. S_{wi} is the function of effective porosity observed from an S_{wt} versus $\emptyset_e$ crossplot of two DSTs from an adjacent well. S_{wt} was used, not S_{we} because it is directly comparable to S_{wi} ($\emptyset_t$). $\emptyset_e$ was used because $\emptyset_e$ is net of the clast effect (9.1.8). These intervals produced traces of water only and are at S_{wi}. The observed relation between $\emptyset_e$ and S_{wi} was:

$$S_{wi} = 1.0 - 8.5\,\emptyset_e$$

(Yields $S_{wi} = 1$ in pure shales and clasts)

for minimum value of $S_{wi} = 0.15$:

i $S_{wi} > 0.15$

t S_{wi}

e 0.15

4) Reducing the sum of K_o+K_w to 0.6 of absolute permeability, k. 0.6 is an approximation based upon relative permeability plots[53] of matrix samples and book plots (Dake, 1978. p122).

Using if-then-else logic, k_w and k_o become:

i $S_{wt} > S_{wi}$

t $k_w = 0.6k\,S_{wt}$

e 0.00...yields *KWE*

i $S_{wt} < 0.70$

t $k_o = 0.6\,k\,(1\text{-}S_{wt})$

e 0.00...yields *KOE*

This corresponds to the effective permeability plot:

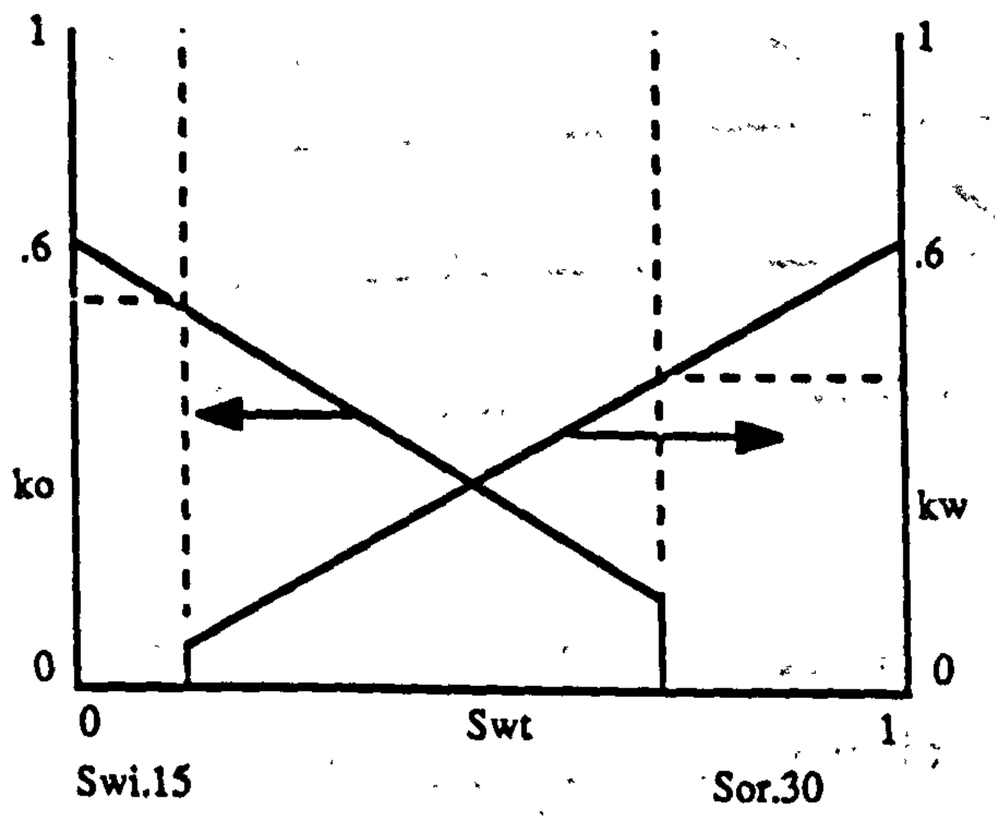


Fig p131 Pseudo relative permeability plot used for estimating single phase flow from calculated saturation.

53 Plots withheld

Fig p132 is not intended to be a pore geometry characterisation. It is being used as a predictive tool. In this form it avoids non-linear expressions of core relative permeabilities.

μ_{oil} and μ_{brine} are assumed equal, consistent with laboratory data. Clearly this linear version is not accurate at S_{wt}=1. This is not necessary since the intervals being used in this calibration were at S_{wi}.

We have now transformed the single phase k predictor (*KE3*) into a k_o (*KOE*) and k_w (*KWE*) predictor using log S_{wt}.

kh mDft values were calculated from the DST reports using the approximation:

$$kh \approx 1000\, Q_o / (p_{res} - p_{well})$$

(Schl, 1987.p150)

These *kh*s provide calibration for the accumulated effective permeability curve (*KOECUM*) over tested intervals. The fit (*kh* v *KOECUM*) was forced through zero and assumed linear since *KOECUM* is proportional to $\emptyset_e$**3. Identical procedures were performed throughout using $\emptyset_t$ in place of $\emptyset_e$. $\emptyset_e$ provided better results.

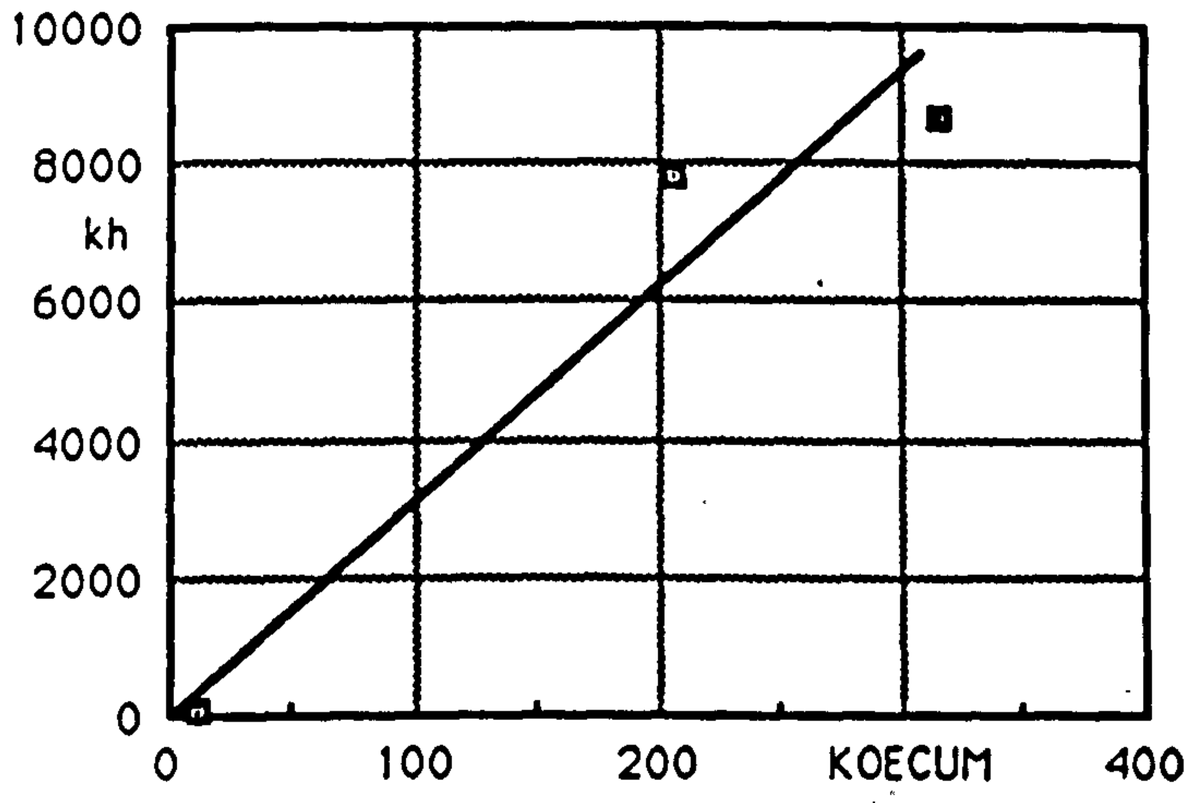


Fig p132 Calibration of the selected log derived oil permeability predictor to actual oil zone test data. Scaling factor = 31

We use this scaling factor, 31, with *KE3* to predict water saturated *kh* values; e.g. water leg injection. *KE3O* is therefore:

$$KE3O = \sum KE3*31$$

This procedure integrates core, logs and DSTs. It enables the continuous record of logs to extend the discontinuous relationship between core permeabilities and DST *kh*s into uncored and or untested intervals. This has been done through the laboratory and log derived continuous values for $\emptyset_e$.

KO

Is the summed effective permeability to oil based upon *KE3*, S_{wt}, the DST scaling factor and a residual oil constraint when $S_O < 0.3$.

i $S_O > 0.3$ *or*

i $S_w < S_{wi}$

t $KOE = 0.6 KE3*S_O$

e 0

then:

$$KO = \sum KOE*31$$

"*or* i" allows oil zones with with high S_{wi}s to be included in predicted oil producibility. *KO* may be used in all zones.

KW

Is the summed effective permeability to water based upon *KE3*, S_{wt}, the DST scaling factor, and an immovable water constraint when $S_{wt} = S_{wi}$.

i $S_w > S_{wi}$

t $KWE = 0.6\ KE3*S_{wt}*31$

e 0

then:

$$KW = \sum KWE*31$$

KW is for use in transition zones or zones with uncertain S_{wt}, or S_{wi} values.

Numerous other parameters were calculated concurrently with the above sequence to continually check for better alternatives. These made no significant contribution.

8.2 ERROR

The internal consistency of log analysis is not necessarily a measure of how accurately it describes the real world. Incoherence[54] factors generated from logs alone do not necessarily show the probable accuracy of log analysis. Quality control during formation evaluation would be better achieved by a system of credibility ratings which prefixed each formation evaluation parameter, including non-log and log analysis parameters. Prefixes would also aid communication between geologists and engineers. They would establish objectively how to weight parameters when decisions have to be made, for example, S_w as a function of height or as a function of resistivity.

Calibrations and Environmental Corrections

Logging tools were first checked for calibration errors and then environmentally corrected within Petcom[55]. If better alternatives existed, e.g. RTGLOB, or manually edited values over limited intervals, the Petcom output was substituted. The washed out borehole and conductive mud make environmental corrections important in Well A.

8.2.1 SYSTEMATIC ERROR

Systematic error in log analysis is inaccuracy in equations relating tool response to formation properties. An example is the independence from geometry that many response equations show. In clean water saturated formations the following mixing laws are commonly used:

$$\partial t_{log} = \emptyset\, \partial t_{fluid} + (1-\emptyset)\, \partial t_{mtx}$$

$$\varphi_{po} = \emptyset\, \varphi_{wo} + (1-\emptyset)\, \varphi_{mtx}$$

$$rho_{blog} = \emptyset\, rho_{fluid} + (1-\emptyset)\, rho_{mtx}$$

$$\emptyset_{n\,log} = \emptyset\, HI_{fluid} + (1-\emptyset)\, HI_{mtx} \qquad \text{(Schl. 1985)}$$

If clay or hydrocarbon are present these equations are extended by summing the individual component volume fractions. The components geometrical distribution is assumed to have no influence on the tool reading, largely because no data is available to quantify any effect. If we consider the simple case of a sonic pulse's first arrival time it is clear that geometry can have considerable influence on the calculated porosity. In fact the difference between

---

[54] Schlumberger output from Global processing indicating disparity between original tool readings and hypothetical tool readings recreated from results of analysis.

[55] Petroleum Computing Log Analysis Software

$\emptyset_d$ and $\emptyset_s$ has been used as an indicator of (pore) geometry.

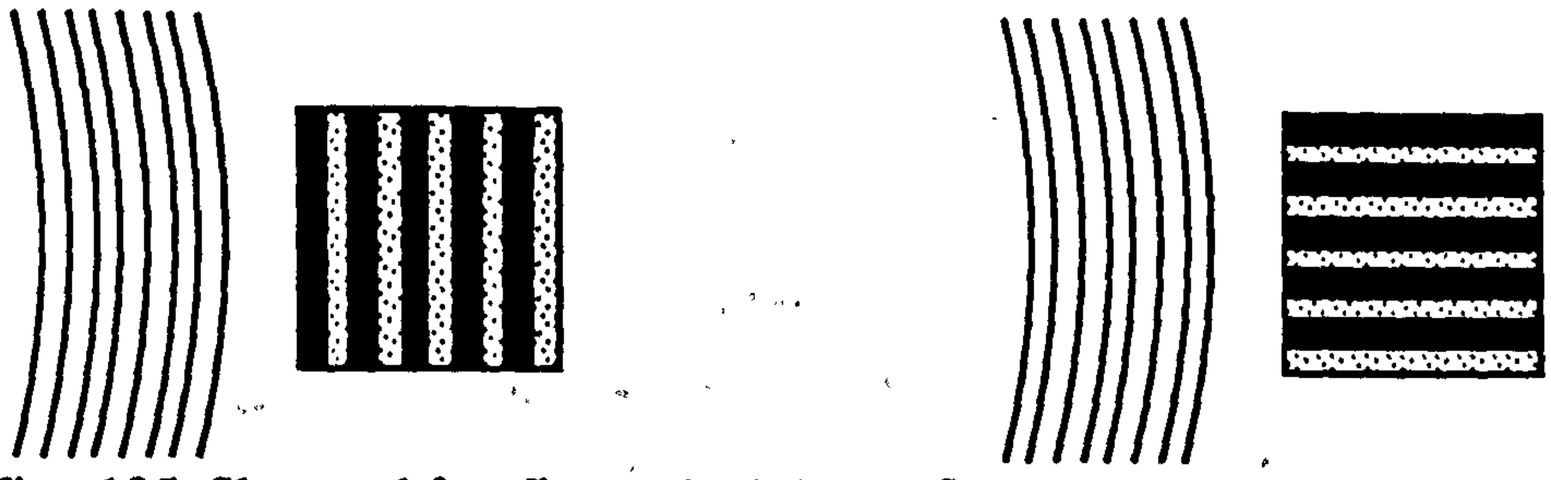


Fig p135 Slow and fast first arrival times (∂t) as a function of geometrical distribution of equal volume fractions.

Also when Hanai-Bruggeman's L factor for an interval of rock $\neq 0.5$ tpo porosities will contain systematic error.

Systematic error will be introduced wherever geometry causes tool response to depart from the method of summing volume fractions. Conglomerates, diagenesis and thin beds will exacerbate systematic error because they represent changing geometrical arrangement. Some equations include geometrical parameters: Archie's m , Hanai-Bruggeman's L . It seems probable that most tool response equations require geometrical factors[56] which are currently absorbed by squashable factors such as shale grain density, m or even a.

Systematic error will increase under the following circumstances:

1) Deviation of logging conditions from calibration conditions.
2) Variation between volume fractions within one tools depth of investigation and another tools, when those tools are used together in log analysis.
3) Heterogeneous pore size and pore morphology.
4) Unknown mineralogy.

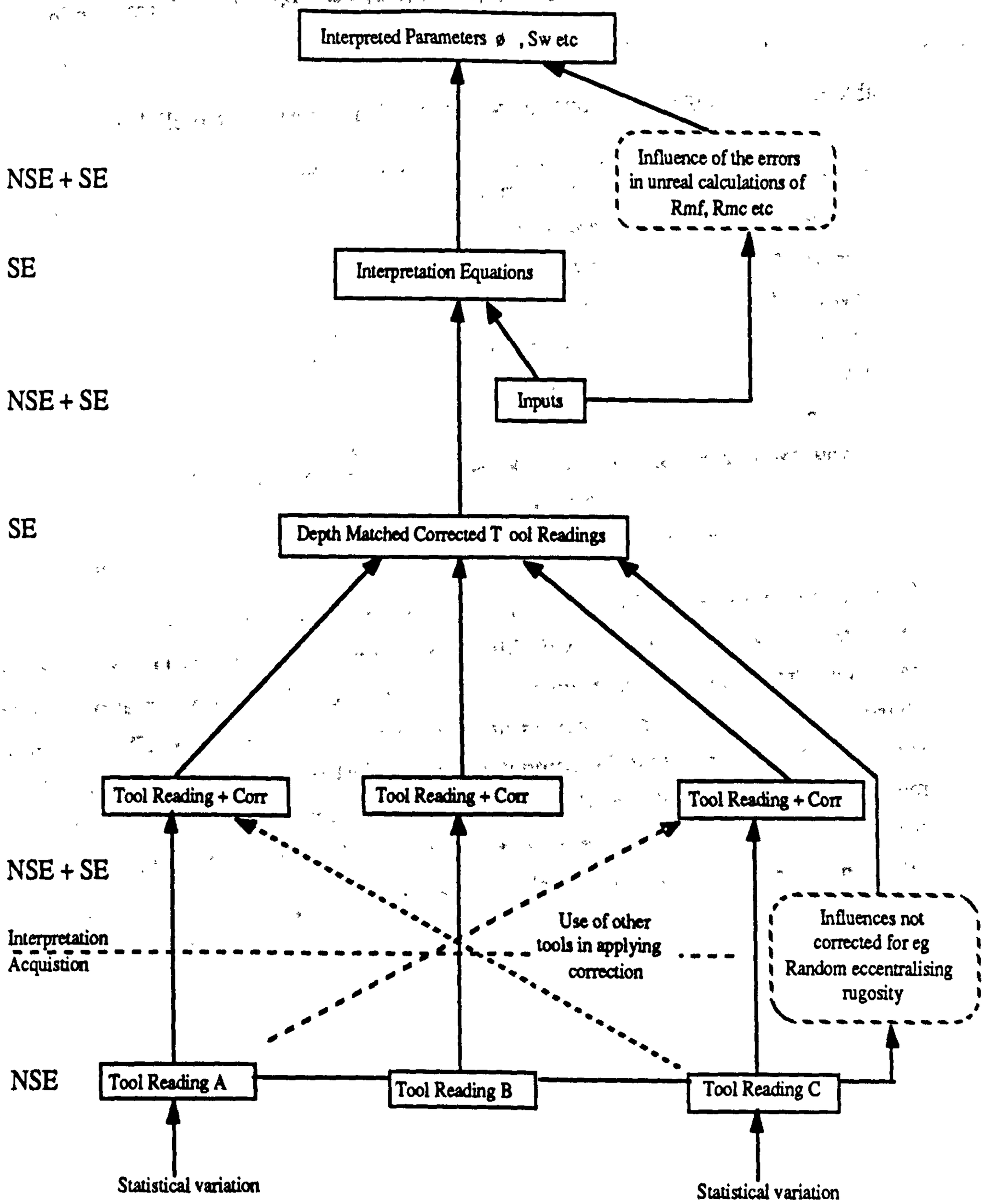
---

[56] This observation means m from logged water zones will be superior to an m value from SCAL since all such geometrical effects will automatically arrive in the log value of m, however calibrating log $\emptyset$ to core $\emptyset$ will alleviate this.

8.2.2 NON SYSTEMATIC ERROR

Non systematic error may be thought of as:

1) Statistical. Evident as a poor repeat logging run.
2) Poor Logging Environment. Deviations of the environment from standard calibration conditions introduce possible errors in corrections. Rugosity and unknown mudcake thickness cannot be accurately corrected for.



NSE = Non Systematic Error; SE = Systematic Error

Fig p137 Sources of error

In the table below tool readings have been assigned a +/- non systematic error by

considering the average borehole conditions over permeable Brae Formation intervals.

Table p138 Average conditions for permeable Brae intervals of Well A.

Log Depth	=	15517ft(4730m)
Resr press	=	8097 psi (DST 2A)
Borehole Temp	=	274 °F
R_{mc} @ 274	=	.188 Ωm
hmc	=	.1 inch, 2.5 mm (Schl. 1985,chart Rxo-1)
CAL	=	11.5 inch
Rugosity	=	.16 inch/ft

(Manual Ave of 220 typically rugose levels. Rugosity= ∂SA/∂fd = SAn - SAn+1 / 0.5)

DRHO	=	+.025 g/cc

Service company error formulae for logging under non calibration conditions were requested but were not made available. The following semi-quantitative dependencies have been drawn up from experience, the literature, and by careful observation of logs and charts. Whether or not these values are accurate will only slightly affect the relative sensitivity to tool error that the computed parameters have. "% Error" inaccuracies only mean that individual tools could deviate more or less than assumed. For the purpose of comparing computed parameter's sensitivity to tool error +/- 5% per tool would be sufficient but not as realistic as the table below.

Do Not Lend Or Copy

Table p139 Non Systematic Error included in the corrected tool readings for average permeable Brae Formation, Well A.

Tool	Error Dependencies	~ % Error @ Ave Brae[1]	High Sensitivity to:
GR	f(§stat, §cal, §mw, §mc, §ecc, §ovl)	+/- 3	
NGTK	f(§stat, §cal, §mw, §mc, §ecc, §ovl)	+/- 20	§stat
NGTU	f(§stat, §cal, §mw, §mc, §ecc, §ovl)	+/- 45	§stat
NGTTh	f(§stat, §cal, §mw, §mc, §ecc, §ovl)	+/- 25	§stat
ΔSP	f(§temp, §Rmf/Rw, §di/cal, §ecc)	+/- 10	
BHC	f(§rug)	+/- 3	
LDTRHOB	f(§mc, §rug, §cal, §stat, §stdof)	+/- 4	§rug
LDTPe	f(§mc, §rug, §cal, §stat, §stdof, §mw)	+/- 12	§mw, §mc, §rug
CNL	f(§mc, §ch, §rug, §cal, §stat, §stdof, §temp)	+/- 7	
EPTTPL	f(§rug, §mc, §stdof)	+/- 3	
EPTATTN	f(§rug, §mc, §stdof)	+/- 10	§mc
ML	f(§rug, §stdof)	+/- 4	
MSFL	f(§mc, §temp, §rug, §stdof)	+/- 6	§rug
DLL	f(§temp)	+/- 1	
SFL	f(§ecc, §temp, §m, §cal)	+/- 3	§m
DIL	f(§cal, §stdof, §temp, §m)	+/- 2	§m

"§" read: Error due to. See Nomenclature for abbreviations.

1) Repeats show a minimum value. 2) Repeats compared on a 3ft(1m) interval basis.

3) In some cases §s are composites of component §s eg: §mc = $\sum$ §Rmc, §hmc.

4) §stdof = §stdof + §ecc.

Table p140 Inputs with Systematic and Non Systematic Error, for average permeable Brae, Well A.

Input	Error Dependency	~ % Error @ AveBrae	High Sensitivity to:
Rmf	f(§temp, §hist, §Rxwe)	? +/- 30	
Rmc	f(§temp, §hist)	? +/- 15	
Rw	f(§temp, §con)	+/- 5	
Rcl	f(Σ §Rt, §sh-cl, §geom, §cltyp)	? +/- 50	
hmc	f(Σ §ML, Σ §Rmc, §rmvl)	? +/- 40	
Rt	f(§di, §mc, §bed, §step, §mf/w, §cal, §ecc)	+/- 20[a]	§bed, §di, Rmf/Rw
Rxo	f(§bed, §mc, §di, §step, §mf/w)	+- 25[a]	§mc, §m
m	f(All Tools & Inputs)	?	
n	f(Laboratory)	?	wettability changes

Notes: a) The primary objective of Schl. Chart Rint 2c is determination of Rt, thus its method includes the error of Rt in Rxo determination.

§con: Recovered formation fluid contamination.

§sh-cl: Influence of non clay minerals on shale bed resistivity.

§geom: Contrasting clay geometrical distribution in shale bed and reservoir.

§cltyp: Contrasting clay types in shale bed and reservoir.

§rmvl: Removal of mud cake by tool. §bed: Bed thickness correction.

§step: Invalid step profile assumption, Rint Charts.

§smpl: Atypical sample of log analysis volume.

The % errors at average permeable Brae Formation have been used to generate a crude index of a parameters average credibility over these intervals. A parameter's credibility will decrease as the number of steps required to calculate it increases because some degree of systematic error is to be expected at each step.

Table p141 Semi-quantitative optimistic and pessimistic values and credibility ratings for mean permeable Brae. (Based on previous tables. Optimistic=low S_{wt})

Tool	Mean Permeable Brae	Error Swing: Optimistic		Pessimistic	Credibility
GR	35 API	3%	34	36	1
NGTK	.08 %	20%	.06	.10	3
NGTU	1.5 ppm	45%	.7	2.2	4
NGTTh	3.0 ppm	25%	2.3	3.8	3
BHC	69 µsec/ft	3%	71	67	1
LDTRHOB	2.45 g/cc	4%	2.35	2.55	1
LDTPe	2.9 Barns/e	12%	2.55	3.3	2
CNL	.060 ØN	7%	.0642	.0558	2
EPTTPL	10.1 nsec/m	3%	10.4	9.8	1
EPTATTN	177 dB/m	10%	159	195	2
ML1x1	1.5 Ωm	4%	1.44	1.56	1
MSFL	11.0 Ωm	6%	10.3	11.7	2
DLL	9.50 Ωm	1%	9.60	9.41	1
SFL	10.2 Ωm	3%	9.99	10.5	1
DIL	5.3 Ωm	2%	5.41	5.19	1
Rxwe	.080 Ωm	30%	.090	.025	3
Rmc	.240 Ωm	15%	.264	.216	2
Rw	.025 Ωm	5%	.024	.026	1
Rclresr	10.0 Ωm(Kimmer)	50%	5.00	15.0	4
hmc	.125inch	Effects on Ø and Rxo cancel			4
RtDIL	5.3 ΩmChartRint2c	20%	6.36	4.24	3
RTGLOB	14 Ωm	17%	15.9	11.6	3
RxoSFL	14.3ΩmChartRint2c	25%	10.7	17.8	3
P	.11	15%	.127	.094	2
E	.09	20%	.108	.072	3
vlogs	≈.1	25%	.75	.13	3
DI	70 inch	35%	95	45	4
BVO	.013	50%	.020	.007	4
ML (PROD)	.15	8%	.16	.14	2
KE3O	30	40%	48	12	4
KW	19	60%	30	7.6	4
KO	2	60%	3.2	.8	4

Error varies with the logging environment and ideally requires continuous evaluation, and presentation as an integral part of each parameter. An automated mathematical process using agreed standard errors for each perturbing influence would be preferable to the incoherence method for two reasons:

1) By informing the user at what stage error had been introduced so useful information can be retained.
2) By enabling better pathways of information flow during difficult formation evaluation through awareness of error.

Chapter 9

LABORATORY WORK

Chapter 9 describes the main data gathering phase of the project. It is divided into 5 reports with their own conclusions: optical thin sections (including diagenesis), X-ray diffraction, scanning electron microscope, nuclear activation and core conductivities. The lab work created large amounts of data which has been bought to bear upon the interpretation in terms of its influence upon the physical processes of the various logging tools (e.g. Fig p157). Chapter 9 also eliminates the possibility of swelling clays or mobile fines, and establishes a firm grounding for the log analysis of a formation in which 90% of the rock volume is rock matrix.

9.1 OPTICAL THIN SECTIONS

9.1.1 PURPOSE OF THIN SECTION EXAMINATION

Thin sections provided an appreciation of the basic nature of the rock type where other methods failed. The rock components geometrical arrangement and relative volumes became clear, a basic weakness of wireline logs.

The advantages of studying thin sections can be summarised as follows:

1) To quantify bulk mineral components.
2) To investigate intrafacies heterogeneity.
3) To highlight distinctions between clast and matrix which influence tool response.
4) To investigate the ability of basic logging tools to differentiate the facies delineated during core description.
5) To evaluate clay types and distribution.
6) To investigate porosity permeability relationships and predict reservoir quality.
7) To investigate fluid and electrical flow pathways, particularly excess conductivity.
8) To catalogue porosity reducing agents.
9) To establish a diagenetic history.
10) To provide point count raw data for the following Non–log–inputs:
The Dry Clay Mineral Point.
$V_{clay\ dispersed}/V_{clay\ total}$ & Illite/Total clay.
HI_{clay}, HI_{shale}, and V_{clay} HI adjusted ;
through knowledge of clay types in the reservoir and shale reference bed.

9.1.2 SIGNIFICANCE OF *"Structural"* AND *"Dispersed"* CLAY USED IN POINT COUNTED PHASES

Structural and Dispersed as opposed to Detrital and Authigenic are used as subdivisions here because the purpose of the research is to upgrade log interpretation by making use of non-log information. Tool response, particularly resistivity, will be dominated by the conducting medium's resistivity and geometry as opposed to its geological origin.

Dispersed Clays: Clays with a film or thread like three dimensional geometry.

Structural Clays: Clays with a grain like or lumpy geometry.[31]

For equal volumes of clay:

$$(\text{Clay Boundary Surface Area})_{dispersed} >> (\text{Clay Boundary Surface Area})_{structural}$$

The importance of this distinction is that volume for volume dispersed clay will influence conductivity far more than structural clay providing their resistivities are approximately equal.

9.1.3 THIN SECTION DESCRIPTION SHEETS

96 detailed description sheets with 109 photomicrographs were compiled from a total of 47 thin sections, and over 11,000 point counts. Some poorly made thick sections and some SEM (Scanning Electron Microscope) polished sections were also seen but quantitative data was not derived from these. The 96 pages which make up (APPENDIX 2) most accurately and fully represent the porosity types of Well A. They are also important because they provided the impetus for directions followed in this thesis.

9.1.4 THIN SECTION STATISTICS

Economy of Point Counts

While a large number of point counts per section would most perfectly determine the percentage of small volume fractions, e.g. pyrite, the counts required to give reasonable accuracy for their occurrence in these rocks was determined using Fig p144. Very rare phases such as tourmaline were grouped together under "Other". The volumetric importance of "Other" was always negligible in terms of the bulk properties seen by logging tools. (APPENDIX 2)

[31] Structural clay may merge laterally into Dispersed clay within a thin section.

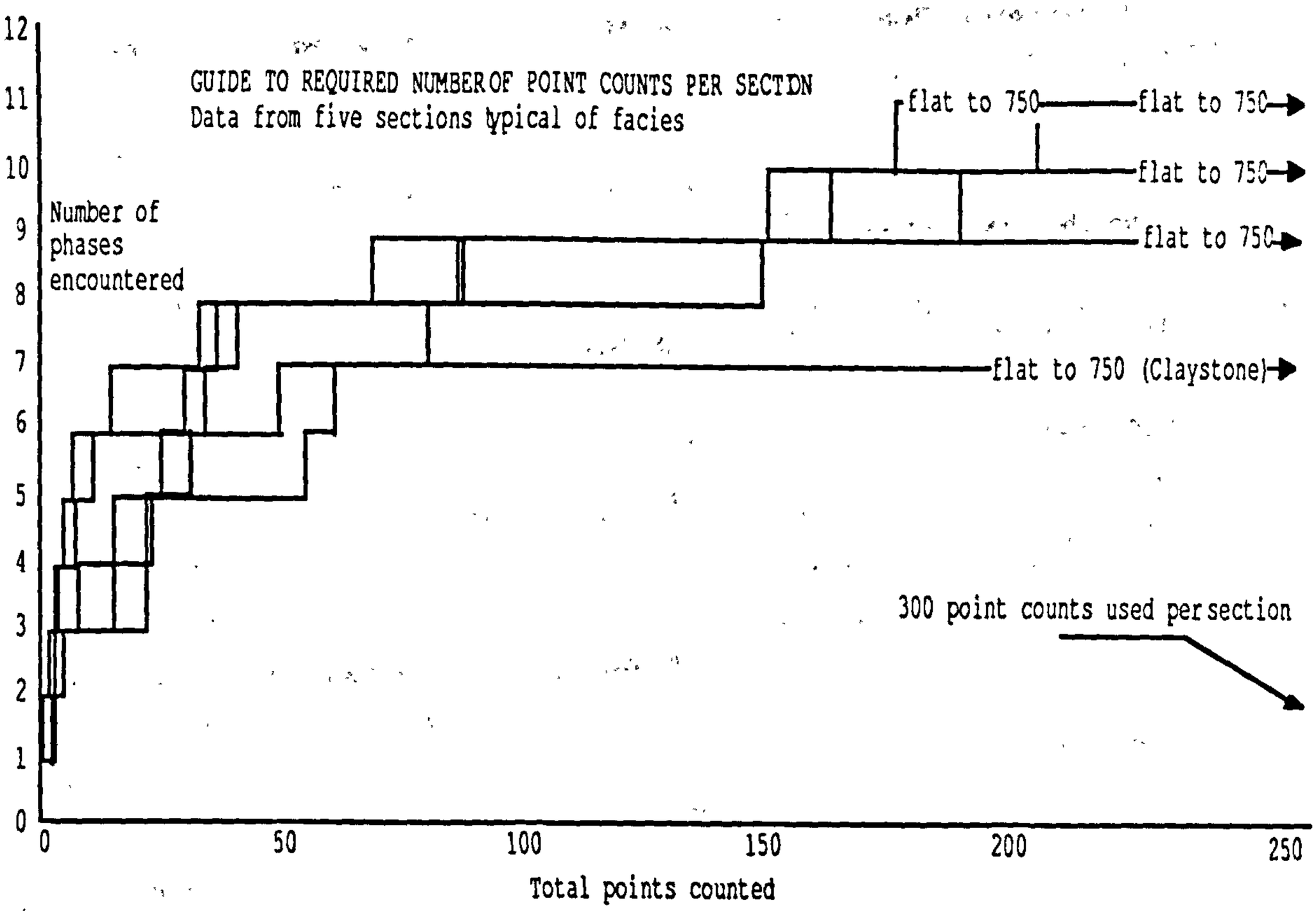


Fig p145 Economy of point counts.

Statistical Variation

Intra and inter-facies variations became apparent after point counting the thin sections. The following statistical treatment of point counts taken from the description sheets provides a medium for these observations.

Table p145 Statistical treatment of point counts

		$\Sigma x/n$	$(\Sigma(x-x)^2/n)^{.5}$	$(StdDev)/n^{.5}$
Ryazanian Sandstone	n = 6	Arith Mean	Stand Devn	Stand Err +/-
Structural + Dispersed Clay		28.67	9.42	3.84
Ø>100 + Ø<100µ		23.33	6.41	2.62
Pyrite		1.50	1.22	0.50
Hydrocarbon + Organic Matter		0.67	0.82	0.33

Clast Supported Cgl, Clasts	n = 4	Arith Mean	Stand Devn	Stand Err +/-
Structural + Dispersed Clay		69.00	9.42	4.71
Ø>100 + Ø<100μ		0.75	1.50	0.75
Pyrite		25.75	19.57	9.78
Hydrocarbon + Organic Matter		5.25	3.77	1.89

Matrix Supported Cgl, Mtx	n = 8	Arith Mean	Stand Devn	Stand Err +/-
Structural + Dispersed Clay		28.25	8.86	3.13
Ø>100 + Ø<100μ		12.25	7.96	2.81
Pyrite		3.38	2.39	0.84
Hydrocarbon + Organic Matter		2.14	1.46	0.52

Bedded Medium Sandstone	n = 12	Arith Mean	Stand Devn	Stand Err +/-
Structural + Dispersed Clay		22.50	6.14	1.77
Ø>100 + Ø<100μ		8.67	3.96	1.14
Pyrite		3.33	1.97	0.57
Hydrocarbon + Organic Matter		4.33	5.18	1.49

contd...

Interbedded Sstn & Claystn	n = 4	Arith Mean	Stand Devn	Stand Err +/-
Structural + Dispersed Clay		36.25	8.88	4.44
Ø>100 + Ø<100μ		3.75	2.22	1.11
Pyrite		2.00	2.71	1.35
Hydrocarbon + Organic Matter		52.00	63.54	31.77

Claystone	n = 4	Arith Mean	Stand Devn	Stand Err +/-
Structural + Dispersed Clay		137.00	59.38	29.69
Ø>100 + Ø<100μ		0.00	0.00	0.00
Pyrite		26.50	18.63	9.31
Hydrocarbon + Organic Matter		41.75	7.80	3.90

Significance of Facies

These numbers concur with the general impression gained from looking at sections, that there is no significant difference in mineral abundances between the Brae Formation sandstone facies. However the total porosity[32] of the Massive Coarse Sandstone facies

[32] Thin section visual porosities may be less than $\emptyset_{he}$

appears to be slightly higher. Facies were chosen from core description with the usual emphasis upon depositional grain size, and not after quantitative laboratory work.

9.1.5 QUANTITATIVE BULK MINERALOGY

The rock name on individual thin section description sheets is based on the original core description. Intrafacies heterogeneity causes some sections to appear typical of other facies.

The main variation in bulk mineralogy was from Quartz to Quartz with Clay minerals. Other constituents, namely pyrite, carbonate, hydrocarbon + organic matter, K–feldspar and muscovite, rarely exceed a total of 7% by volume. The histograms below reveal the similarity in bulk mineralogies of geologically distinct facies. Geologists use depositional energy as a strong criterion for facies demarcation (Selley, 1985. p298). This presents problems for log analysis because tools do not distinguish the sizes of detrital clasts with the same mineralogy. In fact the usual Quartz to Clay minerals facies trend, a trend which reflects depositional energy and logging tool response, is destroyed in the Brae Formation because of clay minerals in the highest energy facies of all; in the clasts of the Clast Supported Conglomerate.

The 11,000 point counts have been used to show the distribution of minerals with respect to facies. Point counts for each channel have been corrected in accordance with SEM work (9.3.4), and summed for each facies by using all the thin sections from one facies. The summed point counts for each phase, and the percentage they represent within each facies have been listed and are included as (APPENDIX 3). Facies are listed in order of decreasing reservoir quality as shown on the ternary plot. The values in (APPENDIX 3) have been displayed as histograms on the following three pages.

Overleaf:

Fig p148 Relative abundance of point counts per channel per facies

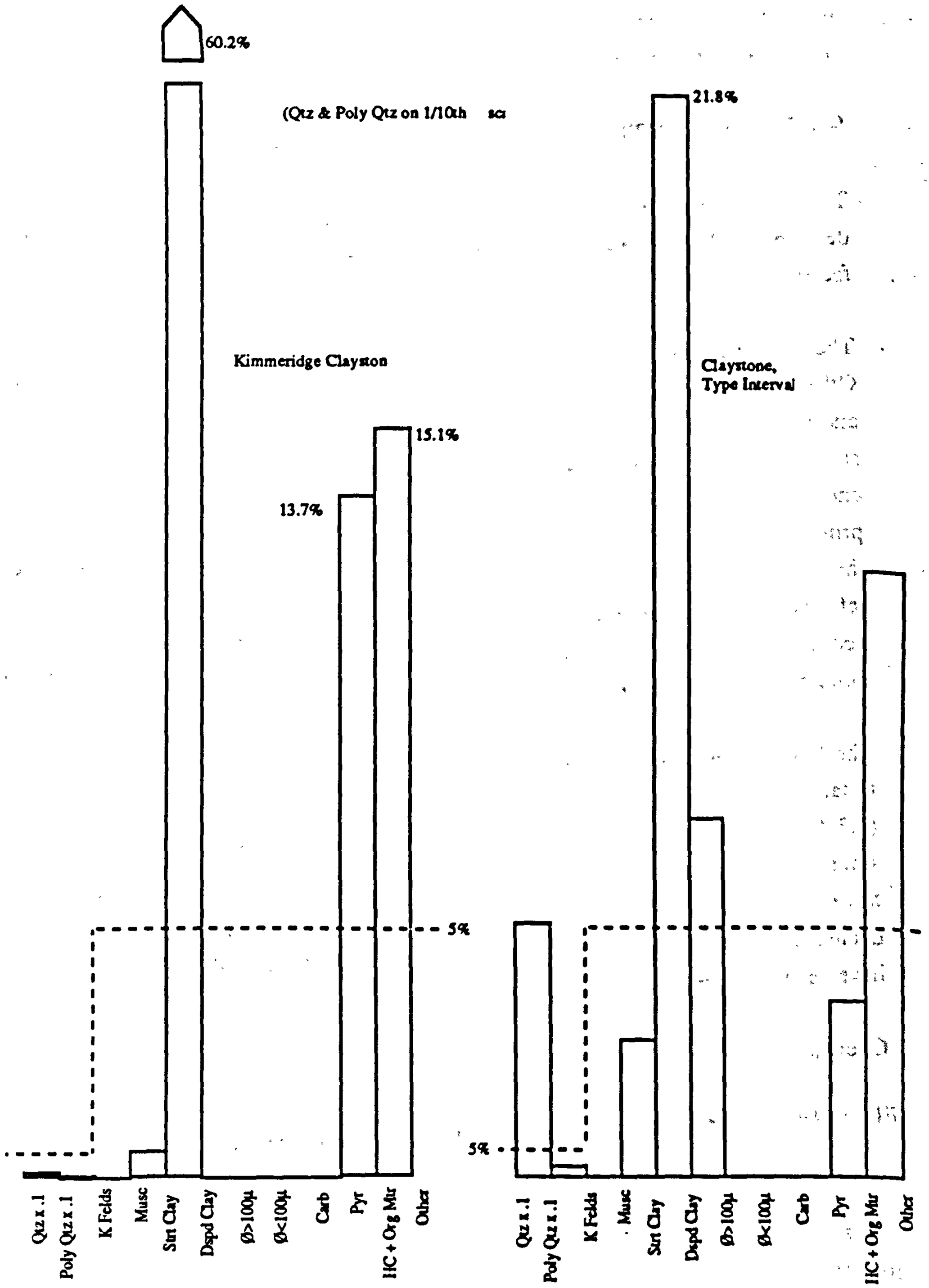


Fig p148 Relative abundance of point counts per channel per facies, contd...

(Qtz & Poly Qtz on 1/10th sc

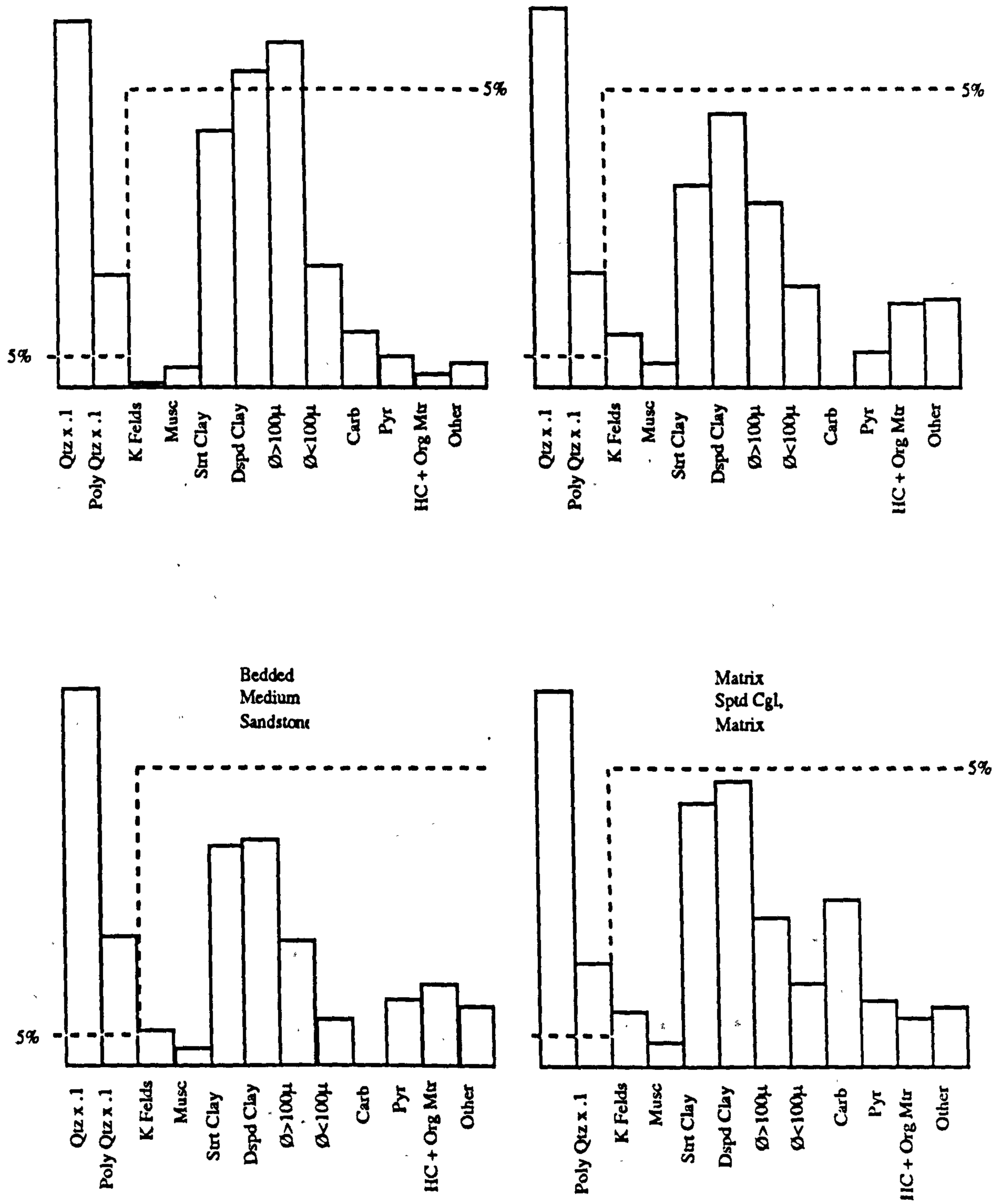


Fig p149 Relative abundance of point counts per channel per facies, contd...

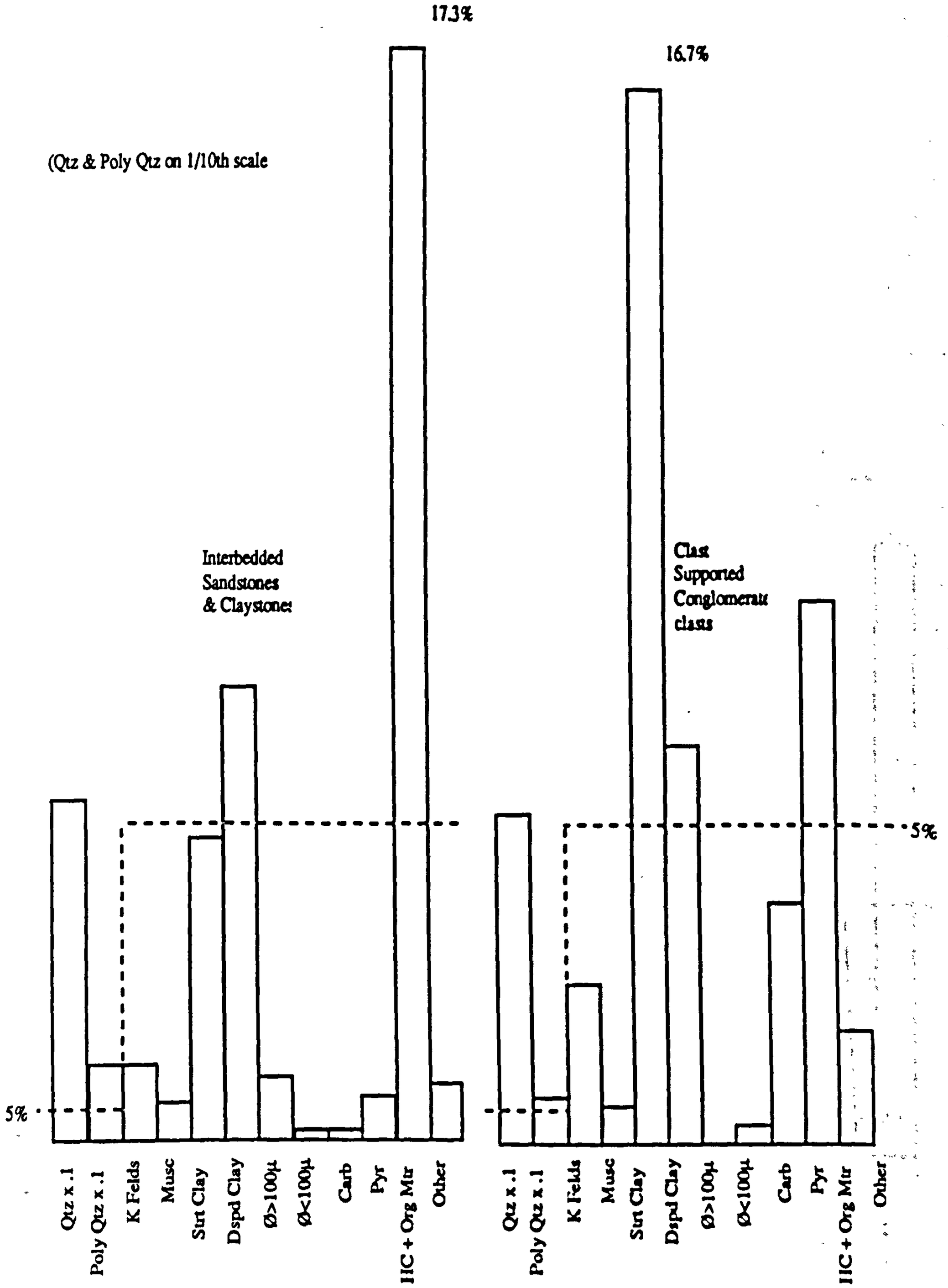


Fig p150 Relative abundance of point counts per channel per facies, end

Three types of sandstone are evident from the histograms.

1) Ryazanian Sandstone. (Protoquartzite)
2) Brae Formation Sandstone facies together with the conglomerate matrix. (Protoquartzites)
3) Conglomerate Sandstone Clasts. (Quartzwacke)
   Brackets: refer Selley, 1982.p81.

Ryazanian Sandstone comes closest to pure orthoquartzite but still contains more than five percent non quartz.

There is no consistent difference in mineralogy between the various sandstone facies of the Brae Formation in Well A, including the conglomerates matrix. The common origin of the Brae sands is indicated by the constancy of all detrital phases across all the Brae sandstone facies. Sandstones deposited before or after the Brae Formation: Ryazanian and Devonian, have markedly different feldspar contents and muscovite/feldspar ratios.

Clay volumes are similar for the Brae sandstones, with less than half the volume found in the sandstone clasts. Some point counts under hydrocarbon+organic matter are sourced from detrital plant debris which has matured in situ, and some from bitumen injection from interbedded or overlying organic shales. There was no obvious relationship between the two types and facies. A portion of both dispersed and structural clays were authigenic. These authigenic clays were slightly more abundant in the conglomerates sandy matrix and the Massive Coarse Sandstones, possibly reflecting a higher ancient permeability.

The remaining point counted phases are controlled primarily by diagenesis and are discussed under Diagenesis (9.1.12) below.

9.1.6 INTRAFACIES HETEROGENEITY

Variations in pore geometry within each facies are considerable and approach the variations seen between facies, with the exception of Bedded Medium Sandstone which appeared relatively homogeneous.

Almost all the porosity in the Brae Formation of Well A is secondary. Leaching has given rise to an inhomogeneous porosity network which appears to have been initiated by scattered feldspars. Leaching has continued with the corrosion of quartz grains (MCS 15144). Pore types varied from rare isolated vugs, of 5+ grain sizes, to slightly better

connected secondary porosity. Vugs usually occur in a very low porosity intergrown quartz matrix (photo:MCS 15144, MSCM 14633).

Porosity has been classified as > and < 100 microns to record pore geometry and assist with any porosity permeability relationships. However no clear relationships between pore type or mineral geometrical distribution, and facies, evolved. Facies, influenced primarily by depositional energy, are not as relevant to formation evaluation as observations based upon pore geometry, especially in the case of Well A's strong diagenetic overprint. The controls which depositional facies exert upon diagenesis have become obscured by successive phases of diagenesis except in the interbedded facies which show less diagenesis due to the restrictions placed on flow by interbedded shales.

Clay distribution was also variable and did not correlate with facies. Authigenic clay coats were extensive in all facies but some individual sections did show less coats, particularly those from the interbedded facies.

9.1.7 A PETROPHYSICAL PLOT

For the purpose of recognising facies from logs, a plot related to petrophysical properties should demonstrate the potential that logs have to separate facies, provided that the plot utilises those distinguishing properties most clearly seen by the logs available. Initially the thin section data was plotted on a "Petrophysical Ternary Plot" by the point counted channels contributions to *rhob*, *HI* and *GR*. The summed contributions were then expressed as fractions of (*rhob*+*HI*+*GR*). However a ternary plot cannot properly represent three tool readings in their absolute terms; it can only present them as fractions of the sum of the three. Unlike thin section counts, the logging tools absolute values carry information and so a three dimensional plot was required.

9.1.7.1 DEDUCTION OF PETROPHYSICAL VALUES FROM THIN SECTIONS

The three standard petrophysical properties with a good ratio of natural spread to tool error are:

Natural Radioactivity,

Bulk Density,

Hydrogen Index.[33]

Conductivity, C_O, is a fourth; however it cannot be used as an axis in a graphical plot

[33] HI as seen by a neutron logging tool, not as measured in geochemistry.

because the influence of each point counted channel is strongly affected by pore geometry which cannot be recorded for each thin section in a manner quantitatively linked to conductivity. Neither is conductivity dominated by depositional mineralogy or processes, but more by authigenic phases such as dispersed clay and remaining porosity. Although the microlog parameter (*ML*,8.1.7) is useful in distinguishing facies this parameter cannot be numerically deduced from point counts. Permeability seen with the Microlog's response to wall cake is a Yes / No indicator, however "Yes" or "No" may apply to more than just one facies.

If we group the point counted channels under axes corresponding to the three standard lithological tools: *rhob* , *GR* and *HI* , the feasibility of using these tools to distinguish facies should become clear (9.3.4). Some phases contribute to more than one axis, i.e. K-Feldspar contributes to *rhob* and *GR* . In order to apportion a point counted channel's influence to an axis, the influence on a channel has been compared to a standard, therefore:

Fresh water is the standard influence for *HI* : 1.0,
Illite is the standard influence for *GR* : 275 API,
Pyrite is the standard influence for *rhob* : 3.99 g/cc. (*rhob* range: 1.00-4.99=3.99)

With these axes mineral volume fractions, not their geometry, is the dominant influence on the tool readings. The presence of adsorbed radioactive uranium on anoxically formed organic matter is unquantifiable from thin sections. Its presence will cause the *GR* value predicted from sections to be less than *GR* true. This will be greatest in the organic rich Kimmeridgian shales.

9.1.7.2 INFLUENCE OF POINT COUNTED CHANNELS PER AXIS, MULTIPLIERS. (Schl, 1985. p104/5)

Table p154 Influence of point counted channels on axes of Petrophysical Plot

CHANNEL	rhob (g/cc-1)/3.99	HI Øcnl/100	GR GR/275
Quartz	.41	-.02	0.00
Polyxln Quartz	.41	-.02	0.00
K Feldspar	.38	-.03	0.80
Muscovite	.46	.20	0.98
Structural Clay	.38	.30	1.00
Dispersed Clay	.38	.30	1.00
Ø > 100 µ	.01	1.00	0.00
Ø < 100 µ	.01	1.00	0.00
Carbonate	.43	-.01	0.00
Pyrite	1.00	-.03	0.00
HC+Org Mtr	*.05	.60	0.00 + see above paragraph

* Bitumen has a marginally greater density than pore water, Ø.

The multipliers have been used to deduce the coordinates rhobcord, *HI* cord, *GR* cord in the following way:

PCs = Point Counts

rhobcord = *(Qtz + Poly Qtz PCs * .41) + (KFelds + Strl Cly + Dspd Cly PCs * .38) + (Musc PCs * .46) + (Carb PCs * .43) + Pyr PCs + (HC+ OrgMtr PCs * .05)*

HIcord = *(Qtz + Poly Qtz PCs * -.02) + (KFelds + Pyr PCs * -.03) + (Musc PCs * .20) + (Strl Cly + Dspd Cly * .30) + (Ø > 100 + Ø < 100 µ PCs) + (Carb PCs * -.01) + (HC+OrgMtr PCs * .60)*

GRcord = *(KFeld PCs * .80) + (Musc PCs * .98) + (Strl Cly + Dspd Cly PCs)*

Each counted phase has been substituted into these formulae for each thin section. Before this was done each thin section was normalised to 300 point counts because the absolute values carry information. The 156 coordinates resulting from these calculations are listed

as (APPENDIX 4). The theoretical positions of the pure standard influences have been shown here to help see the petrophysical plot overleaf in perspective:

Thin section of pure Illite	rhobcord	= 114.00
	HIcord	= 90.00
	GRcord	= 300.00 off plot scale
Thin section of pure Pyrite	rhobcord	= 300.00
	HIcord	= - 9.00
	GRcord	= 0.00 off plot scale
Thin section of pure Ø	rhobcord	= 0.00
	HIcord	= 300.00
	GRcord	= 0.00 off plot scale
Thin section of pure Quartz	rhobcord	= 123.00
	HIcord	= - 6.00
	GRcord	= 0.00 within plot scale

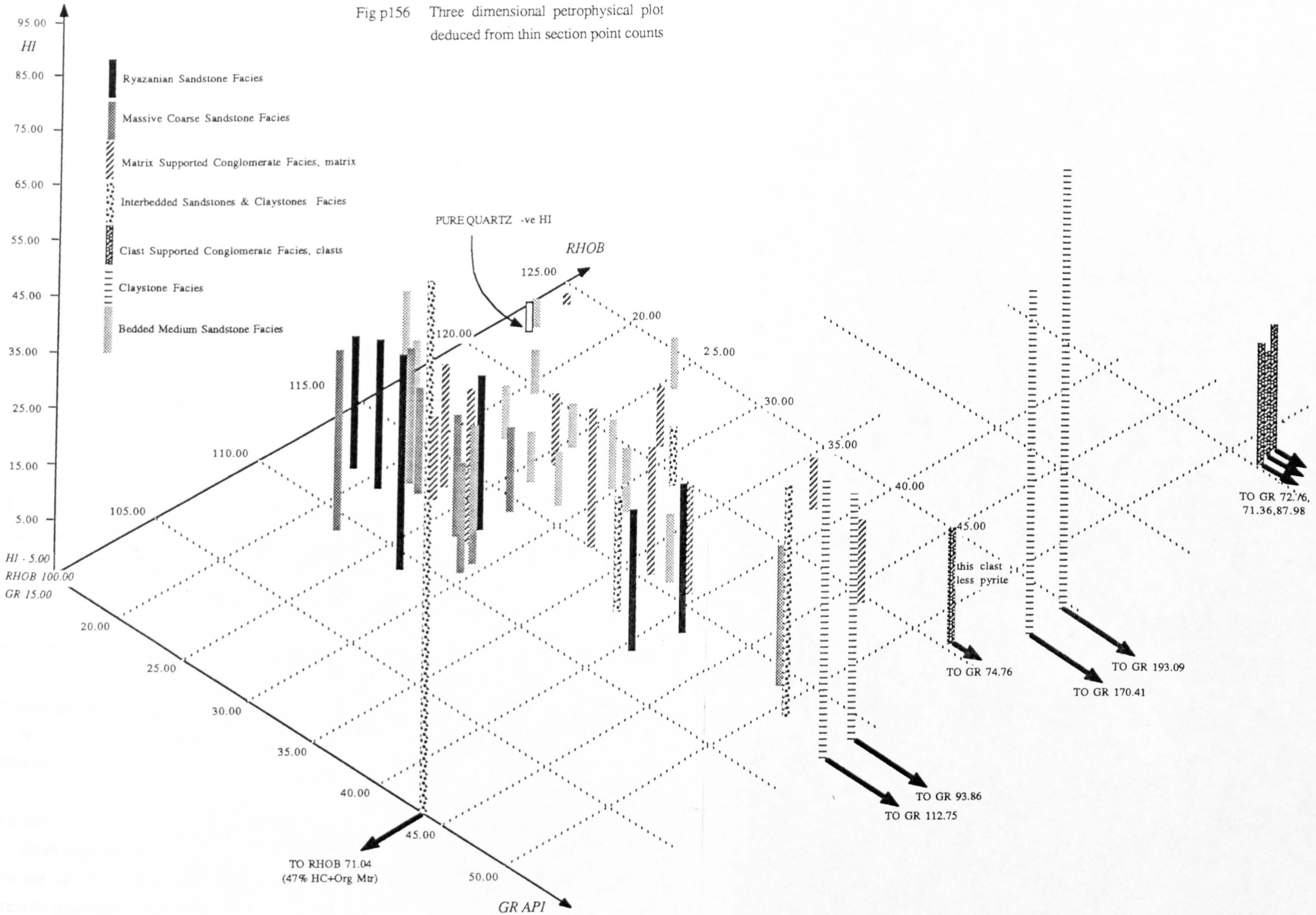
Overleaf:

Fig p156 Three dimensional petrophysical plot deduced from thin section point counts.

Fig p156 Three dimensional petrophysical plot deduced from thin section point counts.

Do Not Lend Or Copy

Fig p156 Three dimensional petrophysical plot deduced from thin section point counts



9.1.8 DISTINCTIONS BETWEEN CLASTS AND MATRIX WHICH INFLUENCE LOGGING TOOLS

There are three main types of clasts,

1) Argillaceous fine sandstone,
2) Polycrystalline quartz granules and pebbles, and
3) Carbonate cemented fine argillaceous sandstone.

There are also minor intraformational shale clasts. All have zero effective porosity and make no contribution to reserves.

The presence of zero porosity pure quartz pebbles does not present problems to log analysis because bulk porosity measurements will be correct, and conductivity through these quartz pebbles will not occur. However the presence of clay, feldspar and microporosity in the argillaceous clasts does require attention. These characteristics will affect bulk porosity and bulk conductivity but arise in the non-reservoir, i.e. non sandy matrix, fraction of the rock.

The mineralogical differences between clasts, predominantly argillaceous fine sandstone, and sandy matrix can be seen in the histograms earlier in this chapter. K–Feldspar, clays, pyrite and carbonate are all significantly increased in the clasts, while porosity is negligible. These will effect the lithological logging tools in the manner quantitatively worked out and displayed in the three dimensional petrophysical plot.

The effect on water saturated conductivity has been dealt with at length in (7).

The petrophysical plot shows that it is feasible to distinguish clasts from matrix using standard lithological logging tools. This fact has been exploited during log analysis in the parameter *vlogs*.

It is interesting to note that "geological" clasts from a core description, and "petrophysical" clasts from logs are not identical for reasons given three paragraph above. Petrophysical clasts are of interest in calculating producibility and reserves, geological clasts are of interest in modelling depositional environments.

9.1.9 POROSITY & PERMEABILITY

Porosity/permeability relationships are strongest when only one type of pore geometry is present in a rock, primary porosity for example. The Brae Formation sandstones contain predominantly secondary porosity with variable pore geometries. A small proportion of primary small pores between quartz overgrowths do remain. The tortuous paths which provide permeability are not always evident from a 30micron thin section. Nevertheless the sandstones did provide a general increase of connected pores (permeability) for an increase of porosity, in all the facies.

Although numerous sections for each facies were observed there was no clear relationship between porosity type and facies, although it must be remembered that a laboratory technician has imposed a bias upon all these samples which can only be overcome by a complete resampling of the core. The lack of a relationship between pore type and facies can be seen in the photographs. The Reservoir Quality ternary plot provides a good indication of the wide variations within facies, as well as the median position of each facies. Use of image analysis software could provide a standard pore geometry classification system for use with fluid and electrical flow. This is the object of the Ø > or < 100µ classes of this project.

The plot also shows the clear superiority of Ryazanian sandstone as a potential reservoir. Porosity/permeability relationships are stronger in this simpler sandstone.

Porosity/permeability relationships based on the Density Neutron combination will include clay microporosity. In rocks of 10% porosity, and 8% clay, effective porosity as a function of the matrix sands clay (V_{shmtx}) will provide a stronger correlation. Core porosity/permeability plots were made by the operator.

The Bedded Medium Sandstones have slightly less porosity than other facies. Their slightly lower clay content and absence of non productive clasts make these predominantly thin intervals better potential reservoirs than their porosities might suggest. Lack of clasts in this and the Massive Coarse Sands allow better log evaluation. Any shale intercalations finer than tool resolution will however make log analysis pessimistic.

9.1.10 TERNARY PLOT OF RESERVOIR QUALITY FROM THIN SECTION DATA

Point counted channels are grouped as they effect reservoir quality. End members are:

1 = (Qtz + Poly Qtz + KFelds + Musc + Strl Cly + Carb + Pyr + HC+OrgMtr + Other) pcs

2 = (Dspd Cly) point counts

3 = (Ø > 100μ + Ø < 100μ) point counts

Then, for ternary plot coordinates:

1cord = 1/1+2+3 *2cord = 2/1+2+3* *3cord = 3/1+2+3*

The presence of the phases in 1 is considered to have neutral influence on reservoir quality, the presence of phases in 2 a negative influence on reservoir quality, and the presence of those in 3 a positive influence on reservoir quality. No account can be made of porosity > 100μ which is vuggy or connected. Although point counted dispersed clay takes up no more pore space per point count than any other phase in 1, it is generally more detrimental to the flow of hydrocarbons and to formation evaluation.

A glance at "Relative Abundance..." histograms, the DST data and core analysis indicates that the relative amounts of porosity > 100μ pore diameter (≈25μ pore throat radius) and dispersed clay do have a strong correlation with reservoir quality. They are clearly the major point counted influences on reservoir quality.

The results of these calculations on each thin section provide the Reservoir Quality Ternary plot coordinates which has been listed as (APPENDIX 5). These have been plotted overleaf as:

Fig p160 Reservoir quality from thin section point counts.

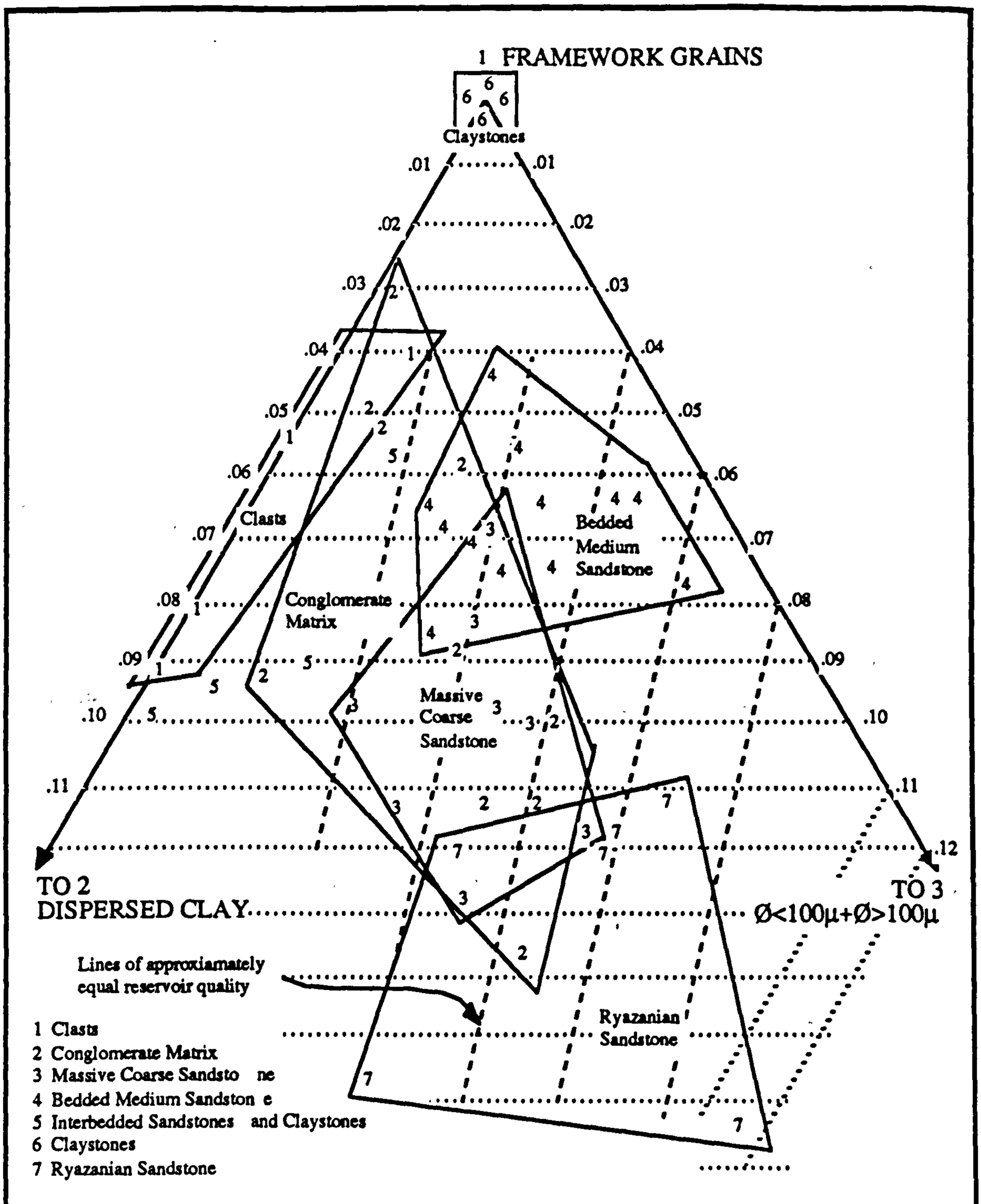


Fig p160 Reservoir quality from thin section point counts

9.1.11 FLUID AND ELECTRICAL FLOW PATHWAYS WITH REFERENCE TO EXCESS CONDUCTIVITY

9.1.11.1 FLUID FLOW

Thin sections from the Brae Formation give the impression of poor and variable fluid flow properties. Some sections, notably BMS 15175, 14633; MCS 14951; MSCM 14622, 14905, showed moderately good pore systems but this was not always corroborated by the core permeabilities from which the sections were cut. Such variations within a core plug mean at least those variations within the facies. To counter this numerous sections were examined from each facies.

Thin sections suggest that Ryazanian flow properties are superior for many reasons. Porosity >100μ approaches double the average for Brae. Visual connection of pores is also better and the pore network is far more homogeneous, suggesting continuity beyond the thin section. However some sections did show zones of intergrown quartz grains, RS 14055 & RS 13884. Primary porosity was also present in the Ryazanian. Point counts of dispersed clay were slightly higher, but clay in the Ryazanian's larger pore throats is not as damaging.

These contrasts between Ryazanian sandstone and the Brae Formation show that when porosities drop below about ten percent, pore geometry and clay distribution become critical to permeability and also to formation evaluation.

9.1.11.2 ELECTRICAL FLOW

Electrical flow can occur in three of the point counted phases.

1) Pore water.
2) Bound water in clays.
3) Pyrite.

The relative importance of these three phases to electrical pathways is variable and not necessarily controlled by their percentage volume. They are controlled by diagenesis, and show heterogeneous geometries bearing no obvious relation to deposition. In many

sections dispersed clay appears to be the greatest conductor, MCS 14680 for example. In others higher counts of structural clay do not seem to provide electrical pathways - remembering that we are limited to two dimensions. Dispersed and structural clay subdivisions were invented to discover any correlation with log derived C_x parameters (6.2.1, 6.2.2.1, 11.3.2). However these effects are obscured by the high (85,000ppm) salinity and by any variations in m.

The proportions of dispersed to structural clay had no clear relationship with facies, or anything else observed in the rock, and so the geometrical distribution of conductive clay remains unpredictable beyond individual thin sections[34]. This unsatisfactory situation prevails for all other petrophysical laboratory tests on all wells; pointing to the use of downhole data wherever possible.

The same is true for pore geometry, m. Clearly m for cubic meters of rock, R_t, with pores like MCS 15144 will be higher than for a rock with pores like MSCM 14905. There is no way to determine the three dimensional extent of an m value beyond those samples tested. With a rock exhibiting such variations in pore geometry, coupled with the bias imposed on sampling by the laboratory technician it is unrealistic to measure R_Os, combine the data in a single plot, and apply th result across the reservoir. This will lead to low m values and artificially low S_ws.

Pyrite does not contribute to electrical pathways in some sections, although it may be present in amounts greater than one percent. It has the highest conductivity and exhibits the most diverse geometry of all the conductors. Geometry varies from isolated nodules partially enclosed in quartz, to thread like replacements of organic matter, or strings of micronodules entrained in clay, BMS 15250, 14924, 14607. In determining S_w, pyrite is usually ignored, whereas vuggy porosity is included. This is a reflection of being able to quantify porosity and not pyrite. Where pyrite occurs in a conducting medium; clay or formation water, it will act as a vug of conductivity in the same manner as vuggy porosity, but with an order of magnitudes greater conductance. Its effect on bulk conductivity is dependent upon its geometry and electrical contact with other conductors. Its volume fraction alone is almost useless as a guide to its conductive pathways. If the LDT[35] detects pyrite, its influence on R_t will remain unknown unless additional geometrical information is available. The image producing FMT[5] should help with empirical translations of image to the various conducting mediums individual m values.

---

[34] Furthermore reservoir temperatures were not available for tests so no clay/electrical correlations could be made.

[35] Schlumberger Trade Mark. Litho Density Tool. Formation Microscanner Tool.

In the Ryazanian the ratio of free water conductivity to excess conductivity will be more stable in view of the general homogeneousness of the conducting phases.

These observations on excess conductivity for the Brae Formation may appear pessimistic. However after examining 53 sections and remembering the resistivities of Formation Water 10^{-2}, Dispersed Clay $\approx 10^{0}$, and Solid Pyrite $\approx 10^{-3}$ Ωm, the method of calculating water saturation by measuring <u>bulk</u> conductivity seems problematic in these rocks. The ratio of free water conductivity to non free water conductivity in pore lined, low porosity rocks is low; and changes in free water conductivity due to hydrocarbon will be blanketed by excess conductivity. The straightforward test of a rock's resistivity sensitivity to saturation is Archie's *n* value. However room temperature *n* values taken on probably atypical and traumatised plugs cannot properly describe the deep reservoir situation. These seemingly naive and qualitative observations cannot therefore be overruled by laboratory results. See also (7).

9.1.12 DIAGENESIS

9.1.12.1 POROSITY REDUCING AGENTS

The diagenetic phases which reduce porosity in Brae sandstones, in order of importance are:

1) Quartz overgrowths,
2) Authigenic Illite,
3) Bitumen, (seen as porosity by logs)
4) Pyrite and
5) Poikilotopic Calcite present below about 15220 (4636m).

A reduction of porosity with depth is superimposed upon these influences.

In the Ryazanian Sandstone above porosity was reduced by:

1) Quartz overgrowths,
2) Authigenic Illite and Kaolinite,
3) Carbonate,
4) Traces of Organic Matter and Pyrite.

9.1.12.2 DIAGENESIS HISTORY

The apparent diagenetic sequence has been recorded under "Inferred Diagenetic Sequence"

on each thin section description sheet.

Quartz

Diagenesis is well advanced in Brae and has given rise to low porosity, low permeability sandstones with unevenly distributed petrophysical properties. The major volumetric influence is undoubtedly quartz overgrowths which have occurred soon after depositional settling and compaction, and also following the development of secondary porosity, as evidenced by euhedral growths into large pore spaces. See BMS 15105, MCS 14959 (APPENDIX 2). A portion of the volume of quartz overgrowth is likely to have been sourced from early smectites altering to illites with release of SiO_2. Quartz overgrowths in Brae are not always easy to identify because "dust rims" of crystal voids, or of partial coatings of early authigenic clay; are not always apparent. Zones of tens of grains have frequently become intergrown forming low porosity "knots", leaving only microporosity between crystal edges. This microporosity, seen with the SEM, has been unable to conduct future porosity creating fluids.

High magnification views of quartz grain/quartz overgrowth boundaries commonly appeared to contain thin clay films. See MCS 15325, MSCM 14622 (APPENDIX 2). These were never convincingly identified as clay minerals, and an early pre-overgrowth phase of authigenic clay is <u>not</u> thought to be present (9.3).

Clays

Authigenic illitic clays are well developed throughout the cored interval of the Brae Formation. They occur as structural and dispersed clay, filling pores and forming extensive grain coatings which frequently seal interparticle porosity, see CSCM 15370A, MCS 14680, BMS 14633. All authigenic clays appear to be illitic and probably share a common origin of either detrital kaolinites and smectites, or detrital potassium feldspars.

Temperatures above 200°C (Hower, 1981), increasingly alkaline conditions and potassium waters all favour a kaolinite to illite transformation. Traces of kaolinite were detected with the SEM and were probably present first, altering to illites as pH rose from acid levels following kerogen maturation, (Curtis, 1983).

Any detrital smectites will have degraded to illites with depth.

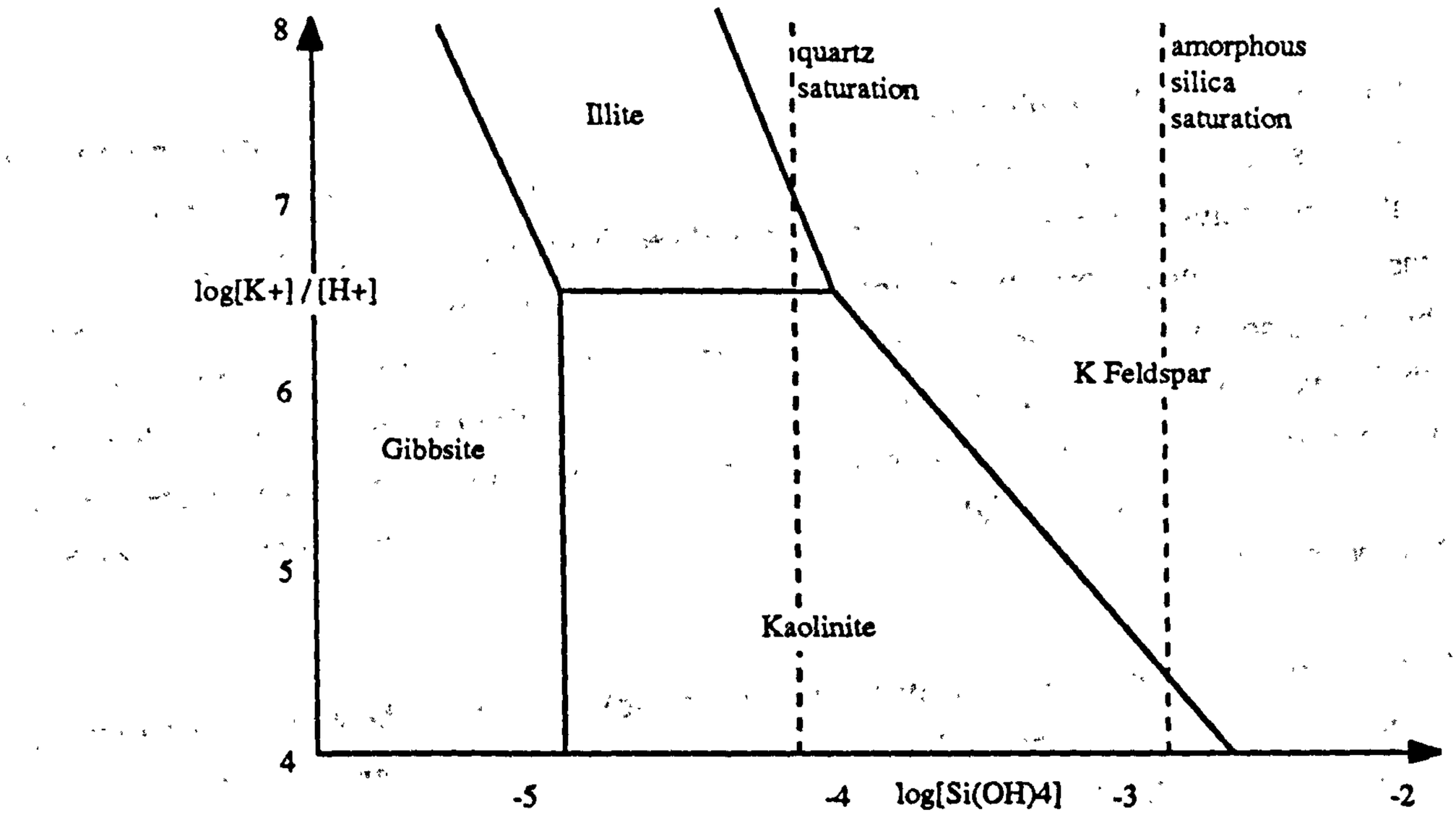


Fig p165 Stability fields of kaolinite, illite and K-feldspar in aqueous solution. Modified after Curtis, 1983.

Rotting potassium feldspars are common, BMS 15175 (APPENDIX 2), and are probably a major source of illite, bearing in mind that it is difficult to determine original feldspar content because of dissolution and quartz cementation. The Brae Formation illites therefore have three sources:

1) The degradation of detrital feldspar to kaolinite and illite.
2) The alteration of detrital kaolinite and smectite to K bearing illite.
3) In-situ mobilisation of detrital illites.

The chronology of the three basic diagenetic events: quartz overgrowths, secondary porosity and clay coats is obscured by observations such as clay coated quartz overgrowths growing into secondary porosity while other secondary pores are entirely filled with clay (MCS 15325).

Fluids which were corrosive to feldspars and quartz, passed through the Brae sandstones following the earlier phases of quartz overgrowth. These acidic fluids were probably sourced from the decarboxylation of maturing sapropelites overlying the formation (Schmidt & McDonald, 1979a). These fluids left an unevenly distributed network of secondary porosity. They may be viewed as the prime force behind the major diagenetic

changes which occurred after the main quartz overgrowth and illite phases.

Organics

Bitumen is a small but ubiquitous diagenetic phase, and occurs filling a small proportion of pores in all facies. It occurs as pore filling, partially pore filling, and entrained in authigenic clays. Bitumen was probably mobilised from organic rich shales and followed the advancement of porosity creating corrosive fluids. Bitumen fills some secondary pores but can also be seen adjacent to vacant secondary pores. The passage of short and long chain hydrocarbons through the irregular secondary porosity network appears to have left viscous long chained hydrocarbons trapped in narrow throated pores. Ancient pressure or temperature reductions may also alter the composition and viscosity of previously mobile hydrocarbons.

Organic matter also occurs as macro (cross fabric) stylolites where insoluble detrital organic debris has collected in the wake of pressure solution. Primary porosity reduction occurred early in the diagenetic history, and so these stylolites have an early origin, and have been isolated from further changes due to their position in very low porosity knots. These knots extend for a hundred or so grains. Stylolites are restricted to these zones.

Pyrite

Framboidal pyrite is the most pervasive diagenetic mineral. It occurs apparently well within[36] detrital quartz grains, as well as in quartz overgrowths, BMS 14607, 15250; and in all types of clay. Some of these occurrences appear to be part of the original detrital grain, but not all. Pyrite is particularly associated with bitumen and frequently replaces plant derived organic matter in strings of ?conductive micronodules. Pyrite and organic matter are both stable in reducing conditions.

Sulphur and iron, the elements of pyrite, and the reducing conditions necessary for pyrite genesis are met with during and after hydrocarbon migration from a sapropelic source (Surdam et al., 1984). Sulphur originates from in-situ organic matter and/or migrated hydrocarbons and H_2S. Fe cations occur in the irreducible formation water of an oil zone in equilibrium with clay minerals. In fact illites are phengite rich: Fe,Mg substitution of octahedral Al ions. Unlike most diagenetic phases small volumes of pyrite could be generated within an oil saturated rock, as well as at advancing oil water contacts. The

[36] Determining porosity from rhob, $\emptyset_{he}$ and core grain densities could accomodate this characteristic if pyrite was homogeneous.

availability of Fe cations is likely to limit the volumes of pyrite from this process but clearly Fe was available during phengitic illite authigenesis.

Pyrite and Carbonate were rarely found together.

Carbonate

Sections containing at least one point count of Carbonate:

13884	1 %	RS
13922	Tr	RS
14011	2	RS
14043	1	RS
14053	Tr	RS
14530 - 15219	BRAE GROUP SANDSTONES, NO CARBONATE.	
.....	No Brae Fm carbonate cements above this line.....	
15220	Tr	Highest Occurrence
15258	14	
15272	Tr	
15343	7	
15367	7	Clast
15370A	2	Clast & Matrix
15370B	3	Clast
15380	5	Clast
15381	4	

Carbonate cemented matrix was apparent in only a few of the deeper sections, notably MSCM 15258, 15343. It does not occur throughout the sections examined, only as a patchy poikilotopic cement. Zones of carbonate free, low porosity, quartz cemented sandstone lie adjacent to the calcite. These quartz zones sometimes contain leached feldspar secondary porosity. If these pores were present before calcite precipitation why did they not fill with calcite? Calcite seems to follow the main phase of porosity reduction, but precede leaching. Conversely, the ancient porosity where the sandstone is calcite cemented is higher; suggesting either early calcite which has been removed from adjacent areas, or quartz corrosion in the calcited areas. Alternatively, small scale brecciation of the

low porosity sandstone could allow selective poikilotopic calcification.

More than the two available sections are required for an unequivocal placing of calcite cementation in the sequence, however it occurred after most porosity reduction. Its presence below a certain depth suggests that it is below an ancient or present day oil:water contact. The coincidence of oil:water contacts, calcite cementation, and Tertiary block tilting needs to be investigated across the field, from information unavailable to the author.

Oil migration

Oil migration occurred after most diagenetic phases, with the exception of some of the pervasive micro pyrite, and calcite, if calcite is below an oil water contact.

Barite fines

Barytes was not detected in pore space observed with thin sections, however the SEM will be used to investigate this further. Thin sections indicate that Barite fines are not a major source of poor flow properties.

9.1.12.3 CONCLUSIONS REGARDING DIAGENESIS

Diagenesis in the Brae Sandstones of Well A has been extensive and ruinous to its reservoir properties. Low porosities have been impaired further by illitic clays in pore throats; and the system of secondary porosity is unevenly distributed, leading to formation evaluation problems and difficulties with the efficient exploitation of any hydrocarbons. During production heterogeneous pore geometries would cause advancing water fronts to enclose pockets of oil. Thin sections and core suggest this would occur on a cm, metre and greater than metre scale; severely impairing the recovery factor of an already low porosity formation.

From a review of the thin section description sheets a diagenetic sequence has been reconstructed overleaf as Fig p165 Diagenetic sequence.

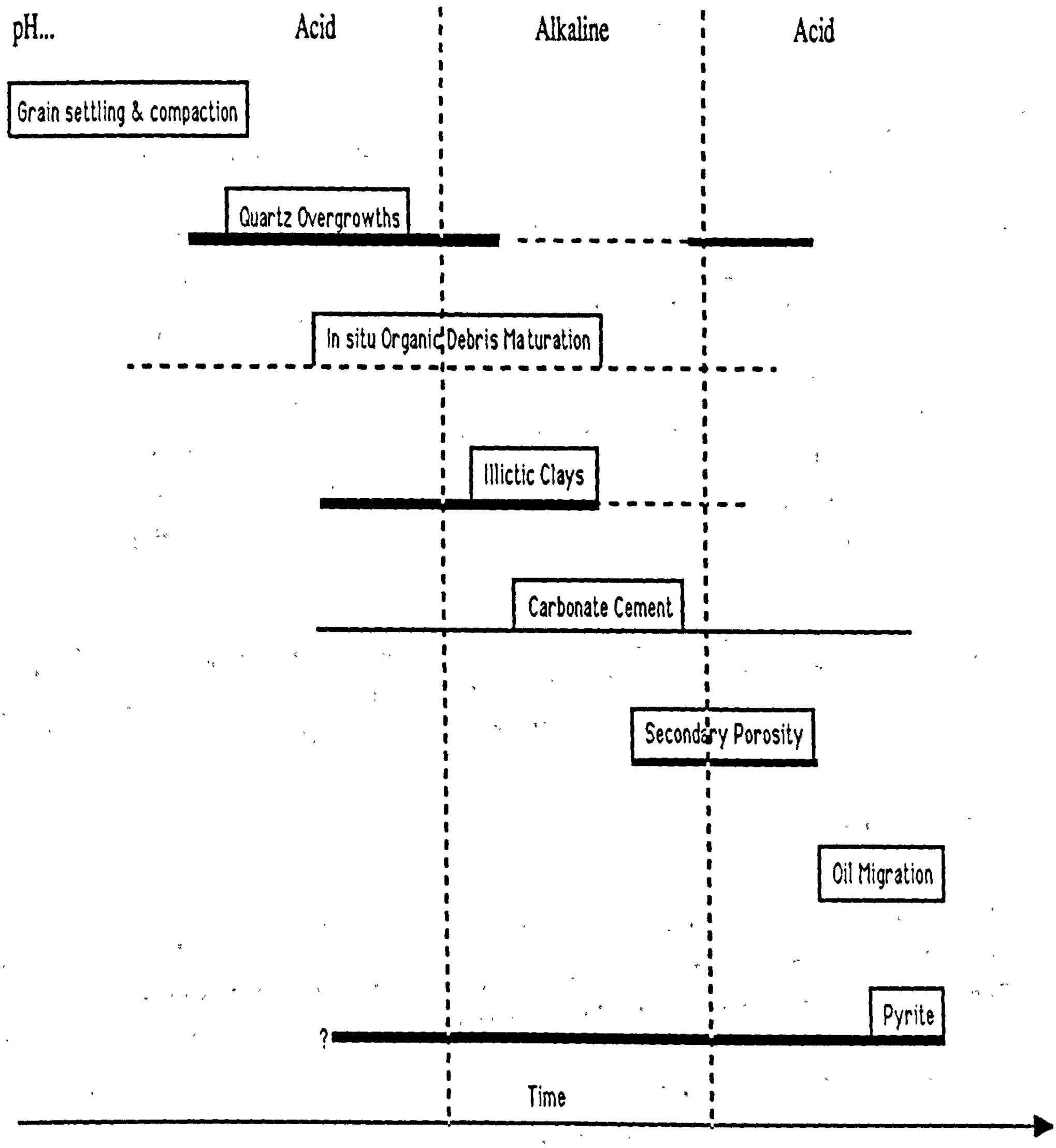


Fig p169 Diagenetic sequence

9.2 X- RAY DIFFRACTION

9.2.1 PURPOSE OF X-RAY ANALYSIS

X-Rays are diffracted by crystal lattices at angles characteristic of lattice spacing, *d*, according to Bragg's law (1914):

$2d\sin\theta = n\lambda$ (Nomenclature)

Characteristic angles and relative intensities provide for mineral identification.

Diffractions were carried out to corroborate the thin section study, and to confidently identify the clay minerals and minor unidentified phases. X-Ray studies were also intended to establish the absence of certain troublesome species such as swelling clays. Clay formation damage needed to be positively eliminated from explanations of Well A's anomalous results.

Differences in facies bulk mineralogy were established partly through X–Ray diffraction. Bulk mineralogy provides calibrations for tool responses which can be extended beyond cored intervals, assisting predictions of mineralogy, clays and pore geometry.

9.2.2 BULK SAMPLES

A full sweep X-Ray analysis was carried out on the 39 samples listed below. Samples were taken from core plugs where available, or whole core, and powdered in an agate Tema mill. They were packed into aluminum trays and run through a '*Phillips PW1010 X-Ray Diffractometer* '; with the following settings:

$2\emptyset = 3^\circ \text{--> } 71^\circ$ @ 2° per minute.

Chart Drive = 2cm per minute @ 1000 counts for full scale deflection.

The facies and core depths of the 39 samples are listed in the results table below.

9.2.2.1 BULK MINERAL ABUNDANCE PER SAMPLE

Each samples X-Ray diffraction trace has been interpreted semi-quantitatively. The mean of the results for each facies are tabulated below. The individual values of all 38 samples are included as (APPENDIX 26). The samples 38 annotated original traces (APPENDIX 6) are held at the Imperial College Lyon Playfair Library, and may be scrutinised upon request.

Table p171 X-Ray diffraction. Semi-quantitative, bulk mineral abundance per sample. Mean values per facies. (Semi-quantitative: Area beneath the peaks rated from 1-10 with quartz =10) Arag=Aragonite

Sample Core Depth	Qtz	Illite	Kao	Mcr Feld	K-Feld	Dio Mic	Mic	Pyr	Dol	Calc2Ø
Ryazanian Sandstone										
Mean	10	.8	.2	0	3.2	.4	.6	0	2.2	1.6
Massive Coarse Sandstone										
Mean	10	1.7	0	3.0	2.7	1.6	1.0	.9	0	0
Bedded Medium Sandstone										
Mean	10	3.0	0	1.6	2.7	2.3	1.4	.9	0	0
Interbedded Sandstones and Claystones										
Mean	10	3.1	0	2.5	2.3	2.8	2.4	1.8	.1	0
Sands of the ISC Facies are cleanest, 14848 15013 15027 more complex										
Clast Supported Conglomerate, Clasts										
Mean	10	4.4	0	3.5	2.5	3.1	3.8	2.9	2.1	.4
CSCC Facies many minerals present										
Claystone, Kimmeridge and Type Interval										
Mean	8.0	4.5	5.0	3.0	3	5.0	5.5	7.3	1.0	0
Extra phase present in non-Kimmer clays @ 2Ø = 32										

Unidentified phases are of minor importance, with peaks areas of ≤ 2. Their *d* spacings are as follows:

2Ø	d Å	Probable mineral (I/Io)
30.4	3.41	Aragonite? (100), but should show other (100) reflections
55.7	1.915	
20.7	4.98	Muscovite (50)
27.1	3.82	Muscovite (40), Feldspar (40)
41.8	2.51	
50.4	2.101	Barite (80)
13.5	7.62	NOT Chlorite, NOT Smectite

These bulk mineral compositions compare well with, and confirm the thin section study. This data also shows the association of each mineral with the various facies.

Overleaf

Fig p173 Relative occurrence of each mineral across six facies, from X–Ray diffraction bulk samples. Semi–quantitative.

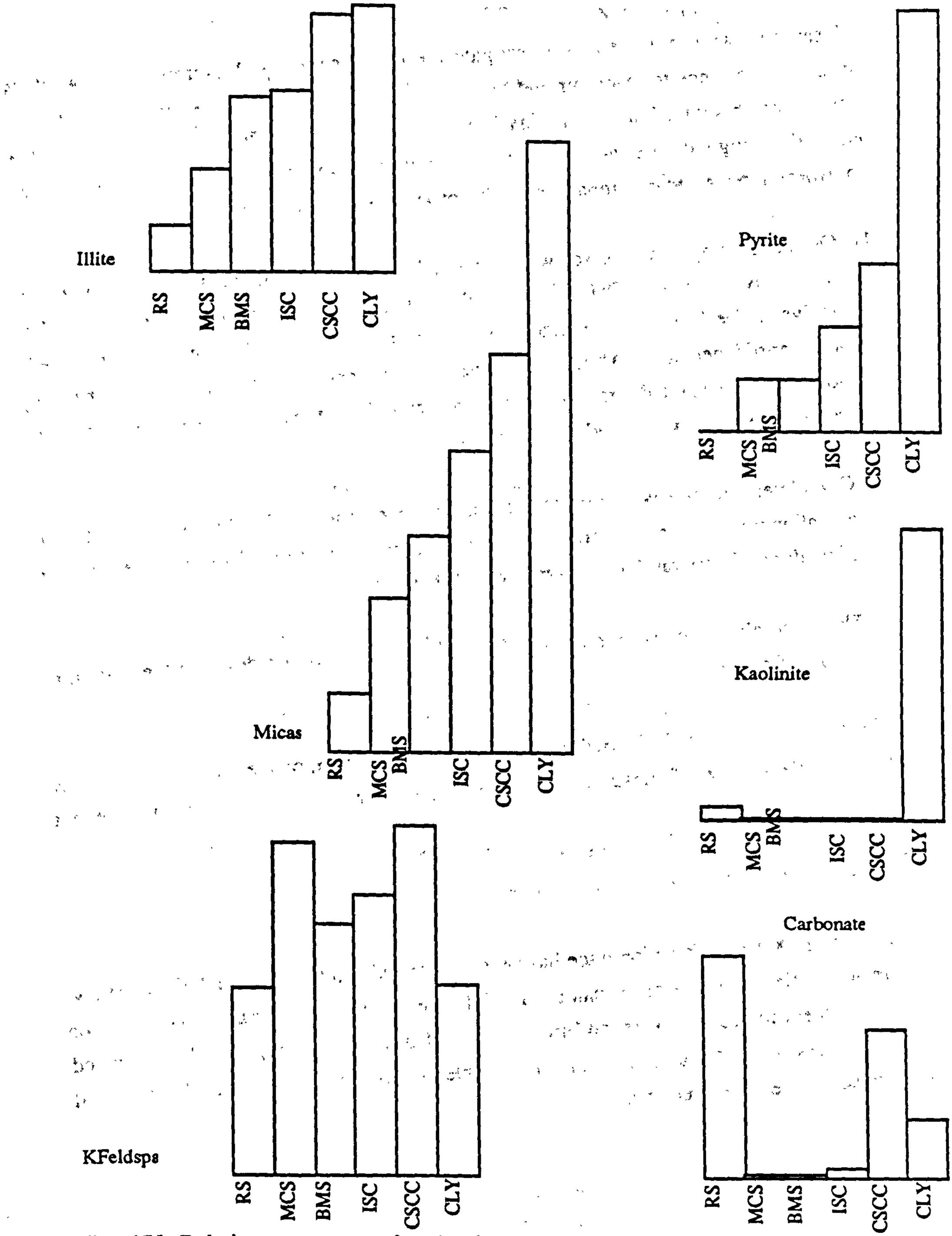


Fig p173 Relative occurrence of each mineral across six facies, from X–Ray diffraction bulk samples. Semi–quantitative.

9.2.3 CLAY FRACTION SAMPLES

11 samples were prepared to investigate the clay fraction, < 2 microns, in view of its special importance to reservoir and petrophysical properties. Samples were chosen from depths which showed abundant clay in thin section, or high Th and K content from the equivalent logged interval. Diffractograms were taken from each of these samples following three standard preparations. The procedure was as follows:

1) Orientated clay coated discs were prepared by adding 50mls of deionised water and five drops of dilute NaOH solution to the Tema milled bulk samples selected for clay analysis. The beakers were placed in an ultrasonic bath for 20 minutes, then stirred, and centrifuged at 1000rpm for between a half and four minutes. The remaining solution was decanted into a funnel plugged with the porcelain disc over a low pressure vessel. The discs were dried in a dessicator.

2) Glycolated samples were prepared by adding two drops of Ethyl Glycol to each disc and allowing them to stand for four hours at room temperature. This causes expansion of randomly interstratified illite-smectites (Shaw, 1985).

3) The same clay discs were heated to 550°C for 1 hour, which destroys the Kaolinite 7.15Å reflection.

Diffractograms were made following each stage of preparation, on the same diffractometer used for bulk samples. Diffractogram settings were slow enough to observe all relevant reflections:

2Ø = 3° --> 33° @ 0.5° per minute.
Chart Drive = 1cm/min. @ 1000 counts full scale deflection.

Each samples X-Ray diffraction trace has been interpreted and the results tabulated below. There was little point in a semi-quantitative interpretation since the sample composition will be subject to settling rates, and the clay's tendency to disaggregate. The annotated original traces (APPENDIX 7) are held at the Imperial College Lyon Playfair Library, and may be scrutinised upon request.

9.2.3.1 CLAY FRACTION X-RAY DIFFRACTION RESULTS

Table p175 Clay fraction X-Ray diffraction results

Smpl CoreDepth	Orientated	Glycolated	550°C
14657 CLTI	ILT, Kao	ILT, Kao	ILT Peak hts 1: 2.5 Kao:ILT
14661 CLTI	ILTbroad@20.7, Kao	ILT, Kao	ILT Peak hts 1: 5.0 Kao:ILT
14031 RS	ILT	ILT	ILT
14049 RS	ILT saddle	ILT saddle	ILT saddle
15098 MCS	ILT	ILT	ILT
15129 MCS	ILTbroad@20.7	ILT	ILT
14978 BMS	ILT	ILT	ILT
14848 ISC	ILT	ILTsharp	ILT
15120 CSCC	ILT	ILT	ILTbroad@20.8
15380 CSCC	ILT	ILT	ILT
15377.5 CSCC	ILTsharp	ILTsharp	ILTsharp

All the Illites showed I/Io values of approximately:

10.1Å = 100 4.99Å = 50 4.48Å < 20

Most available table values (Brindley & Brown, 1980) for field and synthetic illites show approximately:

10.1Å = 100 4.99Å = 50 4.48Å = 90

Table values from Sultan Basin, Washington, show intensities of 100, 53, 19 respectively. These illites have a 3T polytype structure. The illites from Well A appear to be of this type.

Broad and narrow illite peaks are caused by variations in the lattice layer spacings. This is caused by hydrated cation substitution between layers and octahedral substitution within layers. This phenomenon is also evident in quantitative SEM analysis.

Air Dried Orientated Clay Discs

In no cases were the characteristic 15Å basal spacing of smectites, or 14Å basal spacing of vermiculites or chlorites present. The 001ILT/001SMT basal reflection was in all cases equal to or less than 10.2Å. This indicates 100% Illite with no regular or random mixed

layering with smectite or vermiculite.

The characteristic 7.15Å basal reflection for Kaolinite was completely absent from all sandstone samples. However the two Claystone Type Interval samples both contain significant proportions of Kaolinite, and differ from the reservoir clays primarily in this respect.

Ethyl-Glycolated Clay Discs

Glycolation of all samples in no case revealed the characteristic 17Å spacing of smectites or 14.5Å spacing of vermiculites. In no case are discreet smectites or vermiculites present. Furthermore, the ratios of any mixed layer ILT/SMT, if present, is < 30% smectite (Johns & Kurzweil, 1979).

14049 RS showed a raised saddle between the 10Å Illite reflection and the start of the trace, about 34Å. This saddle is unaffected by glycolation or heating and is therefore not due to expandable smectites or vermiculites. Its persistent presence indicates a non swelling mixed layer species such as ILT/CHLORITE, of < 10% chlorite. This is certainly insignificant in terms of bulk log analysis, or reservoir properties, representing a non-swelling species of less than 1% of one sample.

Heating @ 550oC for 1 hour

Heating had no effect on the size, shape or *d* spacing of the basal 10Å or 5Å Illite reflections, for all the samples; again indicating illites with a low or nil proportion of mixed layering. The 7Å Kaolinite peaks in the Claystone Type Intervals were destroyed, confirming Kaolinite's presence.

9.2.4 CONCLUSIONS REGARDING X-RAY DIFFRACTION

Illite is the overriding clay mineral in the matrix of the Brae Group Sandstones, the clasts of the Brae Group Conglomerates, and the Ryazanian Sandstones; illite is also approximately 70% of the clay minerals of the Brae Group Claystone Type Intervals. Nevertheless other methods of analysis show very considerable variation in the morphology, and some variation in the chemistry of these illites. Therefore this geological classification of clay minerals in itself is of limited use in predicting reservoir quality. The use of an adjectival noun such as "hairy illite" is essential when dealing with illite in a

formation evaluation context.

Formation damage due to swelling clays or mobile fines of kaolinite or barite is not present. There is no evidence of formation damage from thin sections or X-Ray diffraction.

Table p177 Summary of X-Ray results relevant to dry clay mineral points

	%Kaolinite	%Illite
Kimmeridge Clay	40	60
Claystone Type Interval	30	70
Brae Reservoir Interval	0	100
Ryazanian Reservoir Int.	5	95

9.3 SCANNING ELECTRON MICROSCOPE

9.3.1 PURPOSE OF SEM STUDY

9.3.1.1 QUANTITATIVE

Apart from images of pore geometry and diagenetic phases one of the intentions of the Scanning Electron Microscope (SEM) study was to fully investigate the SEM's various functions with a view to discovering new methods of core/log integration. The intention was to develop a standardised SEM program that could benefit formation evaluation generally (9.3.5). The function of a standardised program would be to provide numbers for quantitative Non–log–inputs which could be fully integrated with log analysis, in a manner analogous to core data for log porosity for example.

Stoichiometric data from SEM work was used in conjunction with thin section and X–Ray results to synthesis the *Non-log-inputs* . SEM Polished Sections (PS) were used primarily to establish the stoichiometric variations within any single phase that had already been point counted in optical thin sections, enabling a closer chemical definition of minerals and their log responses. Intraphase variations in the claystone reference beds, the reservoir matrix, or the conglomeratic clasts were important in predicting differences in matrix[37] log responses; particularly during clay typing which may be necessary in log analysis.

P_e log values from the Litho Density Tool[38] are related to mean Atomic Number thus:

$$P_e = Z^{3.6} / 10$$

Mean Atomic Numbers were calculated by combining SEM stoichiometries with their thin section mineral proportions.

Th, U, K contents were investigated via the laborious process of Wave Dispersive Analysis. This was done for an independent comparison with the Natural Gamma Log. Obviously the SEM approach suffers from low Th and U contents and very small sample sizes, but nevertheless this opportunity for possible calibration data seemed a prudent addition to a prototype SEM program.

---

[37] In a logging context "matrix" equals solid volume fraction.

[38] Mark of Schlumberger

The SEM also provided a check on previously undetected, unidentified or misidentified phases, although these were insignificant in terms of the bulk properties seen with logs.

9.3.1.2 QUALITATIVE

Standard scale photographs of pore geometry from fractured surface samples were compared to Reservoir Type Signatures (RTS) to gain insight into the ability of an RTS to convey useful pore geometry information. These forced standard scales of x45, x300, x3000 also avoid undue attention to minutiae.

The textural diagenetic relationships have been noted to clarify diagenetic history.

These last two qualitative uses represent the conventional use of an SEM in reservoir geology.

9.3.1.3 LIMITS OF SEM ANALYSIS

All quantitative SEM work is limited to spot analysis. The results therefore have to be synthesised with other quantitative surface data before being used in log interpretation. Initially whole pores containing different phases were scanned and a "mean elemental formula" arrived at. At first these results were thought to be more relevant to the bulk properties of logging tools than spot probes. However the necessary process of assumptions involved in the mathematics of the ZAF4 interpretation made these results untenable. Unfortunately all quantitative work was therefore limited to spot analysis.

Clearly, such spot analyses constitute a minute fraction of the logged rock volume. However the small differences between numerous point analyses reduced concern over this problem.

9.3.1.4 SEM RELATED *Non-log-inputs*

SEM related *Non-log-inputs* arising in whole or in part from the above were:

DCMP Shale bed (*rho* dry clay sh, *HI* dry clay sh),
DCMP Reserv bed (*rho* dry clay res, *HI* dry clay res),
DCMP Clast (*rho* dry clay clast, *HI* dry clay clast),
rho_{mtx},

HI_{mtx},
(∂_{mtx}),
P_e,
$V_{clay\ dispersed} / V_{clay\ total}$, and Illite / Total
K %, Th ppm, U ppm

9.3.2 POLISHED SECTIONS, QUANTITATIVE

9.3.2.1 POLISHED SECTION PROCEDURE

Samples from each facies were chosen from depths which were most important for well evaluation. Namely, depths that would contribute most to production, or most to log analysis, such as reference shale beds, typical clasts or typical matrix. 28 sections were cut, polished and sputter carbon coated. Some of these were optically point counted to complete the optical thin section study. All polished sections were then optically examined. Holes were identified optically and distinguished from bitumen, because elements with atomic numbers less than sodium such as carbon, are not detected by Energy Dispersive Spectrum techniques.

Polished sections showing optically typical dispersed clay, structural clay, feldspar, pyrite; or showing questionable or rare minerals were ringed. Location maps of the polished sections were sketched prior to mounting in the SEM vacuum chamber.

The section was first scanned at x40 magnification in the "COMP" backscatter mode. From a polished flat surface this mode displays variations in mean atomic weight as contrasting grey levels (Shaw, 1985). Quartz, kaolinite and illite have similar grey levels. Contrast was enhanced with maximum "GAIN", minimum "BRIGHTNESS" and maximum "DISPLAY CONTRAST". Locations of grey levels were noted and each grey level spot-probed using the qualitative "Analyser" software. Typical EDS spectrums for the common mineral phases were printed (APPENDIX 64, see also Welton, 1984). Large areas were periodically scanned at x40 and the resulting spectrum checked for exotic element peaks.

The EDS spectrum provides a quick means of identifying most phases, and provides some indication of the elements present within that mineral. However, the element must constitute more than 1–2 percent, and be heavier than sodium. Scanning, the grey levels,

and the EDS spectrum provided the means for identifying:

1) All phases, and
2) Variations in elemental make-up of one phase, illite for example.

Having now gained an impression of the minerals and mineral variations; typical minerals were spot probed using the quantitative "ZAF4" software. ZAF4 attributes peaks to elements entered by the user. A formulae, based on oxide analysis, is calculated by the ZAF4 program, which then requires judicious interpretation before arriving at a geologically sensible answer (9.3.2.3). Special attention was paid to feldspars and clays, particularly kaolinite, although little kaolinite was found in the sands.

Pyrite can be an important variable in the log analysis of low porosity pyrite bearing rocks. Pyrite is best addressed through the LDT[39] tools reading of P_e, barns/cm3. Pyrites P_e at U=85 stands clear of rock forming silicates and carbonates of 5 and 14 respectively, and 0.8 for porosity filled with brine or hydrocarbons.

9.3.2.2 POLISHED SECTION SAMPLE LISTING

1.	14672	MCSTI
2.	14679	MCSTI
3.	14873	MCS
4.	14960	MCS
5.	15347	MCS
6.	14626	MSCTI
7.	14633	MSCTI
8.	14642	MSCTI
9.	14906	MSC
10.	15108	MSC
11.	15375	MSC
12.	15380	MSCC
13.	15367	CSCC
14.	15370B	CSCC
15.	15377.5	CSCC
16.	14615	BMSTI
17.	14864	BMS
18.	15002	BMSTI
19.	15236	BMS
20.	14848	ISC
21.	15013	ISCTI
22.	15033	ISCTI
23.	15183.5	ISC
24.	14062	CLKM
25.	14066	CLKM
26.	14068	CLKM
27.	14661	CLTI
28.	14657	CLTI ... END

[39] Mark of Schlumberger

9.3.2.3 POLISHED SECTION QUANTITATIVE INTERPRETATION TECHNIQUE

ZAF4 does not provide unique solutions. The calculation printouts (APPENDIX 8) which follow each timed spot probe, represents a comparison of that sample's spectrum to the spectrum of a 100% Cobalt standard. Previous calibrations with element standards enable the samples spectrum peaks to be attributed to elements entered by the user. Unassigned peaks are flagged. Element percentages are then processed in a manner similar to standard oxide mineral analysis (Deer et al, 1966, p515). With ZAF4 in the "DIFFERENCE" mode the volumetric shortfall, computed from the detected elements, is attributed to undetected Oxygen. ZAF4 therefore does not provide an unequivocal list of mineral formulae as percentages of the total spot volume. The mineralogy has to be deduced by the user who must interpret the ZAF4 output in its geological context.

When an Energy Dispersive Spectrum (EDS) is the source for the ZAF4 analysis it should be remembered that:

1) Elements where Z < Na will not be detected e.g. O, C, N, H. Their presence will show as total oxides < 100%.
2) Elements in an oxidation state less than that assumed by ZAF4 will show as total detected oxides > 100%.e.g. FeS_2.
3) A detection volume covering more than one phase results in a composite spectrum which has to be mentally deconvolved into a geologically feasible combination; or scrapped if this becomes too complex.

The following formulae were referred to during interpretation:

Illite	*K1-1.5 Al4 [Si7-6.5 Al1-1.5 O20] [OH]4*
Smectite	*[.5Ca,Na].7 [Mg,Fe,Al]4 [(Si,Al)8 O20] [OH]4 . nH2O*
Muscovite	*K2 Al4 [Si6 Al2 O20] [OH,F]4 Dioctahedral*
Vermiculite	*[Mg,Ca].7 [Mg,Fe,Al]6 [(Al,Si)8 O20] [OH]4 . 8H2O*
Chlorite	*[Mg,Fe,Al]12 [Si,Al]8 O20 [OH]16 Trioctahedral*
Biotite	*K2 [Mg,Fe]6-4 [Fe,Al,Ti]0-2 [Si6-5 Al2-3 O20] [OH,F]4*
Kaolinite	*Al4 [Si4 O10] [OH]8*
K-Feldspar	*K [Al Si3 O8]*

(Deer et al, 1966)

Although clays were overwhelmingly illitic the printout invariably showed some degree of illite / smectite mixed layering and / or Fe,Mg octahedral Al substitution; known as *phengite*. In response to these results the following method was devised for interpreting

the proportions of clay minerals from printouts:

1) Remove Fe contribution due to S in pyrite. (Pyrite commonly occurs as disseminated submicroscopic framboids).
2) In an illite/smectite mix K is confined to illite and Na, Ca are confined to smectite. It can be seen from the text-book formulae above that:

$$\frac{\textit{UNIT CELLS ILT}}{\textit{UNIT CELLS SMT}} \approx \frac{\textit{(K)*0.7}}{\textit{(Na,.5Ca)*1.25}}$$

3) Fe, Mg are from smectite layers or from the substitution of octahedral Al in the illite layers (phengite) thus Fe, Mg are non-exclusive and cannot reliably show ILT/SMT ratios (Deer et al, 1966, p202). The K:Al:Si printout ratios however do provide insight into the phengite proportions.

The intuitive assimilation of all information relevant to interpretation are difficult to document as a fixed procedure, but these "soft" rules played an important role.

This method indicated that all spots were within the limits:

Illite 100-80
Smectite 0-20

This is consistent with all other experimental data and is geologically feasible.

The processes 1-3 may appear imprecise but X-Ray results had established the absence of free smectite, vermiculite, chlorite, and biotite; and very limited kaolinite in the sands, enabling procedures to be followed that would not otherwise be possible.

The clay fraction X-Ray diffraction results preclude significant proportions of smectite or vermiculite in any possible mixed layered illites. The highest proportions from the CLTI being ~ ILT90 / SMT or VRM10; with zero free smectites or vermiculites. The SEM results suggest higher Fe, Mg components. Substitution of octahedral Al with Fe, Mg in the illites may explain this; however, ultimately, greater weight must be put on X-Ray results than SEM results because the SEM results rely upon sensitive calibrations and complex computations, a situation reminiscent of cores and log analysis. This is especially true when the diagnostic elements are only a small percentage of the whole probed volume, and when more than one phase is convolved in one spectrum.

The small proportion of smectite layers and phengitic substitutions have been quantitatively incorporated in the *Non-log-inputs* .

9.3.2.4 REPRESENTATIVE ENERGY DISPERSIVE SPECTRUMS

Quartz
K Feldspar
Illite
Kaolinite
Pyrite
Rutile
Zircon

These spectrums may be viewed in (APPENDIX 64): Representative energy dispersive X-Ray spectrums.

9.3.2.5 POLISHED SECTION INTERPRETIVE SHEETS (Stoichiometry to 1 decimal place)

(APPENDIX 9) is the stoichiometric interpretations resulting from the computer printouts which followed each timed spot probe of the SEM. The bulky computer printouts themselves are not included in this appendix, but as (APPENDIX 8), both in the Lyon Playfiar Library

9.3.2.6 POLISHED SECTION WAVE DISPERSIVE K, Th, U

Originally K, Th, U ratios were to be used to indicate illite/totalclays and so $V_{clay\ dispersed}/V_{clay\ total}$, i.e. an indication of clay distribution from clay type. Following thin section and X-Ray studies no correlation was established between illite content and dispersed clay because both dispersed and structural clays were overwhelmingly illite. Knowledge of K/Th ratios from the logs of this well would therefore be of no help with formulations for clay distribution and its effect on excess conductivity or permeability.

A non-log assessment of K, Th, U contents could be included as part of a prototype SEM program. If the reservoir contained kaolinite or chlorite this would provide external data for log analysis.

After delays with setting up the SEM for Wave Dispersive Spectrum (WDS), overnight 15

hour runs were made on two polished sections of Kimmeridge Clay which, according to the Natural Gamma Log[40], bore high concentrations. The results of 306 times 20micron spot floods, at 0.25μamps averaged:

K 3.11% *Th 39 ppm* *U 79 ppm*

Although the results are good, this method of determining independently K,Th,U ratios fails because it is extremely laborious and extremely complex, and is therefore too labour intensive and error prone to be used routinely as a well evaluation technique. After this abortive attempt 30 samples were dispatched to the Nuclear Reactor Centre for K,U,Th content (9.4).

9.3.3 FRACTURED SURFACES, QUALITATIVE

9.3.3.1 FRACTURED SURFACE PROCEDURE

Since tool and therefore RTS resolution is coarser than 3ft(1m), samples have been chosen which are typical of the lithology above and below for at least three feet. The SEM study was performed as an adjunct to log analysis: the common practice of using core plug chips was avoided because core plugs will have suffered greater alteration than chips taken from the centre of the core. Central chips are better representatives of the volume of rock influencing logs. A good core/log depth match is essential for a comparison of photographs and log results (3.2.1) which occurs in RTSs.

RTSs in the Interbedded Sandstones & Claystones (ISC) facies will bear no relation to individual samples; they will be composites of sandstone and claystone interbeds.

9.3.3.2 FRACTURED SURFACE SAMPLE LISTING

Facies	Depth	Block Ref	Lithology Continues... Above	Below, FT	
RS	13887	1			
RS	13895	2	3	10	Calcareous zone
RS	13921	3, 4	3	13+	Carbonaceous, Normal
RS	14016	5	6	5+	
RS	14031	6	12+	7	
RS	14049	7	6	8	

[40] Mark of Schlumberger

BMS	14604	8	1+	16	Could be clast?
MSCMTI	14626	9	5	5	] RTS will show Clasts also
MSCCTI	14633	10	12	9.5	] "
MCSTI	14672	11	3	9.5	] Should be same
MCSTI	14679	12	10	2.5	] "
BMS	14840	13	?	3	
BMS	14864	14	8	3	
MCS	14873	15	6	3	
MCS	14893	16	1+	2	
MSCM	14906	17	2	2.5	
MCS	14960	18	9	4+	
BMSTI	14978	19	7+	6	
BMSTI	15002	20	17	9	
ISCTI	15033	21	0.5	0.5	No RTS comparison, ref only
BMS	15084	22	5	10	
MCS	15098	23	4	4	
CSCCTI	15120	24	8	1	
MCS	15147	25	5	2+	
MSCM	15258	26	3	1+	2pics: Rd pbl clst.Poik carb mtx
CSCC	15370	27	4	1	

9.3.3.3 FRACTURED SURFACES STANDARD SCALE PHOTOGRAPHS AND RESERVOIR TYPE SIGNATURES, RTS

Standard scale photographs were taken of the gross grain–pore arrangement, x45, the geometry of a complete typically largish pore contributing to flow, x300, and of micropores which contribute to total porosity and conductivity but not to flow, x3000. Standard scale photographs are important for the purpose of rapid comparison, and for use with the pore geometry sector of the RTS. It was hoped that an RTS would reveal something of pore geometries, and the photographs are partly intended to show any such relationship. Ideally thousands of photographs would be taken covering the volume of rock giving rise to the RTS. Typical samples, and typical pores within those samples was the best approximation available. Even small scale heterogeneities are clearly very important in this equivalence of photograph and RTS.

The photographic suite is displayed adjacent to the RTS interval in (APPENDIX 53).

9.3.3.4 FRACTURED SURFACE PHOTOGRAPHIC CAPTIONS

83 - - numbers are those in the middle at the bottom of each photograph seen in (APPENDIX 53).
Also "@40" refers to a 0-99 location: 4/10 across, 0/10 down, i.e.centre top.

8319*45	MSCM14906	Overall grain/pore geometry, clean broken quartz grains with sparse authigenic clay.
8320*300	MSCM14906	Geometry of typical pore, showing illitic coats which do not intrude significantly into pore volume. Conductive yes, permeability OK.
8321*3000	MSCM14906	Typical µØ. Illitic flakes adjacent to quartz overgrowth wall.
8322*45	MCS15098	Overall grain/pore geometry, clean, common euhedral quartz overgrowth faces, two pores primary, two secondary leached?
8323*300	MCS15098	Secondary pore w quartz wall and illite carpets.
8324*3000	MCS15098	µØ. Partially leached feldspar, K bearing. Trapped connate water, low additional conductivity, permeability OK.
8325*45	RS13921	Pore/grain arrangement, vuggy pores @57, 58.
8331*3000	RS13921	Illite hairs lie on quartz overgrowth, µØ, generally clean.
8332*45	RS14016	Excellent open primary pores, leached feldspar grains @95, sparse illite.
8333*300	RS14016	Excellent clean large open primary pore. Numerous quartz overgrowths @54 on detrital grain surface@52.
8334*3000	RS14016	µØ bounded by quartz, interlocking quartz grains, single illite strand.
8335*45	RS14031	Excellent primary porosity, open connected pores, authigenic dispersed clay @68.
8336*300	RS14031	Primary pore, multi smal and large quartz overgrowths @33, and authigenic illitic clay coates @16. High % of replaceable brine.
8337*3000	RS14031	µØ caused by quartz. Represents a small fraction of Øt.
8338*45	MCS14893	Good Ø, some primary @22, smal volume but extensive dispersed clay coates.
8339*300	MCS14893	Clean primary channel pore. Permeable, low connate water, low non Archie conductivity.
8340*3000	MCS14893	Flaky illite µØ, small dry volume of clay creating large effect. Rare in this sample.
8341*45	BMS14064	Sparse secondary leached pores in tight matrix. Abundant illite on all pore walls, fractured quartz grains and separation of abutting overgrown grains leave clay free surfaces.
8342*300	BMS14604	Brkn quartz grain and illite carpeted early vuggy pore. Permeability OK, but excess conductivity in hc saturated leg.
8343*3000	BMS14604	Densely packed illite carpeted surface, bound water.
8344*45	MSCM14626	Small homogenous secondary Ø, illite coated.
8345*300	MSCM14626	Typical corroded secondary pore. Nest of quartz overgrowths and hairy illite.
8346*3000	MSCM14626	Typical illite lattice next to quartz overgrowth wall.
8347*45	MSCC14633	Featureless broken surface, sparse Ø.

8348*300	MSCC14633	Illite clothed rare pore, fractured quartz grain, feldspar overgrowth @46.
8349*3000	MSCC14633	Macro + μ Ø, pyrite nodules associated with illitic mat.
8350*45	CSCC15120	Small vuggy pores, almost all pore walls clothed in illite.
8352*300	CSCC15120	Typical pore, quartz overgrowths appear to post date illite @17.
8353*3000	CSCC15120	Typical illite μØ @34 and quartz overgrowth fingers @75.
8354*45	MCS14679	Sparse exclusively illite on rough moderately sorted sandstone. Roughness is interface between two grains with very fine separation. Leached vug @78, Vug invaded by quartz overgrowth @32.
8355*300	MCS14679	Isolated vug lined by detrital grain or corroded grain, illite and overgrowths. Overgrowths clearly postdate authigenic illite.
8356*3000	MCS14679	Typical μØ, flowering illite.
8358*300	BMS1480	Typical pore bounded by quartz, illite framboidal pyrite @35. This illite is more compact.
8359*3000	BMS1480	Framboidal pyrite creating μØ. This pyrite would be counted as solid in optical thin section.

9.3.4 MODIFICATIONS TO THIN SECTION DATA

Point Counts

The SEM's increased resolution and stoichiometric information enables fine tuning of the optical thin section data which is to be integrated with log data. *Non-log-inputs* must be expressed in the form of bulk properties before entering the log analysis environment. The major SEM observations requiring attention were:

1) Small proportion of smectite mixed layers in illites.
2) Silt grade quartz in structural clays.
3) Kaolinite in shales but not in sands.
4) Submicroscopic pyrite framboids in organic matter.
5) Pyrite framboids which contain microporosity.
6) Fine grained feldspar sometimes counted as quartz.

Greater detail appears on the 33 sheets comprising (APPENDIX 9).

Mineral percentages from optical thin sections have been modified in the manner shown below, and the results are listed under (9.1.5).

Table p189 Modifications to optical thin section data following SEM study

Ryazanian Sandstone	
Quartz	= Quartz + Structural Clay * 0.20
Structural Clay	= Structural Clay * 0.80
Kimmeridge Clay	
Quartz	= Quartz * 0.95
K-Feldspar	= K-Feldspar + Quartz * 0.05
Pyrite	= Pyrite * 0.90 + HydroCarbon + Organic Matter * 0.10
Hydrocarbon + Organic Matter	= HCOM * 0.90 + Pyrite * 0.10
Claystone, Type Interval	
Quartz	= Quartz * 0.80
K-Feldspar	= K-Feldspar + Quartz * 0.20
Massive Coarse Sandstone	
Quartz	= Quartz + (Structural Clay)x 0.25
Structural Clay	= Structural Clay * 0.75
Bedded Medium Sandstone	
Quartz	= Quartz + (Structural Clay)x 0.25
Structural Clay	= Structural Clay * 0.75
Matrix Supported Conglomerate, matrix	
Quartz	= Quartz + (Dispersed Clay)x 0.08
Dispersed Clay	= Dispersed Clay * 0.92
Clast Supported Conglomerate, clast	
K-Feldspar	= K-Feldspar + Quartz * 0.07
Quartz	= Quartz *.93 + (Structural Clay) * 0.10
Structural Clay	= Structural Clay * 0.90

Petrophysical Plot

Ideally the formulae for the *rhob* , *HI* and *GR* coordinates of the optical thin section petrophysical plot (9.1.7) should be corrected in two ways:

1) By correcting point counts, e.g. where submicroscopic pyrite has been found embedded in clay minerals, and

2) By entering the log response for SEM stoichiometries as opposed to using the ideal stoichiometries of the Schlumberger tool response table. (Schl, 1985)

Since the coordinates (APPENDIX 4) took a great deal of time to calculate and plot this has not been done. However it can be seen from the coordinate formulae that changes would be small, with the exception of ≈7% increase in the claystone gamma ray coordinate. The purpose of the plot is to demonstrate the inadequacy of *HI*, *rhob* and *GR* to clearly distinguish the various sandstone facies delineated at core description; and this conclusion has not been affected.

9.3.5 Non-log-inputs

9.3.5.1 DRY CLAY MINERAL POINTS

The $DCMP_{shalebed}$ (12.1) corresponds to the mean SEM stoichiometries of clay minerals from the shale bed. By using the SEM stoichiometries of the reservoir beds to position $DCMP_{resbeds}$, the LDT/CNL[41] combination can be corrected accurately for clays present in the reservoir, by calibration to the clay mineral assemblage present (12.1). The same principle can be used to correct for the effects of clays in the clasts. Refer to Fig p "Review of stages..." four pages forward.

Table p190 Effect of stoichiometry on clay densities

Clay min. (MẆ)	%	Mean SEM stoichiometry	MW/MWshale
Shale bed:			
*Kaolinite	40	(Ca,Mg,K,Fe).4 Al4 Si4 O10 (OH)8	1.000
*ILT/SMT/PHN (806)	60	Na.1 K1.4 Mg.4 Fe.2 Al5.0 Si7.3 O20 (OH)4	1.000
Reservoir beds:			
Kaolinite	0		na
ILT/SMT/PHN (813)	100	K1.5 Mg.3 Fe.2 Al5.5 Si7.1 O20 (OH)4	1.009
Clasts:			
Kaolinite	0		na
ILT/SMT/PHN (823)	100	Na.1 K1.7 Mg.3 Fe.3 Al5.3 Si7.1 O20 (OH)4	1.021

*See Deer et al, 1966 p257 & 261 respect.

[41] Mark of Schlumberger

9.3.5.2 DRY CLAY DENSITIES

The density tool is taken as responding proportionally to any volume of equal density, whether this volume is submicroscopic between clay sheets, or millions of times greater in vuggy pores. "Dry" clay densities are therefore needed for the calculation of porosity because the tool responds to this <u>total</u> porosity. The solution to the problem of variations in laboratory clay density with humidity is to standardise[42] the relative humidity and temperature of core $\emptyset_{he}$ measurements, and to determine clay densities at these standard conditions. rho_{mtx} as a function of V_{clay} then yields equivalent $\emptyset_{he}$s across uncored sections with varying amounts of clay. i.e. Clay matrix densities need not be assumed equal to the sand matrix densities.

The "dry" clay density, that which would furnish a $\emptyset_t$ calculation, of the stoichiometries revealed by SEM is difficult to establish precisely. Muscovite, structurally similar to illite but with more potassium, less silica and greater stacking regularity has a density of 2.77-2.88, (Deer et.al., 1966, Berry & Mason, 1959). This provides a maximum value for illites because of its structural similarity, increased degree of order, and relative lack of adsorbed water. Illite, with fewer interlayer cations and less regular stacking is quoted as 2.6-2.9; depending primarily upon adsorbed water and secondly upon cation substitutions. The "dry" densities lie at the upper end of this range i.e. > 2.75. Illite has little interlayer water (non-swelling), and dehydration of the adsorbed surface water and crystal edge water associated with exchange ions comes off rapidly below 110°C, (Deer et.al., 1966, p262). 110°C concurs with the proposed standards for $\emptyset_{he}$ (footnote). The molecular weights (and densities) of the clay minerals in Well A is affected only slightly by elemental substitutions such as phengite:

K2 Al(4-x)(Mg,Fe2+)x Si(6+x) Al(2-x) (OH)4 O20 (Deer et al., 1966 p261)

when x = 0: MW = 797. when x = 1: MW = 810.

i.e. *MW PHN / MW ILT = 1.016*

According to Deer et al, 1966, the density of pure kaolinite, Al4(Si4O10)(OH)8, varies from 2.61-2.68 depending upon hydration (p258), and to some minor extent upon the species of exchangeable cation. We can conclude that dehydrated kaolinite has a maximum value of 2.68. Therefore it is reasonable to assume that the shale type interval dry clay densities, from which the shifts to reservoir and clast clay mineral assemblages will be based, are:

---

[42] 105°C, vacuum, 48hrs. Juhasz, 1988.

Table p192 Book values of dry clay densities

	Illite	Kaolinite
Dry density, g/cc	2.80	2.67

It should be noted that the correctness of these absolute values is not of paramount importance to the determination of reservoir or clast clay volumes. The shift in tool response from a shale bed to 100% reservoir or clasts clay minerals is our primary concern, since this is where the error lies in the traditional use of shale beds for reservoir analysis. Thin section point counts have already linked the actual tool responses to the actual volume and types of clay minerals present in the shale bed, i.e. 61 %.

Table p192 Density and Hydrogen Indexes of the three dry clay mineral assemblages

	Dry Clay Mineral Assemblage: Density	Hydrogen Index	
Shale Type Interval	2.75[43]	.199	(section 13.1.1)
Reservoir Beds	2.83[44]	overleaf	
Clasts	2.86[45]	overleaf	

9.3.5.3 DRY CLAY HYDROGEN INDEXES

The hydrogen index response of the neutron tool is caused primarily through the slowing of neutrons by hydrogen atoms which have a similar mass. The SEM does not detect hydrogen in EDS mode and so a direct measurement of dry clay *HI* values for shale, reservoir and clasts cannot be made. However the three clay mineral assemblages, and the ratios of book values of their *HI* s, can be used to shift the DCMP *HI* from its known value of 0.199 for the shales, (12.1.1) to that of the reservoir or clasts. It is comforting to note that the book value *HI* s for the shale clay mineral assemblage is surprisingly close to the DCMP value, deduced from logs and laboratory data.

---

[43] 2.8*.6+2.67*.4 = 2.75
[44] 2.8*1.009 = 2.83
[45] 2.8*1.021 = 2.86

Do Not Lend Or Copy

				HI dry clays in shale
Book value:	0.60*0.12 +	0.40*0.36	=	0.216
	Illite	Kaolinite		(0.12, 0.36: Fertl 1987)
DCMP procedure:			=	0.199

Therefore:

Table p193 LDT and CNL tool response to the dry clay mineral assemblages of the three petrophysical rock types of Well A, deduced from laboratory and wireline data.

	Dry Clay Mineral Assemblage: Density	Hydrogen Index	
Shale Type Interval	2.75	.199	(ILT/KAO section 12.1.1
Reservoir Beds	2.83	.111[46]	(ILT
Clasts	2.86	.111[47]	(ILT

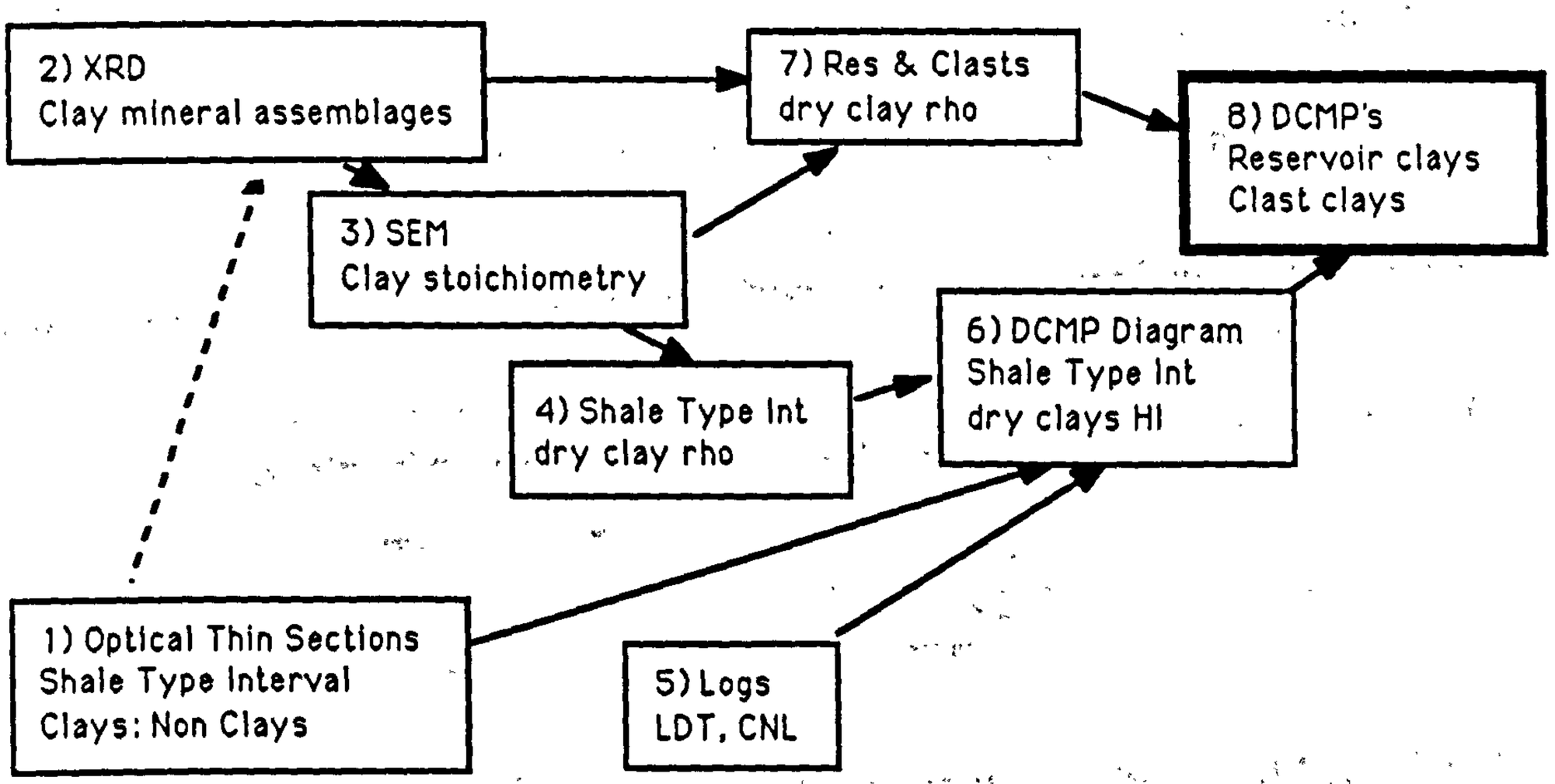


Fig p193 Review of stages 1-> 8 followed to determine the density / neutron DCMPs.

9.3.5.4 *rhog, HI$_{matrix}$*

The clay volume determined from the NGT™(12.2) is used in conjunction with DCMP to continuously modify *rhog* and *HI $_{mtx}$*.

[46] .199*.12/.216 = .111 HI sh cl multiplied by ratio of book value HI res: HI sh cl
[47] .199*.12/.216 = .111

9.3.5.5 P_e

Barite (U=1091) weighted mud invalidates use of the Pe curve in this well. However SEM stoichiometries can predict U matrix values. In barite free wells deviations above predicted values can be attributed to high U matrix minerals such as pyrite (U=85). This new mineral assemblage provides a modified *rhog* value for total density porosity calculations.

9.3.5.6 Vclay dispersed : Vclay structural

The SEM spot probe spectrums and ZAF4 analysis revealed a lack of chemical variation in the clays. Differing clay distributions therefore display similar chemistry and are invisible to most lithological tools. The SEM therefore did not assist in predicting dispersed clay from logs (12.2).

9.3.5.7 K, Th, U

Wave Dispersive Spectrum analysis performed upon two shale type interval samples provided the following results:

Table p 194 Wave Dispersive Spectrum analysis of shale type interval samples

	K %	Th ppm	U ppm
Sample 1	2.36	52	63
Sample 2	3.86	25	95
Average CLTI	3.11	39	79

9.3.6 MODIFICATIONS TO X-RAY DATA

No modifications required.

9.3.7 CONCLUSIONS REGARDING SEM STUDIES

The increased time and expertise required for the SEM study failed to yield a proportionately equal contribution to formation evaluation as the optical thin sections. Nevertheless the following conclusions can be drawn from the SEM work:

1) SEM data (Appendix SEM Stoichiometric Interpretation Sheets) have been used to synthesise quantitative *Non-log-inputs* .

2) In the sands and sandy conglomerate matrix (potential pay) no additional relationship could be found between properties that influence tool response[48] and the geometrical distribution of micro and macro-porosity.
3) A standardised photographic record of pore geometry per facies has been compiled for use with RTSs.
4) Compact fringed stacks of illite and diffuse spider legs of illite are chemically identical, and therefore difficult to distinguish with logs, but will have radically different effects upon reservoir quality.
5) The optical thin sections diagenetic study (10.1.12) has been corroborated by the detrital and authigenic minerals spatial relationships seen under SEM.
6) Small errors which occur when evaluating optical sections can be rectified with the SEM. However these minor changes are not quantitatively significant to the formation evaluation of this well, and are unlikely to be important in most wells.

9.3.7.1 ROLE OF SEM IN FORMATION EVALUATION

A standardised SEM program is proposed overleaf in answer to the opening paragraph of (9.3). It results from the qualitative and quantitative investigations documented in (9.3) as well as the large volume of data and interpretation contained in (APPENDIX 8, APPENDIX 9, APPENDIX 10, APPENDIX 11, & APPENDIX 53).

The logic overleaf recommends that petrographic uncertainties are <u>not</u> investigated with the SEM unless cores, logs and DSTs are incomprehensible.

In addition to the scheme overleaf SEM fractured surface photographs may be taken purely for comparison with RTSs.

---

[48] *(Øsonic - Ødensity)/Ødensity* will respond negatively to vuggy porosity, and positively to dispersed clay and pyrite. However the formation has too many disturbing influences to assume such a parameter is a proper reflection of only one formation characteristic such as macro: micro porosity.

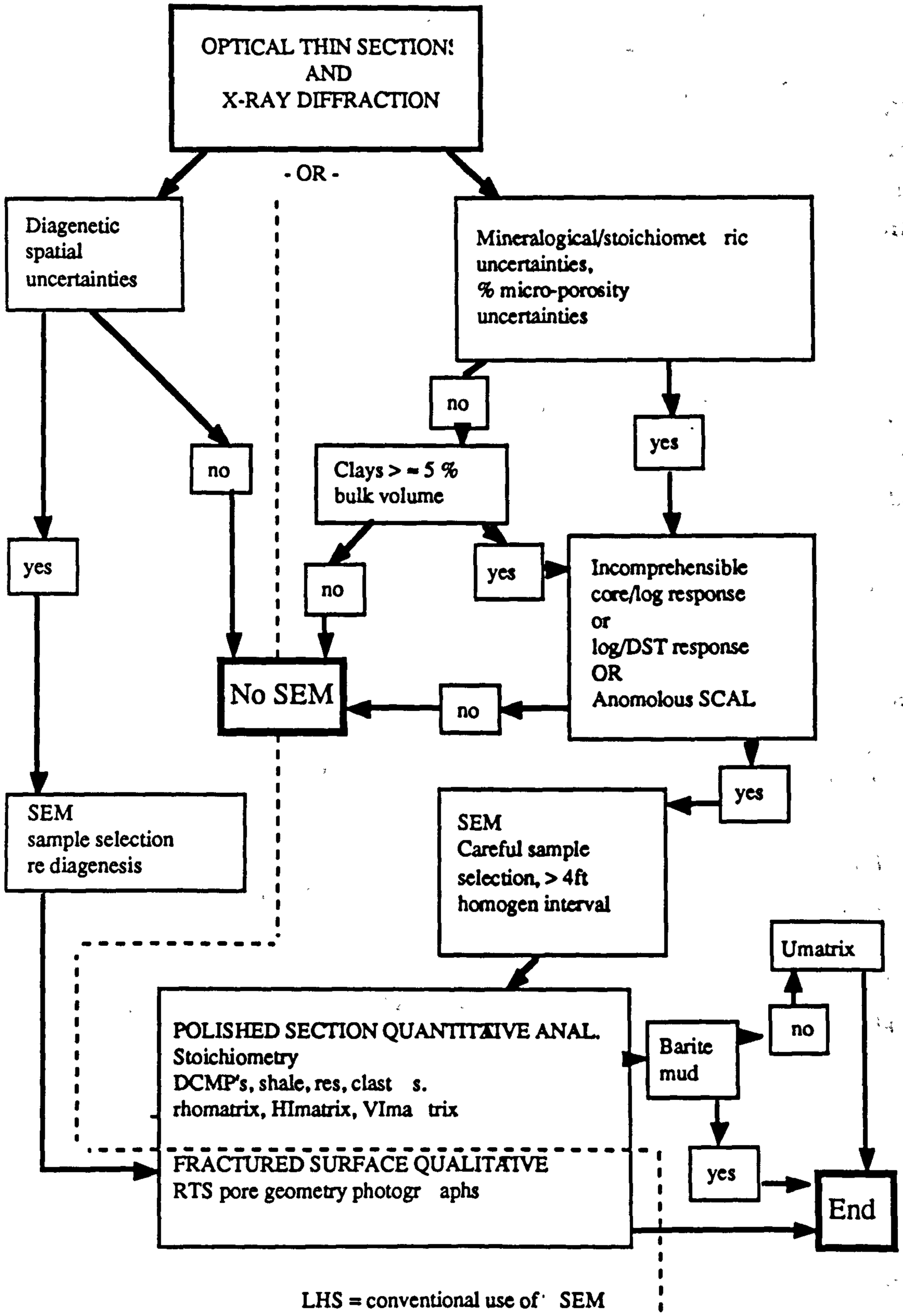


Fig p196 Role of SEM in formation evaluation

9.4 NUCLEAR ACTIVATION

Notwithstanding service company literature, e.g. Schlumberger, 1982 p23, a precise check on the NGL was thought necessary. This was done by neutron activation of K,Th and U in actual rock samples. The NGL runs at 900fph logging speed, has a radius of investigation of 5-25cm, with six inch sampling, and involves a three to one sampling smoothing process (p19). This results in a minimum of 2.5 vertical feet(.75m) creating any log value. Three core chips covering 3ft(1m) centered about the log reading were milled, combined proportionately and analysed for K,Th and U at the Reactor Centre. The results are listed below, and are self explanatory, showing a fair correlation between log values and activated samples. Mud contaminants such as Thorium in Bentonite may impair this data, although care was taken in washing samples.

Table p197 Values of radioactive elements from logs cf. nuclear activation of milled core.
Log values plain, Nuclear Activation values underlined

	GR TotalAPI	^{40}K %	^{232}Th ppm	^{238}U ppm	K + Th/U
14011 RS	40	0.6 <u>0.67</u>	3.5 <u>2.24</u>	2 <u>1.60</u>	<u>1.8</u>
14068 CL KM	235	3.0 <u>2.50</u>	14 <u>8.12</u>	16 <u>23.4</u>	<u>0.5</u>
14661 CL TI	157	3.8 <u>3.68</u>	12 <u>10.1</u>	7 <u>12.9</u>	<u>1.1</u>
14672 MCS TI	32	0.8 <u>0.64</u>	2 <u>1.48</u>	1 <u>1.20</u>	
14899 MCS	30	0.7 <u>0.96</u>	3 <u>2.77</u>	1 <u>1.26</u>	
15098 MCS	25	0.7 <u>0.55</u>	3 <u>1.33</u>	0 <u>0.59</u>	
15347 MCS	28	1.0 <u>0.55</u>	3 <u>1.34</u>	0 <u>0.63</u>	<u>matrix 2.8</u>
15370B CSCC gn fgss	38	1.0 <u>1.56</u>	3 <u>4.70</u>	1 <u>1.13</u>	
15377.5 CSCC gn fgss	45	1.2 <u>1.46</u>	4 <u>2.15</u>	17 <u>0.60</u>	
15108 MSCC wh qtzt Not frm one depth	<u>0.87</u>	<u>1.81</u>	<u>0.66</u>		<u>clasts 5.2</u>

9.5 CORE CONDUCTIVITIES

Purpose of Electrical Experiments

Provided there is a contrast in resistivity between formation water and hydrocarbons the presence of hydrocarbons will affect formation resistivity. Before using resistivity to interpret what portion of the pore space is hydrocarbon filled, certain formation characteristics must be quantified, namely the resistivity the formation imparts to the water, F; the sensitivity of a formation's resistivity to the presence of hydrocarbons, n; and, in some rocks, the maximum amount of resistance the formation can provide when its pore space is filled with a non conductor, (the reciprocal of) excess conductivity (6.1.2). Cores enable the in-situ values of these three formation characteristics to be approximated, allowing estimates of hydrocarbons in place.

In view of the importance of interpreting resistivity it was thought preferable to select suitable samples, and perform the laboratory measurements of C_x, F_g, n, and n-y, for use in the $C_t = (C_w / F_g) S_{we}^{\ n} + C_x S_{we}^{\ n-y}$ equation. However, C_x could not be determined with the facilities available (see 9.5.4) and so the corresponding set of Archie parameters were investigated, at room conditions. i.e.

$$F = \emptyset_t^{-m}, \quad \text{and} \quad S_{wt}^{-n} = R_t / R_o$$

Sample Selection

Samples were chosen in consideration of the following points:

1) Samples should be particularly instructive to log analysis, e.g. end members such as pure clasts, pure matrix etc.
2) Depth matching between core and logs must be good. (APPENDIX 13)
3) Samples should be towards the middle of an 8 foot(2.4m) or greater petrophysically homogeneous interval.
4) Samples should be from depths which appear favourable to production.
5) Some samples should be selected from pyritic intervals with low porosity and low clays.

Ryazanian sandstone plugs were included because this interval flowed water, and therefore

F_{log} may be compared with F_{lab}. Drill Stem Tests in the Brae Group were less conclusive.

Plug No	Core Depth Facies	Log Depth Refer MicroLog
072	14014 RS	14022
083	14035 RS	14045
189	14631 MSCMTI	14644
225	14672 MCSTI	14691 pyritic
228	14675 MCSTI	14694
272	14877 MCS	14896
365	14980 BMSTI	14998
493	15119 CSCCTI	15136
546	15192 BMS	15210
681	15363 MSCC	15393

ALL PLUGS: Length 1.5 inch , Diameter 1.0 inch

Laboratory Facilities and Limitations

With help from various SPWLA members laboratory facilities were kindly made available by Core Laboratories, London, but for room temperature/pressure measurements only. Reservoir temperatures and pressures could not be simulated for these experiments. Reservoir conditions certainly furnish more valuable information. However, under the circumstances the indeterminate additional amount of time spent trying to locate and reserve this apparatus was unacceptable. The results cannot therefore be allowed to form a crucial role in the overall evaluation. 9.5.4 details the procedure which would have been followed had this apparatus been available.

9.5.1 METHOD

In order to determine R_o and F the ten representative samples were weighed in air, W_{air}. The samples, and two litres of undiluted formation brine, R_w[49], were evacuated for 68 hours and 1 hour respectively, to remove air. The de–aired brine was dripped onto the samples under vacuum and the beaker then vented to atmosphere. The samples were then pressurised to 2000psi under the same brine for 64 hours in order to saturate clay microporosity. The resulting weight, W_{RO}, was taken as the benchmark $S_w = 1$ weight.

9.5.1.1 BRINES

The brine resistivities were measured accurately in a purpose designed resistivity device. Brine resistivity was increased for the C_w v C_o plot by dilution with distilled and de-

[49]From DST3A which produced 5-600bbls of brine. This fluid is very probably close to 100% formation brine.

ionised water. Using formation brine as opposed to NaCl solutions maintains the reservoir ionic ratios which may influence the clay morphology and conductivity of this rock, (Hardwick 1987). This is especially so with dilute solutions where direct surface site 'inter-hopping' becomes proportionally more important to observed conductivity.

Each successive brine was de-aired for 1 hour prior to resistivity measurements. Brine resistivities were measured into and out of the core samples, the latter being recorded. All samples had these two resistivities within 1% before proceeding. Although this is not necessarily synonymous with perfect equilibrium across the entire pore space, it represents a practical procedure for the over 100 resistivity measurements.

9.5.1.2 CORE SAMPLES

Core sample water saturated resistivities (for F and C_x) were measured in a purpose designed unit employing brine soaked leather pads coupled to a digital frequency generator/multimeter. A standard measuring procedure was adopted, under the advice of Core Laboratory technicians, designed to both minimise and standardise experimental errors. The most critical influence was the drying of core sample surfaces, which increased resistivity. Each plug was rolled once on absorbent paper and its resistivity measured (9.5.2.1) within a fixed length of time and with a constant contact pressure. The C_o v C_w plots indicate that experimental errors due to drying are not significant.

A purpose designed unit for the continuous measurement of resistivity during flushing was not available, instead plugs were flushed with successively more dilute brines, between resistivity measurements, by the use of a "strut". This device enabled water, brine or crude oil to be pressure fed at up to ≈4500psi, through the plugs which were held in a thick rubber sleeve (Hassler sleeve) under an external pressure some 400psi greater than the incoming fluid.

Since R_{xoc} and R_{xot} (Nomenclature) were of particular interest the samples had to be tested in this order:

$$R_o, R_{xot}, R_{xoc}, R_{owI} \text{ ...etc.}$$

This resulted in the R_{owI} measurement being a reversal of the normal diluting trend. Consequently, flushing for this measurement was in excess of 20 pore volumes, and for a minimum duration of 1 hour. This resistivity point does not disrupt the linear trend of results. A minimum of 12 pore volumes were flushed for all other water saturated measurements.

9.5.1.3 OIL SATURATED SAMPLES $1/R_t = S_{we}^{n} \emptyset_e^{g} / R_w + C_x S_{we}^{n-y}$

Besides providing hydrocarbon in place figures a saturation curve can provide useful information on reservoir quality and produced fluids. The purpose of electrical SCAL is to assist with the accurate conversion of formation conductivity into saturation. This is usually done by sample cleaning, determining porosity, saturating with brine, determining *m*, desaturating with air, and recording resistivity for *n*. A saturation equation is then assumed to embody the correct downhole relationship between these laboratory determined parameters; and the formation S_w is calculated.

However, if fresh core samples have S_{crude} set in the laboratory at an approximate value for this rock when situated in an oil zone, i.e. if they are pressured with crude to a given reservoir height, then logged R_t can be compared directly with laboratory R_t. If laboratory S_{crude} (1-S_w) is fixed in this manner then logged R_t can be used to indicate a samples position relative to an oil-water-contact with greatly lessened disturbance to the rock characteristics *n*, *y*, *g*, and C_x. The sample can later be destroyed and its porosity and saturation accurately determined. This concept was acted upon in the following way:

Given the absence of more specific S_w data (such as oil based mud core S_ws) core analysis porosities and permeabilities for these samples were used in conjunction with the Coates and Dumanoir chart, 1973, to estimate S_w. This chart relates porosity and permeability to immovable water saturation above the transition zone. The volume of brine to be displaced was calculated and the samples dynamically flushed with dead formation crude until this chart figure was reached, apparatus for crude displacement was not available. The resulting resistivity ratio, R_t/R_{oxc}, was plotted against S_w on a log-log plot (Archie 1942).

9.5.1.4 VARIABLE FREQUENCY DATA

Formation resistivity and capacitance are related to signal frequency and this relationship is likely to be related to the presence of charged surfaces within the formation, namely clays. In view of recent developments with higher frequency resistivity and dielectric tools the resistivity and capacitance of the samples was recorded at 12, 2,000 and 100,000 Hertz for possible later use in regard to in-situ clay conductivity. Low frequency values maybe invalid.

9.5.2 RESULTS

9.5.2.1 CORE RESISTIVITIES Chronological Tabulation

Resistivities at 2 khz and 77 °F unless otherwise stated.

R_w= .0894 Ωm	C_w= 11.24 mho/m
R_{w1}= .130	C_{w1}= 7.69
R_{w2}= .170	C_{w2}= 5.88
$R_{w3} = R_{mf}$ = .284	C_{w3}= 3.52
R_{w4}= .514	C_{w4}= 1.95
R_{w5}= 3.75	C_{w5}= 0.267
R_{wz}=.0898 cf R_w=.0894	
RHO_{crude}= .84 g ml^{-1}	RHO_{Rw}= 1.06 g ml^{-1}

C1= 3.846 Ωm-1, 0.4molar (23,000ppm) NaCl @25C. Published data departure from linear trend on C_o v C_w plot. (Clavier 1984)

A chronological listing of core sample resistivity related measurements was made and is included as (APPENDIX 33). (APPENDIX 33A) is the individual core plug frequency data. (APPENDIX 33B) is the sequence of resistivity related measurements corresponding to the dilution of the saturating brine, and the oil saturated samples.

9.5.2.3 R_{xwe}, FLUSHED ZONE EFFECTIVE WATER RESISTIVITY

R_{xot}, "true" resistivity of the flushed zone, is the resistivity following one pore volume of R_{mf} (R_{w3}) being flushed through the sample. R_{xoc} is the corrected resistivity of the flushed zone when the effective resistivity of the flushed zone water, R_{xwe}, equals R_{mf}. At least 12 pore volumes of R_{mf} are required to flush through the sample before this condition is met.

One pore volume was used to investigate R_{xo}'s dependence upon R_{mf}. The volume of filtrate actually passing through rock adjacent to the wellbore depends upon the volume of mud required to build an effective mudcake, a property of the mud. Close to the mudcake more than one pore volume does pass through the pore space, however this experiment was simply intended to show that piston type replacement of R_w by R_{mf} does <u>not</u> take place, and that R_{xwe} lies somewhere between R_{mf} and R_w. This may be independently observed by calculating F in a known water zone using R_{mf} and a shallow reading R_{xo} tool, and F using R_w and a deep reading R_o tool. These Fs are frequently unequal,

indicating either a genuine difference in F with distance from the borehole or an incorrect entry for R_{mf}. See logs from Ryazanian Sands. An R_{xo} tool reading deeper than invasion amounts to the same problem, that piston type water replacement cannot be assumed to occur during S_{xo} calculations.

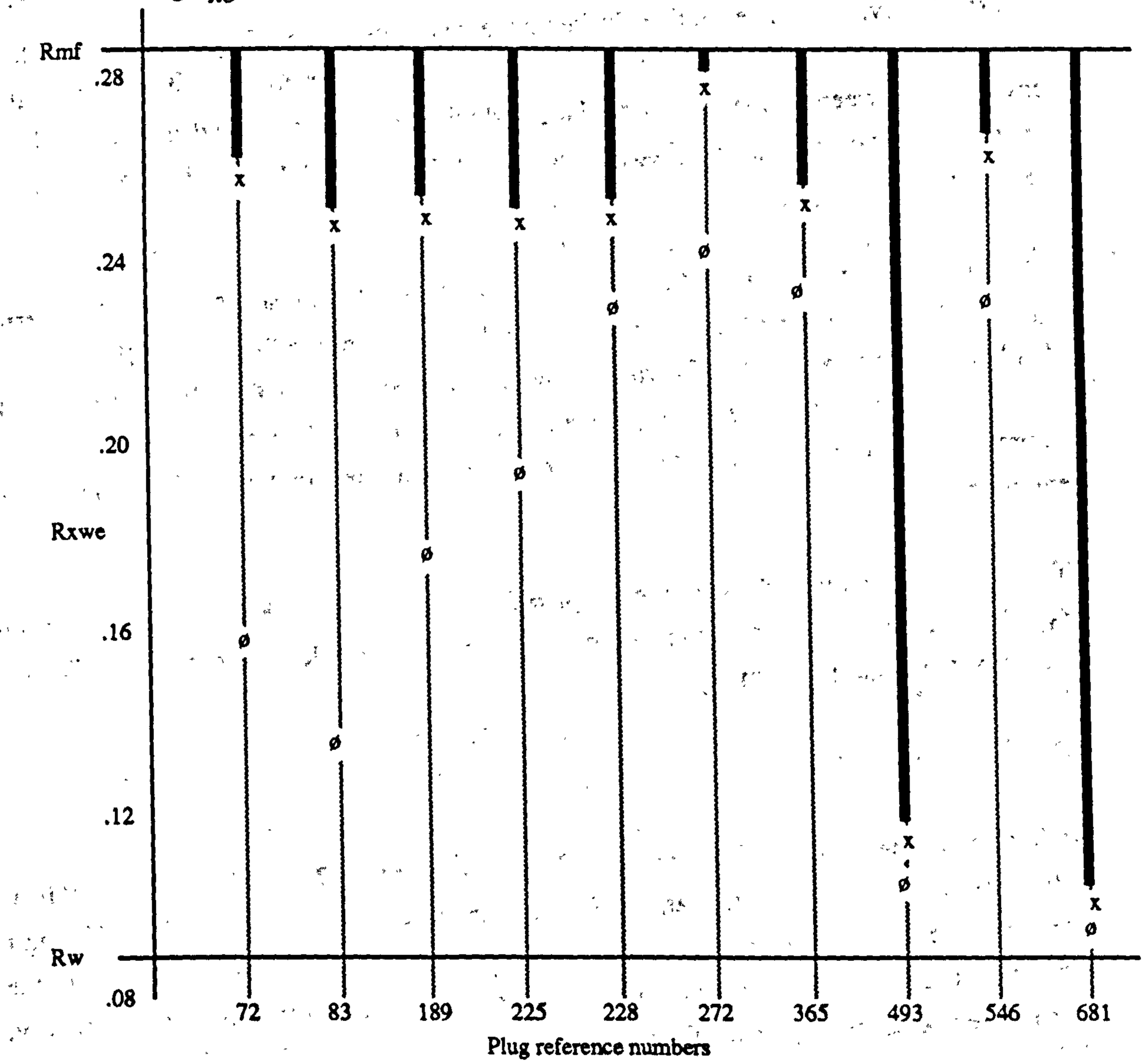


Fig p203 Movement of R_{xwe} with 1 pore volume (Ø) and 12 pore volumes (x) of mud filtrate flushing

If the flushed zone is defined as the zone where $R_{xwe} = R_{mf}$ then Fig p203 suggests that this zone is severely restricted. In most cases after 12 pore volumes $R_{xwe} \neq R_{mf}$, suggesting the depth of investigation of shallow resistivity devices would embrace rock in which $R_{xwe} \neq R_{mf}$. Using this definition a shallow reading device is preferred. This definition creates problems with rock heterogeneity within the rock volume being evaluated by a combination of different tools with different volumes of investigation.

Furthermore the shallow reading R_{xo} device may still not be shallow enough for $R_{xwe} = R_{mf}$.

If the flushed zone is defined as the zone which dominates the shallow resistivity device, an expediency, then the effective flushed zone water resistivity, $R_{xwe} = \text{f.}(R_w, R_{mf})$. This function is not obviously related to the rocks permeability or porosity. A relationship was envisaged between permeability and R_{xwe} which could be translated into a log derived relationship between S_{wi} and R_{xwe}. Such a transform would yield improved S_{xo} and movable oil values.

Invasion charts, with outputs R_{xo}, R_t, and *di* avoid any definition of R_{xo} in fluid terms, R_{xo} is defined in terms of a chart relationship between tool readings. In reality therefore R_{xo} becomes the resistivity of a variable volume of rock proximal to the hole wall. Like other log analysis parameters R_{xo} is an internally derived number which bears an imprecise relationship to the rock properties used in the concepts of geologists and engineers.

If S_{xo} is to be calculated assuming $R_{xwe} = R_{mf}$, the usual method, a shallow reading R_{xo} device, insensitive to mudcake and rugosity is desirable. Dielectric S_{xo} devices overcome the R_{xwe} problem.

9.5.2.4 HYSTERESIS

An hysteresis check (R_{oz}) after flushing 12 pore volumes of R_w produced repeatability of the original R_o of between 6 and 12%. This indicates either residual R_{w5}, 42 times more resistive than R_w, or a non reversible change to pore geometry, F, following the experiments. Changes in clay conductivity are excluded since no intercept is apparent on the room temperature C_o v C_w plots below.

9.5.2.5 R_t

The dynamic flushing of samples with formation crude produced irregular expulsions of water. This indicates an irregular distribution of the phases in the sample (Lyle & Mills, 1989). For a given S_w a patchy distribution of the conducting phase would result in a high resistivity. In the probable equilibrium conditions of the reservoir the same S_w may be expected to provide greater conductivity due to greater continuity of the wetting/conducting phase.

Reducing S_w through dynamic flushing appeared to be inferior to air desaturation over a porous plate, and the laboratory R_t measurements are the least reliable of the results (9.5.2.6).

9.5.2.6 TEMPERATURE

R_{xoc5C}, was recorded to check linearity of resistivities with temperature. The C_o v C_w plots show zero intercepts on the C_o axis in all cases despite the presence of clays. This is because clay conductivity decreases with decreasing temperature (Waxman and Thomas 1974).

The n plots are derived from R_{ozc} and R_t. n values are erratic and unrealistically high for the following reasons:

1) Patchy distribution of water fraction.
2) Inaccurate S_w calculations.
3) Lack of additional clay conductivity at this temperature (9.5.4).

The second reason was addressed by calculating S_ws using the various methods below:

1) Using weights from the following formulae:
   Actual $S_{wt} = 1 - (WR_o - WR_t) / (0.21 \, \emptyset_{he})$;
2) Using expelled water volume in a graduated test tube;
3) Using core analysis helium porosities;
4) Using imbibed water volume effective porosities. This porosity lacks clay water volume at room temperature and humidity.

The most feasible results were from the combination of core analysis porosity and expelled water volume. These were used in the n plots. However, the divergence of weight and water volume S_ws cast doubt upon S_w values.

9.5.2.7 FORMATION RESISTIVITY FACTOR AND THE EFFECT OF TEMPERATURE

With respect to temperature Archie's formation resistivity factor, F, C_w/C_o, is to be distinguished from the geometrical formation resistivity factor, F_g, in this thesis, C_w/C_{oe}. The increasing conductivity of clays with temperature adds to C_o, but not C_{oe},

thus F becomes a function of temperature in shaly rocks, whereas F_g does not. (Waxman 1974, Brannan 1973). Therefore F_g, or Waxman and Smits F^*, may be deduced from the C_O v C_W plots below. (Waxman 1968)

See (APPENDIX 65): LABORATORY RESISTIVITY (DILUTION) PLOTS, 77°F, 2kHz.

9.5.3 CONCLUSIONS REGARDING CORE CONDUCTIVITIES

1) The input R_{mf} in log analysis does not represent the effective flushed zone water resistivity, R_{xwe}. R_{xwe} lies between R_w and R_{mf}. R_{xwe} is dependent upon depth of investigation, porosity, pore geometry, the history of drilling operations, and mud properties during open hole operations. Generally, actual unmoved hydrocarbons will be greater than those calculated with R_{mf}.

2) It has been impossible to determine experimentally each sample's water saturated excess conductivity, C_x, due to the unavailability of reservoir temperature apparatus. This problem is addressed in (9.5.4).

3) n values determined from displacing formation brine with crude oil are unusually high. [A reservoir temperature n value will be determined based upon room temperature service company n values below (9.5.4.1)].

4) Direct comparison of laboratory R_t with logged R_t, to establish the sample's position above or below a transition zone (9.5.1.3), suffers from non-equilibrium laboratory conditions in the distribution of oil and brine, artificially increasing laboratory R_t.

5) F_g has been determined from the dilution plots:

Sample	Fg
14014 RS	40
14035 RS	48
14631 MSCM	54
14672 MCS	94
14675 MCS	79
14877 MCS	75
15192 BMS	54
14980 BMS	124
15119 CSCC	196
15363 MSCC	1667

9.5.4 DEMONSTRATION OF PREFERRED METHODOLOGY

Thin section examination of these low porosity illite bearing rocks indicates that at reservoir temperatures excess conductivity, C_x, could represent a considerable fraction of oil saturated conductivity.

Unfortunately, the lack of high temperature/pressure apparatus disallowed quantifying this excess conductivity during the laboratory work outlined in 9.5.1 & 2.

Excess conductivity can be estimated by resorting to correlated parameters such as clay volume, hydrogen index, $C_{xomsfl} - C_{xoept}$ (5.1), Cation Exchange Capacity etc. These are incomplete or inaccurate descriptions of excess conductivity. They are less valid than parameters which correlate with actual laboratory determined C_x values. These values, determined from a C_o v C_w plot at reservoir temperature, on reservoir samples, are the actual value required for the successful interpretation of conductivity. C_x at reservoir temperatures can be calculated from C_x at room temperatures by reference to Hardwick's 1987 paper. This method requires some value of C_x to be recorded at room temperature which is meaningful in terms of experimental error. This value is then used as the basis for a considerable extrapolation to reservoir temperatures. Intercepts obtained on the ten samples tested were not considered sufficient to base such an extrapolation upon. This would also appear to be the case for Waxmans & Thomas's 1974 data.

It is for these reasons that "Theoretical Examples" for each sample have been generated by the method below, and their values used in the calculations which follow. In this way it is intended to demonstrate the preferred method of using high temperature laboratory C_x values, had they been available.

Two assumptions are necessary:

1) Samples are from above the transition zone.
2) S_{wi} can be crudely estimated from core analysis porosities and permeabilities.

This approach represents a solution consistent with the theme of distinguishing conductivity in fluids that can be replaced by hydrocarbons, and conductivity from all other sources. Using the usual log derived approximations to C_x was rejected because such approaches are already well documented in the literature.

9.5.4.1 CALCULATION OF n AT RESERVOIR TEMPERATURE FROM ROOM TEMPERATURE DATA

The input n characterises the rate of decrease of C_t with desaturation. A corrected n has been derived from the room temperature special core analysis performed for the Operator. The basis of this modification rests upon the fact that clay conductivity is enhanced relative to water conductivity at higher temperatures. This influences n in the following manner: as the sample is desaturated the free pore water is displaced and clay conductivity comprises a progressively greater proportion of the observed conductivity. At reservoir temperatures R_t/R_O is therefore reduced, producing a flatter desaturation plot, corresponding to a lower n value (Givens 1987). This difference between clay and free pore water conductivities, as desaturation progresses, is why the clay term's S_W is raised to n-y while the clean term's S_W is raised to n.

Waxman and Smits' n^* is the saturation exponent corresponding to '...a hypothetical rock having the same pore geometry as the shaly sand, but whose clay content is (electrically) inactive '. However we know that:

$$C_O / C_t = S_w^{-n} \quad \text{(Archie, 1942)} \quad \text{and:}$$

$$C_O / C_t = S_w^{-n^*} (C_w + BQ_v) / (C_w + BQ_v / S_w) \quad \text{(Waxman \& Smits, 1968)}$$

The difference between n and n^* is the effect that electrically active shale has on the saturation exponent. $n^* > n$, since the rate of decrease of C_t will be smaller if the shale is electrically active.

Combining the equations:

$$n = n^* - \log [(C_w + BQ_v) / (C_w + BQ_v / S_w)] / \log S_w$$

The value of B should be that of B_{max} in Fig13 of the Waxman and Thomas paper, at 130°C = 0.200mho cm^2 meq-1, and not B = 0.045 mho cm^2 meq^{-1} from Eqn19 of Waxman & Smits 1968. B_{max} is for formation salinities above ≈23,000ppm NaCl. B_{max} at 130°C is used because the equation is being used here to show the shale effect at reservoir temperature.

The available data are a set of six room temperature n values and Q_vs. It has been established by experiment that room temperature shale effects on these samples are almost negligible (APPENDIX 65). The available n values reflect this and therefore correspond

approximately to the electrically inactive n^*. The reservoir temperature n (electrically active shales) required for the demonstration C_x values can therefore be calculated from the above expression by entering the room temperature values as n^*. The Q_v and S_{wi} data now provide the effective reservoir temperature n values, n in the preceding equation.[50]

Converting n values in this way is in essence making an analogy in the differences between:

1) W-S electrically inactive clays and active clays;

analogous to:

2) Room temperature clays and reservoir temperature clays.

Sample	n rm temp (=n*)	Q_v meq ml^{-1}	Calculated n res temp
14612 BMS	1.93	.11	1.84
14633 MSC	1.79	.13	1.65
14677 MCS	1.92	.08	1.86
14957 MCS	2.00	.13	1.91
14986 BMS	2.02	.26	1.86
15354 MSC	1.93	.09	1.93

Although from these limited figures there does seem to be a greater drop from n^* to n with higher gamma ray, as expected (APPENDIX 13) there is no evident relationship between rock type and the reservoir temperature n values in themselves. An average of

$$n = 1.84$$

is therefore used throughout since the six Q_v samples above were not available and the samples in were used.

y is the only remaining input to solve for C_x. y is introduced and dealt with under (6.2.1).

$n > y > 0$, the default value of y is one, and one is used in this case because its true value is based upon a reservoir conditions desaturation plot. Although the theoretical treatment

[50] W-S model assumes all excess conductivity is due to clay minerals, and the equations are based on Na equilibrating ion solutions. In the *Fg* model it is not necessary to postulate a source for excess conductivity. While the modifications used above may not be accurate because of this disparity, they represent the most accurate method available to generate the required demonstration *Cx* values.

of such a plot has been proposed, creating the plot was not possible during this thesis.

9.5.4.2 THEORETICAL EXAMPLES OF C_x

A theoretical value of C_x may be produced, for demonstration purpose only, by its relationship to the other variables in the F_g saturation equation (6.2)
The equation:

$$C_t = [S_{we}{}^n C_w / F_g] + C_x S_{we}{}^{n-y}$$

is used for when S_{wt}=S_{wi}, immovable water saturation above the transition zone. S_{wt} is converted to the input S_{we}:

$$S_{we} = 1-(\emptyset_t / \emptyset_e)\ (1-S_{wt}) \quad \text{(Juhasz, 1979).}$$

$\emptyset_t$ is converted to $\emptyset_e$ from an estimate of the plugs V_{shale}. The input F_g is known since F_g= 1/slope, from C_O plots. F_g for this formation has the same value at reservoir temperature. This is because with formation water salinities above ~23,000ppm NaCl, F_g = F^* (Clavier 1984). F^* does not vary with temperature. This can be clearly seen from the shaly sands data studied by Waxman & Thomas, (1974).

S_{wi} is taken from its empirical relationship with porosity and permeability (Coates 1973). Each sample's core analysis porosity and permeability values are used for S_{wi}[51].

The value n=1.84 is taken from the procedure detailed in (9.5.4.1). C_t is the logged value. The F_g saturation equation is now solved for C_x for each sample.

[51] If samples are taken from a water or transition zone this procedure will yield artificially high Cx values.

Table p211 Theoretical examples of C_X

R_w, 85,000ppm Nacl =.025Ωm. C_w=40.0 mho/m @ 288°F, 16500ft(5029m).
Temp Grad in Brae =.0172 °F/ft

Sample	C_t	S_{wi}	n	°F	C_w@°F	F_g	C_x	$C_x.S_w^{n-1}/C_t$	C_o
14014 RS	.154	(.14)	(1.84)	254	6.06	40	.002	13%	.154
14035 RS	.156	(.18)	(1.84)	254	6.05	48	.030	19%	.156
14631 MSCMTI	.233	.18	1.84	262	38.7	54	.852	87%	1.57
14672 MCSTI	.154	.40	1.84	263	38.8	94	.168	51%	.581
14675 MCSTI	.222	.44	1.84	263	38.8	79	.227	51%	.718
14877 MCS	.233	.43	1.84	266	39.2	75	.248	52%	.771
14980 BMSTI	.182	.48	1.84	267	39.3	124	.185	55%	.502
15119 CSCCTI	.167	.62	1.84	269	39.7	196	.124	50%	.327
15192 BMS	.200	.53	1.84	270	39.8	54			
15363 MSCC	.192	1.0	1.84	272	40.0	1667	.168	86%	.192

$C_t = ILD_{cor}$

$C_x S_w^{n-1}$ is expressed as a percentage of C_t to indicate its relative importance.

Each samples C_o has been generated from the equation:

$$C_o = C_w/F_g .1 + C_x .1$$

The procedure of the last five pages is <u>solely for the purpose of creating demonstration C_x values</u>, from room temperature experiments, which are likely to correspond approximately to the <u>actual</u> C_x values of those samples[52]. Alternative methods could have been used, as noted on p215. However, his method is consistent with the theme that experimental determination of reservoir conditions C_x is important to formation evaluation in oil bearing complex rocks.

---

[52]The weakest point in generating these demonstration *Cx* values is assumption 2 on p215, to which there is no alternative if the *Co v Cw* plot is to be the source of *Cx* .

10 DRILL STEM TESTS, REPEAT FORMATION TESTS FORMATION INTERVAL TESTS & CAPILLARY PRESSURES

This chapter gathers the remaining engineering data relevant to water zone, transistion or oil zone interpretations. It provides crude limits on some *Non-log-inputs* such as S_w and S_{hmov} and examines the poor quality formation pressure data. Capillary pressures have been used in conjunction with R_t to estimate an interval's position in relation to a possible base of closure level.

10.1 FLUIDS

Fluids recovered from Drill Stem Tests were as follows:

DST 1 (16308-16468)

The formation was open to flow for a total of 45 hours. No flow to surface, reverse circulate: 7.5 bbls 36 API oil.
15.0 bbls mixed oil/water.
18.5 bbls of 12-28,000ppm brine
Total 41.0 bbls of fluid.

18% of fluids were oil. A minimum of 18% of the movable fluid volume in the non-invaded formation was therefore oil, for those intervals with higher effective porosities and lower water saturations. $S_{hmov} \geq .18$, $S_{xo}-S_w \geq .18$

DST 2 & 2A (15050-15320)

DST 2 recovered 38bbls. DST 2A reversed out 40 bbls, and gas lifted ≈ 100bbls. Total ≈ 178bbls of fluid. The fluids were a mixture of completion brine, mud filtrate, and oil scum. 50 kppm NaCl equivalent brine. S_{hmov} = ?

DST 3 (14585-14964)

No flow to surface, gas lift ≈ 550 bbls of formation brine, and oil traces on one sample only. 85 kppm NaCl equivalent brine, of constant salinity, was achieved early in the test. DST 3 was aborted following downhole equipment failure after the interval had been perforated 2,000psi below balance. Pulling and re-running the test string for DST 3A exposed the formation to 11ppg kill brine for 100 hours. The interval was open to flow for a total of 49.5 hours, with a maximum drawdown of 5,800psi (APPENDIX 16). $S_{hmov} \approx 0$

DST 4 (14020-14064), Ryazanian Sandstone

Flowed 1750 bbls water per day, 10 kppm NaCl equivalent. $S_{hmov} \approx 0$

10.1.1 ROCK VOLUMES CORRESPONDING TO PRODUCED FLUIDS

Confidence in R_W, and that DST 3 tested a water zone, can be clarified by volumetrics.

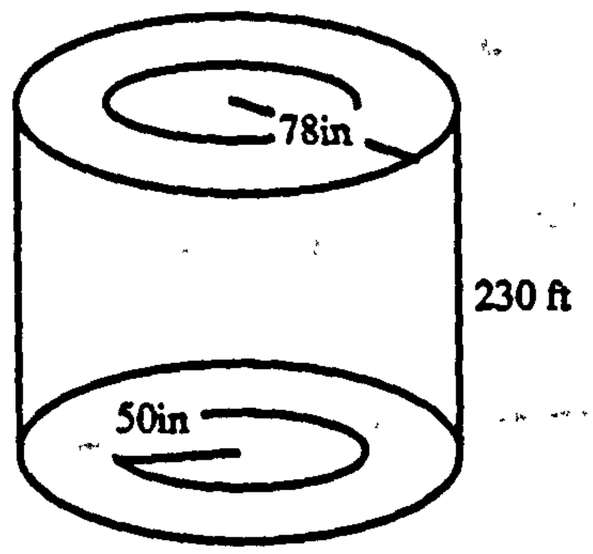


Fig p213 Rock volumes associated with DST3's fluids
and the same interval's mud filtrate (ignores wellbore)

At Ø=.1, and 230ft(70m) contributing to flow, bulk volume of rock associated with DST3:

$550*5.6/.1=\pi*r^2*230$ cu ft, r = 6.5 ft = 78in (2m)

Average *di*=50in over good flow intervals (APPENDIX 52)

The proportion of filtrate to formation brine if produced fluids flowed evenly from 230ft(70m) is 0.7. Although volumetrics allow up to 0.7 of produced fluids to be filtrate three considerations indicate that formation brine was produced; 1) the high salinity consistent with other Brae water tests, 2) constant salinity achieved early in the test, and 3) the probable preferential flow of fluids from a relatively thin interval. Therefore:

a) R_W=0.025 @ 15555ft(4741m), and

b) DST 3 tested a water zone.

10.1.2 EXTRAPOLATION OF R_W VIA RECOVERED FORMATION BRINE AND SP LOG

R_W from recovered uncontaminated formation brine (6.2.1) can be extrapolated with the SP log using Schl.chart SP-1 (Schlumberger, 1985), having first estimated static SP. The table below shows the results.

Table p214 R_W as a function of DST brines and the SP log

Interval	Rw @ res temp	Source of R_w
Ryazanian Sandstone 13830 - 14068	0.165	DST
Upper Brae 14586 - 15500	0.025	DST
Mid Brae 15500 - 16100	0.030	SP
Lower Brae 16100 - 16520	0.040	SP

This produces a vertical distribution as follows:

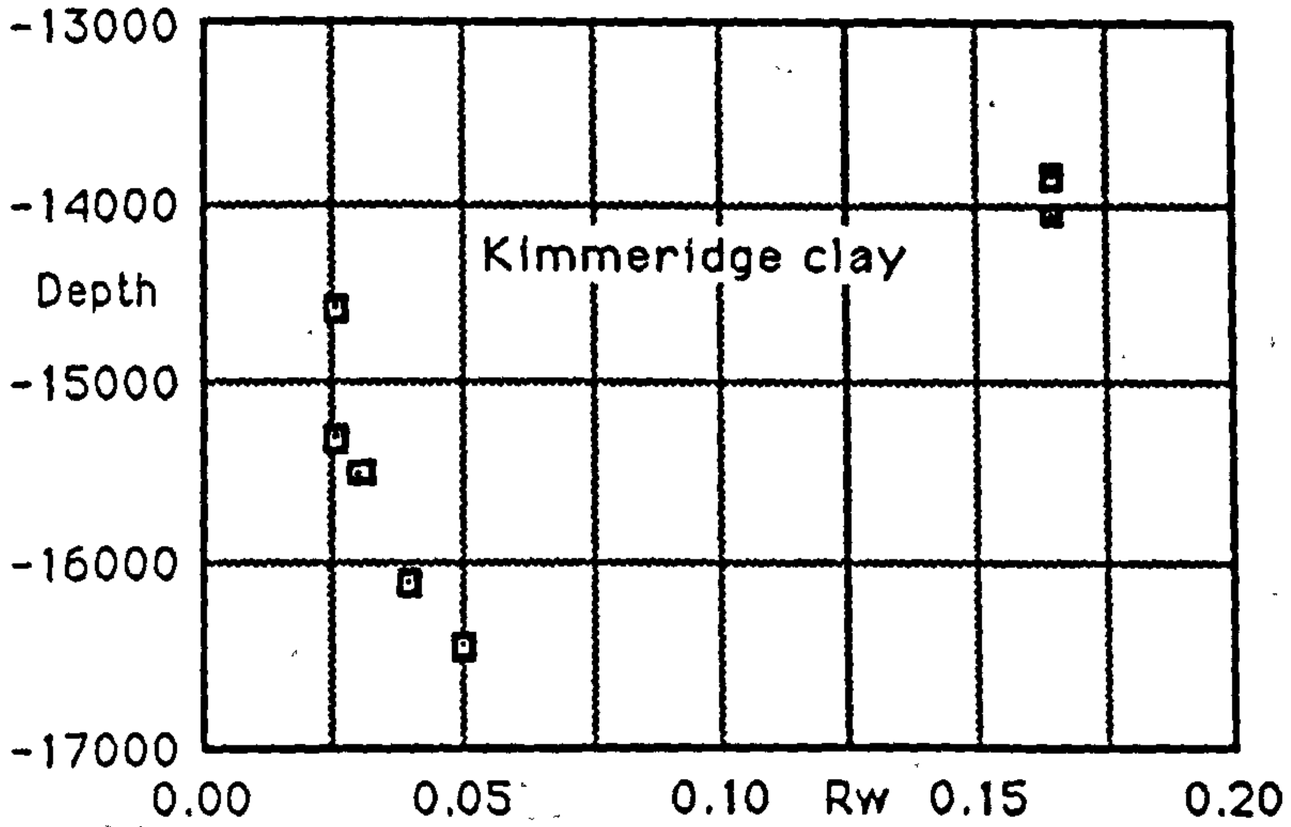


Fig p214 R_W from DST brine extrapolated with the SP log

Using these R_Ws assumes the error incurred by the possibility of hydrocarbons suppressing the SP, is less than that error introduced by ignoring a possibly changing R_W.

The extrapolated R_W will compute less hydrocarbon in lower Brae. Lower Brae flowed 7.5 bbls of oil, and it is possible therefore that R_W remains constant and the SP has been suppressed. However a permeability barrier at least sufficient to block passage of the non-wetting phase clearly does exist between the upper and lower DSTs, as evidenced by the water above oil tests and the low effective porosity (E) calculations seen in the log plots. Therefore a changing R_W cannot be ruled out. This dilemma, whether R_W increases or SP is suppressed by oil, is typical of dilemmas encountered in Well A, however, on balance R_W was left at 0.025 Ωm. Zoned R_W saturations were also computed, but rejected as unnecessarily complicated.

10.2 FORMATION PRESSURES

Pressure data for the Brae Formation was from three sources: Drill Stem Tests, Wireline Repeat Formation Tests and Wireline Formation Interval Tests.

Drill Stem Tests (DST)

DST 1 (16308-16468) suffered a washout in the test string, mud entered the drill pipe, and the test was aborted with two inches of solid barite in the drill pipe. DST 1A's test string failed to enter the well. DST 1B reversed out fluids (10.1), but no formation pressure interpretations were possible.

DST 2 (15050-15320) was aborted due to mechanical failures. DST 2A had five flow and shut-in periods. Horner plots were made with data from all three gauges (APPENDIX 14). The best estimate of initial reservoir pressure was

$$P^* = 8097psi \text{ @ } 14978ft \text{ (4565m)},$$

where P^* is initial reservoir pressure, from the second shut in period. DST 2B provided poorer pressure records resulting in P* = 7652 psi @ 14970ft(4563m).

DST 3 (14585-14964) was aborted, after successful underbalanced perforating, due to a washout in the test string. Qualitative information only can be derived from this test. DST 3A suffered from leakage across the LPR-N valve. Pressure records were complicated by gas lifting the test string fluids, and the final build–up pressures were invalidated by further leaks across the LPR-N valve. No definitive P^* calculations were possible from either DST 3 or 3A, however P^* = 7929psi is an approximate figure from DST 3's initial flow build–up. (APPENDIX 15)

In summary, all eight tests in the Brae formation suffered considerable departures from the ideal conditions required to project initial reservoir pressure from pressure buildup plots. Buildup tests ideally follow a period of constant flow rates, after wellbore storage effects have expired.

Repeat Formation Tests (RFT)

The most striking shortcoming of Well A's data is the lack of RFT pressure points, (10.5). Washouts, rugosity, water based mudcake and low permeability are poor conditions for acquiring RFT true formation pressures. However three open hole pressure tests were attempted, two of which succeeded. The pressure logs show good character; (APPENDIX 13), but cannot be true mobile phase fluid pressures because of their negative gradient. FITs suggest both points were supercharged (footnote, p225).

Log depth ft	Fm psi
14610 (4453m)	7911
14654 (4467m)	7906

Formation Interval Tests (FIT)

Six FITs were performed with explosive charges through casing. Pressures were:

Log depth ft	Fm psi
13904 (4238m)	7696
13965 (4257m)	7708
14978 (4565m)	7911
15348 (4678m)	8078
15390 (4691m)	8123
15736 (4796m)	8125

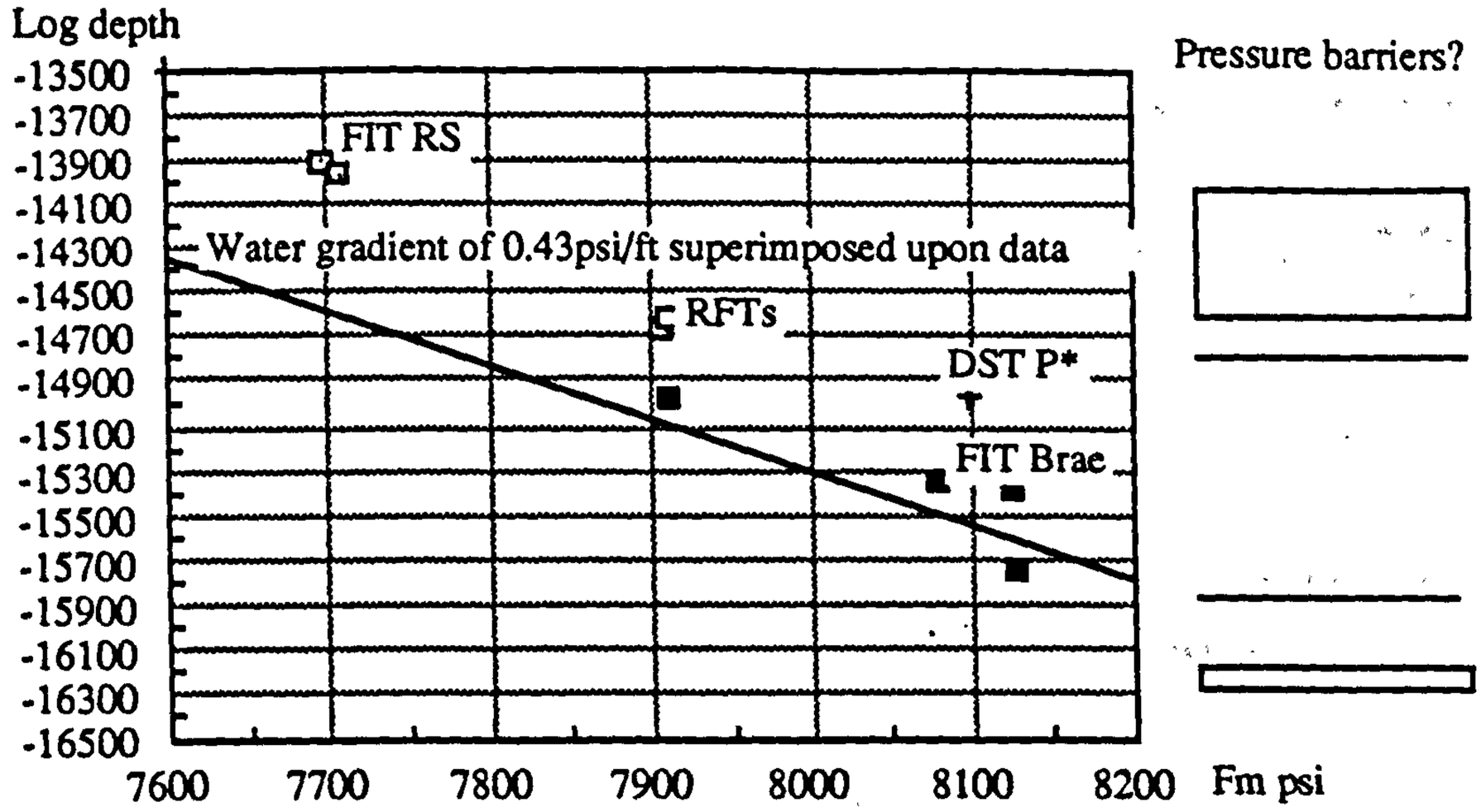


Fig p217 Composite of pressure information from FITs, RFTs, and DST 2A's *P**. Possible vertical pressure boundaries are interpreted from the SP log, GR log and effective porosity calculation.

An unequivocal message from fluid pressures is not present in Well A. The plot fails to provide any clear indication of formation fluids distribution because the undisturbed formation pressure gradients cannot be interpreted with confidence. The Brae interval FIT data has large scatter. This is due to:

a) Imperfect seals between probe and wellbore fluids.

b) Pressures responding partly to historic mud filtrate pressures in a low permeability formation "supercharging"[53].

c) Possibly (not probably) actual lithological/pore throat size pressure compartments in the formation within the interval providing the gradient.

If the difficulties with evaluating Well A had been evident at the time numerous FITs may well have provided a more confident picture of the reservoir gradient(s). Although the various data is not inconsistent with a superimposed water gradient, the scatter is too great to positively eliminate an oil column(s). This plot may contain data from basal sections of transition zones, with each rock volume within closure showing an oil gradient rising from a common aquifer. This unsatisfactory result is discussed in the conclusions of this thesis.

[53] Supercharging is more probably caused by the RFT removing wall cake, which causes a pressure gradient to arise within the formation, simultaeneous with the test, as new filtration occurs during build up of the new cake. The pressure gradient occurs across the cake as soon as it becomes impermeable and the mud column pressure dissipates.

10.3 *kh*

DST 1, 1A, 1B (16308-16468). Inadequate data for *kh* calculations.

DST 2, 2A, 2B (15050-15320). An estimate of *kh* mDft has been calculated from the build–up pressures of the second shut-in period of DST 2A. The principles for this calculation follow those of Earlougher (1977); in particular p.93. (APPENDIX 14)

$$kh = (162.6\, q\, \mu\, B_w) / m\,, \text{ where}$$

k = mD

h = 270ft(82m), tested perforated interval height

q = flow, 35 bbls water per day

μ = 0.23cp@ 290°F & 1 atmos = 0.23*1.06@ 8000psi = 0.24cp (p.241)

B_w = 1.0 Formation volume factor. Flowed water.

m = 1142 psi/$\log_{10}$cycle

15050 -15320 *kh = 1.24 mDft*

DST 3, 3A (14585-14964). No *kh* values were possible from DST 3 due to annular fluid influxes across the LNP-R valve. DST 3A had five in-flow events. One followed bleeding off the N_2 cushion and four followed the removal of produced fluids from the test string with coiled gas lift tubing. However throughout these periods the formation was continuously exposed to various degrees of drawdown due to valve leakage. (APPENDIX 16, Williams, 1984)

After each gas lift cycle the increase in down hole pressure results primarily from the increasing height of produced fluids above the gauge at 14501ft(4420m). This was used to indicate formation productivity by calculating produced volumes from test string internal volumes. A plot was made of flow rate versus flowing bottom hole pressure. (APPENDIX 17). The plot shows linear trends of rate versus pressure, with the extrapolated pressures at zero flow rate, 7435 and 6875 psi, reducing with time. If these extrapolations are valid the depletion effects indicate a small drainage volume. However these data are not convincing.

Bbls per day / psi of drawdown can also be calculated from:

$$kh = [\, q\, \mu\, B_o\, \ln(r_e / r_w)\,] / [\, 7.08 (P_e - P_{wf})\,]\,, \text{ where}$$

q = bbls/day, 120

B_o = 1, Flowed water

r_e / r_w = reservoir boundary radius/wellbore radius = 2000/0.3 = 6667

$P_e - P_{wf}$ = boundary press - wellbore flowing press, 6880-5120 = 1760

μ = 0.24cp see above.

14585-14964 *kh = 0.2 mDft*

This extremely low value has been deduced from very poor data. Nevertheless the result is quite insensitive to most of the variables: for example with the reservoir boundary pressure at 8000psi (10.2) *kh* remains below 1mDft. *q* is the parameter which requires scrutiny. For *q* to be significantly increased, by a factor of say 100 for *kh* to approach 100mDft, is difficult to envisage, since ≈550 bbls of formation brine were produced during this test. The only destination for the unnoticed disappearance of ≈5,000 bbls of brine is loss to the adjacent formation. Even with mechanical failures such a major event would not have gone unnoticed, and *q* therefore remains low.

Despite the poor data it is possible to conclude either that:

a) This interval has extremely low permeability, or,

b) The formation has been severely damaged, for which there is no other evidence.

10.4 SKIN

Skin is a dimensionless pressure drop assumed to occur at the wellbore face caused by a "skin" of altered flow properties proximal to the well (Earlougher, 1977. p5). Conventional skin calculations cannot be made for any Brae Formation interval because of the extremely poor data quality.

10.5 CAPILLARY PRESSURES, P_c

10.5.1 METHOD

Despite significant core residual oil, strong indications of oil while drilling, and DST 1 recovering oil from apparently below a water zone; Well A shows no significant shift in resistivity over its entire 1,932 ft (589m) of potential reservoir, except for a general porosity trend. This constancy suggests the whole 1,900 ft (579m) is either entirely above or entirely below any possible oil:water contact. Capillary pressures can assist in deciding the position of Well A's Brae formation in relation to such a contact.

Capillary data provides a means of estimating the immovable water saturation, S_{wi}, in an oil zone. The saturation equation then enables this S_{wi} to estimate an oil zone resistivity. Providing *n* is not abnormally low there will be a significant difference in R_t above and

below the transition zone, and this difference will depend upon S_{wi}. In the case of Well A, using typical values:

R_O =3.0 Ωm,
if S_{wi} =.40 then R_t = 14 Ωm, however
if S_{wi} =.15 then R_t = 65 Ωm.[54]

The capillary pressure data is converted to a composite oil/brine P_C-S_w plot, from which at a given P_C a Ø -S_W relationship will be derived. This procedure enables Ø from logs to estimate S_{wi} and the corresponding R_t, at the given P_C or height above free water. Since FWL is unknown, a deep FWL will be assumed, because as previously stated, the formation is either entirely above or below any transition zone. The resulting R_t prediction is then compared to the logs.

The data consists of ten plugs: six using nitrogen/brine and desaturated to a pressure of 180 psi, and four using mercury/air, injecting mercury at up to 2000 psi (APPENDIX 39). The mercury plugs are from the same depth as the brine plugs. One low porosity mercury plug is included to facilitate an even spread of data over a wider porosity range. Using and converting the data assumes:

1) Core plugs are a statistically proper representation of the bulk reservoir rock under investigation.
2) Insignificant changes in pore geometry have occurred during core retrieval and cleaning,
3) Insignificant changes in wettability have occurred during core retrieval and cleaning,
4) The same P_C-S_{wi} relationships derived in the laboratory for a sample hold true for the uniaxially compacted reservoir pore volumes. (Conversions to compacted porosities and their new S_Ws are not possible, crack like pore geometries will be altered)

These assumptions may be invalid.

10.5.2 P_C PLOTS, PREDICTIONS AND RESULTS

The P_C values converted to an oil/water system are plotted in the three figures below. *Pc res oil / brine* has been derived from (APPENDIX 39) and the formula:

Pc wx / Pc yz = (TcosØ)wx / (TcosØ) yz (Core Lab, 1982)

where *w, x, y* and *z* are any fluid phases. *T*=interfacial tension, dynes/cm. Ø=contact angle, degrees.

Therefore: *Pc res oil / brine = .36Pc lab air / brine*

Pc res oil / brine = .071Pc lab air / Hg

[54] C_W=40 Ø=0.12 *g*=2.30 *n*=1.84 C_x=0.03 (C_x=10% of *Coe*)

Approximate heights above FWL were calculated from:

$$H = Pc\ res\ oil\ /\ brine\ /\ 0.11$$

where H = Height in feet above FWL

0.11 = Water gradient - Oil gradient, psi/ft = 0.44 - 0.33 (Core Lab. 1982)

All three plots show the heterogeneous pore geometries within Well A, whether using porosity or permeability as a reference. Although the 8.7, 8.9, 11.1 and 11.2 porosity plugs all show a general dewatering trend with pressure, their relative proportions of small, medium and large pores are clearly dissimilar. The $\emptyset_{he}$ versus S_w trend at ≈600 feet (183m) above free water, high in the oil zone, will be used to derive an $S_w = f.(\emptyset_{he})$ relationship so that logs can be used to approximately predict Swi at different porosities.

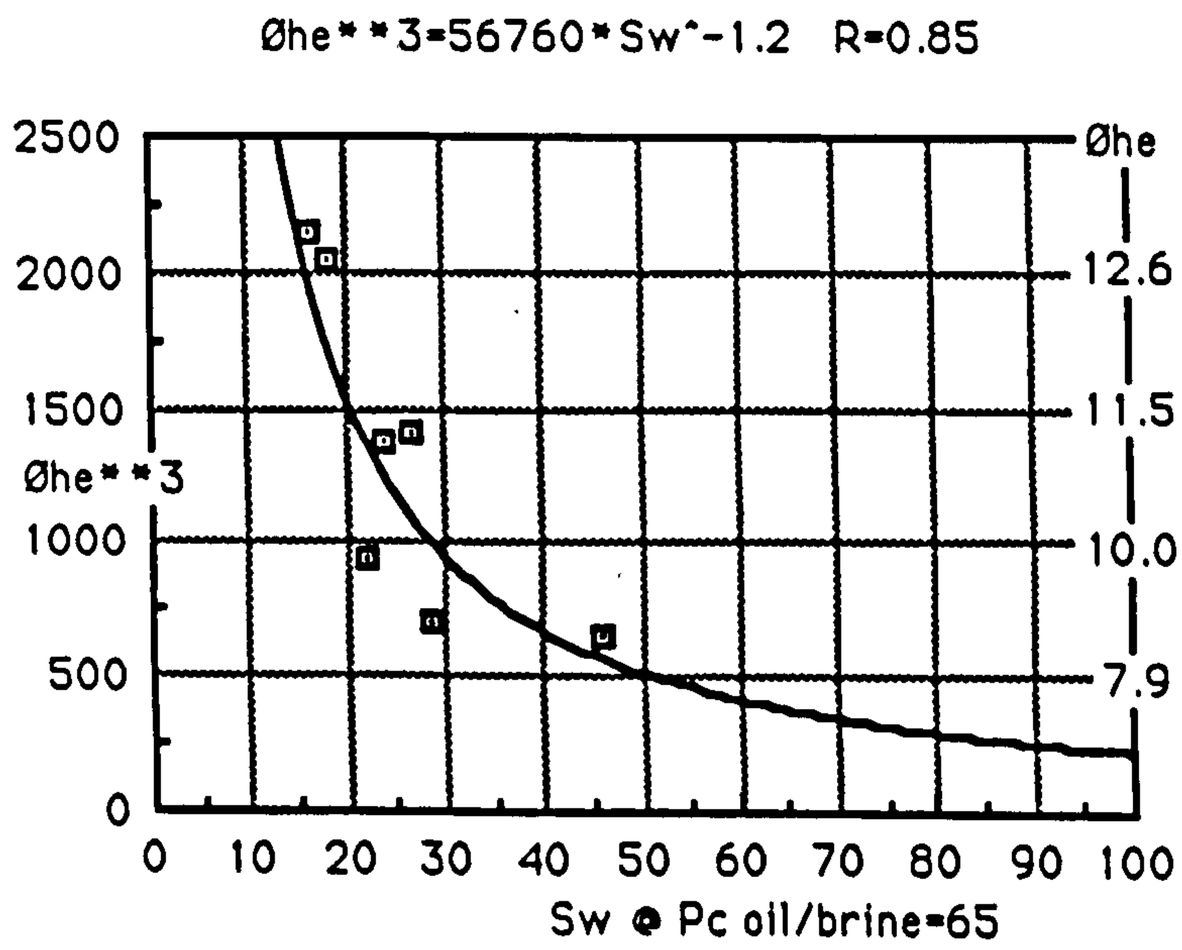


Fig p221 Means of estimating S_{wi} above ≈600 feet (183m) of height, by using porosity. (See previous plot.)

Porosity was chosen in preference to permeability because

a) the fit is slightly closer, and

b) logs cannot measure permeability as directly or as precisely as porosity.

Fig p222 Water saturation versus reservoir fluids capillary pressures for six samples of varying porosity

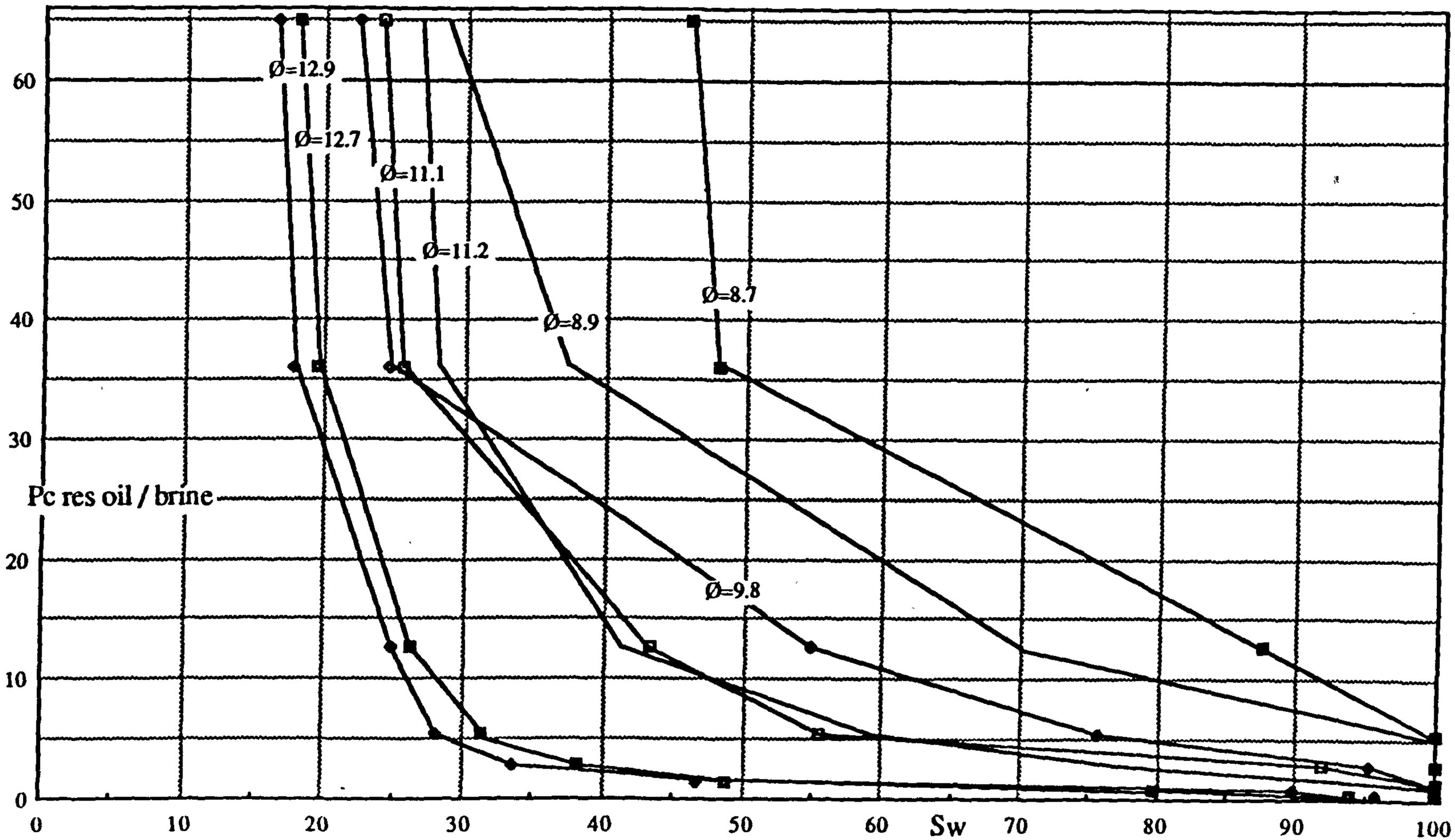


Fig p222 Water saturation v reservoir fluids capillary pressure for six samples of varying porosity

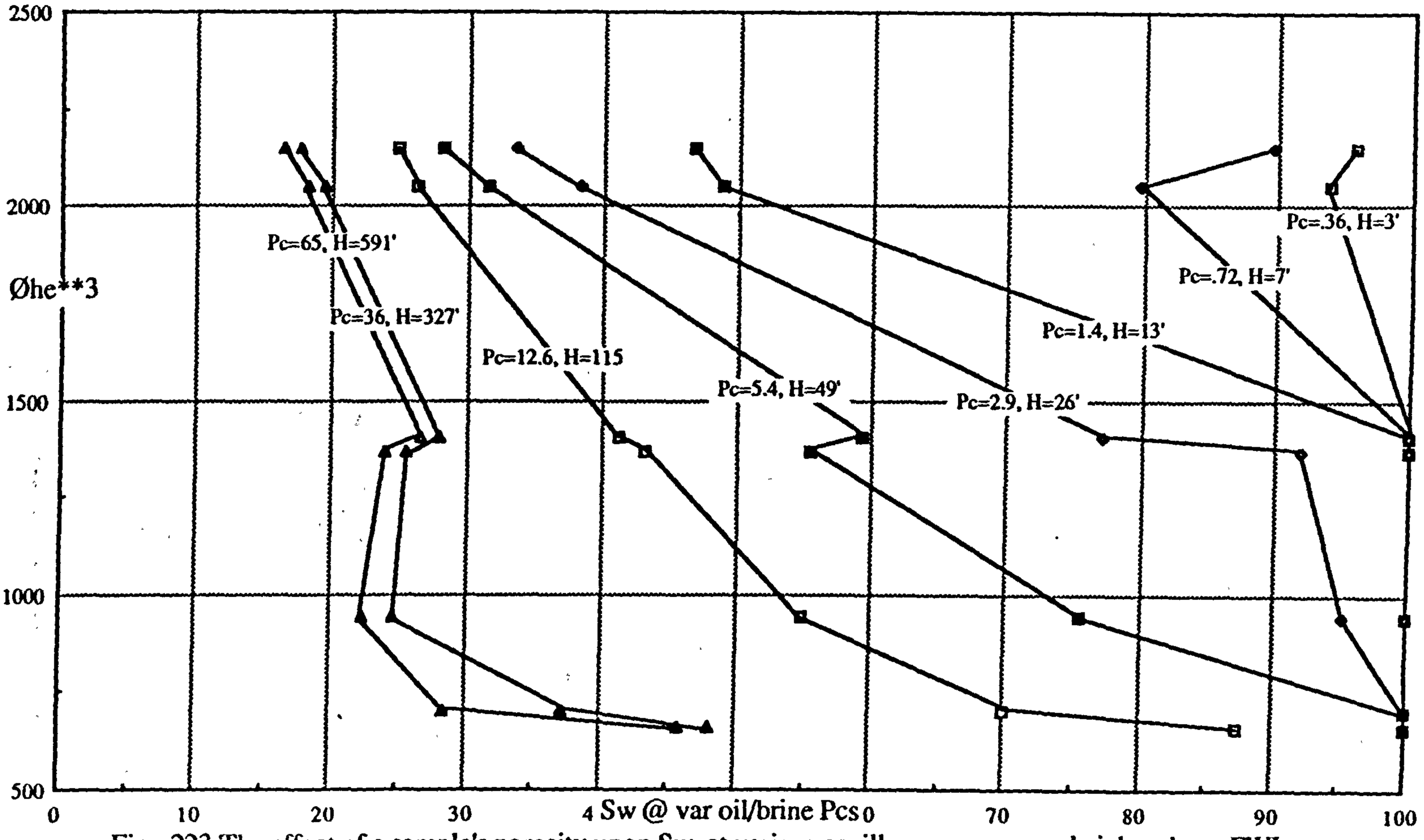


Fig p223 The effect of a sample's porosity upon Sw, at various capillary pressures or heights above FWL

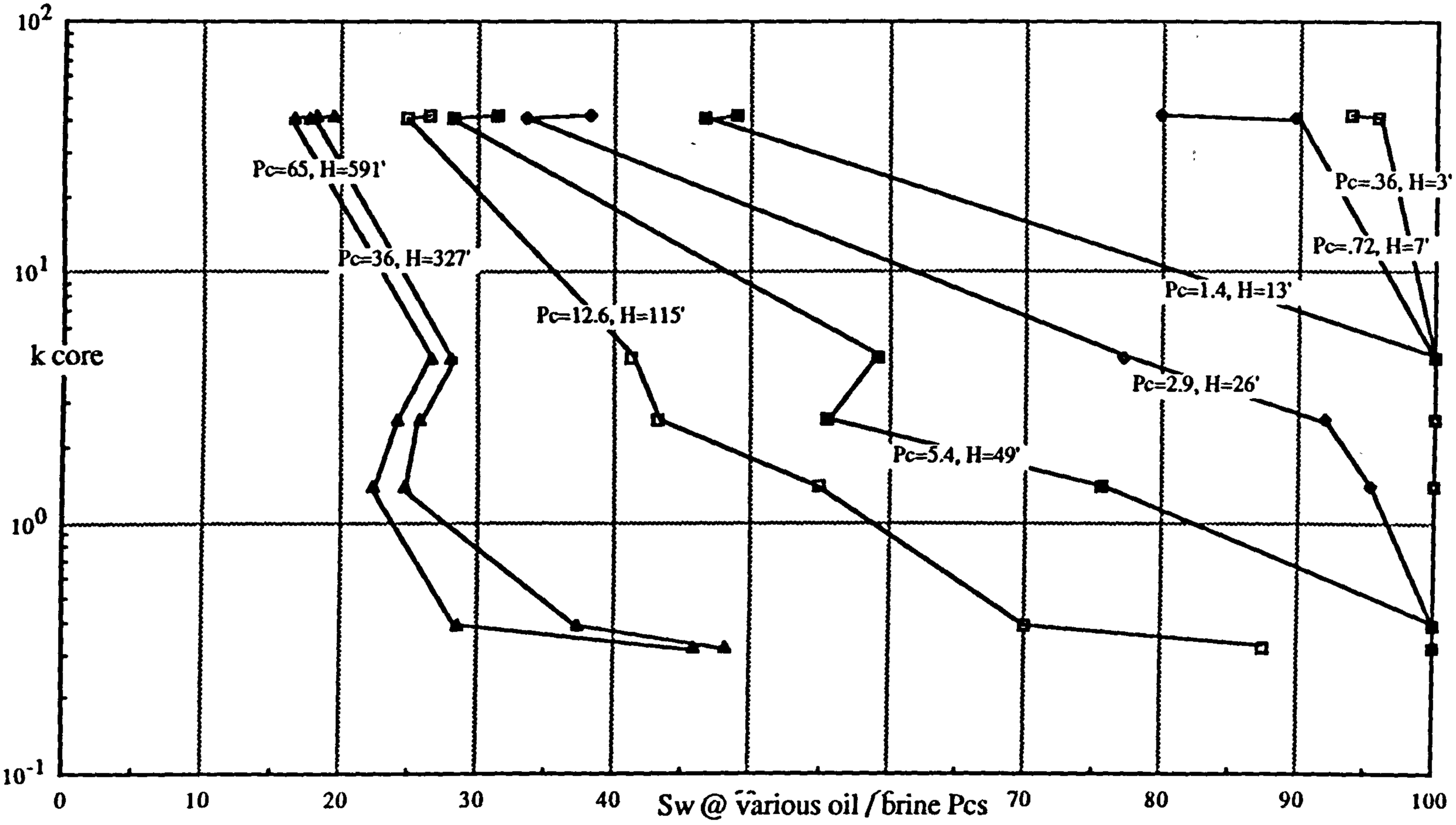


Fig p224 A sample's permeability and Sw, at various capillary pressures, or heights

10.5.2.1 CAPILLARY PRESSURE PREDICTIONS OF R_t

Using the fit:

$$S_{wi} = (56760 / \emptyset_{he}**3)^{0.833}$$

the following S_{wi}s and corresponding R_t values have been calculated for Brae rock situated 600 feet (183m) above FWL.

At a porosity of 0.12, S_{wi} = .18 Therefore in the oil zone if C_x varies from 0.030 –> 0.015 mhom: R_t --> 50 – 60 Ωm; R_O=3.0 - 3.1Ωm

At a porosity of 0.09, S_{wi} = .38 Therefore in the oil zone if C_x varies from 0.030 –> 0.015 mhom: R_t --> 25 – 30 Ωm; R_O=5.3 - 5.8Ωm

At a porosity of 0.06, S_{wi} = 1.00 Therefore in the oil zone if C_x varies from 0.030 –> 0.015 mhom: **R_t --> 11 – 13 Ωm; R_O=11 - 13Ωm**

The above exercise indicates the extreme difficulty of formation evaluation in deep, low porosity rocks. Any errors in core or log analysis influence results dramatically. This SCAL program has failed to investigate the range of logged porosities encountered in the only oil yielding interval. Any conclusions are therefore the results of extrapolation.

Alternative fit equations alter 6% porosity S_{wi} considerably. However, if the capillary pressure derived S_{wi}s, and n and m are realistic, oil zone sandy matrix resistivities will increase with porosity. Also at ≈ 6% porosity greater than 600 feet (183m) of oil column is required to reach capillary threshold pressures, replace brine, and raise resistivity above that seen for a 6% rock in the water zone.

(APPENDIX 41) shows Schlumberger's estimate of R_t from the six resistivity curves of the laterolog and induction runs. Firstly, the broad trend of resistivity with porosity over the lower interval, 15600-16520, is inconsistent with an oil zone. Secondly, R_t matches R_O predicted (water saturated) from the saturation equation over porosities from 0.06 – 0.12.

10.6 CONCLUSIONS REGARDING DSTs, RFTs FITs & P_c s

10.6.1 *Shmov*

Some Non–log–inputs may be gained from this chapter. Below 16308ft(4971m) movable fluids, $S_{hmov} = S_{xo} - S_w \geq 0.18$. We can assume that this figure applies to the higher porosity, lower S_w intervals such as 16340ft(4980m) from which any hydrocarbon will have preferentially flowed in a water-wet rock.

Likewise between 15050-15320ft(4587-4670m) $S_{hmov} \approx 0$ in the higher porosity intervals such as 15170-15180ft(4624-4627m); and finally in the upper Brae test, 14585-14964, the hydrocarbon content of movable fluids is also practically zero.

If $S_h > 0$ then $S_h = S_{hr}$, residual hydrocarbon saturation. Residual hydrocarbons could be viscous or solid varieties such as bitumens; or an oil-wet surface. An oil-wet formation of 11% porosity is likely to be more resistive than the 5Ω seen in this formation. Although SCAL wettability tests are open to criticism these tests show no evidence of oil–wetness. Given that the formation flowed water and is not oil–wet the simplest conclusion is therefore that:

$$S_{hmov} = 0 = S_h$$

Therefore:

Log depth ft	S_{xo}-S_w = S_{hmov}	S_{wt}
14585-16255	≈ 0.00	≈ 1.00
16255-16465	≥ 0.18	≤ 0.82

10.6.1.2 EFFECT OF FILTRATE INVASION ON PRODUCED FLUIDS

Previous indications of hydrocarbons, and trace amounts of oil on DST2&3 imply relative permeability to oil may have been reduced by water filtrate invasion. This phenomenon would also explain reluctance to flow, since $k_W+k_O<k$. However an increase of k_W over k_O cannot explain water production from a zone at connate water saturation.

10.6.2 FLUID PRESSURE GRADIENTS

Pressure information could normally provide *Non-log-inputs* in the form of probable limits on S_W by indicating fluid contacts. In Well A's case definite oil or water gradients cannot be identified, and Non–log–inputs cannot be derived (10.2). The absence of sufficient (>20) RFT pressures allowed considerable confusion when the initial log analysis had to be reconciled with tests. This absence of critical data shows the value of petrophysical supervision at the wellsite, who could have persisted in relocating adequate RFT pressure points in this difficult situation.

10.6.3 CAPILLARY PRESSURE DATA

Capillary pressure predictions of oil zone water saturation coupled with the F_g saturation equation indicate the entire interval to be in a water zone, despite indications of oil from core, cuttings, chromatograph, standard log analysis and DST 1.

11 RECONNAISSANCE IN CORED & LOGGED WATER ZONE

If we wish to analyse the conglomerates accurately we need to separate and quantify three influences on C_t:

1) The effect of clasts.
2) The effect of excess conductivity in the sandy matrix.
3) The effect of hydrocarbons in the sandy matrix.

In this case the reservoir conditions special core analysis required to examine these influences was unobtainable (6.2.1). This unsatisfactory situation was dealt with by attempting to find useful data from other sources, by making approaches to all operating companies with interests in the Brae conglomerates. Adequate SCAL was not found; but a large well organised database was found at Marathon Oil Company, London. The database included log and core data from conglomeratic intervals that had been cored through both oil and water zones with water based mud (WBM), together with core photographs. The reconnaissance log analysis runs were made with the kind assistance of Mr Harold King at Marathon.

Cores in a known water zone provide valuable information for formation evaluation because the major variable under investigation, the conglomerate's sandy matrix saturation, is constant, $S_{wm} = 1$[55]. This allows a better understanding of other influences which might otherwise be falsely attributed to S_{wm}. Furthermore, no core preservation or laboratory problems arise.

The Marathon cored water zone data was used for determination of the constant *"d"* in the diffusion equation (7.1). Cored water and oil zone data was used to deduce the C_{tm} chart (7.3). The role of this chapter is depicted in the box diagram below.

---

[55] Localised closure below FWL may trap migrating hydrocarbons and form the lower portions of transition zones (15).

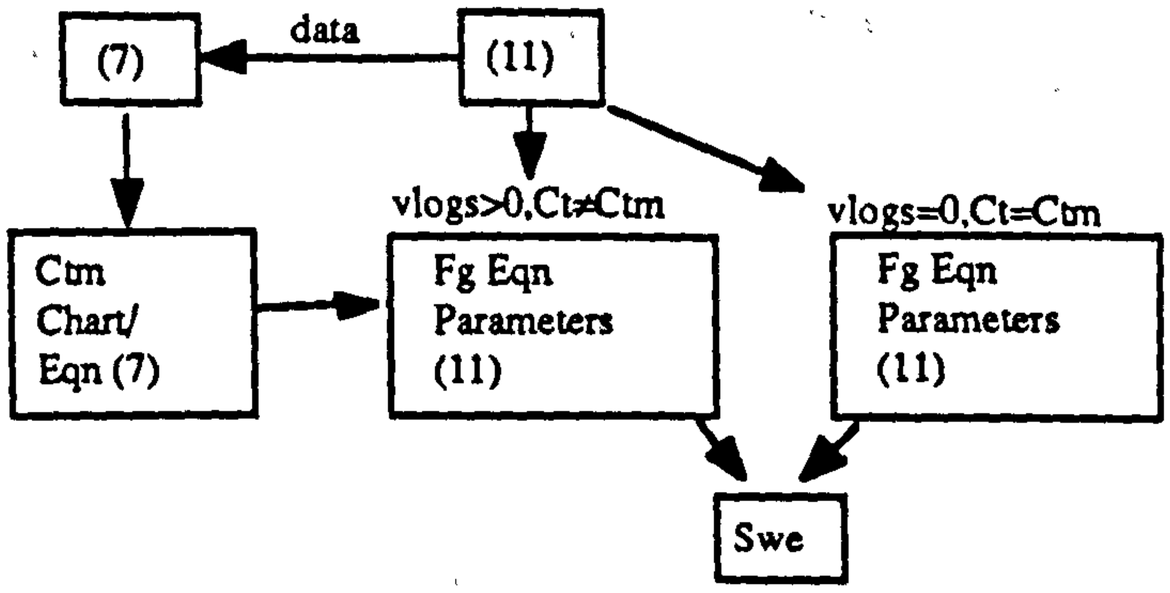


Fig p229 Relationship between chapters 7 and 11 and solving for S_{we}

The object of the pilot runs was therefore:

1) To furnish data to establish the diffusion equation constant d from known clast:matrix ratio in S_{wm}=1 intervals (7.2.1 & 7.2.2). (The diffusion equation yields C_{tm}, conductivity of the conglomerate's sandy matrix.)
2) To generate log parameters for $\emptyset_e$, g and C_x in the sandy matrix for the continuous application of the F_g saturation equation in the sandy matrix:

$$C_t = C_w \, \emptyset_e^{\beta} \, S_{we}^{n} + C_x \, S_{we}^{n-y}$$

3) To compare the equation's prediction of R_O with actual logged R_O values below the FWL.

11.1 FIELD WIDE TOOL NORMALISATION AND POROSITY MATCHING

Laterally extensive thick shale intervals provide a continuum of approximately constant physical properties against which tools may be normalised. Low energy shales have little lithological variation, and units within the Kimmeridge clay are sufficient for this purpose.

Density tools varied by up to 2.5 porosity units in the Kimmeridge, due to influences such as tool face wear. This creates artificial separation of a saturation equation's predicted C_O value from well to well if a tool cannot be calibrated due to lack of core. For these uncored wells tools were normalised via modal values of tool readings from histograms of correlated lithological units. Only the same tools were normalised. i.e. the FDC tool and LDT[56] from two wells should not be normalised.

In cored wells *rhob* is first plotted from clay free and clast free intervals in the water zone[57]. A best fit is then made between *rhob* and $\emptyset_{he}$; fixing nil $\emptyset_{he}$ at the modal

[56] FDC & LDT Mark of Schlumberger: Formation Densiy Compensated & Litho Density Tool.

[57] Hydrocarbon zones may be used seperately, but not transition or unknown zones. Hydrocarbon zones have less

grain density and 1.0 $\emptyset_{he}$ at *rhof*. (Uniaxial stress core porosities were not available.)

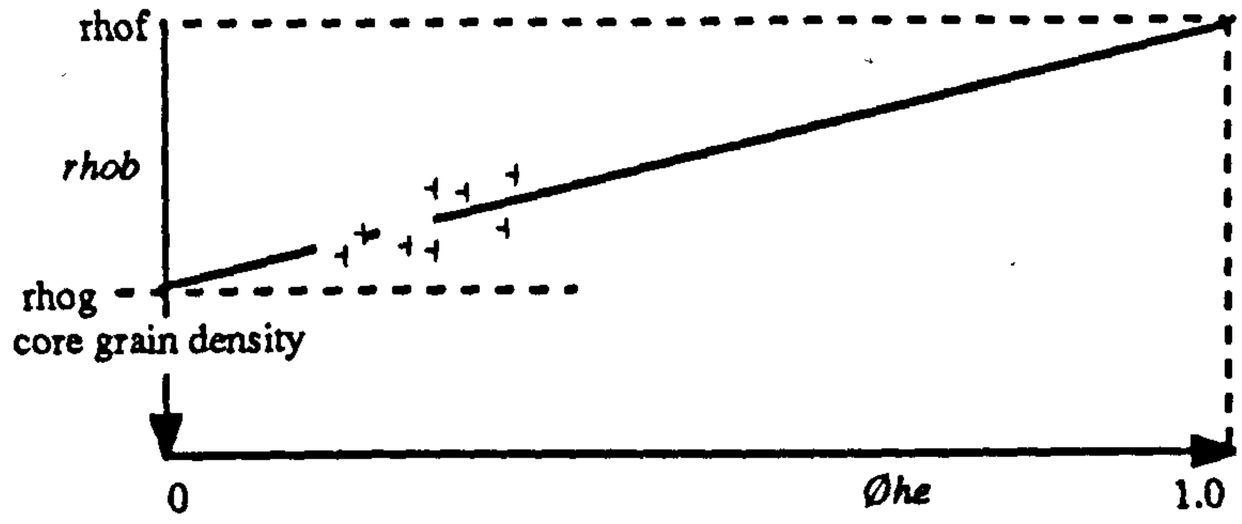


Fig p230 Matching $\emptyset_d$ and $\emptyset_{he}$

This provides core matched $\emptyset_d$s in water zones for cored wells. The well whose *rhof* is closest to 1.00 is used as the reference density trace for uncored wells. The density traces over the lithological unit in uncored wells, and the reference well, are histogrammed. The entire density trace of uncored wells is now shifted to the reference trace by an amount equal to the difference apparent in the histograms. This method was followed by using frequency plots of $\emptyset_{he}$, $\emptyset_d$ over net intervals (H.King, pers comm). (APPENDIX 35A–F)

Other environmentally corrected tools can have their traces matched over lithologically persistent units. This reduces ghost parameters, and artifacts created by a mismatched database.

11.2 PROCEDURE FOR ESTABLISHING MATRIX CONDUCTIVITY, C_{tm}

The core photographs were studied and an estimate of clast:matrix ratio throughout the cored intervals was plotted on the wireline raw log. This was done for all wells drilled with water based mud with cored conglomeratic intervals, through oil and water zones. (APPENDIX 18A-F)

The results furnish data for d (7.2.2), and produce a chart for C_{tm} (7.3). The C_{tm} chart can then be used with $\emptyset_e$ in the F_g saturation equation.

---

certain fluid densities than known water zones drilled with water based mud.

11.3 GENERATING LOG PARAMETERS FOR $\emptyset_{e,g}$ & C_x

Pickett Plot

In clean water bearing matrix sands g=m, because C_x=0 and $\emptyset_e$=$\emptyset_t$. A Pickett plot of log$\emptyset_t$ versus logR_t can therefore be used to find g, (APPENDIX 19). R_w was set at 0.028Ωm from the large volume of produced formation water. The results show the exponent g required to predict R_o from $\emptyset_e$ is not a constant, $\emptyset_e$ can more accurately predict R_o if g varies with porosity. This may be real, or indicate a tool resolution mismatch, or a log to log depth shift. The density curve was ramped over four feet (1.2m), *POROdenAVE*, and the curves manually depth shifted to reduce these two problems. Different physical processes for R_t and *rhob* disallow perfect compatibility in a heterogeneous system. However, the ramped plot provided a satisfactory g value of 2.30. Although g=f.($\emptyset$) predicts C_o accurately over a wider range of porosities it was treated as constant during this exercise. At average porosity g=2.30 is as correct as g=f.($\emptyset$). However it can be seen from (APPENDIX 20A–B)[58] that g in reality is not constant even for a unique value of porosity. Nevertheless g=2.30 must be considered more valid for this log analysis than other methods mentioned in this thesis, because of its in-situ derivation from the same rock type.

Compatibility of g with Switched $\emptyset_t$

g=2.30 has been derived with $\emptyset_d$. The method of switching parameters for $\emptyset_t$ detailed in (8.1.5) does not conflict with $\emptyset_d$ derivation because g is an attribute of $\emptyset_e$. The optimum method of deriving $\emptyset_e$ therefore becomes the overriding consideration. $\emptyset_e$ derivation has been calculated (8.1.6) to be most accurate if various methods for $\emptyset_t$ are employed.

11.3.1 $\emptyset_e$

A useable definition of $\emptyset_e$ for non-clean intervals, based on shale water volumes was adopted:

$$\emptyset_e = \emptyset_t - V_{sh}\emptyset_{dsh}$$

---

[58] Helium porosity multiplied by a uniaxial stress compaction factor of .95, a reasonable value, would lower a porosity of .150 to .143, however for the purpose of S_w, g=2.30 is compatible with the non-compacted porosties used, even if these porosities themselves are slightly high.

11.3.2 PARAMETERS FOR C_x

$$C_x = C_{olog} - (C_w \ \emptyset_e^g)$$

Various parameters for C_x from non conglomeratic water zones were tried including:

1) $(V_{shGR} \ \emptyset_{dsh})/\emptyset_d$,
2) $(\emptyset_n - \emptyset_d)/HI_{drcl} \ \emptyset_d$, ($HI_{drcl}$ = 14 not critical, absorbed by constant k below)
3) $(\emptyset_s - \emptyset_d)/\emptyset_d$, and
4) SP; an electrically sourced parameter.

Correlations were not acceptable from deep reading tools. The major reason for poor correlations is g's foot to foot variations (APPENDIX 20), thus using a constant porosity exponent usually predicts an incorrect free brine conductivity, which when subtracted from logged C_o yields an incorrect C_x (APPENDIX 21). This is the crux of the argument for reservoir conditions laboratory plots of C_o versus C_w for determining C_x. In the laboratory it is not necessary to predict conductivity with a porosity exponent.

In the flushed zone the free brine salinity and conductivity are reduced, which increases the proportion of C_x to C_o. Before the flushed zone could be used to discover a valid C_x parameter the effective conductivity of the fluid inhabiting the flushed zone, C_{xwe}, had to be determined. This is somewhere between C_{mf} and C_w. (9.5.2.3) and was determined from clean zones where C_x=0. i.e.

$$C_{xo} = C_{xwe} \ \emptyset_e^g, \text{ where}$$

$C_{xo} = 1/R_{msfl}$, good hole only.

R_{msfl} was chosen because of its similar depth of investigation to other tools involved in the C_x procedure. A histogram plot from clean clast free water intervals showed 18 mho/m as an acceptable value for C_{xwe} (APPENDIX 21).

The C_x parameters 1-4 were plotted against C_x (APPENDIX 22A–D). (1) was chosen as the best indicator of C_x. Automatic correlation coefficients were not used in this choice. Now, let k=C_x/(1). All pairs of C_x and (1) were calculated and the modal value of this ratio determined via histogram (APPENDIX 23). Thus k = 0.06, and:

$$C_x = 0.06 \ V_{shGR} \ \emptyset_{dsh}/\emptyset_d$$

The neutron Q_{vn} type C_x parameter also appears an attractive candidate, however the neutron response is subject to many poorly understood influences. A possible change of this relationship in the oil zone favoured the GR parameter. (The influence of clasts on

GR is corrected via *vlogs* in the final analysis.)

We now have values for $g, \emptyset_e$ and C_x.

m_{sand} and m_{shale}

It should be pointed out that using $\emptyset_e{}^g$ and not $\emptyset_t{}^m$ in the $C_x = C_{msfl} - 18\emptyset_e{}^{2.3}$ axis allows for different <u>total</u> porosity exponents being required for sand and shale conductivities. A <u>total</u> porosity exponent, Archie's m, would not be expected to be the same for sands and shales because of the different pore geometries of sands and shales. (APPENDIX 24) suggests a difference, although the conductivity of the shale bound water itself, and m_{shale}, are in practice inseparable quantities and therefore should never be separated in log analysis, i.e. An m_{shale} derived from the porosity and conductivity of a shale bed should not be exported for use with a hypothetical bound water volume in another lithology. $\emptyset_e$ circumvents this problem, even if it entails others.

11.4 PREDICTION OF LOGGED R_o

The F_g saturation equation is now used to predict R_o in the water zone (APPENDIX 34A-C):

$$C_t = C_w \emptyset_e{}^g S_{we}{}^n + C_x S_{we}{}^{n-y}$$

C_t = *logged*
C_w = 35.71
$\emptyset_e$ = $\emptyset_t - V_{sh}\emptyset_{dsh}$
g = 2.30
S_{we} = *fractional water saturation of the effective porosity*
C_x = $0.06(V_{sh}\emptyset_{dsh})/\emptyset_d$
n = 2.00
y = 1.00

The equation has been deduced from clast free intervals. At 13834-13870, and below 13966 it overlies logged R_O satisfactorily. Inequality, at any particular depth, is due to the following, in order of importance:

Clean or shaly zones: 1) $g \neq 2.30$
2) R_o *logged* $\neq R_o$ *actual*
Shaly zones only: 3) $(V_{shGR}\ \emptyset_{dsh})/\emptyset_d \neq C_x$, and/or $\emptyset_e \neq \emptyset_t - V_{sh}\emptyset_{dsh}$

The inability of the equation to track R_O precisely, even when derived from the same data, indicates the inherent inaccuracy of resistivity interpretations.

Conglomeratic Intervals

The response of the F_g equation over clast intervals requires some thought. Surprisingly, $R_{O\ predicted}$ and $R_{O\ logged}$ track where $vcors > 0$, despite the F_g parameters being deduced from clast free intervals. This is because, coincidentally, the reduced logged $\emptyset_e$ and response of the C_x parameter to clast's V_{sh}, changes the composite term $\emptyset_e{}^g + C_x$ approximately equally to changes in $R_{O\ logged}$ adjacent to clasts. Alternative methods of deriving g and C_x may respond differently. This F_g equation appears to successfully predict bulk conglomerate conductivity in the water zone, and not simply sandy matrix conductivity. This could not be observed or assumed[59] prior to this reconnaissance since Well A's saturations were unknown. The water zone provided a controlled environment for observations of this type.

This coincidence need not persist in hydrocarbon zones because the $\emptyset_e{}^g$ and C_x terms are affected differently by S_w. The influence of clasts upon the oil saturation parameters n and y, which would be compatible with bulk measurements, needs to be quantified if C_t is to be used. The purpose of C_{tm} is to circumvent this problem by enabling the use of a sandy matrix equation. The C_{tm} chart (7.2) requires data from this reconnaissance to achieve this.

11.4 CONCLUSIONS REGARDING RECONNAISSANCE RUNS

1) $d \approx 0.57$ (7.2.2)
2) g is not constant but varies from foot to foot.
3) C_x is of less importance than variations in g.
4) Clasts are at least partially self-compensating in saturation calculations due to their low porosity and shalyness.
5) The C_{tm} chart shows that if $S_{wm} > \approx 0.20$, $C_{tm} > C_t$. Therefore the F_g equation used with C_{tm} will yield higher water saturations. The horizontal 0.20 S_{wm} line indicates C_t is adequate for low S_{wm} s, regardless of clasts. $C_{tm} \neq C_t$ errors are most important at high water saturations, i.e. close to oil water contacts, or in conglomerates with high sandy matrix connate water saturations.

[59] Unless laboratory determinations of m and C_x for matrix and clasts were found to be equal and credible.

12 NON LOG INPUTS

The function of *Non-log-inputs* is to integrate logs and non–log data (4.2). *Non-log-inputs* are the interface between the continuous and discontinuous data. These inputs are detailed in this chapter.

12.1 DEDUCTION OF THE DRY CLAY MINERAL POINT, DCMP

The calculation of the DCMP is a correction of the environmentally corrected shale bed log response for all non–clay minerals present in the shale. The downhole response to clays of porosity tools allows a more precise clay correction during log analysis of the reservoir, with its possibly different clay mineral assemblage (9.3.5.3).

12.1.1 SHALE TYPE INTERVAL

[60]The fractions present in the Shale Type Interval are:

.608	Clay Minerals, includes ØClay. All shale Ø assumed to occur in clays.
.149	HC + Organic Matter. Taken as equivalent log response to Bitumen
.139	Pyrite
.104	Quartz
1.000	Total

The shale type interval has corrected tool readings of:

$$rho = 2.569, \qquad \emptyset_n = 0.319$$

(Schl. Por-15a, Por-14b, 1985)

The Dry Non Clay Mineral Point

The presence of hydrocarbon, pyrite and quartz requires a density/neutron plot for these phases, to be superimposed upon the density/neutron chart CP-1c (Schl, 1984). The influence of these phases must be quantified before the clay response becomes evident.

The DNCMP is plotted in a non-clay mineral ternary plot with end members (hydrocarbon + organic matter), pyrite and quartz:

[60] The density tool is treated as responding to total porosity, seeing clay bound water as porosity.

Phase cord = Vol fraction of phase / Total non clay min vol fraction

HC+OM cord	*= .149 / (.149 + .139 + .104)*	*= .380*
Pyrite cord	*= .139 / (.149 + .139 + .104)*	*=. 355*
Quartz cord	*= .104 / (.149 + .139 + .104)*	*=. 265*

The plot defines the DNCM assemblage present in the logged shale, in terms of tool readings. The intersecting lines overleaf show the relevant proportions.

The graphical DNCMP is:

$$rho = 2.92, \quad \emptyset_n = 0.212$$

The Wet Clay Mineral Point

The logged shale point is due to three influences

1) Dry Clays
2) Clay porosity, (1)+(2) = .608
3) Dry Non Clays = .392

The density of wet clay minerals, *rhowcmp* , is found from the logged *rho* shale value of 2.569; i.e.

Logged Shale rho = 2. 569 = . 608 *rhowcmp* + .392 * 2. 92

rhowcmp = 2.343

Logged Øn = 0 .319 =. 608 *Ønwcmp* + . 392 * 0. 212

Ønwcmp = .388

The Dry Clay Mineral Point

By summing the density volume fractions at the WCMP:

rhowcm = rhodcm (1-ØClay) + 1. 00 ØClay

2.343 = rhodcm (1-ØClay) + ØClay

and by summing the neutron volume fractions at the WCMP:

Ønwcm = Øndcm (1-ØClay) + 1.00 ØClay

.388 = Øndcm - ØClayØndcm + ØClay

Having defined the WCMP through observation we know the DCMP must lie on an extrapolation of the water to WCMP line. The slope of this line is 2.16. The equation of this line is:

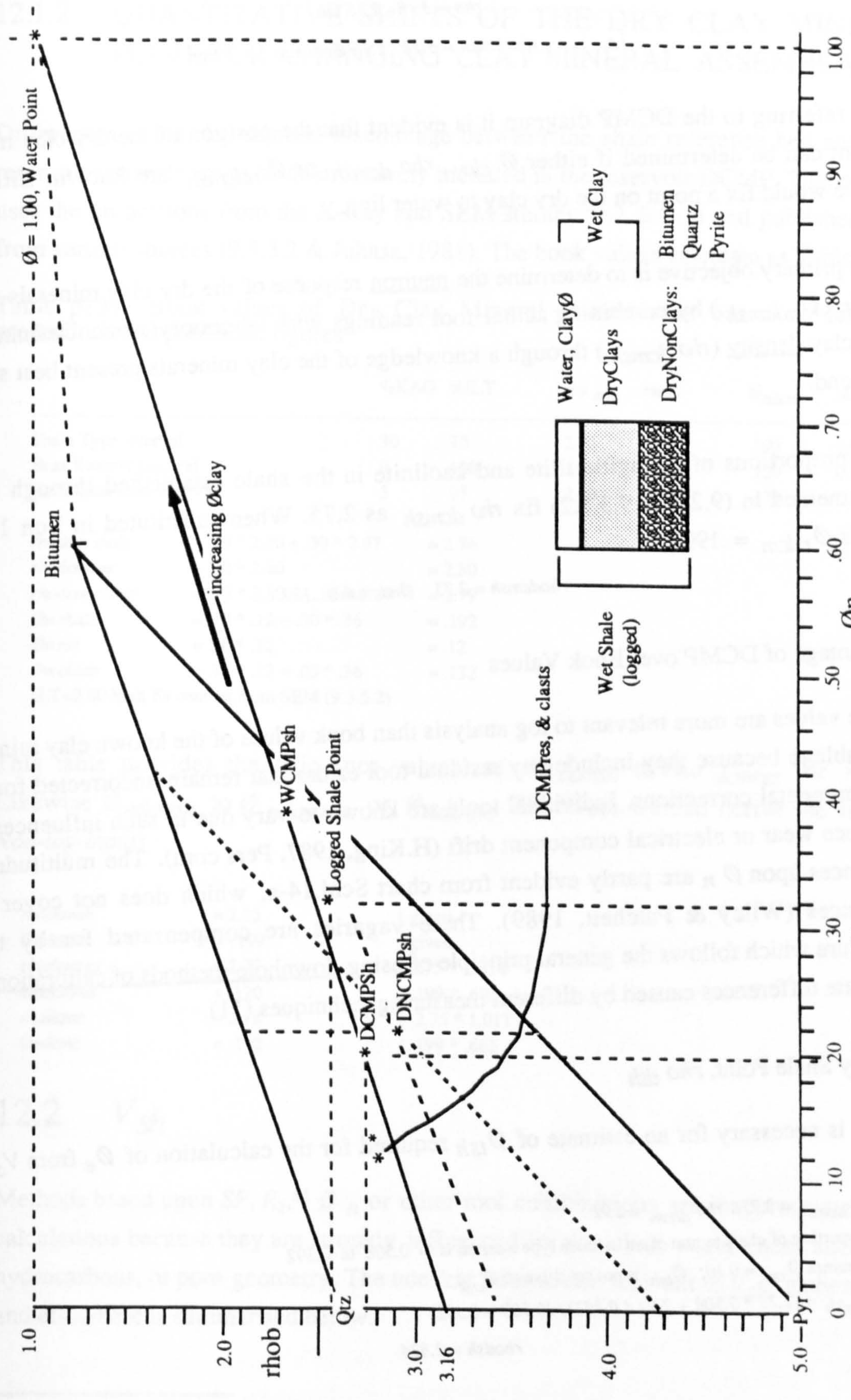


Fig p237 Deduction of the Dry Clay Mineral Point

$$rho = 3.18 - 2.16\,\emptyset n$$

$$i.e. \qquad rhodcmsh = 3.18 - 2.16\,\emptyset ndcmsh \qquad \text{Eqn 1}$$

By referring to the DCMP diagram it is evident that the position of the dry clay mineral point can be determined if either $\emptyset_{clay}$, rho_{dcmsh} or $\emptyset_{ndcmsh}$ are known. Either of these would fix a point on the dry clay to water line.

The primary objective is to determine the neutron response of the dry clay minerals in the shale ($\emptyset_{ndcmsh}$) by combining actual tool readings with laboratory work. Defining the dry clay density (rho_{dcmsh}) through a knowledge of the clay minerals present best serves this end.

The proportions of phengitic illite and kaolinite in the shale established through steps documented in (9.2.3 & 9.3.5.2) fix rho_{dcmsh} as 2.75. When substituted in Eqn 1 this yields $\emptyset_{ndcm} = .199$

$$rhodcmsh = 2.75, \quad \emptyset ndcmsh = .199$$

Advantage of DCMP over Book Values

These values are more relevant to log analysis than book values of the known clay mineral assemblage because they include any residual tool errors that remain uncorrected for by environmental corrections. Individual tools are known to vary due to such influences as tool face wear or electrical component drift (H.King, 1987. Pers com). The multitude of influences upon $\emptyset_n$ are partly evident from chart Schl.14-a, which does not cover all influences (Wiley & Patchett, 1989). These vagaries are compensated for by this procedure which follows the general principle of using downhole methods of calibration to eliminate differences caused by different measuring techniques (11).

The Dry Shale Point, rho_{dsh}

rho_{dsh} is necessary for an estimate of $\emptyset_{tsh}$ required for the calculation of $\emptyset_e$ from V_{sh} $\emptyset_{dsh}$.

$rho_{dcmsh} = 2.75$, $rho_{dncm} = 2.92$

Proportion of clays to non clays in shale type interval is ≈ 0.508 to 0.392

(assumes $\emptyset_{cn} = 0.10$; $\emptyset_{tsh}$ is not sensitive to $\emptyset_{cn}$)

$rho_{dsh} = (2.75 * 0.508 + 2.92 * 0.392) / (0.508 + 0.392)$

$$rhodsh = 2.824$$

12.1.2 QUANTITATIVE SHIFTS OF THE DRY CLAY MINERAL POINT FOR CHANGING CLAY MINERAL ASSEMBLAGES

Differences in the clay mineral assemblage between the shale reference bed and typical reservoir intervals are to be quantitatively included in the reservoir DCMP. This procedure uses the proportions from the X-Ray and SEM studies (9.2 & 9.3) and published figures from various sources (9.5.3.2 & Juhasz, 1981). The book values calculate as Table p239.

Table p239 Book values of Dry Clay Mineral assemblages based on laboratory proportions and published figures

	%KAO	%ILT	rho_{dcm}	ratio	$\emptyset_{ndcm}$	ratio
Shale Type Interval	30	70	2.76	1.000	.199	1.000
Brae Reservr Interval	0	100	2.80	1.014	.120	0.603
Ryazanian Resr Interval	5	95	2.79	1.011	.132	0.663

rhodcm shale	= .70 * 2.80 + .30 * 2.67	= 2.76
rhodcm res	= 1.0 * 2.80	= 2.80
rhodcm clasts	= .95 * 2.80 + .05 * 2.67	= 2.79
Øn shale	= .70 * .12 + .30 * .36	= .192
Øn res	= 1.0 * .12	= .12
Øn clasts	= .95 * .12 + .05 * .36	= .132

ILT=2.80 high Fe content from SEM (9.3.5.2)

This table provides the ratio (not values) of rho_{dcmsh} to rho_{dcmres} or rho_{dcmc}. Likewise $\emptyset_{ndcmsh}$ to $\emptyset_{ndcmres}$ or $\emptyset_{ndcmc}$. Therefore we can derive the following *Non-log-inputs* :

rhodcmsh	= 2.75	(given
Øndcmsh	= .199	(given
rhodcmres	= 2.79	(2.75 * 1.014
Øndcmres	= .120	(.199 * .603
rhodcmc	= 2.78	(2.75 * 1.011
Øndcmc	= .132	(.199 * .663

12.2 V_{sh}

Methods based upon *SP*, R_t,[61] $\emptyset_n$ or other tool combinations are inappropriate for V_{sh} calculations because they are strongly influenced by non-shale occurrences such as R_w, hydrocarbons, or pore geometry. The non-log information relevant to V_{sh} gathered in (9) and elsewhere is summarised below.

[61] Increased log analysis S_{wc} could be explained by undetected shale, or other infuences.

Table p240 Non-log information relevant to V_{Sh} calculation

	Shale	Reser
Clasts		
Kaolinite %	30	0
5		
Illite %	70	100
95		
	HI	GR
Kaolinite	36	≈100
Illite	12	≈275

(Juhasz, 1981 & Schl. 1985)

	%	rhog	
Claystone Type Interval			
Quartz	52.5	2.64	
KFeldspar	0	2.54	
Muscovite	2.7	2.82	
Kaolinite	11.6	2.61	
Illite	17.4	2.67	
Carbonate	0	2.71	
Pyrite	3.5	4.99	
HCOM	12.2	1.24	
Other	0	2.65	
	99.9	255.54	Claystone Type Interval rhog = 2.56
Massive Coarse Sandstone			
Quartz	82.9	2.64	
KFeldspar	0.9	2.54	
Muscovite	0.4	2.82	
Kaolinite	0	2.61	
Illite	8.0	2.67	
Carbonate	0	2.71	
Pyrite	0.6	4.99	
HCOM	1.4	1.24	
Other	1.5	2.65	
	95.7	252.34	Sandy Matrix Typical rhog = 2.64
Clast Supported Conglomerate, Clasts			
Quartz	59.3	2.64	
KFeldspar	2.5	2.54	variable from clast to clast
Muscovite	0.6	2.82	
Kaolinite	0	2.61	
Illite	23.0	2.67	variable from clast to clast
Carbonate	3.8	2.71	variable from clast to clast
Pyrite	8.6	4.99	variable from clast to clast
HCOM	1.8	1.24	
Other	0	2.65	
	99.6	281.45	Clasts Typical rhogc = 2.83

The variation of *rhog* with the presence of clasts or carbonate cement (2.71+) tell us that a density/neutron crossplot or regression should not be used for V_{Sh}. In these circumstances *Th+K* is most suitable for estimates of reservoir V_{Sh}. *GRCC* is the borehole corrected *Th+K* ppm curve. The radioactive elements in the shale and reservoir were distinguished and quantified in (9). This allows *GRCC* to be used accurately for V_{Shres} by enabling a V_{Sh}=1 *GRCC* to eb calculated for the reservoir beds different

minerals. Th and K bearing minerals are listed below. Hydrocarbon and organic matter are excluded because uranium radiation is excluded from *GRCC*.

Table p241 The volumetric normalisation per rock type of *GRCC* using Non–log–data.

	%Ill	%Mica	%Kao	%KFelds	Total%	Multiplier	Ratio[62]	
Shale TI	20.3	2.7	8.7	0	31.7	3.2	23120	Kao effect
Res Sandy mtx	8.5	.4	0	.9	9.8	10.2	26964	
Clasts	21.3	.6	0	6.2	28.1	3.6	26581	

$$GRCCres = 1.17 \times GRCCsh$$

In the shale type interval $GRCC = 116$ equiv 1.0

$$Vshres = [(GRCC-23)/(116-23)] / 1.17$$

$$V_{shres} \approx .01(GRCC-23)$$

Since V_{shres} is not corrected for *vlog's GRCC*, it is a whole rock parameter.

12.2.1 $V_{dry\ clay\ reservoir}$

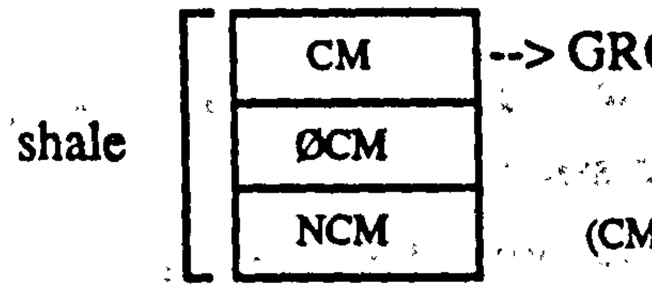


Fig p241 Source of *GRCC* in Shale type interval

Change in *GRCC* adjacent to unit volume of shale's dry clay minerals is:

(116-23) / Fraction DCM in sh

= 93/WCM (1-Øcl) ≈ 93/(0.55*0.90) = 187 = ∂ *GRCC*

Change in *GRCC* to unit volume of typical sandy matrix DCMs is: 187 (26964/23120) = 218 = ∂*GRCC*

Therefore: $V_{dryclres}$= (*GRCC*-23)/(218-23)

$$V_{dryclres} = 0.0051(GRCC-23)$$

In summary, this equation uses the *Th+K* count, calibrated to the radioactive minerals in the reservoir, to provide the whole rock reservoir dry clay mineral's volume.

[62] To obtain the ratios of *GRCC* to these mineral proportions the Total % is normalized to unit volume via the "Multiplier". The *GRCC* ratios of a unit volume of those minerals is obtained when this multiplier is multiplied by the sum of the component's book value gamma ray response (Schl 1985, pp104-5)

12.2.2 CORRECTING $\emptyset_n$ FOR RESERVOIR CLAYS: $\emptyset_{nc}$

$\emptyset_{nc} = \emptyset_n - (\emptyset_{ndcmres} \quad V_{dryclres})$

$\emptyset_{ndcmres} = 0.120$ (see 12.1)

$V_{dryclres} = 0.0051(GRCC\text{-}23)$ (see 12.2.1)

Therefore:

$$\emptyset_{nc} = \emptyset_n - [\, 0.120 - 0.0051(GRCC\text{-}23) \,]$$

$\emptyset_{nc}$ is a total porosity value, corrected for reservoir clays, rock matrix and environment, but not light hydrocarbons.

($\emptyset_{rfac}$, a zero porosity, zero clays, neutron response rock matrix correction, could be calculated from the bulk mineralogies of facies (12.2 & Schl. 1985) and switched in following facies identification. The correction is minor in Well A, and has not been quantified.)

12.2.3 DISPERSED & TOTAL CLAY

Pore lining dispersed authigenic clays are damaging to reservoir properties and S_w calculations whereas structural grain sized clays tend to be detrital and less problematic. The ratio of dispersed:total clay was recorded for every thin section (APPENDIX 2), and the tool response determined for each clay type. If, as expected, Illite:Kaolinite had correlated with Dispersed:Structural clays, the parameter:

$$V_{shres} / (\emptyset_n - \emptyset_d)$$

responding to the contrasting *GRCC* and *HI* s of illite and kaolinite, could be calibrated with (APPENDIX 2) and used to provide the ratio Dispersed:Structural clay. In Well A dispersed and structural clays are both illitic, and no log parameter is able to distinguish clay distribution in this well (6.1.3).

12.3 *rhog*

Non-log mineralogical information (9) combined with the log derived parameters V_{shres}, *vlogs* and *vcalc* provide control on all volume fractions which significantly affect *rhog* and the calculation of $\emptyset_d$. Calculating *rhog* in this manner involves either an approximation or iteration of $\emptyset_t$; and is to some degree tautological since *vlogs* and

vcalc already involve *rhob* , which is re-used for $\emptyset_t$ with the calculated *rhog* . The impact of this on $\emptyset_t$ has been mollified by a switching routine. (8.1.5)

12.4 S_{oc}

Water mud filtrate enables $S_{oil\ core}$ to provide a qualitative "soft" maximum value for S_w calculations: being discontinuous and subject to the core analyst's sampling bias. S_{oc} rarely exceeds 20% (APPENDIX 37), with its highest values at ≈15000ft(4572m), but is almost absent in the upper permeable $S_{hmov} = 0$ interval (10.5) above 14945ft(4555m).

12.5 Non-log-inputs, LISTING

The table below summarises the quantitative input that non–log information has during evaluation. Non-log information also provides qualitative assistance in the choice of parameters. With more computing time Non–log–inputs per facies (or flow units), e.g. $\emptyset_M.\emptyset_m$, could be developed and used in conjunction with flow units recognised by RTSs, to assist with producibility predictions.

Overleaf:

Table p244 Non-log-inputs

Table p244 Non-log-inputs. 2 pages

Non-log-input	Theory proposed	Quantified	Value(s)	Curve= c Single value= s	Used in Thesis	Is Theory Exportable?	Is Value Exportable?	Chapter	Comment
g	y	y	2.30	s	y	y	y in Fm	6.2.1	
C_x	y	y	many	s	y	y	n	6.2.1	{Ideally per plug
R_t/R_o	-	y	many	s	y	y	n	9.5	{ "
n res temp	y	y	1.84	s	y	y	n	6.2.1/9.5.4.1	{ "
y	y	n	1=default	s	y	y	n	6.2.1	{ "
F_{cgl}	y	y	Eqn Fig p107	c	y	y	y	7.2.1	F_{cgl} eqn may alter in other Fm's.
d	y	y	0.57	s	y	y	?	7.2.1	? Further research required.
C_{tm}	y	y	0.020	s	y	y	n	7.3	{ C's used for Ctm Chart Eqn 7.3.2
C_{tc}	y	y	0.022	s	y	y	y in Fm	7.2	{ computing not available for Ctm curve.
C_{om}	y	y	0.303	s	y	y	n	7.2	{
C_{oc}^*	y	y	0.055	s	y	y	y in Fm	7.2	{
X_{100}	y	n	-	s	n	y	n	6.2.2.1	{ Height-Sw-Rt relationship.
$Ø_{100}$	y	n	-	s	n	y	n	6.2.2.1	{ "
X_{pc}	y	n	-	var	n	y	n	6.2.2.1	{ "
R_{xwe}	y	y	many	s	y(11)	y	n	9.5.2.1	Transform not discovered 5.5/9.5.2.3
rhodsh	y	y	2.824	s	y	y	n	12.1	rho dry sh, rqd for Øtsh
rhodcmsh	y	y	2.75	s	y	y	n	12.1	
rhodcmres	y	y	2.79	s	y	y	n	12.1	
rhodcmc	y	y	2.78	s	y	y	n	12.1	
Øndcmsh	y	y	0.199	s	y	y	n	12.1	
Øndcmres	y	y	0.120	s	y	y	n	12.1	
Øndcmc	y	y	0.132	s	y	y	n	12.1	
Ønc	y	y	var	c	y	y	n	12.2.2	
Ønfac	y	n	many	s	n	y	n	13	
Vshc	y	y	0.10	s	y	y	y in Fm	12.2	
rhog	y	y	2.65	s	y	y	n	11.1	rhog sandy matrix, clean matrix plugs

Non-log-inputs, contd...

Non-log-input	Theory proposed	Quantified	Value(s)	Curve= c Single value= s	Used in Thesis	Is Theory Exportable?	Is Value Exportable?	Chapter	Comment
rhogc(clasts	y	y	2.83	s	y	y	y in Fm	12.2	Mineral assemblage
rhogsh	y	y	2.824	s	y	y	n	12.1	Rqd for Øtsh from rhob
rhofl	y	y	0.98	s	y	y	n	8.1.5	Ave of brine & filtrate
Vshres	y	y	Eqn p249	c	y	y	n	12.2	Mineral assemblage & GRCC
Øhe	-	y	many	c	y	y	n	13.	{ Plugs
kasdymtx	-	y	many	c	y	y	n	8.1.7	{ "
Soc	-	y	many	c	y	y	n	12.4	{ "
vcors	y	y	variable	c	y	y	n	11	Cores & core photos
Vcldspd:Vclstrl	y	y	many	s	n	y	n	12.2	Opitcal thin sections
calcite	y	y	Eqn p118	c	y	y	?	13	
Shmov	y	y	0 & >.18	c	y	y	n	10	DSTs
Pe	y	n	-	s	n	y	-	9.3	Barite invalidates PEF
Th	y	y	many	s	y	y	n	9.4	{ Poor correlation.
K	y	y	many	s	y	y	n	9.4	{ "
U	y	y	many	s	y	y	n	9.4	{ "
kh	y	y	many	s	y	y	n	8.1.7	DSTs in Fm
ko	y	y	Eqn	c	y	y	n	8.1.7	
kw	y	y	Eqn	c	y	y	n	8.1.7	
ko factor	y	y	0.6	s	y	y	y	8.1.7	
kw factor	y	y	0.6	s	y	y	y	8.1.7	
µo/µw	-	-	1.0	s	y	y	y	8.1.7	
Scaling Factor	y	y	31	s	y	y	n	8.1.7	KOECUM: kh
khsm/khc	-	y	20	s	y	y	y	4.5	k sandy mtx : k clasts
ksoc	y	n		c	n	?	n	5.2	Requires plot: Core ka v Sor
Rw	-	y	0.025	s	y	-	-	10.	DST
ØM: Øm	y	y	many	s	n	y	n	APPX 2	Optical thin sections & SEM
SEM Photos	y	-	-	s	y	y	n	APPX 33	

Non-log-inputs, end.

Table p245 Non-log-inputs. 2 pages

13 PROPOSED INFORMATION FLOW

The figures in this chapter show the processes followed in the text schematically. Additional processes have been documented in the text. Furthermore some *Non–log–inputs* were plotted and used qualitatively to assess reservoir quality, or to help with future directions in the evaluation, for example: Calcit, $\emptyset M{:}\emptyset m$ and S_{hmov}.

These diagrams are intended to assist in understanding the general thrust of finer details. They also represent the proposed flow of formation data for an exhaustive and quantitatively balanced evaluation.

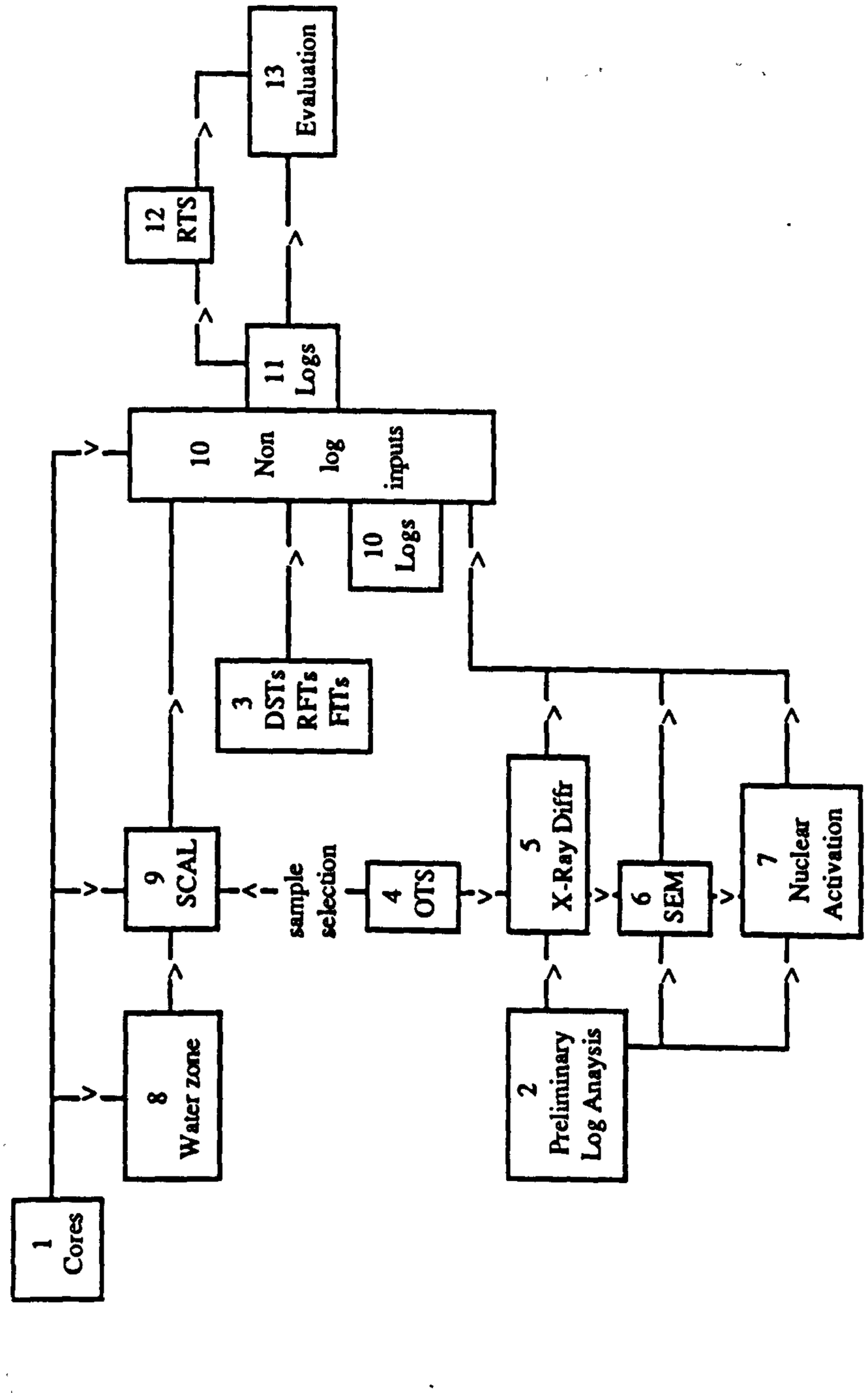


Fig p247 Generalised Information Flow for Integrated Evaluation, sequential

Fig p249 Information Flow 1: Deriving *Non-log-inputs*

Figp249 Info Flow 1: Deriving *Non-log-inputs*

Fold out page, with a blank reverse side.

13 Proposed Information Flow

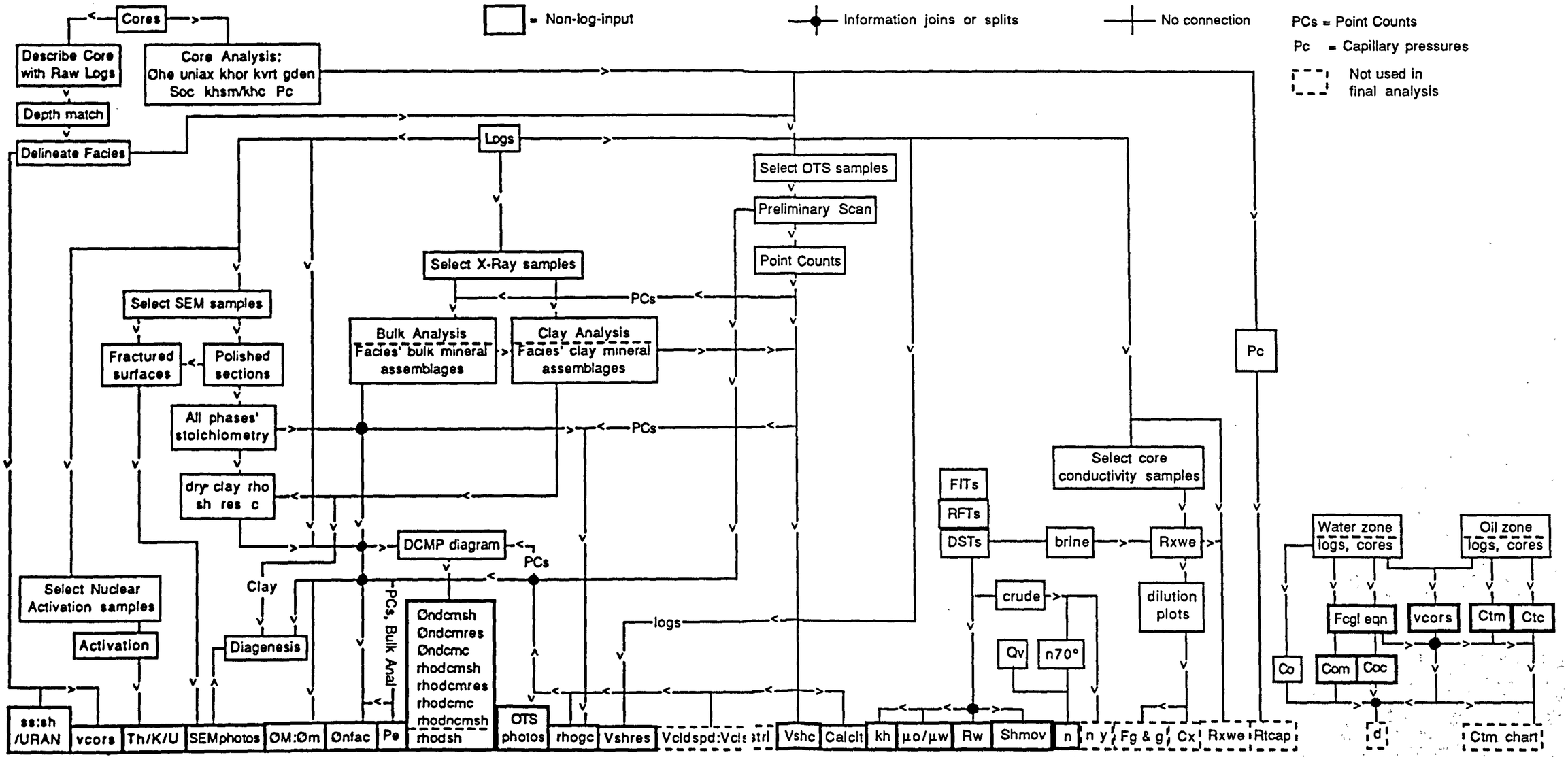


Fig p249 Information Flow 1: Deriving Non-log-inputs

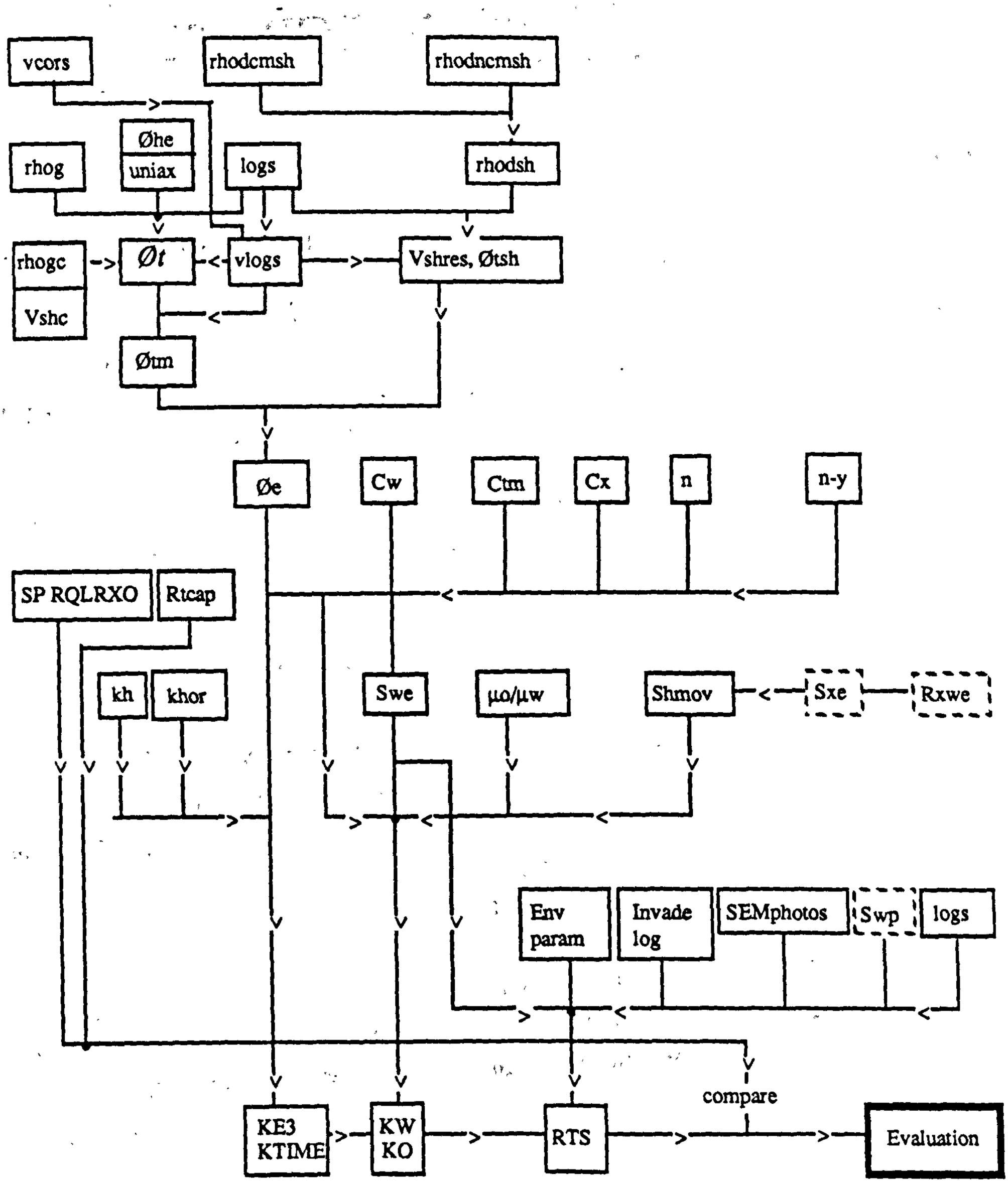


Fig p251 Information Flow 2; Processing Log and *Non-log-inputs*

14 RESULTS of INTEGRATED EVALUATION

This chapter's main concern is the hard copy made during a period when computing facilities became available towards the end of the experimental work. It steps sequentially through the results comparing various analyses and clarifies the essential problem. This project has been a continuous learning process and so these plots do not always coincide with current thinking, however computing facilities were not available after March 1988, and so later developments could not be plotted. The plots available are:

APPENDIX 42A,B	Amalgamated Raw Log Data. Plots A&B
APPENDIX 30	Selected Clast Finders
APPENDIX 31	Input for *vlogs* Scaled from 0-1
APPENDIX 45	Construction of Total Porosity
APPENDIX 27	Shifted v Unshifted Core Porosity
APPENDIX 47	Final Total Porosity cf. Helium Porosity
APPENDIX 48A,B	Resistivity Ratio. Plots A 1:200 & B 1:1000
APPENDIX 49	Effect of Dividing a V_{sh} Type Parameter by Porosity
APPENDIX 50	The Effective Porosity Required for a Constant S_{we} Calculation
APPENDIX 51A&B	S_{we} From F_g Equation, A=Using RTGLOB B=Using LLD
APPENDIX 52	Invasion and Calculated Parameters
APPENDIX 53	Bulk Volume Fractions, Porosity, Saturation & Producibility, Reservoir Type Signatures and SEM Photomicrographs

Discussion of these plots follows.

14.1 RAW LOGS AND LOGGING COMPANY LOG ANALYSES

Water based mud allowed a large number of final logs to be run including the NGT™, SP™, SFL™, Laterolog, Microlog and EPT™; however the logging environment is

unusually poor. Earlier logs were spliced to make full use of the reduced invasion and in–gauge hole..

Resistivity

The laterolog and induction resistivity runs show quantitative differences; but similar trends. (APPENDIX 42A,B; 58A,B; 59A,B) Standard log analysis, i.e. (APPENDIX 54-57, Schlumberger's Cyberlook, Coriband and Global) in which a=1, m=1.9-2.0, n=2.0, and R_W=.025–.028, calculate 30-70% oil saturation over the entire interval. These plots show how meaningless stand–alone log calculations can be in low porosity rocks where porosity and m become critical. It is interesting to remember that at this stage the Operator had drilled and logged an appraisal well into some 2,000 ft (610m) of apparently oil bearing rock, within a known oil producing formation. The CPI logs simply confirmed the mudlog and core description (APPENDIX 60). However, the raw logs contain some lingering doubts:

Firstly, assuming only that a) the LLD and ILD record deeper resistivities than the LLS and ILM, and b) that the formation brine is more conductive than mud filtrate, then above 15780, either brine resides in the pore space or the volumes of moved hydrocarbon are so limited that they fail to offset the increased conductivity of the formation water.

Secondly, both later resistivity runs over 14588-14980 show higher R_{deep} s, betraying invasion into a conductive zone. No assumptions about $\emptyset$, m,or n are required. Below 15780 invasion profiles are more difficult to interpret, but still indicate high S_ws, which unfortunately are possible in low permeability oil zones.

Electro-magnetic Propagation

When water filled porosity is computed from EPT (APPENDIX 61), and divided by $\emptyset_t$, the result shows patches of unmoved hydrocarbon, 15080-15670. These rarely exceed 20% S_{hr}. The upper permeable zone shows less and patchier S_{hr} . This S_{hr} calculation is independent of R_{xwe} and C_x. However the only oil seen is from intervals with poor microlog response, and since EPT oil always occurs with increased log porosity (SxoEPT = f($\emptyset_t$)) rugosity or bitumen could account for this apparent oil. Bitumen is present in core.

Microlog

The microlog (APPENDIX 13) is an extremely useful qualitative log because of its vertical resolution and clear delineation of permeable mudcaked intervals. The microlog also confirms whether log calculations of fair $\emptyset_e$s are valid, or simply due to bad porosity logs. The log also displays characteristic signatures for sands and conglomerates.

14.2 CLAST PREDICTIONS, *vlogs*

Method is discussed in (8.1.1&2). The clast sensitive parameters resulting from the laboratory work and core-log correlations can be seen in (APPENDIX 30); core clasts are mounted on the left. The two basic problems of *vlogs* are its dependence upon porosity, and its derivation from a limited data set: the upper cored sections. Despite *vlogs* good predictions in (APPENDIX 31) two factors reduce confidence in *vlogs* with depth, firstly the reduced porosity contrast between sandy matrix and clasts, and secondly calcite cements. The parameter *Calcclst* (APPENDIX 31) is designed to identify calcite which, from observations made on other Brae core (11), can occur with or without clasts.

A log prediction of clast rock volume in the Brae Formation which relies upon more than density log calculations will improve the foundation of reserves estimates.

14.3 POROSITY

Log porosities are less than satisfactory when washouts, low porosities, varying lithologies and mineralogies, lack of representative core, and bias core sampling all prevail. However knowledge of mineralogy and hole conditions enables the switching method (8.1.5.1) to select the best porosity calculation for any detectable condition. Switching is disconcerting in that the movements seen with one tool are lost, however these movements are not necessarily caused by porosity. The parameter with the highest sensitivity to porosity in comparison to error should always be used. The (shifted) equality of different methods under good conditions, and the subsequent switching to the least deviant method for a given change of conditions, must guarantee the closest approximation to $\emptyset_t$.

14.3.1 *NET*

NET (8.1.6.3) sand is 803 ft(245m). The additional *ML* requirement reduces *NET* from 1096 to 803 feet. Net : Gross is therefore 0.42, which in itself indicates the severely impaired condition of these predominantly coarse grained diagenetically altered sediments.

14.3.2 POROSITY ZONES

Porosity distribution in the coarser grained facies is broadly controlled by diagenesis, depth, and the presence of clasts and calcite. Diagenesis is discussed in (9.1.12).

The best $\emptyset_t$ lies between 14605-14670 at 10.5% (APPENDIX 45,52). These values are the most reliable log porosities in the well. They correspond to high $\emptyset_e$ values and yielded most of the 550bbls of brine on DST3. 10% is reached intermittently down to 14950, but some high values are related to rugosity and should be ignored. At 14905 all porosity logs show two feet of high porosity in good hole. Other logs and the core (APPENDIX 1@ 13884) indicate this interval to be bituminous, with sooty carbonaceous laminations.

Between 14985-15360 the hole is caved by up to 5 inches, porosity is approximately 9.5%. It is uncertain whether this caving reflects lithology or drilling practices. It commences at the base of the earlier logging run, but improves 350 ft(107m) deeper. Although $\emptyset_t$ frequently switches to sonic, avoiding the density neutron excursions, road noise and cycle skips degrade the porosity result. Core porosity confirms ≈10%, but plugs tended to avoid tight samples, giving logs a theoretical advantage (in good hole) for bulk porosities across heterogeneous intervals. This rugose interval corresponds with DST2. High log porosities, computing as hydrocarbon, probably encouraged this test.

15409-15460, interpreted as Bedded Medium Sandstone facies, shows unusually good porosity for this depth, ≈12%. This is below the deepest core, *∂rho* and caliper indicate reliable porosity. R_t rises into this higher porosity zone, suggesting hydrocarbons. R_t should rise in a hydrocarbon zone with <u>increased</u> porosity if bulk connate water volumes decrease, as commonly occurs with low porosities (Coates & Dumanoir, 1973). The induction and laterolog invasion profiles conflict, which confuses their interpretation. This 50ft(15m) interval of 12% porosity is difficult to explain, except by deeper invasion. Lack

of an upper seal probably discouraged testing this zone of interest.

Sandy intervals between 15460-16130 have porosities declining from 9 to 7% with depth. This interval has washouts up to 4 inches, corrected for. The *∂rho* correction is generally low. Six excursions to very low near zero porosities show the onset of calcified zones (*Calcclst*), not seen in Well A's core. These are not laterally extensive and should not be thought of as pressure boundaries or horizons below which significant volumes of migrating hydrocarbons can become trapped.

16130-16305 is a zone of very low porosity, rarely exceeding 5%, frequently with nil $\emptyset_e$. This 175 ft(53m) is interpreted as calcified conglomerates, sands, interbedded facies and shales, which do provide a hydrocarbon seal. At these depths the facies' porosity contrasts observed in core are greatly reduced. All logs used to identify facies are influenced by porosity, and have become less facies characteristic.

Between 16305-16520 porosity rises to an acceptably reliable 6-9%. DST1 recovered 7.5bbls of oil from this interval at the foot of well.

$\emptyset_e$ follows $\emptyset_t$ but is reduced by immobile water associated with clay minerals and clasts (8.1.5.2). There is no means by which to test $\emptyset_e$'s usefulness in predicting flow specifically within Well A, because only DST3 flowed appreciable formation fluids. However, the $\emptyset_e$ parameter correlated well with DSTs in adjacent wells. $\emptyset_e$ around 16250 also explains the oil below water test.

14.3.3 FRACTURES

Naturally occurring sub-vertical fissures can render low matrix permeability rocks commercially productive. The poor reservoir quality of Well A combined with its uncertain fluid content make fracture detection important for the regional reservoir potential. The full sonic wavetrain display was not included in the data, but the caliper, small arm caliper, density correction, photoelectric, microspherically focused resistivity, microlog and electromagnetic propagation logs were all examined for evidence of fractures. The poor hole shape makes many logs appear to log fractures, however the combination of PEF > 8, a conductive MSFL, and a small arm caliper deflection rarely occurs. 15984–15992, 16030 & 16040, 16380–16382 meet these conditions, and the lower 400 ft(122m) of Well A may contain some small degree of natural fractures. This bears upon DST1's interpretation in that oil filled fractures would overcome the relative

permeability problems associated with a water based mud system, allowing oil to flow .

14.3.4 APPENDIX 49

(APPENDIX 49) shows the effect of dividing a V_{shale} type of parameter by porosity, thus creating a Q_{vn} type of parameter. As porosity decreases, the amount of conductivity associated with the V_{shale} parameter is confined to a smaller pore volume, increasing C_{we}, the effective pore water conductivity (Waxman&Smits, 1968). In shales this accounts for all logged conductivity.

14.4 HYDROCARBON SATURATIONS, S_w

This section is the most important in the thesis. It discusses the possibility of a 2000 foot oil column in a known producing formation. A variety of methods have been explored to clarify this issue.

14.4.1 HAND HELD INTERPRETATION

Unfortunately there is a difference between RTGLOB, the deepest resistivity parameter, and RLLD corrected. m =2.30 was derived from LLDs in known water zones in other wells. An m for RTGLOB is not available, but will be lower, ≈2.10, based upon 14890-14925, a porous zone at the base of DST3's water test.

9 feet (3m) of pay (14588-14597) results from S_w's significantly less than 1 (.47); and more importantly, no increased resistivity between logging runs (APPENDIX 59B, 58B, 36A). i.e. over this interval the invading fluid is no more resistive than the movable pore fluid. In contrast to these 9 feet, all remaining porous intervals down to 15411 appear water wet.

15411-15460 shows better character. All three porosity tools show slightly increased porosity, including sonic. Resistivities are slightly increased, and crossover occurs between ILD and ILM. S_w≈.6, depending upon R_{we}, but no obvious upper seal exists. This zone may yield water and hydrocarbons but is excluded from pay on the basis of large *di* s. No hydrocarbons are encountered between 15460-15960. Orange marked sections (APPENDIX 59B) are resistive due to lower porosity.

All zones appear water wet down to 16305, the top of DST1. 16308-16336 shows very

subtle increased resistivities, compared with equal sonic porosities elsewhere, and marginally greater crossover. Using RTGLOB, $S_w \approx .8$, however reservoir quality pay criteria are not reached. This leaves only the uppermost 9 out of 1932 ft (589m) as pay.

14.4.2 RESISTIVITY RATIOS

(APPENDIX 48A & B), the log of the ratio of flushed and deep zone resistivity, $\log(R_{xo}/R_t)$, is a qualitative indication of moved hydrocarbons which does not require assumptions about $\emptyset$, m, or C_x, and only involves R_w and R_{mf} non–log–data.

The compatible scaling of $\log(R_{xo}/R_t)$ and SP has used the R_w changes between the "Ryazanian Sand" and the Brae Formation, but is only intended as a guide for changes in R_w, and in this case is best ignored. The flushed zone and deep tool's investigation depths may not coincide with the actual invasion depth, i.e. *di* will influence this ratio, but not reduce it below zero unless deep fluids are more resistive than proximal zone fluids. Both RTGLOB and laterolog corrected tools have been used for R_{deep}. $R_{flushed\ zone}$ is:

$$Rxo = RMSFL \ \textit{if} > SFLC, \ \textit{else} \ SFLC$$

This logic rejects RMSFL when rugosity causes it to read mud, but ensures shallow investigation.

Below 15400 the invasion profile shows shallow, medium and deep readings as resistive, conductive, and intermediate respectively. This is not consistent with a water or an oil zone; or an annulus of flushed formation brine or flushed oil. It could be explained by borehole conductivity affecting the medium tool.

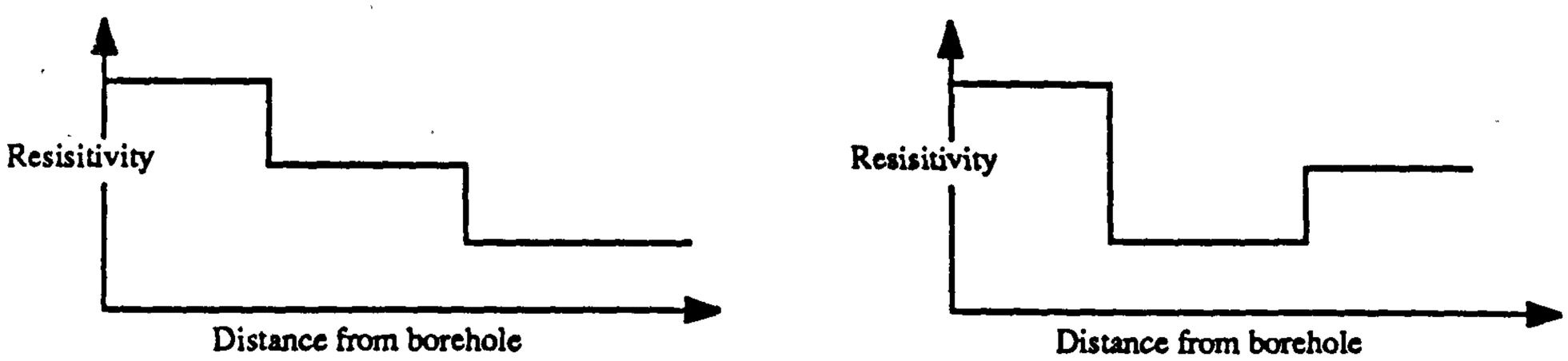


Fig p258 Expected water zone invasion profile (left) and invasion profile commonly observed below 15400 (right)

See (14.4.3) for discussion of resistivity ratio results.

14.4.3 APPENDIX 52: INVASION & CALCULATED PARAMETERS

This plot is a summary of evaluation parameters, clearly showing their relationships. i.e. the effect of clasts and shale upon $\emptyset_e$'s divergence from $\emptyset_t$, the uncertain effect of CALiper and DRHO upon $\emptyset_t$ and S_w, and the effect of invasion upon S_w.

Invasion effects any resistivity method for determining hydrocarbons. For example, Rmf on the earlier runs was .090Ωm, compared with an R_w of .025Ωm, providing a water zone value for $\log(R_{xo}/R_t)$=.56. The logged values (APPENDIX 48) which look most encouraging for hydrocarbons, adjacent to porous intervals, are ≈.20 above 15700, and ≈.10 below. However, there are at least two factors which will bring the observed ratio below .56 without hydrocarbons:

a) $R_{xwe} < R_{mf}$, formation brine left in the flushed zone decreasing R_{xo} (9.5.2.3).
b) Deep invasion of R_{mf} into zones investigated by the deep tool.

di, from Schlumberger's GLOBAL shows 60-100 inches of invasion in upper and most of Brae. *di* is a poorly defined output, but relative to other wells 60-100 inch is high and "R_t" is probably affected. The 11.1ppg mud had an acceptable High Temperature Filtrate of 22-28 mls/30mins. The only anomalous values being Cake=3–4/32 inch cf. the usual 1-2/32. However numerous trips with removal of wall cake, open hole duration and low porosities will the increase resistive filtrate invasion.

R_{mf} = 0.09Ωm=19,000ppm
R_{xwe} =.08, (flushed zone crossplot), and
R_{wa} from a 1:1 dilution with filtrate:
R_{wa} =(85,000ppm+20,000ppm)/2 --> .04.
Therefore with invasion in a water zone $\log(R_{xwe}/R_{wa})$ is equivalent to:

$$\log(R_{xo}/R_t) = .30$$

An invaded water zone ratio may therefore be reduced from .56 to .30, but does not reach the logged .20, suggesting limited oil in the deep zone of upper Brae.

The R_{wa} required for $\log(R_{xo}/R_t) = 0.20$ is .050, which using Archie's
$S_w = (R_w/R_{wa})^{.54} = (.040/.050)^{.54} = .88$
Below 15700 R_{wa} required for $\log(R_{xo}/R_t) = 0.10$ is .063, which using Archie's
$S_w = (R_w/R_{wa})^{.54} = (.040/.063)^{.54} = .78$

These oily calculations assume the tools measure R_{xo} and R_t. If RTGLOB is used in place of RLLD, then above 16300 $\log(R_{xo}/R_t) = \log(R_{MSFL}/R_{TGLOB}) = .60$, approximately equalling $\log(R_{mf}/R_w) = \log(.090/.025) = .56$ for a normal water zone.

Below 16300 $\log(R_{xo}/R_t) = .20 = \log(R_{xwe}/R_{wa})$; R_{wa}=.057, which using Archie's $S_w = (R_w/R_{wa})^{.54} = (.025/.057)^{.54} = .64$; or $(>.025/.057)^{.54} => .64$ with deep invasion.

Using Schlumberger's optimum R_t computation from six inputs, RTGLOB, is more reasonable than using LLD corrected. However, being unable to locate the corresponding ?"RXGLOB" for R_{xo} means the RMSFL/SFL logic has to be used for R_{xo}. Above 16300 this results in the dilemma of S_w=1 with RTGLOB, and S_w<1 with the resistive LLD.

In summary, although it is recognised that under estimating invasion creates ghost oil, it is difficult to ignore the apparent oil below 16300. Deep invasion and the more conductive RTGLOB cannot remove it. Therefore ratio methods, free of porosity and porosity exponents, indicate S_h=0 above 16300 while $S_h \approx .2$ over porous intervals below 16300; a log analysis result which concurs with tests and the (14.4.1) analysis.

14.4.4 APPENDIX 51A & B: S_{we}

The F_g equation, $C_t = C_w \emptyset_e{}^g S_{we}{}^n + C_x S_{we}{}^{n-y}$, was used to calculate saturation. The C_x parameter was derived from crossplotting of $C_x = C_{xo} - (12.5(\emptyset_e{}^{**}2.3))$, i.e. logged flushed zone conductivity minus free water conductivity (C_{xwe}=12.5) against various parameters over water zones. See (11.3.2). C_x could not be determined in the laboratory (9.5), so near certain water intervals had to be used, namely 14610-14660 (DST3) and 16055-16260. This C_x parameter must deal with the non-free water volume's conductivity, because the F_g equation predicts the free water volume's conductivity through $\emptyset_e$ and g. The best C_x parameter was $C_x = [(.08 V_{shsdymtx}) + (.06 vlogs)]$, and its water saturated value is displayed in the same track as total conductivity to show its size. The n-y exponent remains undetermined (6.2.1.1) and the industry standard of one is used.

Little difference between SWTB1X (Archie), and SWEFG is detectable in the cleaner porous zones where C_x is insignificant, or indeed over any interval. The position of the well in relation to any possible fluid contact remains unclear, with 15400 showing $\approx .80 S_{we}$, and $.90 S_{wt}$. The $\emptyset_e$ saturation equation does not help in this situation, nor

does Archie. The F_g equation appears conceptually valid from these plots, but its refinements are swamped by the less subtle factors which dominate the results, namely invasion and R_t (14.3.3).

14.4.5 OIL ZONE R_t PREDICTIONS FROM CAPILLARY PRESSURE DATA

Briefly (10.5) shows that if Well A is high in an oil zone, for porosities greater than 6%, R_t s should be higher than RTGLOB or LLD corrected values. Therefore all intervals including 15411-15460 are water bearing, except 14588-14597, which is not at S_{wi}, but at the base of a height /S_w curve.

14.4.6 MUDLOG, EPT AND CORE HYDROCARBON SHOWS

Mudlogs

Mudlogs shows are good, with favourable chromatograph C1:C2:C3:C4 ratios and fair fluorescence and cuts. "Instant white blooming cuts" are reported from ≈15300. However no comments were made regarding oil scums at the flowline or shakers, and no increased oil content was reported on Milchem daily mud checks. Some oil is therefore present, but probably not at producible saturations.

Electro-magnetic Propagation

The EPT™ is independent of R_{xwe} and C_x. When water filled porosity is computed from EPT (APPENDIX 61), and divided by $\emptyset_t$, patches of unmoved hydrocarbon appear between 15080-15670. These rarely exceed 20% S_{hr}. The upper permeable zone also shows patchy S_{hr}. However the oil seen with this technique is from intervals with poor microlog response. Since this oil usually occurs with increased log porosity (SxoEPT = f($\emptyset_t$)), and follows no discernible trend, rugosity or bitumen are probably partly responsible for this phenomenon. Bitumen is present in core.

Core S_{OC}

Core oil saturations are low for an oil reservoir rock, rarely exceeding 20%, and are virtually absent in the upper permeable region above 14945.

14.5 APPENDIX 53: BULK VOLUME FRACTIONS, SATURATION, PRODUCIBILITY, RESERVOIR TYPE SIGNATURES & SEM PHOTOMICROGRAPHS

The facies column in this plot shows fining upwards sequences, on two scales. One of approximately 25 ft(8m), and the other approximately 180 ft(55m). Cycles are recognised by conglomerates grading to the interbedded or shale facies. 10 larger cycles are recognised commencing at:

Below total depth, 16270, 16165, 15796, 15706, 15595, 15517, 15296, 15000, and 14670 ft(4471m).

Larger cycles represent periodic tectonism (3.3.1), the significance of which lies beyond the scope of this single well study.

Calculated bulk volume fractions assist in facies recognition, but do not completely replace the human eye and raw logs. The Microlog holds a great deal of facies character, for example showing the individual bed resistivities of bedded sandstone compared with the homogeneously resistive massive sands. Massive sands have porosity without clasts or *GR*, and therefore become harder to separate from the slightly less porous but similar bedded sands with depth. As porosity declines the expected facies sequences inevitably become an influence on one's interpretation. Massive sands occasionally contain clasts which are successfully located by *vlogs*. *Calcclst* cannot see calcified units of the interbedded facies because of *GR*:

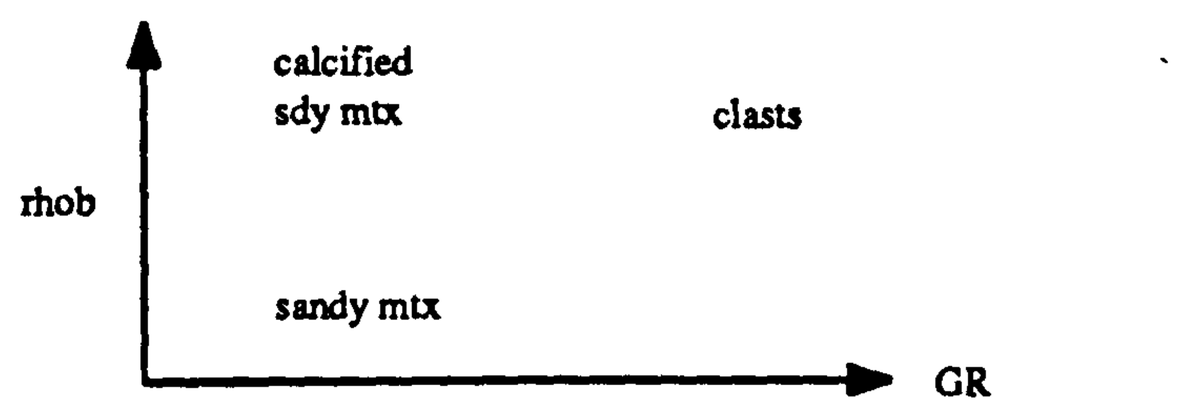


Fig p262*Calcclst*'s method of distinguishing calcified sandy matrix from clasts

The unit at 16250 may be the low permeability "muddy matrix breccia" (Marathon) observed during (11) in other, generally more proximal Brae cores than Well A.

14.5.1 RESERVOIR TYPE SIGNATURES, RTSs

Averaged parameters maybe a more suitable presentation of certain parameters than accumulated values, and have recently been hand calculated and displayed. However the intention at the time was a standard presentation to predict untested DST's *kh* mDft values, accumulated permeabilities.

Matrix

The matrix sector parameters NVSH and NVLOG (8.1) are accumulated curves over the RTS interval. Only the two most powerful matrix parameters are displayed. Full use of the matrix sector can occur only when RTS intervals are fine enough to enclose only one rock type. Limited facilities precluded such detail, and RTSs cannot add to rock type delineation on this scale.

Environmental

This sector indicates the interval's log analysis credibility, *di* and NCAL being primarily relevant to R_t whereas DRHO is relevant to porosity. The sector does not show reservoir mineralogical or geometrical heterogeneity, which can invalidate log analysis transforms (systematic error). The uppermost RTS 14588-14964 indicates fair porosity and R_t determinations. *di* in this well is important for the R_{we} problem (14.3.1), and is worst over RTS 15042-15681. DRHO and NCAL, |Cal-8.5|, are also high. The sector indicates that the log analysis for a test over this interval would be unreliable. RTS 15681-15931 shows a greatly improved environmental sector, whilst RTS 15931-16281 is poor. The lower oil bearing RTS 16281-16500 shows conditions allowing adequate log analysis.

Porosity

Parameters P ($\emptyset_t$) and E ($\emptyset_e$) are summed. E/P generally decreases with depth, from .84 to .63. E does not include any P_c pore throat size distribution relationship. If pore throats are larger in porous zones E/P may decrease more than indicated and it may be legitimate to also make E a function of P, however insufficient data (APPENDIX 62) is available for this refinement. E reflects clay micro-porosity and clast's porosity, with clasts tending to be exaggerated with depth as the porosity contrast declines, and more of the matrix becomes classified as clasts. Calculated clasts increase sandy matrix's clay free porosity and these two opposing effects tend to counter each other. E, as an indication of hydraulic

or replaceable porosity should remain acceptable. Discounting the poor environmental RTS 15042-15681, E per foot also reduces with depth reflecting decreased P, and increased clasts. Average porosities are more useful because summed flow parameters have also been calculated.

Saturation

SOX, shallow zone oil saturation, shows low values at the upper water test, .047 /ft, and highest values at the lowest RTS, .075 /ft, consistent with tests. BVO, deep zone bulk volume oil, trends less favourably with test results, showing .059 at the upper test and .059 at the lower oil bearing test. This poor deep calculation compared with the shallow, which uses R_{xwe} for water resistivity, is an additional indication of how deep filtrate invasion spoils the deep S_w which uses R_w=0.025. It shows that an R_{we} based on DI, R_{mf} and some function of R_t's investigation depth is essential for a realistic S_w calculation. See "DI" (APPENDIX 52)

Flow

Flow sector parameters are best accumulated if *khs* are to be predicted. Accumulated values are shown in both RTS displays. ML is a good semi-quantitative single phase flow indicator because it is independent of the tools or theory of P or E. It shows the upper RTS interval to be most conducive to flow, 34, and the lower the least, 15. ML is plotted on (APPENDIX 30), in which the encouraging 15409–60 interval shows poor character. KE30 (blue), E's single phase flow predictor, decreases in relation to ML with depth. This reflects the on/off nature of ML compared with the more quantitative nature of E. Although ML maintains an "on" status with depth, E is nevertheless reduced.

KW and KO are summed water and oil flow parameters in a two fluid phase system, where S_w<1. If invasion did not invalidate S_w these curves would be useful, and are included to cover this possibility. However the interpretation is that intervals where S_w<1 above 16300 are caused by invasion or inflated log porosities. Below 16300 effective oil permeability is clearly non–commercial.

A comparison of the upper and lower RTS indicates how RTSs contrast a relatively tight oil bearing interval with a more permeable water interval. Two RTSs show high environmental sector parameters, 15042 and 15931, undermining all other parameters. A more useful RTS display could be achieved by experimentation with parameters, the scales of each parameter, and more importantly with smaller RTS intervals.

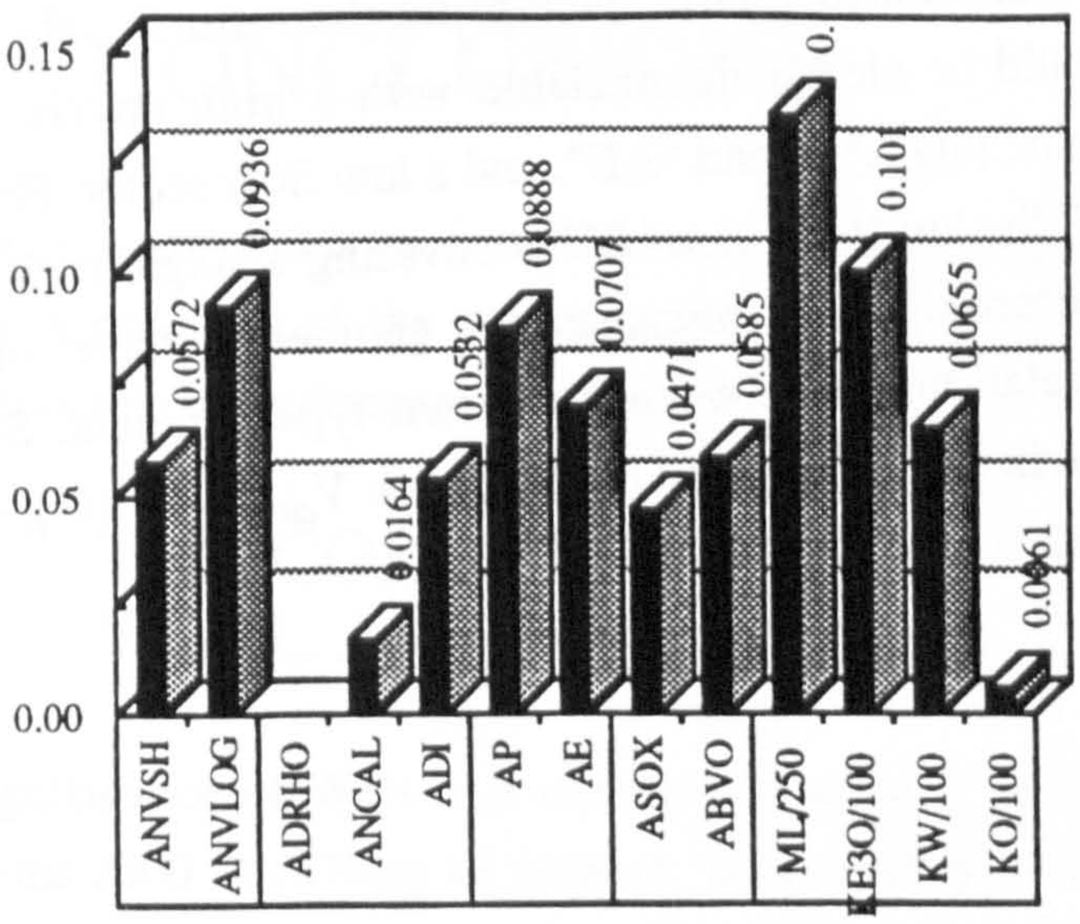


Fig p265 Comparison of RTSs from known water and hydrocarbon bearing intervals within the Brae Formation.

14.5.2 SEM x45, x300 & x3000 PHOTOMICROGRAPHS

The standard scale photographs show the gross arrangements of grains and pores (x45), the nature of a typical pore from the sample which itself was selected as being typical (x300), and lastly of typical micro-porosity geometry (x3000) associated with non-replaceable brine. "Typical" photographs are an attempt to overcome the scale problem. Photographic captions can be found in (9.3.3.4). The greatest contrast appears between Massive Coarse Sandstones and Clasts. Pores in clasts (14633) appear as isolated vugs in

the clay matted fractured surface. MCS pores are larger, better connected and boast a greater proportion of uncontaminated quartz, increasing the ratio $\emptyset_e/\emptyset_t$. A clast RTS covering 15129-15139 would be clearly identifiable with a high matrix sector, a low porosity sector containing unequal "AP" and "AE", and a low flow sector. Photographs are intended to compliment RTSs, but the lack of RTSs covering a single rock type, and the formation's extremely heterogeneous microscopic geometry, have obscured any immediately recognisable relationship between these two types of data. Short interval RTSs with additional matrix sector parameters such as $V_{dryclres}/(\emptyset_n - \emptyset_d)$ would greatly improve this situation.

Do Not Lend Or Copy
Ph.D. THESIS. M. DEAKIN

15 CONCLUSIONS

The conclusions of this project fall under three headings: the commercial significance of Well A, a criticism of the methodology used in the project, and finally some general statements regarding formation evaluation.

15.1 THE COMMERCIAL SIGNIFICANCE OF WELL A

The significance of Well A is not only in its own producibility, but whether or not it represents 2000 ft (610m) of closure. It is a difficult well to evaluate for a number of reasons, both natural and man made. The primary natural causes of difficulty are:

- low porosities combined with varying matrix physical properties.
- heterogeneous porosity distribution on a cm scale and the consequent uncertainty in any core-log porosity transform.
- the similar densities and *HI* s of an oil over water situation compared with the more easily recognisable gas over water situation.
- the unknown effect of fine grained argillaceous clasts upon the porosity/resistivity relationships of an oil saturated low porosity rock.

Man related causes include:

- deep invasion of resistive mud filtrate and the consequent uncertainty of R_t.
- lack of formation fluids pressure data.
- a water based mud system.
- lack of conclusive production test data.
- a poor logging environment.
- lack of core from deeper intervals, particularly from an (unexpected) deep oil bearing interval.
- apparently contradictory data.

15.1.1 ESSENTIAL OBSERVATIONS

In deciding the position of Well A in relation to an oil-water-contact it is helpful to list the important observations, from which a conclusion becomes more obvious:

1) Using any family of parameters discussed in this thesis S_w's are trendless for 1,700 ft(518m). This is inconsistent with a transition zone. Well A is therefore entirely within a water zone or entirely within a hydrocarbon zone.

2) Over the twice logged interval 14588-14980, both LLD and ILD show increased resistivity on later runs. This is caused by invasion of mud filtrate, and proves the filtrate is more resistive than the movable fluids it is replacing.

3) Borehole corrected invasion profiles generally translate as increasing conductivity with depth from wellbore (Schl charts Rcor-1, 2a, 4, Rint 2c, 9).
This implies a) a water zone, or b) extremely limited movable hydrocarbons.

4) DST3 flowed ≈550 bbls of formation brine (10.1.1). By definition the permeable interval is not at immovable water saturation. It is therefore at best a transition zone under closure with impaired effective oil permeability, or at worst a water zone.

5) It is just possible that DST3 is transitional, and only produced brine because water filtrate quashed effective oil permeability. However, DST1 yielded oil. Therefore DST1 strongly implies DST3 did test a genuine water zone, regardless of the effects of a water filtrate on relative oil permeability .

6) Calculations of oil (15400-15480) are associated with deep invasion. Calculations approaching water are associated with reliable porosities and < 50 inches of invasion (14890-14925).

7) Other Brae Formation commercial oil wells, drilled with oil or water based mud, show deep reading resistivity tools increasing from 10-20 ohmm in Kimmeridge Clay, up to 30-70 ohmm in the sands or conglomerates below. By contrast Well A decreases from 10-20 ohmm, confirming the comparison, down to 3-8 ohmm. Although this does not disprove an oil zone with poor reservoir quality and high S_{wi}, it strongly suggests a water zone.

8) It is the quantitative interpretation of resistivity which stands out as the basic inconsistency when interpreting Well A.

Less significant observations are:

9) Movable oil from DST1 requires at least one oil trap within Well A.

10) Capillary pressure data coupled with RTGLOB suggest Well A is water wet.

11) Mudlogs, EPT™ and core saturations suggest residual or "paleo" oil.

12) S_W calculations, or its trend with depth are insensitive to the effects of clays or clasts, and clays need not be an important consideration during evaluation.

13) Formation damage: low permeability tests can be caused by invading fluids altering S_W such that $k_O+k_W<<k$. Furthermore the ratio of produced oil and water may be dramatically altered from their volumetric ratio in the virgin reservoir, favouring the reservoir fluid which is miscible with the invading fluid.

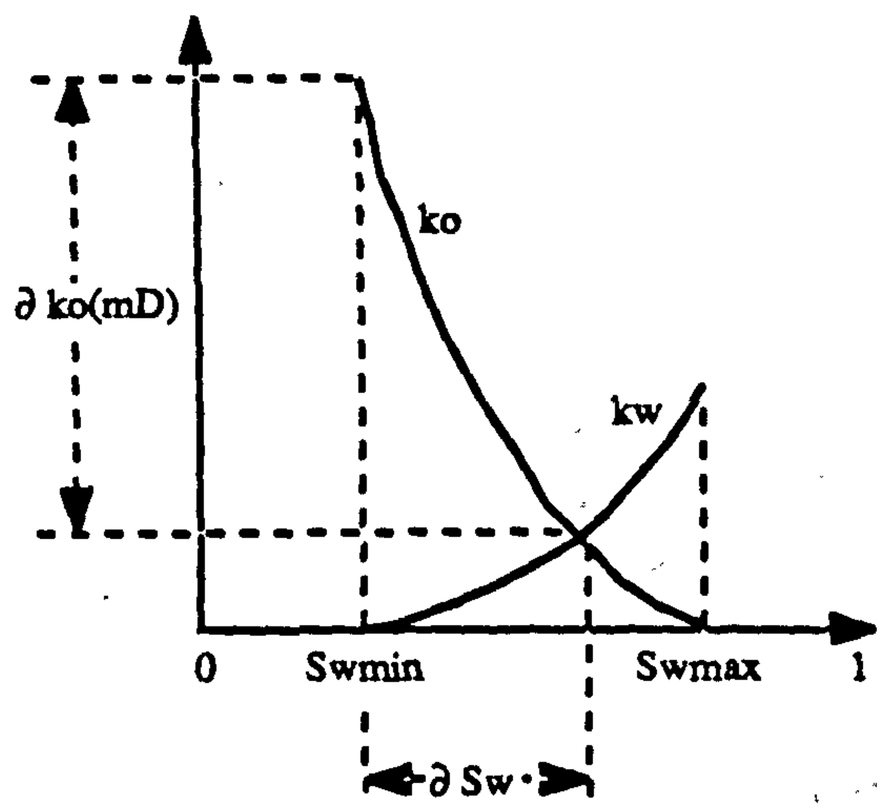


Fig p269 Decreased oil permeability due to water invasion into a zone at S_{wi}

14) Formation damage through swelling clays or mobile fines is not present.

15) There is no evidence of oil wettability.

16) The possibility of fractures below 16300 does not erase the negative implications of items 1-8, and is inconsistent with the sealing mechanism at 16300.

15.1.2 INTERPRETATION

In view of the above, inparticular the combination of 1, 2, and 8, it becomes clear that Well A lies in a water zone. However Well A intersects local accumulations of hydrocarbon trapped beneath oil-water capillary barriers. All such accumulations are non–commercial and do not indicate a regional lowering of the commercial OWC.

Hydrocarbons will be detected in these zones by cores and logs. DSTs may yield oil from these zones depending upon oil phase continuity (movable or residual), relative permeability, and drawdown. RFTs cannot show oil gradients in these zones if the oil phase is discontinuous. A water mud filtrate may break up the oil phase; therefore RFTs would provide the most pessimistic impression in these hydrocarbon intervals.

The origin of these hydrocarbons can be explained by at least three mechanisms:
The sandy conglomerates of Well A lay in the migration path of hydrocarbons which today fill structurally higher rock volumes. Any capillary barrier with a concave lower surface formed local closure and trapped migrating hydrocarbons. A capillary barrier is created wherever the available capillary pressure is inadequate to breach the pore throat it is confronted with. Capillary barrier surfaces today cap the lower sections of transition zones containing movable oil.

Alternatively, Well A previously resided in an oil zone and subsided into a water zone. Subsidence accounts for residual oil, which need not currently be under closure. Subsidence into a water zone also accounts for trapped movable oil under current local closure.

A third alternative is a raised spill-point causing a paleo oil–water–contact to move up through Well A. Like the second alternative, this situation results in residual and movable oil wherever concave capillary barriers exist.

This interpretation is consistent with all data available for this project, including the 7.5 bbls of oil from DST1. The maximum pore throat size of the rock forming closure will limit oil column height. Cemented sands such as those at 16300 with nil $\emptyset_e$, are interpreted as providing an oil-water capillary barrier, even if shales are absent.

15.1.3 SIGNIFICANCE

The project has attempted to overcome natural and man made difficulties by incorporating all data relevant to fluids content. These conclusions may appear straightforward and obvious, but nevertheless contradict all previous log analyses, and interpretations of other data. The inconclusive results of DST2 were the first firmly negative results, and could be optimistically explained by the reduced effective permeability to oil (10.6.1.2), caused by increased S_{xo} from mud filtrate.

The standard formation evaluation parameters resulting from the project are listed below.

Gross interval	1932 ft (586m)
Net	803 ft (245m)
N:G	0.42
Average Net Porosity ($\emptyset_t$)	8.1%
Pay	9 ft
Average Pay Porosity ($\emptyset_t$)	11.0%
Average Pay hc. Saturation	47%
hcft.	0.47 (0.14hcm)
Top Transition Zone	Not present
Bottom Transition Zones	14597ft (4449m), 16336ft (4979m). Possibly 15469ft (4715m)
Free Water Level(s)	Inadequate data
Vertical Permeability Barriers	16305-16254, 15878-15855, 15690-15678 and 14870-14762 ft RKB

15.1.3.1 PERMEABILITY TO BRINE INJECTION

The brine saturated condition, absolute permeability, is predicted in curve KE3O, mD. KE3O indicates adequate permeability for injection purposes with intervals of 25-50 mD, and adequate oil permeability if this rock were higher than 300 ft(91m) above free water (10.5.2). With respect to porosity/depth trends Well A's depth alone would not rule out oil producibility from intervals above 14950, if the rock were oil saturated. The predicted absolute permeability to brine, in mDft is:

14585-14945	14950-16500
9,958	25,238 (+/- 15% for locally inflated KE3O)

It should be noted that carbonate cements, not conglomeratic clasts, are the major negative

influence on reservoir quality.

15.1.4 EXPLANATION OF $R_t \neq R_O$

Whenever a saturation equation predicts an R_O lower than logged R_t, hydrocarbons are calculated. In this well the primary problem the equation has is that R_w is less than the R_{we} encountered by the deep reading resistivity tools. In fact, with the possible exception of RTGLOB, the tools are unable to escape the influence of the more resistive invaded zone, because a) invasion is deep, and b) filtrate resistivity is significantly higher than formation water resistivity.

Filtrate invasion around Well A was the primary cause of the problems addressed by this thesis. The invasion problem was exacerbated by:

- miscible filtrate/formation fluids
- a strong R_{mf}:R_w contrast (x4.4)
- low porosities (8%)
- open hole time (33days)
- overbalance (850psi)
- permeable mud cake (not proven), and
- mud cake removal from trips and wall collapse.

The solution to this R_{we} problem is to ensure R_{mf}=R_w. This results in any increases in R_t being due to hydrocarbon filled porosity. In this situation calculated $S_h \geq S_{h\,virgin}$, regardless of invasion.

The phenomenon of progressive invasion has been highlighted recently by the introduction of monitoring while drilling resistivity devices. (J. Breitmeier et al, 1989)

The equation's second problem with predicting R_O is artificially inflated porosities. The saturation equation calculates any increase in porosity as hydrocarbon since no corresponding conductivity is found. If inflated porosities are due to solid hydrocarbons such as bitumen, they are in fact non-matrix material, i.e. porosity, but filled with solid not fluid.

The equation's least significant R_O error arises in its conversion of porosity to conductivity via the water saturated parameter m or g. The derivation of m and g is

discussed elsewhere at length (6.2), and below (15.2&3). Briefly, wherever m or g varies from its assigned constant value, the equation's R_o will diverge from the actual water saturated resistivity, resulting in the possibility of calculating $S_w < 1$.

The equation's problem with n or y are not relevant in a water saturated rock. Nevertheless they can marginally increase or decrease the S_w error. C_x problems are also negligible in Well A.

The cause of Well A's resistivity problem is therefore firstly invasion, and secondly porosity.

15.2 CRITICISM OF THESIS METHODOLOGY

The project began with a considerable amount of data on one well, including reports of standard interpretations. Early geological studies consumed extremely large amounts of time, in the belief that understanding the rock would solve all the formation evaluation problems, a currently popular view. This was not the case; petrophysics lies between rocks and fluids. If a large number of wells had been presented it would have been correct to employ standard methods, develop a geological model, and predict porous permeable geometries. However, the problem of correctly interpreting one well's contradictory data, resulted in a project concerned with a general methodology for integrating data, as much as the actual results.

Some topics which require discussion or revision due to considerations after late 1987, when hard copy was formulated, are set out below.

15.2.1 *vlogs*

The main petrophysical problem with clasts is their 5% $\emptyset_t$ but nil $\emptyset_e$, and to some extent the difference between m_{clast} and $m_{sandy\ matrix}$ (7.2.1). Fortunately clast mineralogy is dense, and if *rhob* is used in porosity determination $\emptyset_t$ will be preferentially reduced over clast intervals, thus compensating for their lack of $\emptyset_e$. The widespread use of *rhob* for porosity has helped operators over this phenomenon, and with hindsight, *vlogs* does not bear heavily upon the basic conclusions of formation evaluation. It is however valuable as a defensible approach to reservoir rock volumes and equity.

15.2.2 REVISED $\emptyset_t$ SWITCHING METHOD

In response to the lack of calibration of the rate of change of log and actual porosities, and the need to use different tools in different circumstances (8.1.6.1), the following revised switched $\emptyset_t$ is now viewed as providing the closest match of log and actual $\emptyset_t$s.

15.2.2.1 DENSITY TOOL

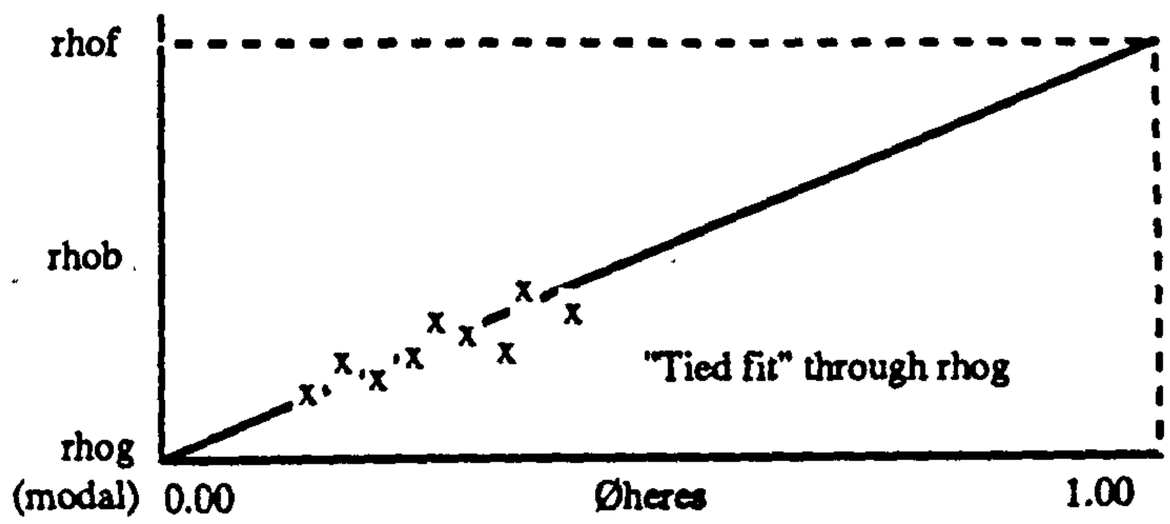


Fig p274 Determining *rhof* for use of *rhob* in determining $\emptyset_t$.
Plugs from clean intervals only.

Then: $$\emptyset_d = (rhog - rhob)/(rhog - rhof)$$

Observe $\emptyset_d$ value at V_{shres}=1, label as $\emptyset_{dsh}$.

Assuming $\emptyset_t$=0.1 when V_{shres}=1

Then: $$\emptyset_{heresD} = \emptyset_d - V_{shres}(\emptyset_{dsh} - 0.1)$$

15.2.2.2 SONIC TOOL

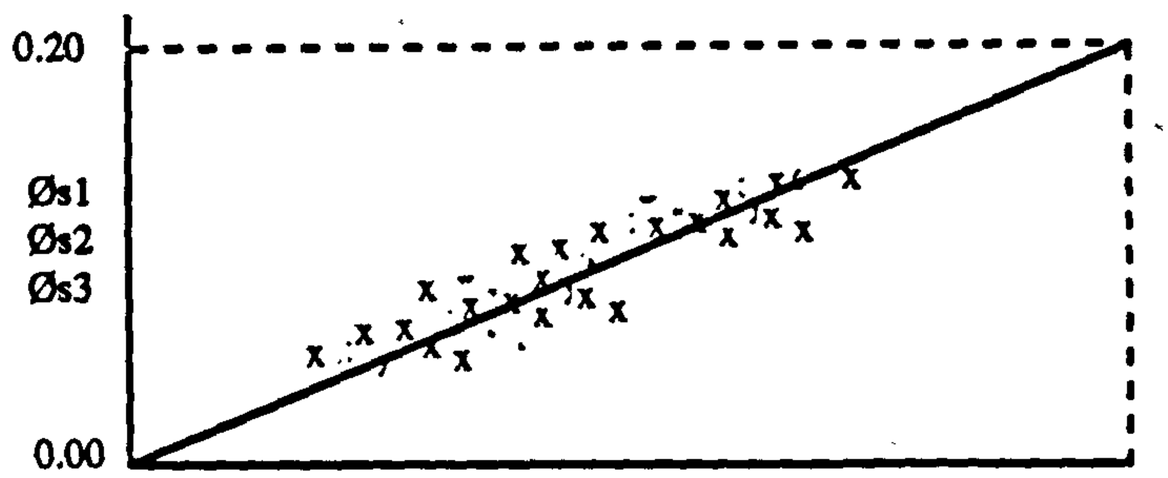


Fig p274 Determining the constant "c" for use of ∂t in $\emptyset_t$. Plugs from clean intervals only.

Compute the curves:

$$\emptyset_{s1} = 0.62(\partial t - 56)/56, \quad c_1 = 0.62$$
$$\emptyset_{s2} = 0.66(\partial t - 56)/56, \quad c_2 = 0.66$$
$$\emptyset_{s3} = 0.70(\partial t - 56)/56, \quad c_3 = 0.70$$

Overlay crossplots of $\emptyset_{s1}$, $\emptyset_{s2}$ and $\emptyset_{s3}$ versus $\emptyset_{heres}$. Choose c value with the least deviation from the diagonal, or make c=f.($\emptyset_{heres}$) for minimum deviation from the diagonal. Compute the corresponding $\emptyset_s$= c (∂t -56)/56 curve.
Observe $\emptyset_s$ value at V_{shres}=1, label as $\emptyset_{ssh}$.
Assuming $\emptyset_t$=0.1 when V_{shres}=1
Then: $$\emptyset_{heresS} = \emptyset_s - V_{shres}(\emptyset_{ssh} - 0.1)$$

15.2.2.3 NEUTRON TOOL

$\emptyset_{nc} = \emptyset_n$-[0.120-0.0051(*GRCC*-23)], where

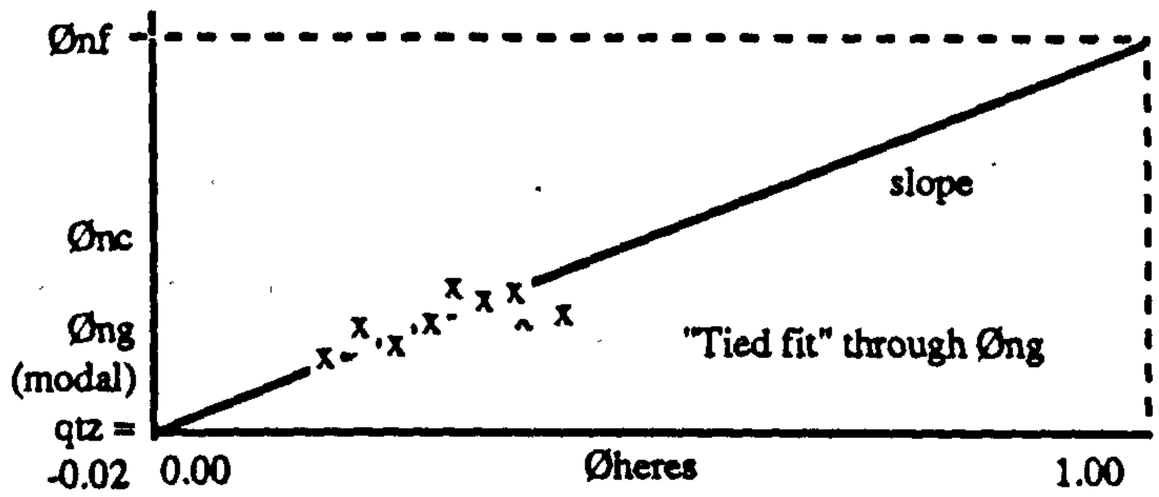


Fig p275 Determining $\emptyset_{heres}$ in terms of $\emptyset_{nc}$. $\emptyset_{ng}$ (grain) is determined by the modal value of neutron response for the matrix of the core plugs. i.e. -0.02 for sand, 0.00 for limestone

Then: $$\emptyset_{heresN} = (\emptyset_{nc}\text{-intercept}) / \text{slope}$$

$\emptyset_{nc}$ is already corrected for matrix, environment, and reservoir clays, but not light hydrocarbons. The switching routine is then applied to these coexisting curves in the same manner as (8.1.5.1), creating a clay corrected $\emptyset_t$ curve largely immune to changing matrix or borehole. If *rhof* is found to vary significantly less than 1.0 an initial S_{xo} HC correction can be applied to the raw *rhob, nphi* and *dt* curves, however this is more relevant in higher porosity wells.

As previously outlined (8.1.6.1), $\emptyset_t$ switches in response to mineralogy and borehole conditions, causing the ratio of [porosity error : porosity actual] to be maintained at a minimum. This method has all the advantages of the accepted *rhob* -$\emptyset_{he}$ method, but also remains true to porosity over low porosity, variable *rhog* intervals, where density count rates are low, by switching to $\emptyset_{nc}$, and over rugose intervals by switching to $\emptyset_s$, whose first arrival time will be little affected by an uneven borehole wall.

Log analysis programs such as ULTRA™ or GLOBAL™[63], which could be adapted to weight inputs as a function of porosity or environment, could make full use of the switched porosity method.

15.2.3 F_g SATURATION EQUATION $C_t = (C_w / F_g) S_{we}^{n} + C_x S_{we}^{n-y}$

The basis of the F_g equation is separating C_x from C_o. This allows F_g to characterise the geometry of the non C_x pore system. It seems reasonable to assume that the non C_x pore geometry, characterised by g, will be more constant than a total porosity exponent m, because it is subject only to free water geometry, whereas m is subject to numerous other variables such as micro-porosity. The importance of this is that g can reasonably be assumed to be a constant, whereas m cannot.

However, in the reservoir F_g must be predicted from porosity. What measurable porosity can be used to create F_g? Will the porosity we measure be identical to the porosity not involved with C_x? We can define the porosity associated with C_o- C_x (i.e. C_{oe}) as $\emptyset_e$. Since in most cases the porosity associated with C_x will be:
$vlogs\emptyset_c + (1-vlogs)\emptyset_{shsdymtx}$, in this thesis $\emptyset_e$ is used to represent the non C_x or free porosity. C_x is the daughter of F_g's free, replaceable, porosity and may or may not be related to the bulk volume ($1-\emptyset_e$). F_g therefore creates a family of parameters:

$$F_g,\ C_{oe},\ \emptyset_e,\ S_{we},\ g,\ C_x,\ n\text{-}y \text{ and } C_w.$$

Some defense should be made here of the method used for determining g. g was derived from water zone Brae Formation wells with water filtrates, ≈2000 ft(610m) shallower than Well A, and logged with the Laterolog (11.3). Log porosities were matched to core. This method involves less error than the more obvious choice of Well A's own SCAL (15.3.2). SCAL samples were poorly selected, poorly preserved, extracted from a deep low porosity formation and tested at non-reservoir conditions. Unfortunately the same facies in the water wells had ≈2% higher porosity with less quartz overgrowths, and therefore possibly slightly different pore geometries. Since g was derived from the laterolog it might seem appropriate to use the laterolog in Well A, however this is not satisfactory because the thick invaded zone raises the series resistivity measurements above R_t. The important point is to use the best estimate of R_t for the derivation of g, and the best estimate of R_t during Well A's evaluation. This is judged to be RTGLOB. i.e RTGLOB and g are compatible.

---

[63] ULTRA: Halliburton Trademark. GLOBAL: Schlumberger Trademark

The problem of exactly how S_{we} affects the C_x's conductivity is ideally dealt with in the lab by *n-y* (6.2.1.1). For oil-mud core see (15.3.2).

The parameters presented above can be calibrated to core. $\emptyset_e$ can be measured in the laboratory, by the non-wetting phase pore volume at a standard capillary pressure; I suggest $P_{c\ air/brine}$ =100psi., ≈300 ft(91m) into an oil reservoir. Like $\emptyset_t$ and $\emptyset_{he}$, $\emptyset_e$ becomes an independently measurable parameter, capable of calibrating the log's $\emptyset_e$ parameter to core.

The thesis proposes a family of formation evaluation parameters more powerful than those of $\emptyset_t$, because $\emptyset_e$ is the usable reservoir volume, which can also be calibrated with core. (6.2.1.2: Positive Features of the F_g.., & 15.2.3.1)

15.2.3.1 USE OF CONSTANT S_{we} CONCEPT TO OPTIMISE LOG ANALYSIS

(APPENDIX 50), The Effective Porosity Required For A Constant S_{we} Calculation, is a very interesting plot in relation to the concepts of the F_g equation, or any other effective porosity saturation equation. It seems logical that even in heterogeneous pore systems S_{we} should be constant in a hydrocarbon zone once capillary effects have become asymptotic. This is to say that the effective "hydraulic" geometry of the total porosity should be occupied by the same volume fraction of oil (close to unity) because this effective porosity should not contain immobile water. An S_{we} greater than zero shows either that the calculation of effective porosity does not square with the actual $\emptyset_t$ minus immobile water, or that one or more of the saturation equation parameters is invalid.

Admittedly this leaves the field open for debate, however conversely, if we find S_{we} to be constant across different porosities and lithologies, we can feel confident in our analysis, and we can create a curve very closely allied to producible fluids: $\emptyset_e(1-S_{we})$. The constant S_{we} concept contains the rudiments of an internal consistency check on the log analysis. If we are clearly above transition, and confident of $\emptyset_e$ and R_t, a variable S_{we} informs us that probably *g*, or possibly *n* are changing.

The plot (APPENDIX 50) uses a fixed value of S_{we}=.4[64] to compute $\emptyset_e$ from:

$$S_{we} = 1 - (\emptyset_t / \emptyset_e)\ (1 - S_{wt}) \qquad \text{(Juhasz 1979)}$$

where S_{wt} is a saturation calculation fixed to show hydrocarbons, and $\emptyset_t$ is the total

[64] Lower value preferrable

porosity curve. The required $\emptyset_e$ diverges considerably from $\emptyset_e$. If the calculated $\emptyset_e$ was close it would indicate hydrocarbons, and approximately the correct saturation equation parameters in the "fixed" calculation. If the saturation equation's parameters refuse to be adjusted in such a manner as to create matched $\emptyset_e$s for a constant low S_{we} then the conclusion must be that R_t is not responding to immobile water in a hydrocarbon zone, but in fact responding to a water saturated rock, or to a transition zone. Fig p278. The concept of a constant S_{we} thus provides the means to optimise saturation equation parameters and bulk volume hydrocarbon. This potential does not seem to have been seized upon by service companies intent upon the internal consistency of log analysis. The mutual attractions of *rhob* , total porosity, C_{we} and m are currently irresistible.

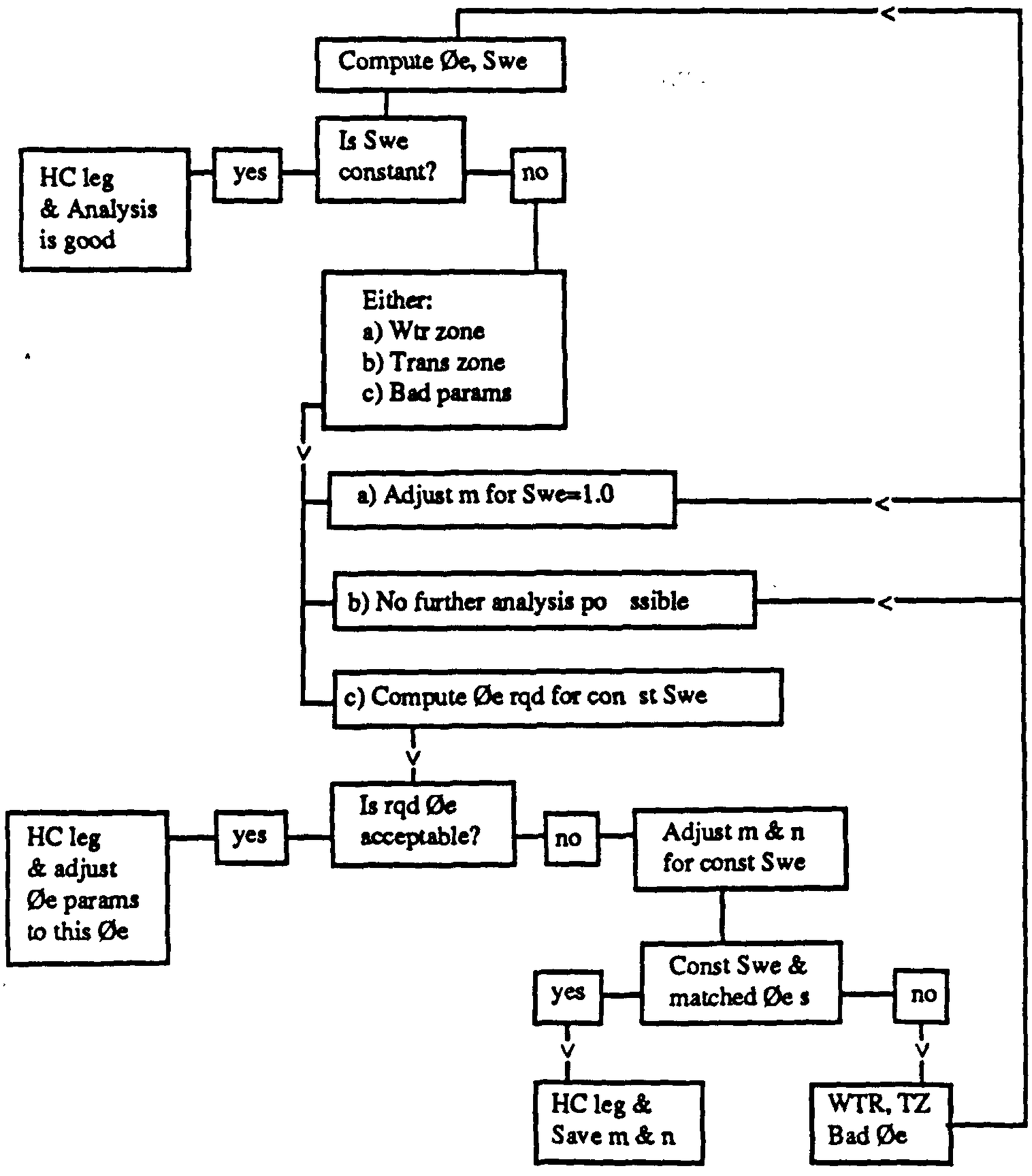


Fig p278 Use of Constant S_{we} Concept to optimise Bulk Volume Hydrocarbon calculations.

15.2.3.2 INDICATIONS OF AND SOLUTIONS TO PROBLEMATIC S_w s

The problems which Well A presented for an accurate S_w calculation have been summarised in a semi-quantitative table below. In Well A R_{we} could be made a function of *di* and R_{mf} in the water zone. R_{we} could then be used in place of R_w in other zones, allowing an improved S_w calculation. This circumvents R_t's inability to read beyond a partially invaded zone, however one should be aware that the derived R_{we} function will partly result from any departures of g from its assigned value.

The table contains general indications and solutions which are believed to be applicable to other wells. The values are calculated from an F_g equation with the following values:

$$C_t = (C_w / F_g) S_{we}^{\ n} + C_x S_{we}^{\ n-y},$$

$$0.13 = (40*0.08^{2.3})\ 1.00^{1.84} + 0.01*\ 1.00^{0.8}$$

$$C_x = 0.06\, V_{shGR}\ \emptyset_{dsh}\ /\emptyset_d \qquad (11.3.2)$$

Table p280 Indications and recommendations regarding S_w equation error

Parameter	Probable typical deviation in Well A, %	Effect upon S_{we} @1.00	Indications of problem	Recommendations
C_t	+100	0.70	*di* , hole history, R_{mf}:R_w, Time lapse resis profiles, High mud api water loss. Conductive shoulder beds	OBM, R_{mf}=R_w, Vigilant drlg practices, R_t from CPI. Rcor5, LLD, IMPH™, w OBM ILM?
C_w	25	1.17, 0.90	Poor water smpls, Thick divided pay zones, Post emplacement aquifer diagenesis.	OBM core wtr smpls with OBM H2O tracer.
$\emptyset_e$	15	1.30, 0.86	$\emptyset_d \neq \emptyset_{nc} \neq \emptyset_s$, Inconsistent & erratic S_w s, Rugosity & caliper, Variable *rhog* core.	Switch $\emptyset_t$ as function of borehole & facies.
$g(m)$	- 8	0.80	Heterogeneous pore geom, $S_w \neq 1$ in wtr zone, S_{we} varies w $\emptyset$ in hc zne, Atypical SCAL smpls.	Generate R_o in wtr zone, (15.2.3.1) Iterate, Are SCAL smpls typical of R_t volume?
n, y	10	1.00 (affected in hc zone)	S_w $\emptyset \neq$ const in hc zne, Unusual S_w/ height curve, Is oil wetness possible? Variable S_{we} in hc zone.	OBM core S_ws for n, Native state core SCAL.
C_x	500	0.98, 1.02 (greater in hc zone)	Res S_w > Cap pres S_w , Res S_w > Tests imply, Res S_w apparent f.V_{sh} , Fresh connate water. Variable S_{we} in hc zone.	(6.2.1) , S_w = f.(Height, Log perm), EPT™, OBM core S_ws for C_x & n.

This table is intended to suggest <u>which</u> parameters require attention by referring to the indications column, and directing attention to that parameter first.

This project has spent a great deal of time on the quantitative interpretation of resistivity, especially m and C_x, a reflection of their prominent position in the literature. For the purposes of evaluating Well A this was a unnecessary. Simpler but less discussed phenomenon dominated Well A's interpretation. Greater weight should have been placed upon direct <u>qualitative</u> observations, and less faith placed upon the assumptions required for a quantitative interpretation.

15.2.4 C_{tm} CHART

It was shown in (11) that little difference in calculated S_{we} results from using C_t or C_{tm} for reservoir sections at S_{wi}s of ≈ 0.20. The horizontal S_{wm} =0.20 line indicates this. This is a function of the particular physical properties of the clasts and matrix of the Brae Formation, not a general condition for conglomerates. Any arrangement of oil and water saturated conductivities on the chart giving rise to non-horizontal S_{wm} lines requires a correction to C_t if S_{we} is to be calculated. Assuming it is possible to calculate $\emptyset_e$ and C_x accurately in conglomerates, a conglomerate whose clasts and matrix had equal g, n and y values can also use C_t to calculate S_{we}.
Note: $S_{we} \approx S_{wm}$ since $\emptyset_e = \emptyset_t - V_{shsdymtx}\ \emptyset_{tsh}$ in the matrix, and matrix shale volume is generally < 0.07

15.2.5 RESERVOIR TYPE SIGNATURES

Reservoir Type Signatures are an attempt to summarise and present complex information in a readily understandable format; over the same intervals covered by other data such as core-facies or DSTs. The RTS concept (4.3) is inadequately tested in this project, no facilities were available after the first prototype RTSs.

The main problem with the RTSs shown is improper zoning. The rapid facies changes in Well A prevented them from evaluating the matrix. RTSs would be more successful if zoned in two passes, firstly over bed thicknesses for facies and reservoir quality evaluation, and secondly over gross flow units for fluids and production test predictions. The DST RTSs would depend upon the facies RTSs, and would consist of accumulated parameters, reflecting fluid bulk volumes and flow such as "hcft" and "mDft". Facies RTSs would consist of averaged parameters reflecting mineralogical components.

15.3 SOME GENERAL STATEMENTS REGARDING FORMATION EVALUATION

15.3.1 A VARIETY OF DATA

Reliable formation evaluation usually results from a balanced appraisal of data from a variety of sources, not a meticulous interpretation of one source. Individuals experienced

in dealing with their own data are required to judge how important or trivial contradictory data from an unfamiliar source is. For example, whether a tight test from an apparently excellent sand means reservoir quality is poor. In some wells lack of a variety of information is fatal to an evaluation, for example the lack of ≈20 RFT pressures in Well A allowed a disconcerting ambiguity between the initial log analysis and tests. However in wells of porous thick quartz sands, with conductive water, RFTs are hardly required. The confusion that followed the lack of RFTs in Well A also shows the value of experienced wellsite supervision, who might have persisted in establishing a reliable gradient in this difficult environment.

The value of combining data is also shown by resistivity curves. Schlumberger created up to sixteen resistivity measurements in Well A. The difference between the commonly used raw curve, LLD, and the processed R_t curve is 2-300%. Full use should be made of these curves to determine R_t, not to mention R_{xo} and *di*. A wellsite version of RTGLOB should be viewed as an integral part of purchasing a resistivity run, unless we prefer to ignore the resistivity of the virgin reservoir, and analyse some other undefined volume of rock. The intricacies of design involved in an R_t tool suggest that the designers themselves are best equipped to extract R_t from its responses, therefore, with water based mud processed R_t should appear on the log as part of the purchase. Consequently an R_{mud} curve should be available at no extra cost in water and oil muds, for borehole signal corrections and proof of oil phase continuity respectively.

15.3.2 USE AND ABUSE OF CORE

$\emptyset_{he}$, *rhog* , k_{hor} , k_{vert} , k_{ro}/k_{rw} , P_c, C_x

Core has an unquestioned value for sedimentological studies, and certain petrophysical parameters which can be physically measured at surface in a manner not possible with remote sensors. The most important are $\emptyset_{he}$ and *rhog* which anchor log analysis to a directly measurable quantity. In addition k_{hor} and k_{vert} provide a useful guide to single phase permeability profiles, and k_{ro}/k_{rw} to two phase flow. Capillary pressure curves are a rich source of pore geometry information, the basic nature of which withstands the rigors of preparation and experimentation. Finally laboratory C_x values circumvent assumptions about porosity exponents (11.3.2).

Estimating Closure from "oil-down-to" wells

Once accurate S_W values have been obtained from an integrated core log evaluation core capillary pressure data can be used to estimate free water levels (FWL) in gas or oil–down–to wells. This rests upon the fact that reservoir hydrocarbon saturation (Fig 6.2.2.1) is controlled by capillary pressure, and that core capillary pressure data reveals the required pressure for a given saturation. A relationship between S_W, P_C and a strongly correlated parameter such as *khor* or $\emptyset_{he}$, here designated X, should be deduced form the core P_C data. The X parameter must also be correlatable to logs. The log's S_W and X can then be used to generate a continuous curve of P_C throughout the reservoir. Providing the hydrocarbon density is known, the corresponding FWL results from extrapolating the log predicted P_C curve to zero. In this method every logging sample point provides its own estimate of the FWL, thus a best fit can be applied. Furthermore the fluid density can be used as a control on the slope of the fit, as is done with RFT data. In thick reservoirs the fluid slope can act as an internal check on the predicted P_C, which it should duplicate.

It is interesting to note that in this case a poor reservoir rock will generally be of greater use than good reservoir rock. This is because desaturation will continue to occur at high P_C levels high above the FWL, whereas good reservoir rock will have desaturated to asymptotic levels within 25 feet. SCAL plugs from gas or oil–down–to wells should be selected with this in mind.

S_W, n

A further important use of core is measurement of S_W in oil mud systems (Woodhouse, 1987). Like $\emptyset_{he}$ this is also a direct measurement of an important petrophysical parameter, S_W, although more problematic. Core boiled in toluene can provide S_W providing:

- core is from the immovable water zone of a reservoir,
- immovable water has not been flushed by filtrate induced wettability changes,
- no de-emulsified oil-mud water, or other water, has become mixed with the connate water,
- $\emptyset_{heres}$ is calculated from overburden porosities to calculate S_W,
- salts are added back to distilled water to increase S_W to reservoir conditions.

Like $\emptyset_{he}$ core S_W not only determines S_W at that sample, but enables logs to extend this information beyond core; in this case through the saturation exponent n. n links R_t, R_O and S_W. The correct value of n is the value which yields the core measured S_W for the

logged R_t. This n value is certainly more relevant to log analysis than a lab value from traumatised (Refs) core plug, desaturated at non–reservoir stresses and temperatures, containing non–reservoir fluids at non–equilibrium distributions (de Waal et al, 1989). The main criticism with core S_w appears to be oil filtrate induced wettability changes which may have changed the connate water saturation prior to measurement at surface. However lab n values must be answerable to this and more obvious criticisms such as C_x log-log plot curvature (6.2.1.2), $\emptyset_M$:$\emptyset_m$ curvature and nonuniform water distribution ((9.5.2.5) & Lyle, 1989). Also, the n value from logged R_t is specifically derived from the actual S_w value in the reservoir, as opposed to a best fit through numerous S_w values, and so the curvature problem is not (as) relevant. The final important advantage is that the same resistivity device, logged R_t, is used during core-log calibration and reservoir evaluation. R_t and n thus become paired parameters in which error in R_t becomes absorbed by the n value.

Large volumes of routine core analysis S_{wc} measurements already exist in databases. These may provide more accurate S_w s, when used discriminatingly to derive n, than S_ws currently based on SCAL. In conclusion, if oil-mud core from above movable water levels has been retrieved SCAL n values are redundant.

Water Zone Core, m and R_w

The second misuse of core is generating SCAL m values. A SCAL m value from clean sandstone at less than 10,000 ft(3048m) has been observed to vary from 1.74 at room conditions to 2.02 at 5000psi net confining pressure, a change in S_w of ≈17 %@0.5[65]. Deeper more complex low porosity samples are likely to be yet more sensitive to trauma (Refs). A further limitation of rocks containing unevenly distributed pore geometries, is the minute volume of R_t that a SCAL m sample represents. In Well A, samples have been withdrawn from large overburden pressures. Overgrowths and pore geometries are formed in equilibrium with these pressures. In samples with slot like low porosities, small shape changes constitute significant changes in conductive pathways. Samples containing pore lining authigenic clays are also vunerable through their altered geometries (g) and altered intra–clay conductivities (C_x).

An accurate m value is best derived from a cored water zone in which diagenesis is no more advanced than oil zone diagenesis. Water zone core enables precise determination of porosity in the $R_O/R_W=\emptyset^{-m}$ equation, but is probably only essential in gas wells, where

[65] $S_w = (0.4 / [40*0.15**1.74])**0.5 = 0.521$; cf. $0.15**2.02 = 0.679$

log porosities may be difficult. Thin sections can be used to compare oil and water zone diagenesis, and should be requested in the water zone for this purpose. Oil and water zone core *m*s can also be checked for equality; but not used for S_w.

Water zone *m*'s contain few of the uncertainties of SCAL *m* values. They are derived at reservoir conditions on unaltered virgin zone samples, with reservoir fluids, and use the same sensors that are to be used to evaluate the reservoir. If water zone core is not taken to settle the diagenesis question then log parameters for clay type, lithology and porosity are available to positively establish if pore geometries are likely to differ. If pore type variations are seen within the field, and few water zones are available, SCAL samples may be the only alternative. However, if few water zones exist and SCAL seems the obvious solution, the question becomes: Are field differences greater or less than the differences between actual reservoir *m* s and lab *m*s? This can be investigated by porosity typing parameters such as $(\emptyset_d+\emptyset_s)/\emptyset_d$, $\emptyset_e/\emptyset_t$ and R_t - $\emptyset_t$ -*height* relationships. Such investigations should be standard precursors to SCAL.

Reservoir R_w may be difficult to establish, and to prove equal to the water zone value, but the R_w problem is common to either method for *m*: it is caused by a lack of recovered immovable water. Criticism of the water zone *m* method based upon unequal R_w is therefore unjustified. It is perhaps worth noting that if a transitional test is used for R_w the water is movable and is probably in chemical equilibrium with the underlying aquifer i.e. the same R_w as the water zone *m* method. The best source of R_w is oil mud core connate water, with mud water tracers.

Water Zone, General

In complex rocks requiring delicate log analysis water zone cores provide calibration points for log parameters where S_w is fixed at unity. In this project the effect of clasts on R_O, from water zone core: $F_{cgl} = 118 + 0.3\%\text{clast} + 0.05\%\text{clast}^2$ (7.3) allowed the effects of clasts on the apparent S_w to be understood. In general, log calibration measurements should be sourced downhole where possible, as in the Dry Clay Mineral Point (12.1), not in the laboratory.

Routine Core Analysis

Precise depth matching is required for integrated studies. Matching $\emptyset_{he}$ to *rhob* is unsatisfactory across mineralogically different facies, or where unevenly distributed porosities are closely spaced. In Well A *rhob* was misleading. A sensitively recorded whole core gamma log is a continuous measurement and directly comparable to logged *GR* and provides a valuable alternative to *rhob*.

Integrating petrophysical data requires compatible data sets resulting from similar sampling techniques. Logs sample a volume of rock every 6 inches(15cm), regardless of lithology. Core must likewise be sampled every 12th inch(30cm), regardless of lithology, if core log transforms are to be genuine. Irrelevant data (bed boundaries, shales) should be excluded from the transform data set after acquisition of the compatible core data by excluding samples from all correlated parameters over the same depth interval. If plugs are selected from favourable locations, resulting from a philosophy of "Why investigate non-reservoir?" the logs are actually being calibrated to a subset of the true data. This approach is reminiscent of times before computerised statistical analysis when only a few core plugs were analysed. Genuine integration of core data is only possible if rigorous data acquisition has been followed. Even the most optimistic analyst does not turn off the density tool when low porosities are being logged; and then interpolate between points!

15.3.3 DRILLING FLUIDS

A comparison of three oil wells, two drilled with oil-based mud and one with water, showed an apparent advantage of oil-based-mud from intervals with similar $\emptyset_e$s. Increased near wellbore oil saturations, via invasion and/or oil wetness, is a certain advantage to effective oil permeability, especially in low permeability formations. However introducing oil into a tight gas reservoir may be more damaging than drilling with water muds, because a third phase is introduced. The increased water saturation from a water based mud will be higher than S_o from an oil mud, and so relatively mobile, and able to rapidly clean up.

High water loss muds combined with oil bearing low porosity low permeability rocks must be avoided. Water invasion can exceed deep reading tools confusing log analysis, and oil resident in the virgin zone cannot flow through the zone of low oil saturation when drawdown is applied. Water invasion can be minimised by thin impermeable cakes with a low high temperature/high pressure fluid loss. Minimum overbalance also reduces flow through partially permeable cakes. Generally the formation should be invaded with the same phase which is intended to be produced. Ideally a produced formation fluid in chemical equilibrium with the virgin reservoir. This also helps during evaluation (15.1.4).

REFERENCES

(SPWLA = Society of Professional Well Log Analysts)

Anderson, D. and Morgenstern, N.R. 1973 'Physics, Chemistry and Mechanics of Frozen Ground: A Review' N.American Contribution to Permafrost: Second International Conference, 257-258, National Academy of Sciences, Washington D.C.

Anderson, W.G. 1986a 'Wettability Literature Survey-Part1: Rock/Oil/Brine Interactions and the Effects of Core Handling on Wettability' Journal of Petroleum Technology. October 1986. Vol38,No11.pp1125-1144

Anderson, W.G. 1986b 'Wettability Literature Survey-Part3: The Effects of Wettability on the Electrical Properties of Porous Media' Journal of Petroleum Technology. December 1986 vol 39, no1. pp1371-1378

Archie, G.E. 1942 'The Electrical Resistivity Log as an Aid in Determining Some Reservoir Characteristics' Transactions, AIME 1942. 146, pp54-62. Also: Petr Tech, Jan 1942.

Baker, P.L., W.E.Kenyon & J.M.Kester 1985 'EPT Interpretation Using a Textural Model' SPWLA 26th Symposium. Transactions. Paper DD.

Barrer, R.M. 1967 'Chapter 6: Diffusion and Permeation in Heterogeneous Media' in: 'Diffusion in Polymers' Editors Crank and Parker Publishers Academic Press, London, 1967

Berilgen, B.A., Sinha, A.K. and Fertl, W.H. 1985 'Estimation of Productivity of Lobo 6 Sand (Lower Wilcox, Tx) by Identifying Diagenetic Clays Using Well Log Data' SPE 14278

Berry, L.G. and B. Mason 1959 'Mineralogy Concepts Descriptions and Determinations' Publ. W.H.Freeman & Co. San Francisco, Calif.

Berteig, V., T. Langeland & D.van der Wel. 1985 'Lithofacies Prediction from Well Data' SPWLA 26th Symposium. Transactions. June 1985. paper TT

Bjorlykke, K. and H. Dypvik 1975 'The Kimmeridge Shale, It's Composition and Radioactivity' Jurassic Northern North Sea Symposium, Stavanger. Norweigian Petr Soc.

Bouma, A.H. 1962 'Sedimentology of some flysch deposits' Publishers Elsevier, Amsterdam. 168pp

Brannan, G.O. and Van Gonten, W.D. 1973 'The Effect of Temperature on Formation Resistivity Factor of Porous Media' SPWLA 14th Annual Logging Symposium. Paper V

Breitmeier J. et al, 1989 Investigation of Radial Invasion of Mud Filtrate. SPWLA 30th Annual Symposium. Paper S

Brindley, G.W. & and Brown, G. 1980 'Crystal Structures of Clay Minerals and their X-Ray Identification' Mineral Society London. 495pp

Bruggeman, D.A.G. 1935 Annln. Physik. Volume 24, 636

Burck, L.J.S. and Forsyth, D. 1985 'Permeability Prediction in Shaly Sands' Transactions: European Formation Evaluation Symposium. paper 19

Bussian, A.E. 1982 'A Generalized Archie Equation' 23rd SPWLA Symposium. Transactions. 1982 Vol.1 Paper E

Clavier, C; Coates & Dumanoir 1984 'The Theoretical and Experimental Bases for the "Dual Water" Model for the Interpretation of Shaly Sands' SPEJ April 1984 pp153-167

Coates, G.R. and Dumanoir, J.L. 1973 'A New Approach to Improved Log Derived Permeability' SPWLA 14th Symposium. Transactions. Paper R

Cohen, J.M. 1988. Dept of Geology, Imperial College, London SW7

Cooke-Yarborough, P. 1987 'A Method for Reconciliation of Log-Derived and Core-Derived Porosity' SPWLA 28th Symposium. Transactions. Paper DD.

Core Laboratories, Inc 1982 'A Course in Special Core Analysis' (Manual)' 7501 Stemmons Freeway, Box 47547, Dallas, Tx 75247.

Crocker, M.E. and L.M. Marchin. 1988 'Wettability and Adsorption Characteristics of Crude-Oil Asphaltene and Polar Fractions' Journal of Petroleum Technology. April 1988. vol40,No4. pp470-474

Curtis, C.D. 1983 'Link Between Aluminium Mobility and Destruction of Secondary Porosity' AAPG Bulletin.v67.p380-384.

Dahlberg, K.E. and M.V. Ference. 1984 'A Quantitative Test of the EPT Log for Residual Oil Determination' SPWLA 25th Symposium. Transactions. June 1984. Paper DDD.

Dake, L.P. 1978 'Fundamentals of Reservoir Engineering' Publishers: Elsevier Scientific Publishing Co. ISBN 0-444-41830-X

Deer, W.A., Howie, R.A. and Zussman, J. 1966 'An Introduction to Rock Forming Minerals' p202. Publishers: Longman. London. ISBN 0 582 44210 9

Delano, J.M. and R.P. Wharton. 1982 'An EPT Interpretation Procedure and Application in Fresh Water, Shaly, Oily Sands' SPE 10738.

Delfiner, P., O. Peyret and O. Serra. 1987 'Automatic Determination of Lithology from Well Logs' SPE Formation Evaluation, September 1987. vol2, No3 pp303-310

Delhomme,J.P., T.Pilenko, E.Cheruvier, & R.Cull. 1988 'Reservoir Applications of Dipmeter Logs' Journal of Petroleum Technology. February 1988. Vol40, No2 pp180-186

Desbrandes, R. and J. Gauldron. 1987 'In-Situ Rock Wettability Determination with Formation Pressure Data' SPWLA 28th Symposium. Transactions. June 1987. Paper Z.

Earlougher, R.C.Jr. 1977 'Advances in Well Test Analysis' SPE Monograph. ISBN 0-89520-204-2

Etris, E.L. et al, 1989 'Petrographic insights into the relevance of Archie's Equation: Formation factor without *m* and *a*. SPWLA 30th Symposium Trans, paper F.

Fertl, W.H. 1987 'Log-Derived Evaluation of Shaly Clastic Reservoirs' Journal of Petroleum Technology. February 1987. Vol39, No2 pp175-194

Freeman, D.W. and K.C. Henry. 1983 'Improved Saturation Determination with EPT' SPE 11466

Ganer, B.L. 1985 'Case History of Cotton Valley Sand Log Interpretation for a North Louisiana Field' Journal of Petro Technology. November 1985. Vol37,No12. pp1995-2005

Gant, P.L. and W.G. Anderson. 1988 'Core Cleaning for Restoration of Native Wettability' SPE Formation Evaluation. March 1988. vol3 No1 pp131-139

Glanville, C.R. 1984 'A Method for Direct Log Calculation of Excess Conductivity Applied to Shaly Sand Log Interpretation' SPWLA 25th Symposium. Transactions. June 1984. Paper X.

Givens, W.W. 1987 'A Conductive Rock Matrix Model (CRMM) for the Analysis of Low-Contrast Resistivity Formations' The Log Analyst. March-April 1987 p138-151

Griffiths, C.M. and S.Bakke. 1987 'Semi-Automated Well Matching Using Gene Typing Alogorithims and a Numerical Lithology Derived from Wireline Logs' SPWLA 29th Symposium. Transactions. Paper GG.

Gubbins, J. 1988 Core Laboratories Inc., London. SCAL supervisor. Personal communication.

Hagiwara, T. 1984 'Archie's m for Permeability' SPE 13100. 59th Annual Technical Conference, Texas, September 1984

Hardwick, A. 1987 'The Effect of Brine Composition on Excess Conductivity In Shaly Sands' SPWLA 28th Annual Logging Symposium. Paper VV

Harms,J.C., P.Tackenburg, E.Pickles & R.E.Pollock. 1981 'The Brae Oilfield Area' Petroleum Geology of the Continental Shelf of North West Europe. Eds: L.V.Illing and G.D.Hobson. pp352-357.

Harms, J.C. and McMichael. 1982 'Sedimentology of the Brae Oilfield Area, North Sea' Journal of Petroleum Geology. 5,4, pp437-439

Helander, D.P. 1983 'Fundamentals of Formation Evaluation' Oil & Gas Consultants Int Inc. ISBN 0-930972-02-3. p332

Hensel, W.M. 1985 'Improved Formation Evaluation From Pressure and Conventional Cores Taken With Stable Foam - Bennet Ranch Unit (Wasson Field)' Journal of Petroleum Technology. December 1985. vol37,No13.pp2203-2210

Herron, M.M. 1987 'Estimating the Intrinsic Permeability of Clastic Sediments from Geochemical Data' SPWLA 28th Symposium. Transactions. June 1987. PaperHH.

Hilchie, D.W. 1984 'Reservoir description using well logs' Journal of Petroleum Technology. July 1984.vol36.no8.pp1067-1073

Hilchie, D.W. 1988 'NML-The Hope for Production Prediction' Journal of Petroleum Technology. March 1988. Vol40,No3.pp273-276

Hill, H.J., Shirley, O.J. and Klein, G.E. 1979 'Bound Water in Shaly Sands - Its Relation to Q_v and Other Formation Properties' Edited by Waxman and Thomas. The Log Analyst. May-June 1979

Hingle, A.T. 1959 'The Use of Logs in Exploration Problems' Society of Exploration Geophysics paper Los Angeles 1959

Hosseini, M.S. and A. Hayatdavoudi. 1986 'Reservoir Characterisation Of Tuscaloosa Sand by Mineralogical and Petrophysical Data' SPE Formation Evaluation, December 1986, vol 1, no 6 pp584-594

Hower, J. 1981 'Shale Diagenesis' In: Longstaffe, F.J. (Ed), q.v., 60-80.

Hoyle, W.R. 1984 'An Interesting Concept' The Log Analyst. Jul-Aug 1984. pp7-13

Hurst, A. 1987 'Mineralogical Analysis and the Evaluation of Vshale for Reservoir Description' Marine and Petroleum Geology. February 1987. vol4,pp82-91

Hunt, E.R., J.D. Walls and C.Scala. 1985 'An Integrated Log and Core Analysis Study of an East Texas Tight Gas Well' SPWLA 26th Symposium. Transactions. June 1985. Paper HHH.

Johns, W.D., and Kurzwell, H. 1979 'Quantitative estimations of illite-smectite mixed phases formed during burial diagenesis' Tschermaks Min. Petr. Mitt. v 26, pp203-215

Johnson, A. 1987 'Permeability Averaged Capillary Data: A Supplement to Log Analysis in Field Studies' SPWLA 28th Symposium. Trans. June 1987. Paper EE.

Juhasz, I. 1979 'The Central Role of Q_v and Formation-Water Salinity in the Evaluation of Shaly Formations' SPWLA Symposium 1979, paper AA

Juhasz, I. 1981 'Normalised Q_v - The Key to Shaly Sand Evaluation Using the Waxman-Smits Equation in the Absence of Core Data' SPWLA Symposium 1981

Juhasz, I. 1986 'Assessment of the Distribution of Shale, Porosity and Hydrocarbon Saturation in Shaly Sands' SPWLA 10th European Formation Evaluation Symposium, paper AA

Juhasz, I. 1988 'Porosity Systems and Petrophysical Models Used in Formation Evaluation' SPWLA London Chapter Porosity Seminar, April 1988

Kapadia, S.P. and D.E.Menzie. 1985 'Determination of Permeability Variation Factor V from Log Analysis' SPE 14402

Kimminau, S. and Schwartz, L. 1987 'A Review of Pore and Grain Geometric Models' SPWLA 28th Annual Logging Symposium. v II, Paper AA

Keith, B.D. and E.D. Pittman. 1983 'Bimodal Porosity in Oolitic Reservoir-Effect on Productivity and Log Response, Rodessa Limestone (Lower Cretaceous), East Texas Basin' AAPG. vol67. no9. pp1391-1399

Kenyon, W.E. and P.L.Baker. 1984 'EPT Interpretation in Carbonates Drilled with Salt Muds' SPE Reprint 13192. 59th Ann Tech Conf & Exhibt SPE Houston. September 1984

Lowe, D.R. 1976 'Grain Flow and grain flow deposits' Journal of Sedimentary Petrology. vol 46, pp188-199

Lockhart, J.S., Burck and D. Forsyth. 1984 'Permeability Prediction in Shaly Sands' Societe pour l'Avancement de l'Interpretation des Diagraphies' 9th International Formation Evaluation Symposium, Paris. Transactions. Paper 19

Lolley, R.L., V.Stallard & A.F.Corrigan. 1984 'The Prediction of the Production Characteristics of a Variety of Lithological Types with Field Examples' 8th European Formation Evaluation Symposium.

Lyle, W.D. and W.R. Mills. 1989 'The Effect og Nonuniform Core Saturation on Laboratory Determination of the Archie Saturation Exponent' SPE Formation Evaluation, March 1989, v4, No1

MacKenzie, A.S., D.Leythauser, P.Muller, M.Radke, and R.G.Schaefer. 1986 'Petroleum generation and migration in the Brae area, central North Sea' 3rd Conference on Petroleum Geology of NW Europe. London.

MacEwan, D.M.C. and Wilson, M.J. 1980 'Interlayer and intercalation complexes of clay minerals. In: Crystal Structures of clay minerals and their X-Ray identification' Editors G.W. Brindley and G. Brown. Mineral Society of Great Britain pp 197-248

Maple, L.C. 1985 'A Crossplot Approach to EPT Interpretation' SPWLA 26th Symposium. Transactions. Paper N.

Mayer, C. and A.Sibbit. 1980 'Global, a new approach to computer-processed log interpretation' SPE 9341. SPE 55th Annual Tech Conf & Exhbtn. Dallas. Tx.

Maxwell, C. 1873 'Treatise on Electricity and Magnetism' Volume 1, p365 Oxford University Press, London

Middleton & Hampton 1973. ISBN

Mitchell-Tapping, H.J. 1983 'Petrophysical Evaluation of the Smackover Oomoldic Porosity of East Texas and Southern Arkansas' The Log Analyst. July-August 1983. pp3-13

Melvin, J. and A.S. Knight. 1984 'Lithofacies, Diagenesis and Porosity of the Ivishak Formation, Prudhoe Bay Area, Alaska' AAPG Memoir 37. 'Clastic Diagenesis' Ed: D.A.McDonald, R.C.Surdam. pp347-367

Moss, B. and A.Seheult. 1987 'Does Principle Component Analysis Have a Role in the Interpretation of Petrophysical Data?' SPWLA 28th Symposium. Transactions. 1987. Paper TT.

Mungan, N. and E.J.Moore. 1968 'Certain Wettability Effects on Electrical Resistivity in Porous Media' Journal Canadian Petroleum Technology. January-March 1968.p20-25

Nelson, C.H. and L.D.Kulm. 1973 'Submarine fans and Deep Sea Channels. Turbidites and Deep Water Sedimentation' Course: Soc of Econ Palaeont Miner. Pacific Section. 1973, 39-78.

Neves, R and R.C. Selley. 1975 'A review of the Jurassic rocks of North-East Scotland' In: Proc, Northern N.Sea Symposium. (Eds. K.Finstad & R.C.Selley) Norweigian Petroleum Society. Oslo. Paper 5

Normark, W.R. 1970 'Growth Patterns of Deep Sea Fans' American Assc of Petroleum Geologists. Bulletin. vol54,pp2170-2195

North, F.K. 1985 'Petroleum Geology' Publ. Allen and Unwin

Occam, 1349. (William of Occam), Occam's razor: the principle that entities are not to be multipiled beyond necessity.

Patchett, J.G. and E.B.Coalson. 1982 'The Determination of Porosity in Sandstone and Shaly Sandstone. Part Two. Effects of Complex Mineralogy and Hydrocarbons' SPWLA 23rd Symposium. Transactions. Paper T.

Pallet, N., J. Wilson and W. McHardy. 1984 'The Relationship Between Permeability and the Morphology of Diagenetic Illite in Reservoir Rocks' Journal of Petrol Technology. December 1984. vol36,no13.pp2225-2227

Pape, H. and P.Worthington. 1983 'A Surface Structure Model for the Electrical Conductivity of Reservoir Rocks' 8th European SPWLA Symposium.

Parker, K.H. 1987 Department of Physiological Flow, Imperial College, London. Personal communication

Patnode, H.W. and Wyllie, M.R.J. 1950 'The Presence of Conductive Solids in Reservoir Rocks as a Factor in Log Interpretation' Petroleum Transactions, AIME v 189, p47-52

Pickett, G.R. 1966 'A Comparison of Current Techniques for the Determination of Water Saturation from Logs' SPE paper. Denver 1966

Poupon, A., Loy, M.E., and Tixier, M.P. 1954 'A Contribution to Electrical Log Interpretation in Shaly Sands' Transactions AIME, v 201, p138-145

Raiga-Clemenceau, J., C.Fraisse and Y.Grosjean. 1984 'The Dual-Porosity Model, A Newly Developed Interpretation Method for Shaly Sands' SPWLA 25th Symposium. Transactions. Paper F.

Ransom, R.C. 1984 'A Contribution Toward a Better Understanding of the Modified Archie Formation Resistivity Factor Relationship' The Log Analyst. March-April 1984. vol25,No2

Rasmus, J.C. 1983 'A Variable Cementation Exponent, m, for Fractured Carbonates' The Log Analyst. November-December 1983. vol24,No6. pp13-23

Raymer, L.L. and P.M.Freeman. 1984 'In-Situ Determination of Capillary Pressure, Pore Throat Size and Distribution and Permeability from Wireline Data' SPWLA 25th Symposium. Transactions. 1984.

Rider, M.H. and D.Laurier. 1979 'Sedimentology Using A Computer Treatment of Well Logs' SPWLA 6th European Symposium. Transactions. 1979.

Richardson, J.G., J.B.Sangree & R.M.Sneider. 1987 'Permeability Distributions in Reservoirs' Journal of Petroleum Technology, October 1987. vol39,No10

Rink, M. and Schopper, J.R. 1974 'Interface Conductivity and its Implications for Electric Logging' SPWLA 15th Symposium. Transactions. Paper J

Romero, G.M. and C.Perez-Rosales. 1985 'New Relationship Between Formation Resistivity Factor and Primary and Secondary Porosities' SPWLA 26th Symposium. Transactions. 1985.

Ruhovets,N. and Fertl, W.H. 1982 'Digital Shaly Sand Analysis Based on Waxman-Smits Model and Log-Derived Clay Typing' SPWLA Reprint. Shaly Sand. July 1982.

Sallee, J.E. and B.R. Wood. 1984 'Use of Microresistivity From the Dipmeter To Improve Formation Evaluation in Thin Sands, Northeast Kalimantan, Indonesia' Journal of Petroleum Technology. September 1984. p1535-1544

Sawyer, W.K., C.I.Pierce and R.B.Lowe. 1971 'Electrical and Hydraulic Flow Properties of Appalachian Petroleum Reservoir Rocks' US Bureau of Mines Report of Investigations, June 1971. R.I.7519

Schlumberger. 1974 'Log Interpn Vol. II Applications'

Schlumberger. 1982 'Natural Gamma Ray Spectrometry'

Schlumberger. 1984 'Log Interpretation Charts'

Schlumberger. 1985 'Log Interpretation Charts'

Schlumberger. 1987 'Log Interpretation Principles / Applications' Schlumberger Educational Services. 1331 Lamar St. Houston. Tx77010

Schmidt, V. and D.A.McDonald. 1979a 'The Role of Secondary Porosity in Sandstone Diagenesis' Soc Econ Petr & Min. Special Publication No26. p179-207

Schmidt, V. and D.A.McDonald. 1979b 'Texture and Recognition of Secondary Porosity in Sandstones' Soc Econ Petr & Min. Special Publication No26. p209-225

Schoen, U. 1953 'Identification of Clay Minerals by Fixation of Phospate and Cation Exchange' Z.Pflanzenernahr. Dung. Bodenk.; v63, 1-17, 97-199

Scholle, P.A. and P.R.Schluger, Editors. 1979 'Aspects of Diagenesis' Soc. of Economic Paleontologists and Mineralogists. 443pp

Schopper, J.R. et al. 1982 'Calculating Permeability from Surface Area Measurements' 7th SPWLA Europe Logging Symposium Paris 1981. Transactions.No17, 12pp

Selley, R.C. 1982 'An Introduction to Sedimentology' 2nd Edition Publishers Academic Press, London

Selley, R.C. 1984 'Helmsdale Field Trip Guide Book' Printed by R.C. Selley & Co. Ltd., P.O.Box 12, Dorking, RH4 3BW

Selley, R.C. 1984 'Porosity Evolution and Truncation Traps' Northern North Sea Offshore Technology Conference. Stavanger. August.

Selley, R.C. 1985 'Ancient Sedimentary Environments and their subsurface environments' 3rd Edition. Publs Chapman & Hall, London.ISBN 0–412–25730-0.

Sen, P.N. 1980 'The Dielectric and Conductivity Response of Sedimentary Rocks' SPE 9379.

Senecal, J.E. and M.E. Mulhern. 1985 'Monterey Formation Analysis: State of the Art Interpretation of Lithology and Identification of Fractures and Fluid Type in Fine-Grained, Mineralogically Variable Rocks' SPWLA 26th Symposium, Dallas, June 1985. Paper KKK

Serra, O. and H.T. Abbott. 1982 'The Contribution of Logging Data to Sedimentology and Stratigraphy' SPE 9270. SPEJ February 1982. vol22, pp117-130.

Serra, O., P.Delfiner and J.C.Levert. 1985 'Lithology Determination from Well Logs: Case Studies. SPWLA 26th Symposium. Transactions. Paper WW

Shaw, H.F. 1985 'Clays and their effects in Source & Reservoir Rocks' JAPEC Course notes 35, June 1985. c/o Geol Soc., London W1V 0JU

Sherman, M.M. 1983 'The Determination of Cementation Exponents Using High Frequency Dielectric Measurements' The Log Analyst. November-December 1983

Silva, P.L. and Z.Bassiouni. 1985 'A Shaly Sand Conductivity Model Based on Variable Equivalent Counter Ion Conductivity and Dual Water Concepts' SPWLA 26th Symposium. Transactions. Paper RR.

Staal, J.J. and J.D.Robinson. 1977 'Permeability Profiles from Acoustic Logging' SPE 6821. SPWLA 6th European Symposium.

Stow, D.A.V., C.D.Bishop and S.J.Mills. 1982 'Sedimentology of the Brae Oilfield, North Sea: Fan Models and Controls' Journal of Petroleum Geology. 5,2, pp129-148

Stow, D.A.V. 1982 'Sedimentology of the Brae Oilfield Area, North Sea: A Reply' Journal of Petroleum Geology. 6,1. pp103-104

Spencer, C.W. 1985 'Geologic Aspects of Tight Gas Reservoirs' Journal of Petroleum Technology. July 1985. Vol37,No8. pp1308-1314

Surdam, R.C., S.W.Boese & L.J.Crossey. 1984 'The Chemistry of Secondary Porosity' In: 'Clastic Diagenesis', AAPG Memoir 37. p127-149. Editors: McDonald & Surdam. ISBN 0-89181-314-4

Surlyk 1978a 'Fan Sedimentation in Eastern Greenland'

Timur, A. 1968 'An Investigation of Permeability, Porosity, and Residual Water Saturation Relationships for Sandstone Reservoirs' The Log Analyst. July-August, 1968.

Thomas, E.C. and Stieber, S.J. 1975 'The distribution of shale in sandstones and its effect on porosity' SPWLA Symposium, June 1975

Thomas, E.C. 1976 'The Determination of Membrane Potential Measurements on Shaly Sands' Journal of Petroleum Technology. September 1976. pp1087-1096

Truman, R.B et al. 1989 'Shale Porosity-its impact on well log modeling and interpretation' SPWLA 30th Symposium, Paper Q, June 1989

Turner, C.C., J.M.Cohen, E.R.Connell & D.M.Cooper. 1987 'A Depositional Model for the South Brae Oilfield' Petroleum Geology of North West Europe. Editors: J.Brooks & K.Glennie. Publisher: Graham & Trotman.

de Vries. 1952a In 'The Thermal Conductivity of Granular Materials' Bulletin Institute Intern. du Froid, Paris

Waffa, M. and R. Nurmi. 1987 'Calculation of Saturation, Secondary Porosity and Producibility in Complex Middle East Carbonate Reservoirs' SPWLA 28th Symposium. Transactions. Paper CC.

Walker, R.G. 1978a ' Generalised Fan Model'

Walker, R.G. 1984 'Facies Models. Second Edition' Geoscience Canada, Reprint Series 1. Geological Assn of Canada.

Waxman, M.H; L.J.M. Smits. 1968 'Electrical Conductivities in Oil-Bearing Shaly Sands' Transactions. AIME. 243. also: SPEJ. June 1968 pp107-119

Waxman, M.H. and Thomas, E.C. 1974 'Electrical Conductivities in Shaly Sands- I. The Relation Between Hydrocarbon Saturation and Resistivity Index; II. The Temperature Coefficient of Electrical Conductivity' JPT Feb 1974 pp213-224. SPE 4094

Wells, P.R.A. 1988 'Hydrodynamic Trapping in the Cretaceous Nahr Umr Lower Sand of the North Area, Offshore Qatar' Journal of Petroleum Technology. March 1988. Vol40,No3.pp357-361

Welton, J. E. 1984 'SEM Petrology Atlas' Publs. The American Association of Petroleum Geologists

Wendel, D.J. 1987 'Restored-State Core Analysis for the Hutton Reservoir' SPE Formation Evaluation, Decemeber 1987

Wharton, R.P., G.A.Hazen, R.N.Rau and D.L.Best. 1980 'Electromagnetic Propagation Logging: Advances in Technique and Interpretation' SPE 9267

Widdicombe, R.E., P.Noon and D.L.Best. 1984 'Multiwell Faciolog Evaluation, Hartzog Draw Field Powder River Basin, Wyoming' SPWLA 25th Symposium, June 1984. Paper BBB

Wiley, R. 1989 Amoco In-House presentation on Neutron Tool Response

Wiley, R and Patchett, 1989 'Towards a neutron tool response model' SPWLA 30th Symposium Trans, paper

Williams, C.T. 1984 'Well A DST 3 & 3A Summary Report' Occidental Petroleum Aberdeen, Unpublished report.

Wilson, D.A. and W.M.Hensel. 1982 'The Cotton Valley Sandstones of East Texas: A Log-Core Study' SPWLA 23rd Symposium. Transactions. Paper R.

Wilson and Pitman. 'Authigenic Clays and Sandstones' Journal of Sedimentary Petrology. vol 47.

Winlowe, P. 1987 Department of Physiological Flow, Imperial College, London Personal communication

Winsauer, W.O. and McCardell, W.M. 1953 'Ionic Double Layer Conductivity in Reservoir Rocks' Transactions AIME 198, p129-134

Wolff, M. and J.Pelissier-Combescure. 1982 'Faciolog-Automatic Electrofacies Determination' SPWLA 23rd Symposium. Transactions. Paper FF.

Woodhouse, R. 1987 'Problems in Sw Calibration Using Oil Mud Cores and Core Electrical Measurements' The Log Analysts. May-June. vol 28,No3. p289-293

Worthington, P,F. 1985 'The Evolution of Shaly-Sand Concepts in Reservoir Evaluation' The Log Analyst. Jan-Feb 1985 Vol. XXVI No1 pp23-40

Worthington, P.F. et al. 1988 'Effect of Sample Preparation upon Saturation Exponent in the Magnus Field, U.K. North Sea' The Log Analyst. v 29 No1. January-February 1988, pp48-54

Yuan, H.H. and Diederix, K.M. 1987 'The Role of Membrane Potential Measurements in Shaly Sand Evaluation' SPWLA 28th Annual Logging Symposium, June 1987

NOMENCLATURE

a = Apparent

B = Waxman & Smits: Equivalent conductance of clay exchange cations (sodium) as a function of C_w at 25°C. mho cm^2/meq

BHC = Borehole Compensated Sonic Tool

BVO = Bulk Volume Oil, volume fraction of bulk formation.

Bragg's Law:

$2d\sin\theta = nl$, where dÅ =lattice spacing, θ =angle between incident X-Ray and lattice layer, n =integer value, Å =X-Ray wavelength.

C = Conductivity, Ω^{-1} m^{-1}

Cl = Water conductivity above which $\partial C_o / \partial C_w$ is a constant, mho/m

CAL = Caliper, inch

CBW = Volume fraction Clay Bound Water = $Q_v \theta_t$ $(0.0845^{-0.5} + 0.22)$; S= salinity meq/ml. Juhasz, 1981.p9

cf. = compare with

CEC = Cation Exchange Capacity, meq/g

CPI = Computer Processed Interpretation

C_o = Conductivity of rock entirely saturated with brine of conductivity C_w, mho/m

C_{ocgl} = Conductivity of conglomerate entirely saturated with brine of conductivity C_w, mho/m

C_{oe} = $C_o - C_x$, the free or replaceable electrolyte contribution to C_o, mho/m

C_{ox} = The intercept of the linear portion of a C_o vs C_w plot extrapolated to the C_o axis, mho/m. Corresponds with W-S $B.Qv/F^*$

C_x = The formation brine saturated true excess conductivity above that resulting from the free electrolyte, mho/m

∂C_{ox} = $C_{ox} - C_x$, the correction for the reduction in excess conductivity below C1, mho/m

Clay water =

Anion deficient water bound to the clay surface

ch = Chlorine

cl = Clay

con = Contamination

cor = Corrected

CNL = Compensated Neutron Log

C_m = True conductivity of the sandy conglomerate matrix

C_{xo} = Conductivity of flushed zone, mho/m

d = diffusion equation constant (7)

DCMP = Dry Clay Mineral Point, LDT / CNL crossplot

di = depth of filtrate invasion, inch

DIL = Deep Induction Log

DLL = Dual LateroLog

dfln = deflection

DN = Density Neutron

DNCMP = Dry Non Clay Mineral Point

DST = Drill Stem Test

DT = Delta Time, first arrival time sonic tool, µsec/ft

D-W = Dual Water Model of Clavier et al

EATT = EPT Attenuation, dB/m

EDS = Energy Dispersive Spectrum

ecc = Tool eccentered

e = Effective

EPT = Electromagnetic Propagation Tool

exp = Exponent

F = R_o/R_w or C_w/C_o, Archie Formation Resistivity Factor

F_{clast} = R_{oclast}/R_w, Archie's F for clasts

F_{cgl} = C_w/C_{ocgl}, Archie formation resistivity factor of the bulk conglomerate

F_g = C_w/C_{oe} Geometrical Formation Resistivity Factor as in used in the F_g saturation equation (6.2.1)

F_{matrix} = $R_{o\ matrix}/R_w$, Archie's F for sandy matrix.

F_o = $F^*(1\text{-}v^{H}{}_{Q}Q_v)$, Formation Resistivity Factor of the Dual Water model, Clavier et al.

Free Electrolyte = Formation water with an equal charge of cations & anions: uncontaminated recovered formation water

FWL = Free Water Level: capillary pressure = zero. Usually in the order of 10 ft(3m) below the oil water contact, more for small pore radius rocks.

F^* = Formation Resistivity Factor of Waxman & Smits, $\partial C_w/\partial C_o$ from linear portion of C_o v C_w plot, when $C_{wf} > Cl$.

g = Exponent to effective porosity in F_g based conductivity saturation equations, $F_g = \emptyset_e{}^{-g}$

g = Grain

GST = Gamma Spectrometry Tool

GRCC = Th+K API, borehole corrected

hc = Hydrocarbon

HI = Hydrogen Index, neutron tool. $HI_{water} = 1.00$

$HI_{hc} \approx 9[(4\text{-}2.5\text{rho}_{hc})/(16\text{-}2.5\text{rho}_{hc})]\text{rho}_{hc}$ (Schl. 1987, p52)

HIIP = Hydrocarbons initially in place.

hist = Mud chemistry history

hmc = Height mud cake, inch

I = Archie Resistivity Index, R_t/R_o

i = Immovable or "Irreducible" fluid

ILT = Illite

k = Absolute permeability, mD, pores entirely saturated with one fluid phase only. Property of the rock.

k_{hor} = Absolute permeability of horizontal core plugs measured with nitrogen.

k_w = Effective permeability to water, mD, at given S_{wi}.

k_o = Effective permeability to oil, mD, at given S_{wi}.

L = Hanai-Bruggeman depolarisation constant

LDT = Litho Density Tool

m = Exponent to total porosity in F based conductivity saturation equations where $F=\emptyset_t^{-m}$, Archie's shape factor or cementation exponent.

m = Mud

mc = Mud cake

mf = Mud filtrate

ML = MicroLog

MNOR = MicroNormal log from Microlog tool, ohmm

mov = movable

MSFL = Micro Spherically Focused Log

mw = Mud weight, lbs/US gal

n = Exponent to S_w in conductivity saturation equations where $R_t/R_o = S_w^{-n}$, Archie's saturation exponent

NGT/L = Natural Gamma Tool/Log

NML = Nuclear Magnetism Log

Non-log-input

= value used during formation evaluation which is wholly or partly derived from non-wireline sources

o = @ S_w=1 with formation water

ovl = Borehole oval

OWC = Oil Water Contact, the level at which S_w moves from 1 to < 1

P^* = Initial reservoir pressure

Parameter = A mathematical combination of logging tool readings with or without *Non-log-inputs* designed to be particularly sensitive to one formation characteristic and relatively immune from others.

Pe = PEF, Photoelectric Absorption Index, barns/electron

PHN = Phengite: Fe,Mg substitution of octahedral Al in illites

Q_v = CEC/unit pore volume, meq/cc

R = Resistivity, Ωm

rho = Density, g/cc

rhob = Density bulk, g/cc

rhoc = *rhob* corrected for mud density, Schl chart Por-15a

rhodsh = rho dry shale

rhodcmsh= rho dry clay minerals shale

rhodncmsh = rho dry non-clay minerals shale

rhog = grain density, matrix density, nil porosity density

$= 2.634 + 0.000714 GRCC + 0.160 vlogs$ (8.1.5.1)

rhogc = grain density of clasts ≈ 2.83 g/cc

rhof = density of pore fluid influencing *rhob*,

= $rho_{fm\ brine} + rho_{mf} / 2 = 0.98$ g/cc

R_{mf} = Resistivity mud filtrate.19,000ppm, 0.09Ωm@275°F: 15555ft(4741m) mid Brae

RTS = Reservoir Type Signature

rug = Rugosity

R_w = Resistivity of recovered formation brine at reservoir temp.

R_{we} = Effective water resistivity of deep investigation zone, ohmm. Problematic.

R_{wa} = Resistivity of formation brine apparent

R_{xo} = Resistivity of flushed zone

R_{xoc} = Resistivity of flushed zone when the resistivity of all replaceable water inhabiting the flushed zone equals R_{mf}.

R_{xot} = Resistivity of the flushed when one pore volume of R_{mf} has passed through the flushed zone.

R_{xwe} = Effective water resistivity of shallow investigation zone, ohmm. 0.08Ωm@275°F:15,555ft(4741m)

S = Saturation, fractional

sandy matrix = Refers to the volume fraction of the conglomerate which is not clasts; 1–*vlogs* , or 1-*vcors*.

SCAL = Special Core Analysis

SEM = Scanning Electron Microscope

SA = Small arm Caliper on EPT - good rugosity indicator

Schl = Schlumberger

SFLC = Spherically Focused Log borehole corrected

Shale = Shale reference bed used for clay mineral parameters

S_h = Fractional hydrocarbon saturation

S_{hmov} = Fractional movable hydrocarbon saturation

S_{hr} = Fractional residual hydrocarbon saturation

SMT = Smectite

S_{oc} = Saturation of oil in core

SOX = Shallow zone oil saturation

SP = Spontaneous Potential

stat = statistical fluctuation

stdof = Stand off between tool face and borehole wall, inch

S_w = Fractional water saturation, ϕ_t or ϕ_e system deliberately not specified.

S_{we} = Fractional water saturation of the effective porosity, see $\emptyset_e$ below.

$S_{we} = 1-(\emptyset_t/\emptyset_e)\ (1-S_{wt})$ Juhasz 1979, p9.

S_{wi} = Fractional 'irreducible' water saturation in the hydrocarbon leg above the transition zone. With increased P_C S_w will inevitably decrease, but in permeable rocks this becomes negligible above a certain pressure and may be considered a constant.

S_{wm} = Fractional water saturation of the conglomerates sandy matrix only, not the whole rock, ≈ S_{we} since sandy matrix shale content is low.

SWP = (Water saturation * Porosity), commonly considered approximately constant above transition zones in the same rock type.

S_{wt} = Fractional water saturation of the total porosity

S_{xe} = Fractional water saturation of the flushed zone's effective porosity

TDT = Thermal Decay Time

temp = temperature, Mean Brae=275°F. Gradient=0.0172°F/ft

TI = Type Interval, facies

TPL = Time of Propagation Log, of 1.1 GHz signal, µs/ft

Transition zone = zone above which water will not flow on production and below which the hydrocarbon saturation is zero. Zone in which both water and hydrocarbon phases are mobile.

V = Volume

v = volume fraction clasts, notation used in Diffusion Equation

$vcors$ = Volume fraction conglomerate clasts observed in cores, *%clast*/100

$V_{dryclres} = 0.0051(GRCC-23)$ *GRCC's* Th+K count, calibrated to the radioactive minerals in the reservoir. Provides the reservoir whole rock dry clay mineral volume.

$vlogs$ = Volume fraction clasts predicted from logs

$V_{shclast}$ = Volume fraction of clasts which is shale = 0.10

V_{shwhr} = Volume fraction of whole rock which is shale

V_{shres} = 0.01(GRCC-23), *GRCC's* calculation of whole rock volume shale responding to a clay mineral assemblage of equal proportions to that in typical sandy matrix.

$V_{shsdymtx} = [V_{shres} - (0.10vlogs)] / 1-vlogs$, volume fraction shale in the sandy matrix of the conglomerate, required for $\emptyset_e$

V_{shsh} = (GRCC-23)/(116-23), *GRCC's* calculation of volume shale responding to a clay mineral assemblage of equal proportions to that in the Shale Type Interval.

V^H_Q = Clay water volume per counter ion when $C_w > Cl$ (22°C), cm^3/meq

W = Grammes water per meq of exchangeable cation

w = Formation water

WCMP = Wet Clay Mineral Point

WDS = Wave Dispersive Spectrum, SEM